UNIVERSITY OF SOUTHAMPTON

Faculty of Medicine

Clinical and Experimental Sciences

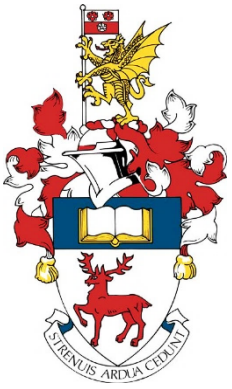

A 3D- Induced Pluripotent Stem Cell-Derived Human Neural Culture Model to Study Certain Molecular and Biochemical Aspects of Alzheimer's Disease.

by

Preeti Prasannan

Thesis for the Doctor of Philosophy

February 2022

UNIVERSITY OF SOUTHAMPTON

ABSTRACT

FACULTY OF MEDICINE

Thesis for the degree of Doctor of Philosophy

A 3D- Induced Pluripotent Stem Cell-Derived Human Neural Culture Model to Study Certain Molecular and Biochemical Aspects of Alzheimer's Disease

Preeti Prasannan

Alzheimer's disease (AD) is the most prevalent form of dementia and currently has no cure. Induced pluripotent stem cell (iPSC) technology is an innovative, cutting-edge technique that is able to recapitulate some key features of neurodegenerative disease pathology *in vitro.* The major advantage of using this technology is that neurons can be generated *in vitro* from AD patients with inherited mutations, thereby allowing patient-specific insight into the biochemical and pathophysiological nature of AD. 3D culture models provide a physiologically and spatially relevant microenvironment, thereby aiding better differentiation and maturation of cells *in vitro*. In this study, we aim to develop a 3D neural model derived from control and AD patient's iPSCs, in which cells can differentiate, self-organize and mature. AD-iPSCs with Presenilin 1 mutation (L286V, M146L, or A246E) and age-matched controls were differentiated in 3D Matrigel for 18 weeks *in vitro*. Characterization of cell morphology and protein profile was performed using immunofluorescence. Western blotting was used to determine disease-associated changes such as hyperphosphorylation of tau. AD and age-matched control iPSCs differentiate into neurons and astrocytes which self-organize into 3D structures by 3 weeks of differentiation *in vitro*. Cells express astrocytic (GFAP), neuronal (beta-3-tubulin, MAP2), glutamatergic (VGLUT1), GABAergic (GAD65/67) and pre-synaptic (Synapsin 1) markers after differentiation. The foetal 3R tau isoforms and 4R adult tau isoforms were detected at 6 weeks post differentiation. We have developed a standardised and validated *in vitro* human 3D iPSCs- derived neural model with mature neurons. In these AD-derived cells, we have shown early changes in AD-associated protein expression levels, presence of Aβ oligomers, an increase in the Aβ42/40 ratio, hyperphosphorylated Tau and presence of aggregated insoluble Tau, as observed in the disease. Our data indicates that this model may recapitulate the early biochemical and pathological disease features and can be a relevant platform for studying early cellular and biochemical changes and identification of drug targets

Table of Contents

LIST OF TABLES

LIST OF FIGURES

LIST OF ACCOMPANYING MATERIAL

DOI: https://doi.org/10.5258/SOTON/D2234

Declaration of Authorship

I, Preeti Prasannan

Declare that this thesis and the work presented in it are my own and has been generated by me as the result of my own original research.

A 3D- induced pluripotent stem cell-derived human neural culture model to study certain molecular and Biochemical aspects of Alzheimer's Disease

I confirm that:

1. This work was done wholly or mainly while in candidature for a research degree at this University;
2. Where any part of this thesis has previously been submitted for a degree or any other qualification at this University or any other institution, this has been clearly stated;
3. Where I have consulted the published work of others, this is always clearly attributed;
4. Where I have quoted from the work of others, the source is always given. With the exception of such quotations, this thesis is entirely my own work;
5. I have acknowledged all main sources of help;
6. Where the thesis is based on work done by myself jointly with others, I have made clear exactly what was done by others and what I have contributed myself;
7. None of this work has been published before submission

Signed: Preeti Prasannan

Date: 02 February 2022

Acknowledgements

First and foremost, I would like to thank my primary supervisor, Dr. Sandrine Willaime-Morawek, for all the warm support and guidance towards the completion of this project. I would also like to wish my second supervisor, Dr. Amritpal Mudher, for all the help and her guidance with the project. A vote of thanks to my third supervisor, Dr. Mariana Vargas-Caballero, for her guidance and warm encouragement in times of need. I would like to express sincere gratitude towards the Commonwealth Scholarship Commission, not just for funding me for PhD but also for the constant support and guidance through my journey. My special thanks to the Gerald Kerkut Trust for funding the project. I would take this opportunity to thank Dr. Ashley Pringle and Prof. John Chad for their helpful discussions and guidance, especially during transfer of this project.

I would like to thank all the people who were directly involved in the project. Special thanks to Dr. Elodie Siney for all the training, guidance, and warm support. Words cannot express my gratitude towards Dr. Shreyasi Chatterjee who has played a major part in my training for Western blot, as well as providing constant moral support that gave me the motivation to keep going in difficult times. I am extremely grateful to Dr. David Johnston from the BIU unit who not only taught me everything about Confocal Imaging, but also has helped me with imaging in general and guided me through this project. Special thanks to Maureen Gatherer, who helped me with cryosectioning when my health prevented me. I would also like to thank Dr. Matthew Brimmell and Matthew Darley for letting me use their Ultracentrifuge when needed. Special thanks to Ben Coles for all the help and warm support.

Finally, I would like to thank my parents, without whose constant support and encouragement I wouldn't have completed this journey. It was a great experience and pleasure working with my fellow team members: Joanna Gould, Diego Ojeda, Eda Sezer, Irene Peral, Megan Sealy, Eva-Daniela Ruiz, and George Devitt for their warm welcome and great support as lovely lab mates. Special thanks to Diana Franco-Bocanegra, Iain Hartnell, David Arcia, Sudha Priya Soundara Pandi, and Yan Ling. A heartfelt thanks to Conor Dinning for his constant support and kindness, without which this journey would have been much more difficult.

Definitions and abbreviations

3R Tau	**3 Repeat Tau**
4R Tau	4 Repeat Tau
AD	Alzheimer's Disease
ANI media	Axol Neural Induction media
ANM media	Axol Neural Maintenance media
APOE4	Apolipoprotein E
APP	Amyloid Precursor Protein
APS	Ammonium Persulphate
ARUK	Alzheimer's Research UK
Aβ	Amyloid Beta
BACE1	β-site APP Cleaving Enzyme 1
BDNF	Brain-Derived Neurotrophic growth Factor
BMD	Becker Muscular Dystrophy
BMP	Bone Morphogenetic Protein
BSA	Bovine Serum Albumin
CaMK2	Calmodulin-dependent protein Kinase II
cAMP	cyclic Adenosine Monophosphate
Cdk5	Cyclin-dependent protein Kinase
CLARITY	Clear Lipid-exchanged acrylamide-hybridized rigid imaging/ immunostaining/ in situ hybridization compatible tissue hYdrogel
CNS	Central Nervous System
CRABP2	Cellular RA Binding Protein 2
CSF	Cerebral Spinal Fluid
CTE	Chronic Traumatic Encephalopathy
DII1	Delta like gene 1
DMD	Duchene Muscular Dystrophy
DS	Down Syndrome

ECM	Extracellular Matrix
EOAD	Early Onset AD
ESCs	Embryonic Stem Cells
FAD	Familial AD
FGF	Fibroblast Growth Factor
FTDP-17	Frontotemporal Dementia with Parkinsonism linked to chromosome 17
GD	Gaucher's Disease
GDNF	Glical cell line Derived Neurotrophic Factor
GFAP	Glial Fibrillary Acid Protein
GSK3β	Glycogen Synthase Kinase
hAPP	human APP
HD	Huntington's Disease
hESC	human Embryonic Stem Cells
hfNSCs	human foetal Neural Stem Cells
hiPSC	human induced Pluripotent Stem Cells
HSC	Haematopoietic Stem Cells
HTA	Human Tissue Authority
ICM	Inner Cell Mass
IGF 1	Insulin-like Growth Factor 1
IGF 1-IR	IGF 1 receptor
iPSCs	Induced Pluripotent Stem Cells
JNK	c-JunN terminal Kinase
LB	Loading Buffer
LOAD	Late Onset AD
MAPK	Mitogen Activated Protein Kinase
MAPs	Microtubule Associated Protein
mRNAs	Messenger RNAs
NFGF	Nerve Growth Factor
NFTs	Neurofibrillary Tangles

NPCs	Neural Precursor Cells
O.C.T	Optimal Cutting Temperature
oRG	outer Radial Glial cells
p70S6	phospho70S6 Kinase
PAK	P-21-Activated Kinase
PBST	PBS with 0.1% or 0.2% Triton-X100
PD	Parkinson's Disease
PHFs	Paired Helical Filaments
PSEN1	Presenilin 1
PSEN2	Presenilin 2
RA	Retinoic Acid
SAD	Sporadic AD
sAPPα	Soluble APP α
sAPPβ	Soluble APP β
SHH	Sonic Hedgehog
TALENs	Transcription Activator-Like Effector Nucleases
TBI	Traumatic Brain Injuries
TGFβ	Tumour Growth-Factor Beta
VGLUTs	Vesicular Glutamate Transporters
α-CTF	α-Cterminal
β-CTF	β-Cterminal

Chapter 1 – Introduction

1.1 Alzheimer's Disease

Alzheimer's disease (AD) is an irreversible age-related progressive neurodegenerative disorder and the most common cause of dementia, for which there is currently no cure. Dementia is a broad term used to describe a group of symptoms (syndrome) that affects multiple brain functions. The characteristic symptoms may include memory loss, difficulty in comprehension and judgement, language, difficulties carrying out movement and daily activities, erratic mood and behaviour. There are various forms of dementia, AD, being the cause, accounts for about 60-70% of the cases. Other types of dementia include vascular dementia, dementia with Lewy bodies, dementia associated with Parkinson's disease and Fronto-temporal dementia. AD and vascular dementia together make up 90% of cases of dementia.

The German psychiatrist and neuropathologist Dr. Alois Alzheimer was the first to describe AD in 1906 when he observed peculiar changes in the brain tissue of his 55 year old female patient Auguste Deter (Alzheimer *et al.*, 1995). He reported AD as, "an unusual disease of the cerebral cortex", which caused memory loss, disorientation, paranoia and finally death after four and a half years of admission. What most people don't know is that Alois Alzheimer was also the first person to report an important stage of the disease progression. The case of Johann F., a 56-year-old male who died 3 years post admission, was different as the autopsy revealed to have the "plaque only" feature in the atrophied brain. Re-examination of the specimens in 1993 confirmed that this was only a different stage of the same disease (Möller and Graeber, 1998). However, even after over a century, the neuropathological features described by Alzheimer remain the key interests in AD research to this today.

Research into the molecular mechanisms of AD is essential, not only to understand the underlying pathogenesis and progression of the disease, but also to generate efficient drug target development platforms for successful clinical trials. In order to study a disease of the aging brain-the most complicated organ system, the use of an appropriate model becomes extremely critical. The lack of availability of viable human brain tissue for research has proven to be quite challenging, since the only source ethically approved for research are samples available post death of a patient or surplus tissue extracted from neurosurgeries. Hence, research in this field relies heavily on transgenic animal models (both vertebrate and

invertebrate). Decades of research on animal models have provided deep insight in understanding neuronal development, the intricate neural network and function of the brain and to a certain extent the molecular mechanisms involved in various neurodegenerative diseases. However, these animal models do not provide for true ageing and behavioural pattern studies. These models can't completely correlate to that of the human system and thus never recapitulate all features of age-related neurodegenerative disease affecting humans. This is primarily due to the vast differences in the basic structure and protein profiles between the brains of the animals used for studies when compared to the human brains. This limits us to study the different stages of progression of the disease from the cellular and biochemical point of view. Non-human primates not only have close resemblance to the human brain circuitry and behavioural characteristics but also have longer life spans compared to other animal models generally used for studies and thus are better candidates for studying neurodegenerative diseases like senile dementia. However, due to strict ethical code of conduct and cost-efficiency they are not commonly used for research. These are some of the reasons why currently all human clinical trials based on animal models for AD have failed to translate into effective life-saving therapies for the patients. The current treatment regimens for AD are regrettably only symptom based. Hence the field is looking towards more human-based models which could mimic key features of the disease in a physiologically relevant manner.

Regenerative medicine is gaining pace in bridging this gap between the known and the unknown. In recent decades, many researchers have generated specific subpopulations of neural and non-neural cells using stem cells. Induced Pluripotent Stem Cells (iPSCs) is a recent technology by which a terminally differentiated cell type like skin cells or blood cells can be used to generate pluripotent stem cells by the introduction of four key transcription factors – Sox2, Oct3/4, cMyc and Klf4 (Takahashi and Yamanaka, 2006). This latest advance in this field has allowed researchers to work with stem cells without the ethical issues that limit use of Embryonic Stem Cells (ESCs) for research purposes. Taking advantage of this state-of-the-art technique, iPSCs derived from patient's skin cells could be used to generate neurons with the disease-specific mutations of interest. This would enable researchers to get in-depth knowledge of a host of diseases from these patient-specific human neural models.

This would not just provide better insight into the disease but also aid in identifying relevant drug-targets to find curative measures for a fatal disease like AD.

1.2 Epidemiology of AD

According to the World Alzheimer's Report (2015), the number of people suffering from dementia will increase from 46.8 million in 2015 to 131.5 million in 2050, a 281% rise (Prince *et al.*, 2015). This report summarized the estimated number of people living with dementia in 2015 as 22.9 million in Asia, 10.5 million in Europe, 9.4 million in Americas and 4 million in Africa. The incidence of dementia is predicted to increase exponentially with an overall rise in life expectancy. Most of the increase in incidence is estimated to be seen in low- and middle-income countries. Dementia is the only disease in the top 10 diseases without treatment for prevention, cure or to slow its progression. According to the Alzheimer's Research UK (ARUK) Dementia Statistics, AD and other forms of dementia were the leading cause of death for women (15.4%) in 2016 (ARUK Dementia Statistics Hub, no date).

1.3 Subtypes of AD

AD is divided into two groups depending on the age of onset of the disease in an individual. These groups are called early onset AD (EOAD) and late onset AD (LOAD). Patients with EOAD start showing symptoms around 40-60 years of age whereas patients with LOAD show symptoms around or after 65 years of age.

Based on the genetic influence AD is categorised as Familial AD (FAD) and Sporadic AD (SAD) (explained in detail in section 1.7.1).

1.4 Symptoms of AD

The symptoms of AD progress slowly over a period of years, though its rate of progression is different for each individual. The initial symptoms can easily be misinterpreted or overlooked as signs of old age as the difference between the two can be quite subtle. Clinically, both EOAD and LOAD patients present similar symptoms, starting with waning of memory gradually progressing with increasing severity ultimately completely debilitating the patient. The symptoms of AD are classified into three stages: the early, middle, and late stages. The early symptoms include loss of memory and inability to remember recent events or information. This is because the first neurons to be affected in the brain are in the entorhinal cortex and hippocampus centres which stores new memories. The middle stage involves worsening of semantic memory stored in the temporal lobe, such as: difficulty recognising known people, confusion and disorientation, increased paranoia and hallucinations, problems with language, change in sleep and mood swings and with loss of information stored in parietal lobe making

spatial judgement difficult and hampering ability to perform daily tasks. At this stage, the neurons in other parts of the brain, including the frontal cortex responsible for different functions including motor functions and speech are damaged. The last stage being the late stage, patients are completely dependent on caregivers for daily tasks like eating, bathing and are bed-ridden. Dysphagia, the inability to swallow, causes dehydration and weight loss. As the disease progresses through various parts of the brain causing atrophy the amygdala, which plays an important role in emotional behaviour and response, emotional memory from amygdala is also affected. With the progression of the disease the symptoms get worse, and some individuals may even get violent and suspicious of their caregivers. They become prone to infections especially to the lungs. AD related pneumonia is the most common causes of death of these patients. Patients with AD live on average between 4 to 8 years after diagnosis. Some may progress faster while some may live up to 20 years with the disease. The progression of the disease may vary from patient to patient.

1.5 Pathophysiology of AD

In AD, the neurons in the brain are damaged over a period of time which leads to symptoms such as memory loss, confusion, disorientation, impairment in language and reasoning, depression and dysphagia.

These symptoms worsen with the progression of the disease. A typical AD pathology at the macroscopic level shows brain atrophy resulting from neuronal death (Bobinski *et al.*, 1996). The presence of intracellular neurofibrillary tangles (NFTs) and extracellular amyloid plaques (formerly called senile plaques) are the classic hallmarks of AD and they were the first well characterised histopathological features associated with the disease (Alzheimer *et al.*, 1995). However, in recent years the secondary features considered are synaptic dysfunction, neuronal loss and chronic inflammation.

NFTs are formed by the abnormal aggregation of hyperphosphorylated Tau. Under normal conditions Tau is a protein that binds to microtubules, thereby providing stability in neurons. This promotes axonal transport in neurons and maintains axonal integrity. Their phosphorylation levels determine their microtubule binding affinity. Tau in its phosphorylated state detaches from the microtubules.

Plaques are formed by the aggregation of amyloid beta (Aβ), a 40-42 amino acid proteolytic fragment of the amyloid precursor protein (APP) whereas intracellular accumulation of hyper phosphorylated Tau proteins leads to NFTs. In AD, hyperphosphorylation of tau leads to a

series of events involving detachment of tau from microtubules, destabilising the axonal transport system (Alonso *et al.*, 1994, 1997) and later aggregation of the hyperphosphorylated forms of tau to form NFTs. This eventually leads to neuronal death. In AD, there is evidence suggesting an imbalance in the regulation of kinases and phosphatases.

1.6 Risk factors of AD

Although there is no clear understanding as to why some people who are not genetically predisposed to AD develop the disease while others do not, there have been many studies pointing towards the various factors which could increase the chances of contracting the disease. These risk factors can be classified into the deterministic and the modifiable risk factors.

1.6.1 Deterministic Risk Factors

1.6.1.1 Genetic factor

AD can be broadly classified as FAD or SAD based on the aetiology of AD. The most common form of AD is the Sporadic AD (>95%). FAD accounts for approximately 2-5% of all AD cases. Having even a single allele of the FAD mutations in the APP, Presenilin 1 (PSEN1) or Presenilin 2 (PSEN2) genes doubles the chance of the next generation acquiring EOAD. Having at least one first-degree relative with dementia increases the risk of acquiring FAD by 3.5 times (van Duijn *et al.*, 1991). So far Apolipoprotein E (APOE4) (more detail in section 1.7.1.1.1) is the only gene identified which could increase the risk of developing SAD. However, presence of APOE4 allele is neither a sufficient nor definitive factor in developing SAD. APOE4 only increases the susceptibility to SAD. The higher the number of APOE4 alleles greater the risk of developing SAD (more detail in section 1.7.1). AD may occur in families with a history for either SOAD or LOAD. Individuals belonging to families with a history of EOAD are genetically predisposed to developing the disease by inheritance. Approximately 60% of the patients with EOAD have a positive family history of AD (Campion *et al.*, 1999).

Down syndrome (DS) is a neurological disorder of individuals carrying an extra copy of chromosome 21 (Lejeune, Gautier and Turpin, 1959a; G.Allen, 1974). Patients with DS show significant levels of AD pathological features including senile plaques and neurofibrillary tangles by age 40 (Wisniewski, Wisniewski and Wen, 1985). With improvements in medical advances over the years the general life expectancy of adults with DS has increased from 58.6

years to 62.9 years, with males showing greater life expectancy by 3.3. years (Glasson *et al.*, 2002). Unfortunately, with increasing age comes the risk of developing clinical symptoms of dementia. However, not all of these patients will live to develop symptoms of AD. Estimates suggest that the proportion of adults with DS developing the clinical symptoms varies significantly.

Estimates based on a small sample size study shows that over the age of 60 years the range of DS patients developing AD-symptoms would vary between 15-77%{reviewed in (E.Head *et al.*, 2012)}. It is still not clear as to why some patients develop clinical signs of dementia and a subset of DS patients show no symptoms at any given age. Interestingly, a study in 1998 showed men with DS were more prone to develop AD than women and those with the APOE4 allele were at an even higher risk (Schupf *et al.*, 1998).

1.6.1.2 Age

The prevalence and the worldwide incidence of the disease points to the fact that increasing age is another major risk factor of developing AD. The risk of developing AD increases every five years once a person reaches 65 years of age and doubles every five years after the age of 65. However, old age alone is not a factor for developing AD. The incidence of AD rises exponentially with increasing age up to the age 90 (Jorm and Jolley, 1998). The percentage of people with AD increases with age with around 3% of people in the age group of 65-74, 17 % of people in age group 75-84 and 32% of people in the age group of 85 years and above having AD (Sposato *et al.*, 2015).

1.6.2 Modifiable Risk Factors

1.6.2.1 Vascular Diseases

Vascular dementia and AD have always been studied and treated separately. AD is attributed to brain atrophy due to neuritic plaques and tangles, whereas vascular dementia was traditionally characterised by vascular damage due to infarction or stroke. Both of these pathologies quite often overlap in the elderly dying with dementia. This co-existence was first reported by Alois Alzheimer (Alzheimer *et al.*, 1995). Vascular risk factors include hypertension, diabetes mellitus, stroke, smoking, obesity and higher cholesterol levels. People suffering from hypertension and diabetes have an increased risk of developing AD (Launer, 2002). However, there are mixed results from different studies making the association of vascular diseases and AD unclear. This could be due to various reasons, such as age of patients

at the start of the study, medical history, lack of follow-ups and treatment with different anti-hypertensive drugs. Some studies have shown systolic hypertension has a more profound effect than diastolic hypertension on the risk of AD. A recent study showed systolic hypertension in midlife can increase the risk of AD by 18-25% and found no association with diastolic hypertension (Lennon *et al.*, 2019).

Similar results were found in another study indicating having raised systolic blood pressure in midlife increases risk of AD while increases in diastolic pressure had no significant effect (Kivipelto *et al.*, 2001). Increased blood pressure, especially untreated in the middle age, may serve as a risk for developing AD around 25 years later in life (Launer *et al.*, 2000).

1.6.2.2 Gender

For most dementias other than AD, men and women face the same risk. 65% of dementia patients are composed of women whereas 35% are men (ARUK Dementia Statistics Hub, no date). However, for vascular dementia men are more prone to develop dementia since men are more prone to strokes and heart diseases. Women are more likely to develop AD than men (Gao *et al.*, 1998) especially at older ages (Jorm and Jolley, 1998). This could just be attributed to the longer average life span of women. According to the ARUK Dementia Statistic Hub, 8.7% men and 16.3% of women in England and Wales died of AD and other dementias in 2017 being the leading cause of death among women. The progression of AD between the sexes is similar approximately around age 75, beyond which it increases for women after the age 80 (Roberts *et al.*, 2014). Women also have a faster rate of cognitive decline from the time after diagnosis of AD (Agüero-Torres *et al.*, 1998).

1.6.2.3 Traumatic Brain Injury

An injury that results in the loss of consciousness or amnesia for 30 minutes or more, or may result in a skull fracture is considered a traumatic brain injury (TBI). There is evidence pointing to the fact that moderate to severe head injuries increase the risk of certain forms of dementia. People with head injuries in early adulthood or those with even a single TBI have a history of developing long-term pathology such as amyloid plaques and NFTs later in life (Johnson, Stewart and Smith, 2012). Those who encounter repeated head injuries may be at even higher risk of developing AD or other types of dementia. Chronic traumatic encephalopathy (CTE) is a pathology of the brain which can be diagnosed only at autopsy and is associated with the development of dementia. However, the cause and risk factors other than head injury are unknown. The CTE autopsy shows evidence of tangles of the protein tau in the brain which

unlike in AD are observed around small blood vessels. Interestingly, amyloid plaques are observed only in certain cases. There is ongoing research to find the exact correlation between head injury and how it contributes to the development of dementia.

1.6.2.4 Education - Social - Cognitive Alertness

Over the years, there has been speculation that people with a greater number of years of formal education are at lower risk of developing AD when compared to people with fewer years of education. The popular saying, "*use it or lose it*", promotes the idea that performing cognitively challenging activities or having formal education throughout adulthood could possibly increase synaptic density. A study in 2013 showed keeping the brain active by reading and doing puzzles through early and late stages of life is important for the health of the brain at old age. In this study 294 men and women, mostly in their 80s, were given cognitive tests every year in the last years of their life and their brains examined post-mortem for evidence of pathology for signs of dementia. They found that people who actively participated in memory challenging activities had a slower rate of decline of memory, despite the presence of plaques and tangles in their brain, as compared to those who didn't participate in such cognitive activities. There was a difference of 14% in the rate of decline between the two groups, indicating that mental stimulation could be a protective measure, decreasing the rate of decline of memory loss (Vemuri and Mormino, 2013; Wilson *et al.*, 2013). The "Nun Study" is a study by David Snowdon, who started studying nuns in Minnesota in 1986 to understand why some brains deteriorated with age while others didn't (Snowdon, 2003). These nuns were tested annually for bloodwork, cognitive assessments, medical exams, and physical assessments and donated their brains at death for future investigation. The study showed that pathology alone could be misleading in understanding the disease. One third of the sisters whose brain was completely covered with plaques and NFTs (in an extreme case where Braak stage score was 6) at autopsy were asymptomatic and scored normal results in their cognitive tests during life (Snowdon, 1997; Iacono *et al.*, 2009). On the contrary, a recent study showed that the pathological progression is independent of the educational level (Rawlings *et al.*, 2019). Cognitive tests revealed an association between educational level and the performance based on intellectual function regardless of the extent of amyloid beta accumulation in the brain, suggesting that education level does not reduce the risk of developing AD but may delay the onset of clinical symptoms. This could mean that testing cognitive function alone may not be a reliable indicator for the progression of the disease. A recent study suggests that lower IQ scores from childhood to adolescence have a link to the presence of the E4 variant of the gene APOE, an allele that is

considered to be a genetic risk factor for SAD (Reynolds *et al.*, 2019). The study suggests that the prescence of the APOE4 allele affects cognitive decline early in adolescence and adulthood. The IQ scores were lowered by 1.91 points per E4 allele, with a much more prominent effect observed in females (a reduction of scores by 3.41 points) than males (a reduction of 0.33 points).

1.7 Aetiology of AD-Genetics

Genetically, AD can be broadly classified into two types: FAD and SAD.

1.7.1 Sporadic AD

The most common form of AD is SAD. SAD accounts for almost 95% of AD cases. Although, SAD may have a similar clinical manifestation to FAD, this form of the disease is not genetically inherited. Many genetic, lifestyle and environmental factors could play an important role in the development of SAD. In most of the cases, symptoms begin at age 65 years or above. Genome wide analysis has led to the identification a number of susceptibility genes that could be a risk factor in developing SAD but are not a determinant like FAD genes.

1.7.1.1 Genes associated with Sporadic AD

1.7.1.1.1 APOE

Apolipoprotein E (APOE) - E4 allele has been the only gene identified as a major risk factor for acquiring SAD (Namba *et al.*, 1991; M. S. Tsai *et al.*, 1994). APOE is a gene on chromosome 19 which encodes for a protein involved in cholesterol and lipid trafficking. There are three alleles of APOE: E2, E3 and E4 with a worldwide frequency of 8.4%, 77.9% and 13.7% respectively (Farrer *et al.*, 1997). Having homo or heterogeneous alleles of the E4 variant increases the chances of a person developing AD (Chartier-Harlin *et al.*, 1994). A single copy of the E4 allele increases the risk by 3-4 times, and the presence of homozygous E4/E4 allele increases the risk 8-12times compared to the other alleles (Corder *et al.*, 1993; Verghese, Castellano and Holtzman, 2011). This however varies a lot from country to country and within countries, with other factors such as sex and ethnicity also playing a role (Farrer *et al.*, 1997). It is also associated with lower age of onset in a dose dependent manner (Corder *et al.*, 1993; William Rebeck *et al.*, 1993; Hsiung, Sadovnick and Feldman, 2004) The mean age of clinical onset and frequency of the disease for homozygous E4/E4 patients is 68 years and 91%,for heterozygous allele is 76 years and 48% and 80 years and 20% in non-carriers (Corder *et al.*, 1993; William Rebeck *et al.*, 1993).Though SAD does not usually run in families, it does increase the chances of future generations developing AD as compared to families with no

history of AD. For instance, a study showed that among the first degree relatives of AD patients, up to 50% of homozygous E4/E4 allele carriers did not develop AD (Farrer *et al.*, 1995).

Genome Wide Association Studies (GWAS) is a study to identify genetic variations seen in different individuals for a particular disease. Although the APOE gene has been implicated as the gene with highest risk factor it is not sufficient to justify the majority occurrence of sporadic AD. For the past decade GWAS have been a critical tool in identifying genetic factors at play in the underlying cause of diseases, such as macular degeneration and diabetes mellitus. Although there are a few reports published, for a complicated disease like AD the approach is still in its early phase. One of the first ever GWAS studies was reported in 2007, wherein a robust sample of 1808 LOAD and 2062 controls from United States of America and United Kingdom were examined for 17343 markers for SNPs known in AD. The study shows 19 significant markers associated with risk of AD, of which 3 SNPs showed most relevance to AD. The SNPs, namely – galanine like peptide precursor (GALP), nonreceptor tyrosine kinase (TNK1) and phosphoenolpyruvate carboxykinase (PCK1) are located near the APOE locus which further validates the approach of the study. These genes possibly affect metabolism or trafficking relevant to AD. Although this study lists a wider range of susceptible genes, replication and further confirmation is necessary to comprehend their role in the pathogenesis in AD (Grupe *et al.*, 2007). A different study of confirmed AD cases and controls from USA and Netherlands reported another significant SNP in association to APOEε4 variant, GAB2 (GRB2-associated binding protein 2), which may have an influence on both tau phosphorylation as well as Aβ due to its binding to both APP and the Presenilins (Reiman *et al.*, 2007). CLU (clusterin; apolipoprotein J), CR1 (compliment component (3b/4b) receptor 1) and PICALM (phosphatidylinositol binding Clathrin assembly protein) – three novel AD risk-genes were reported in 2009, which was later replicated in different studies (Harold *et al.*, 2009; Lambert *et al.*, 2009). CLU has been reported to be involved with the transport of Aβ and Aβ fibrillization (DeMattos *et al.*, 2004; Nuutinen *et al.*, 2009). Nearly three dozen genes have been reported to be associated to AD using GWAS studies over the past decade. Some of these are sortilin-related receptor (SORL1) and glycine-rich protein 2-associated binding protein 2 (GAB2), death-associated protein kinase 1 (DAPK1), ubiquilin 1 (UBQLN1) and adenosine triphosphate-binding cassette transporter 1, subfamily A (ABCA1), low density lipoprotein receptor-related protein 6 (LRP6) and TREM 2. These risk-associated genes have so far been reported to either affect APP catabolism, cholesterol homeostasis, immune system response or

endocytic mechanism. Although these studies are a commendable start with encouraging discovery of a broad range of initial results, these new associations still need to be validated in larger properly representative populations.

1.7.2 Familial AD

This is a rare form of the disease which is genetically inherited in the family. It accounts for less than 5% of all AD cases. The age of onset is quite early at around 40-60 years. It is also called Early-onset AD (EOAD). The familial form manifests due to mutations in one of three major genes: APP (P. St George-Hyslop *et al.*, 1987; Goate *et al.*, 1991), PSEN 1, (Sherrington *et al.*, 1995; Hüll *et al.*, 1998) and PSEN 2 (Rogaev, 1995; Sherrington *et al.*, 1996). The APP gene is located on chromosome number 21, whereas PSEN 1 and 2 are located on chromosomes 14 and 1 respectively. Mutations in the PSEN1 gene are the most commonly found in FAD, followed by mutations in APP and PSEN 2. Currently, 341 PSEN 1 mutations, 70 APP mutations and 84 PSEN 2 mutations have been identified for FAD (ALZFORM, 2019). Patients with EOAD show a more aggressive course with shorter survival time. In affected families (at least two generations have had the disease) it appears early in life, often around age 40. DS patients have an extra copy of chromosome 21 which means they have 3 copies of this chromosome and produce more APP than normal individuals. Hence, people with DS are genetically predisposed to develop pathological signatures of EOAD. It is believed that FAD mutations are responsible for an increase in the generation of an aggregation prone species of Aβ protein peptides which eventually leads to plaque formation. APP is the precursor protein of amyloid beta, whereas PSEN 1 and PSEN 2 are the genes that encode for the PSEN proteins which act as the catalytic subunits of the enzyme complex γ-secretase responsible for the processing of APP.

1.7.2.1 Genes associated with Autosomal AD / FAD

1.7.2.1.1 Amyloid Precursor Protein

Individuals with Down syndrome (DS), a disease caused by the extra copy of chromosome 21, show striking pathological similarities including amyloid plaques as early as 30-40 years of age (Down, 1866; Lejeune, Gautier and Turpin, 1959b; Ellis, McCulloch and Corley, 1974; Glenner, 1983). This raised interest in studying plaques. In 1984, Glenner and Wong discovered the Aβ peptide, which they purified and sequenced, formed amyloid plaques in patients diagnosed with AD and DS (G G Glenner and Wong, 1984; George G. Glenner and

Wong, 1984). Later in 1987, a group of scientists found that APP, a precursor peptide made up of 695 amino acids, includes the Aβ peptide subunit which is 40-42 amino acids long (Kang *et al.*, 1987). With the discovery of Aβ came the question regarding the link between chromosome 21 and the gene or genes responsible for AD. In 1987, genetic data from four families with previous history of AD were used to map the location of the APP mutation to chromosome 21 on the long q arm at position 21 (P. H. St George-Hyslop *et al.*, 1987). However, soon it came under notice that the APP gene accounted for only some but not all cases of FAD. In 1995, scientists using gene mapping studies isolated two other genes associated to AD: PSEN1 on chromosome 14 and PSEN 2 on chromosome 1 (Rogaev, 1995; Sherrington *et al.*, 1995).

1.7.2.1.1.1 Amyloid Beta

Amyloid beta is the protein peptide formed by the sequential proteolytic cleavage of APP by the enzymes β-secretase and γ-secretase respectively (Fig 1.1). APP is a single pass transmembrane protein with large extracellular domains. Once APP is sorted in the endoplasmic reticulum and Golgi complex, it is transported through the axon to the synaptic terminal (Koo *et al.*, 1990). Clathrin coated vesicles mediate the transport to either cell surface for nonamyloidogenic proteolytic cleavage or are reinternalized into the endosomal compartment where Aβ is generated, which is later released into the extracellular space(Koo and Squazzo, 1994). APP is processed by two pathways: a) Nonamyloidogenic and b) Amyloidogenic pathways. It is first cleaved in the luminal domain by (a) α-secretase or (b) β-secretase resulting in the formation of membrane bound α-Cterminal (α-CTF) or β-Cterminal (β-CTF) fragments respectively, and the release of soluble APP α (sAPPα) or soluble APP β (sAPPβ) fragments. This is followed by a cleavage of α-CTF or β-CTF by γ-secretase to eventually release p3 or Aβ peptides respectively into the extracellular domain. In the amyloidogenic pathway following the β-secretase the β–CTF fragment is cleaved at one of many sites by γ-secretase giving rise to Aβ of varying lengths (40-44) Aβ40 and Aβ42 being the most common. The β-site APP cleaving Enzyme 1 (BACE1) is the major β-secretase in the brain.

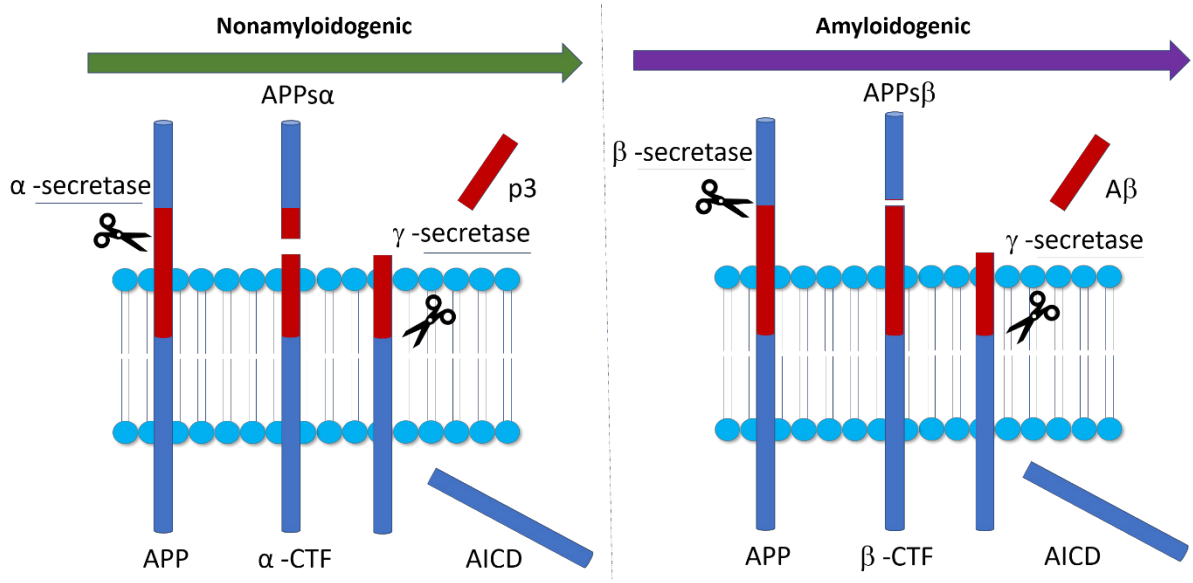

Figure 1.1 : A schematic representation for APP protein processing following the two pathways (O'Brien and Wong, 2011). Adapted from O'Brien and Wong 2011.

The enzyme γ-secretase is a multimeric protein complex which consists of 4 subunits forming a 1:1:1:1 heterodimer (Li *et al.*, 2014) (Sato *et al.*, 2007) :Presenilin 1 or 2 (Carter *et al.*, 2008), Nicastrin (Yu *et al.*, 2000), Anterioe pharynx-defective 1 (Aph-1) (Goutte *et al.*, 2002) and Presenilin enhancer 2 (Pen-2) (Francis *et al.*, 2002) .

1.7.2.1.1.2 Physiological Role

APP is found in many tissues and organs and plays an important role in many biological functions and signalling pathways. Aβ influences cell growth, differentiation, neurite outgrowth and synaptogenesis. APP may also have a developmental role as there is evidence it is processed in a way similar to Notch, which is involved in neural cell differentiation (Kimberly *et al.*, 2001). It is involved in the proliferation of neural progenitor stem cells. Studies have also shown that APP promotes neural and glial differentiation (Baratchi *et al.*, 2012). Cell culture studies have shown that APP regulates neurite outgrowth (Small *et al.*, 1994; Alliquant *et al.*, 1995). The expression of APP drastically increases at the time of synaptogenesis during development (Clarris *et al.*, 1995; Wang *et al.*, 2009).

1.7.2.1.2 Presenilin 1

1.7.2.1.2.1 The gene and protein structure

PSEN 1 is located on chromosome 14q24.2 (Schellenberg *et al.*, 1992), the long q arm of chromosome 14 at position 24.2, which encodes an integral membrane protein (Schellenberg *et al.*, 1992). The gene comprises of 13 exons, 10 exons (3-12) of which contain the coding

sequence (Clark *et al.*, 1995), which generates a 467 amino acid protein. The protein has a nine-pass transmembrane domain topology (Spasic *et al.*, 2006), with an extracellular C-terminus and luminal N-terminus (Thinakaran *et al.*, 1996). PSEN1 remains inactive in its full length form (Ratovitski *et al.*, 1997) and is considered active in its cleaved form (Brunkan *et al.*, 2005).

1.7.2.1.2.2 Function and physiological role

The physiological functions of PSEN1 have not yet been clearly defined yet. PSEN1 is a protein forming a catalytic core of the multimeric γ-secretase complex (see section 1.7.2.1.1 A-Amyloid Beta), which is involved in the proteolytic cleavage of APP (De Strooper *et al.*, 1998; Wolfe *et al.*, 1999). This proteolytic activity of PSEN1 plays an important role in several signalling pathways. One of these is the Notch signalling, it cleaves the Notch receptor. In a PSEN1 null drosophila, Notch signalling was eliminated and a notch-like lethal phenotype was observed (Struhl and Greenwald, 1999). PSEN1-/- mice also show defects in spinal ganglia, somite segmentation and differentiation as a result of reduced Notch1 expression, along with reduced expression of DII1 (delta like gene 1 – a vertebrate Notch ligand) (Wong *et al.*, 1997). However, postnatal inactivation of PSEN1 does not affect expression of Notch or its downstream signalling (Yu *et al.*, 2001). This shows that PSEN1 plays an important role in embryonic development. PSEN1 also plays an important role during the embryonic Central Nervous System (CNS) and skeletal development for axial formation, neurogenesis and neuronal survival (Shen *et al.*, 1997). Loss of PSEN1 function leads to learning, synaptic plasticity and memory deficits and also plays an important role in survival during aging as shown in adult mouse cerebral cortex (Saura *et al.*, 2004a; Wines-Samuelson *et al.*, 2010). PSEN1 binds and stabilises β-catenin, which plays an important role in Wnt signalling. The Wnt signalling pathway is crucial during embryogenesis and development. Mutations of PSEN1 affects this stabilization of β-catenin complex thus leading to degradation of β-catenin in the brains of transgenic mice (Zhang *et al.*, 2009).

1.7.2.1.2.3 PSEN1 and Alzheimer's Disease

With 321 mutations, as reported pathogenic in the Alz-forum database (https://www.alzforum.org/mutations/psen-1), PSEN1 is the most common cause of FAD/ EOAD, thereby accounting for 70-80% of the FAD cases (Cruts, Theuns and Van Broeckhoven, 2012). The PSEN1 family of mutations are known to cause complete penetrance

and cause some of the severe forms of EOAD with age of onset occurring as early as 30 years, thus being one of the most aggressive forms of FAD. However, the PSEN1 mutations come with a wide variability in the age of onset ranging between 29-50 years (Bekris *et al.*, 2010). For example, the M146V mutation seems to have an early age of onset ranging from 36-40 years whereas mutations C410Y and E280A have an age of onset around 45-50 years (Clark *et al.*, 1995; Hutton *et al.*, 1996) Therefore, it becomes crucial to study the physiological role as well as the pathogenesis linked to PSEN1.

Although the exact mechanism of the disease is unclear, there are two hypotheses. The amyloid hypothesis – suggests that PSEN1 mutations interfere with the production of Aβ by increasing the production of Aβ42 (Hardy and Selkoe, 2002), which seems to have more fibril forming tendency. This was supported by evidence from a few of the initial studies from patients with FAD having elevated levels of Aβ42 in their plasma, experiments with transfected cells and transgenic mice in lab settings. However, over the years, inconsistencies with the model have led to criticism and revision of the said hypothesis. With accumulating evidence, there was a shift in the paradigm from absolute increase of Aβ42 levels to increase in the ratio of Aβ42/ Aβ40, which has become a characteristic of PSEN1 mutations in FAD (Borchelt *et al.*, 1996; Selkoe and Hardy, 2016) There is evidence suggesting that Aβ42 deposition may be a preclinical event which precedes other changes in AD with PSEN1 mutation (Lippa *et al.*, 1998). The recent Presenilin hypothesis, which is distinct, but not mutually exclusive, posits that either a loss- or gain- of PSEN1 function caused by PSEN1 mutations triggers FAD. The gain-of- function is more genetic and the loss-of-function is more on the biochemical level. The increase in the ratio of Aβ42/Aβ40 due to PSEN1 mutations could be explained as a gain of toxic function. Conversely, mutations in PSEN1 have shown a partial loss of function in the γ-secretase complex, which disrupts several downstream pathways leading to neurodegeneration in EOAD (Shen and Kelleher, 2007; Heilig *et al.*, 2010) There is evidence that with a PSEN mutation there is a decrease in APP and Aβ generated (De Strooper, 2007). Saura et al 2004 have shown complete loss of PSEN1 function in mice results in age-dependent neurodegeneration in absence of Aβ generation but with increase in hyperphosphorylated tau. With increasing age, these mice show severe neurodegeneration of the cerebral cortex, impairment of memory and synaptic plasticity (Saura *et al.*, 2004b). This hypothesis contradicts the amyloid hypothesis, leading to the notion that Aβ accumulation is not required for developing AD.

1.7.2.1.3 Presenilin 2

In 1995, Presenilin 2 was reported as a gene associated with AD (Levy-Lahad *et al.*, 1995). The PSEN 2 gene is located on chromosome 1 at location 1q42.13. Like PSEN1, PSEN2 is a subunit of the γ-secretase which is responsible for cleavage of Aβ. Studies in mice and humans suggest that PSEN 2 mutations alter Aβ42: Aβ40 ratio (Scheuner *et al.*, 1996; Citron *et al.*, 1997) Studies have also reported PSEN2 mutations decreases Aβ40 production (Walker *et al.*, 2005; Braggin *et al.*, 2019). Knocking out PSEN1 is lethal at the embryonic stage in mice, whereas PSEN2 knockout has no lethal effects (Herreman *et al.*, 1999).

1.8 Amyloid Cascade Hypothesis

More than 30 years ago the amyloid hypothesis was first proposed by George Glenner. He suggested that cerebral amyloid initiates and drives pathology in AD (G G Glenner and Wong, 1984). This was the first report which later came to be known as the *Amyloid Hypothesis*. Over the years, in 1991 this has been refined as the *Amyloid Cascade Hypothesis* by John Hardy and David Allsop (Hardy and Allsop, 1991). This hypothesis states that the aberrant processing of the APP protein was the initiating point of AD pathology which subsequently leads to aggregation of protein Aβ especially Aβ42 forming plaques which ultimately leads to loss in neurotransmission, death of neurons carrying tangles eventually leading to dementia. The autosomal dominant mutations involved in EOAD are either in the APP gene (clustering more around the γ-secretase cleavage site) or the Presenilin gene, the catalytic unit of γ-secretase (reviewed in) (Hutton and Hardy, 1997; Hardy, 2009). The end result of both these mutations is an increase in the production of less soluble and more cytotoxic Aβ42 as compared to Aβ40. Aβ is chemically sticky in nature and forms clumps to eventually form plaques. Studies have suggested that Aβ in small clumps (oligomers), rather than whole plaques are more damaging as it may block cell-cell communication and transfer of neurotransmitters at the synapse (Deshpande *et al.*, 2006).

1.9 Tau

Tau protein was first discovered in the mid-1970s as a protein which was co-purified with microtubules and noted for its ability to induce assembly or disassembly of tubules (Weingarten *et al.*, 1975). Thus, the name tau was designated, and the protein came to belong to the Microtubule Associated Protein (MAPs) family known for its role in assembly and stabilisation of microtubules. In 1977, tau was identified as a phosphoprotein phosphorylated by a protein

kinase, which co-purified with tau proteins (Cleveland, Hwo and Kirschner, 1977). By 1983, a study showed that tau in the dephosphorylated state induced polymerization of microtubules (Lindwall and Cole, 1984). It was only in 1986 that the interest in the protein increased when studies found abnormally phosphorylated tau proteins formed a major component of the paired helical filaments (PHFs) responsible for the formation of NFTs found in AD brains (Grundke-Iqbal *et al.*, 1986, 1987; Kosik, Joachim and Selkoe, 1986) Studies on tau protein gained focus, until the discovery of mutations in the APP and Presenilin genes involved in Aβ formation were believed to be causative factors in FAD. However, with the discovery of mutations in the tau gene responsible for an autosomal dominant neurodegenerative disease known as frontotemporal dementia with parkinsonism linked to chromosome 17 (FTDP-17) with characteristic tau pathology and no implication on amyloid plaques, research on tau proteins has regained its foothold (Poorkaj *et al.*, 1998; Spillantini *et al.*, 1998; Dayanandan *et al.*, 1999)

1.9.1 Transcription and Translation

The human tau gene is located on the long arm of chromosome 17 at band position 17q21 and has 16 exons (Fig 1.2). The exon 4A is found in peripheral tissues and is never detected in the messenger RNAs (mRNAs) in the human brain, whereas exons 6 and 8 have never been observed in humans (Buée *et al.*, 2000). The exons -1,1, 2,3,4,5,7,9,10,11,12,13 and 14 form the primary transcript (Fig 1.2). The exons 2, 3 and 10 are alternatively spliced to form the 6 isoforms in the human adult brain (0N3R, 1N3R, 2N3R, 0N4R, 1N4R, 2N4R) (Andreadis, Brown and Kosik, 1992). The exon -1 constitutes the promoter, hence is transcribed but not translated. Exon 14 is found in the mRNA but also not translated (Andreadis, Brown and Kosik, 1992). The exon 2 can be present alone unlike exon 3 which never appears independent of exon 2 (Andreadis, Broderick and Kosik, 1995). The alternative splicing of exons 2 and 3 encodes for the single or double amino acid containing inserts at the amino terminus. The exon 10 encodes for one of the repeat regions which is responsible for microtubule binding. Alternative splicing of exon 10 leads to the formation of either the 3R repeat isoform (3R Tau) or the 4R repeat isoform (4R Tau). The mRNA transcript without the exon 10 produces the 3R tau isoform whereas the one with exon 10 produces 4R tau isoform (Goedert *et al.*, 1989a). Thus, alternate splicing of exons 2, 3 and 10 leads to the formation of the 6 isoforms in the human brain.

1.9.2 Tau and its Isoforms

Tau is primarily found in neurons, but to a lesser extent also in oligodendrocytes (LoPresti *et al.*, 1995) and astrocytes (Papasozomenos and Binder, 1987; Müller *et al.*, 1997). There are differences in expression of tau isoforms between rodents and humans. In adult rodent brains, three isoforms of 4R tau are expressed either with no (0N), one (1N) or two (2N) amino acid inserts, with an absence of 3R tau isoforms (Takuma, Arawaka and Mori, 2003) in contrast to humans with all 6 isoforms present in the adult brain (Fig 1.2). The expression of tau isoforms are developmentally regulated. 0N3R is predominantly expressed during the early stages of development and found in the foetal human, rat, mouse and guinea pig brain (Janke *et al.*, 1999; Takuma, Arawaka and Mori, 2003; Liu and Götz, 2013) The expression of 3R Tau in rodent brains declines after foetal development. 4R Tau which is absent in the rodent foetal stage and progressively increases through the adult stage (Hanes *et al.*, 2009; Hernández *et al.*, 2020) The human brain expresses all 6 isoforms. All the 3R Tau isoforms are expressed during foetal stage and the 4R Tau isoforms are more adult specific. In human, the 3R Tau and 4R Tau are expressed in equal proportions (1:1) (Kenneth S. Kosik *et al.*, 1989; M. Goedert and Jakes, 1990) These isoforms vary in size from 352 to 441 amino acid residues and differ from each other by the presence of either a 3R or 4R tubulin binding repeats (31 or 32 amino acid residues) in the C-terminal region of the protein, along with the absence or presence of a single (1N) 29 amino acid or double (2N) amino acid containing insert in the N-terminal region of tau protein.

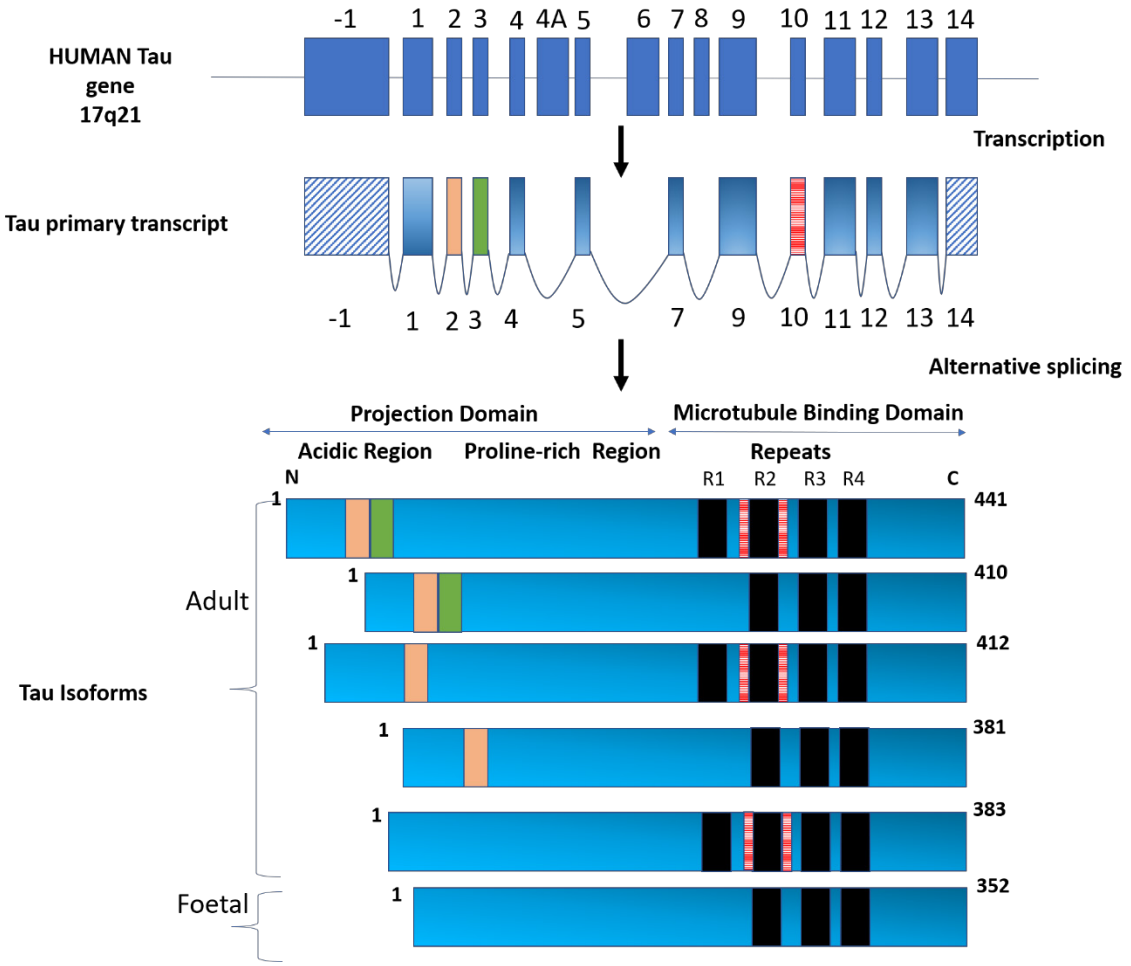

Figure 1.2: A schematic representation of the human Tau – the gene, primary transcript and the six isoforms of the protein. Adapted from Buée et al 2000.

The repetitive regions called the repeat domains (R1-R4) in the C-terminal end encoded by exon 9-12 are the binding sites for microtubules on the tau protein (Lee, Neve and Kosik, 1989). These 3R and 4R repeats are composed of highly conserved 18 amino acid residues each and are spaced from each other by 13-14 amino acid long regions. The conserved 18 amino acid region binds to microtubules with different binding affinities between 3R and 4R repeats (Butner and Kirschner, 1991). 4R tau forms bind to microtubules with a higher affinity as compared to the foetal forms (Michel Goedert and Jakes, 1990). Tau protein basic structure is divided into two large domains; the amino /N-terminal (also called the projection domain) and the carboxy/C-terminal (also called the microtubule binding domain). The projection domain can be further divided into the acidic residue or amino terminal and the proline-rich region.

Tau is a protein with a random coil and βstructure in R2 and R3 binding repeats. Tau protein is highly hydrophilic and is soluble and heat stable. An imbalance in the equimolar ratio of 3R:4R Tau isoforms is generally observed in tauopathies and this shift away from equimolar ratios favours aggregation of the protein. This disrupts its function of microtubule stability (Adams *et al.*, 2010) . *In vitro* and *in vivo* studies have indicated an excess of 3R tau can inhibit aggregation, thereby reducing tau pathology and improving cognitive deficits (Adams *et al.*, 2010; Damianich *et al.*, 2018)

1.9.3 Function of tau in the healthy brain

Tau plays a vital role in various cellular processes such as maintenance of cell morphology and intracellular trafficking. One of the roles of tau protein that has been studied extensively is its regulation in maintaining assembly and stability of microtubules (Fig 1.3) (Drubin and Kirschner, 1986).

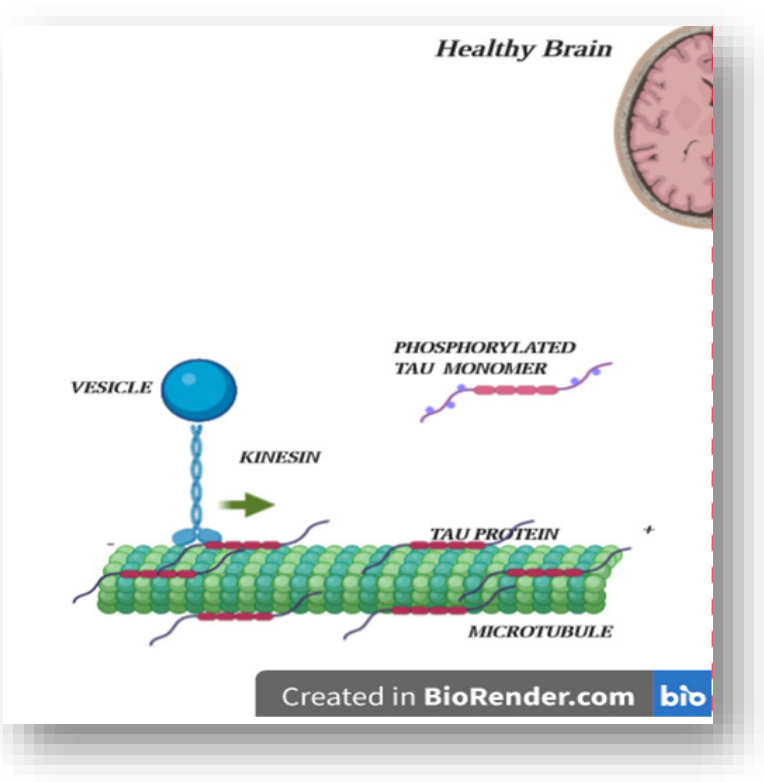

Figure 1.3: Function of tau protein under physiological conditions. The four binding domains (in red) bind to microtubules thereby stabilizing the structure. This binding is regulated by kinases and phosphatases. Phosphorylation of tau at specific sites (in purple) regulates binding of tau to microtubules thereby regulating axonal transport. Kinesins may regulate this function by inhibiting the plus-end transport along microtubules. Created with BioRender.com

Tau proteins are known to initiate tubulin polymerization and play a major role in axonal transport (Cleveland, Hwo and Kirschner, 1977; Brandt and Lee, 1993). The binding of tau to microtubules is regulated under normal physiological conditions by kinases and phosphatases. Kinases such as GSK - 3β (Wagner *et al.*, 1996) are responsible for phosphorylation of tau while phosphatases are involved in dephosphorylation. Like for the Microtubule Associated Proteins (MAPs), the extent of phosphorylation dictates the biological activity of tau. Phosphorylation of tau at multiple sites affects its binding to microtubules and axonal transport (Lindwall and Cole, 1984). It causes a conformational change in the protein structure (Hagestedt *et al.*, 1989). This conformational change leads to a decrease in the binding affinity of the protein towards microtubules (Biernat *et al.*, 1993) thereby promoting the unstable dynamic state (Drechsel *et al.*, 1992; Trinczek *et al.*, 1995) This promotes disassembly of microtubules (Lindwall and Cole, 1984). Tau in its dephosphorylated state supresses the microtubule dynamic instability state by reducing the rate and extent of shortening of tubule formation (Panda *et al.*, 1995). Site-specific phosphorylation of tau is the key to regulating the dynamic instability state of microtubules. For instance, phosphorylation at the site Serine-262 on the repeat domain disables tau to bind to microtubules completely (Drewes *et al.*, 1995) whereas phosphorylation at sites within the proline rich region only decreases the ability to induce nucleation (Brandt *et al.*, 1994). However, inhibition of tau using anti-tau antibodies does not have an effect on axon extension (Tint *et al.*, 1998). This effect is confirmed in tau knock-out mice, which showed no abnormalities, including with axonal elongation (Harada *et al.*, 1994). However, a compensatory mechanism may play an important role involving MAP associated proteins like Map1A (Harada *et al.*, 1994) and Map1B (DiTella *et al.*, 1996). These results show that tau may not be an essential element for axonal growth and development.

Each of the isoforms perform a particular physiological role as they are expressed at different stages during development of the human brain. This shows that tau may have different roles depending on the presence or absence of sequences encoded by exons 2, 3 and 10. For instance, 0N3R is the only isoform present in the foetal human brain, while all the six isoforms are expressed in the adult human brain (K S Kosik *et al.*, 1989; Michel Goedert and Jakes, 1990) The 0N3R tau is called the foetal tau, whereas the 4R isoforms are only expressed in the adult stage (Goedert *et al.*, 1989b). The foetal to adult developmental switch corresponds to the dominant expression of 3R to 4R repeats at the C-terminal end and is conserved between different species. However, the difference in the N-terminal expression varies from species to species (Takuma, Arawaka and Mori, 2003). The ratio of 3R:4R in the adult human brain is

equimolar 1:1.This developmental switch, which essentially is the addition of the exon 10 coded region- repeat 2- R2 in the microtubule binding region is suggestive of the switch from a more plastic function of tau (3R) during neuronal development (Hanger, Anderton and Noble, 2009) to a more stabilised and equimolar (3R:4R) expression in adult human brains. At the foetal stage, tau is highly phosphorylated and there is more tubulin available for microtubule assembly and growth (Kanemaru *et al.*, 1992). As the development progresses, activation of phosphatases leads to a decrease in the phosphorylation levels (Mawal-Dewan *et al.*, 1994).

Tau isoforms may not be expressed equally in different neuron types. For example, tau variants with exon 10 may not be expressed in the granular cells of the dentate gyrus (Goedert *et al.*, 1989a). Studies have also shown that tau plays an important role in axonal outgrowth as well as in the establishment of neuronal polarity (Caceres, Kosik and S., 1990; Caceres, Potrebic and Kosik, 1991; Kempf *et al.*, 1996)

1.10 Tau in AD

Tauopathies are a class of neurodegenerative disorders caused by the deposition of misfolded-hyperphosphorylated protein tau in neurons and glia. Depending on the cause, they can be classified as primary and secondary tauopathies. Picks disease and Frontotemporal Dementia with Parkinsonism linked to chromosome 17 (FTDP-17) are categorised under primary tauopathies; where mutations in the tau gene leads to development of an autosomal dominant neurodegenerative disease. Secondary tauopathies are rather a group of heterogeneous disorders such as AD and Down syndrome wherein the tau-pathology is prevalent although the disease is driven by other factors. Despite the genetic heterogeneity causing AD, NFTs and amyloid plaques are consistently observed in AD brains. Abnormal phosphorylation of tau is consistently found in PHFs in AD brains (Grundke-Iqbal *et al.*, 1986).

1.11 Phosphorylation and Hyperphosphorylation of Tau

As stated previously, the steady state dynamics of microtubule assembly is regulated by the balance between phosphorylation by various kinases and dephosphorylation by various phosphatases which causes binding and uncoupling of tau respectively from the microtubule assembly. When this equilibrium is disturbed, tau becomes hyperphosphorylated and through loss of function leads to destabilisation of the microtubule assembly. This destabilisation and the eventual death of neurons is thought to be the characteristic phenotype in AD. Hyperphosphorylation is known to uncouple tau from the microtubule, thereby inhibiting assembly and microtubule organisation affecting vesicle trafficking (Alonso *et al.*, 1994, 1997)

This causes a conformational change and misfolding in the protein which makes it prone to aggregation. Abnormally phosphorylated monomers aggregate to form dimers, trimers and larger aggregates called oligomers leading to the formation of PHFs. This eventually aggregates to form the larger insoluble species – the NFTs in the neurons of affected individuals (Fig 1.4). Elevated levels of tau and displacement leads to inhibition of kinesin mediated transport of vesicles, mitochondria and endoplasmic reticulum thereby leading to cell death (Mandelkow *et al.*, 2011).

Studies have shown an increase in the number of kinases associated with AD, including glycogen synthase kinase (GSK3β), cyclin-dependent protein kinase (Cdk5), Calcium-Calmodulin-dependent protein kinase II (CaMK2), phospho70S6 (p70S6) kinase, mitogen activated protein kinase (MAPK), c-JunN terminal kinase (JNK) and p38 kinase.

These are all protein-Serine-Threonine Kinases. GSK3, a kinase that is involved in a number of pathways including the Wnt and insulin signalling pathways, and is an enzyme that is constitutively active, unlike other kinases. In 1992, studies found that GSK3 could phosphorylate tau at multiple sites and is a key component in AD-related abnormal hyperphosphorylation (Hanger *et al.*, 1992; Mandelkow *et al.*, 1992) In 1993, an isoform of GSK3- GSK3β, was reported to be a tau protein kinase 1 which provides multiple epitopes of PHFs (Ishiguro *et al.*, 1993). GSK3 was one of the kinases that was shown to be upregulated while testing the effect of Aβ peptides on tau phosphorylation. This was proven when Lithium, a known GSK3 inhibitor, was used to prevent Aβ-induced neurodegeneration(G. Alvarez *et al.*, 1999). Thus the sudden increase in the interest of GSK3 as a therapeutic target began (Eldar-Finkelman and Martinez, 2011). Unfortunately, since GSK3 is a very important kinase which is involved in multiple cell regulating functions, its inhibition lead to other unwanted adverse effects in control animals (Hu *et al.*, 2009).

It is found there is at least a 3-4 fold increase in phosphorylation of tau in brains of AD patients compared to healthy aged-matched individuals (Kopke *et al.*, 1993). Hyperphosphorylation of tau makes its turnover slower than normal tau (Poppek *et al.*, 2006), as it also makes it resistant to proteolysis by proteases (Wang *et al.*, 1995). The lower rate of clearance could be a possible explanation for higher levels of tau in the AD brain (Khatoon, Grundke-Iqbal and Iqbal, 1992). Another possible reason for some of the increased levels of tau in AD brains would be the activation of the ribosomal S6 protein kinase, p70 S6 kinase, which is a key regulator of the

cell-cycle progression, cell size and cell survival. Activation of p70 S6 kinase increases the cells translational capacity thereby possibly increasing total tau levels (An *et al.*, 2003).

Cdk5, a unique member of the cyclin-dependent kinase family, is another kinase involved in AD-associated tau phosphorylation (Ishiguro *et al.*, 1992; Baumann *et al.*, 1993) It is primarily involved in neuronal development (Tsai *et al.*, 1993; Ino *et al.*, 1994), migration (Chae *et al.*, 1997; Gilmore *et al.*, 1998) outgrowth and differentiation (Nikolic *et al.*, 1996) and synaptic function (Matsubara *et al.*, 1996). Cdk5, a monomeric enzyme, requires binding to regulatory factors for activation. Two such activators identified are p35 (L. H. Tsai *et al.*, 1994) and p39 (Humbert, Dhavan and Tsai, 2000). Neurons, when exposed to a neurotoxic insult, cause calpain-mediated p35 cleavage thereby generating a fragment-p25 (Kusakawa *et al.*, 2000; Lee *et al.*, 2000) In AD, increased levels of p25 is observed in the human brain (Patrick *et al.*, 1999). P25 is more stable and thus keeps Cdk5 constitutively active. P25/Cdk5 complex hyper phosphorylates tau and its accumulation is involved in cytoskeletal disruption and eventual degeneration of neurons (Ahlijanian *et al.*, 2000). A study wherein adverse effects of Aβ-induced neuronal toxicity was prevented by inhibition of Cdk5 activity in rat hippocampal cells confirms the role of Cdk5 activation in AD related pathogenesis (A. Alvarez *et al.*, 1999).

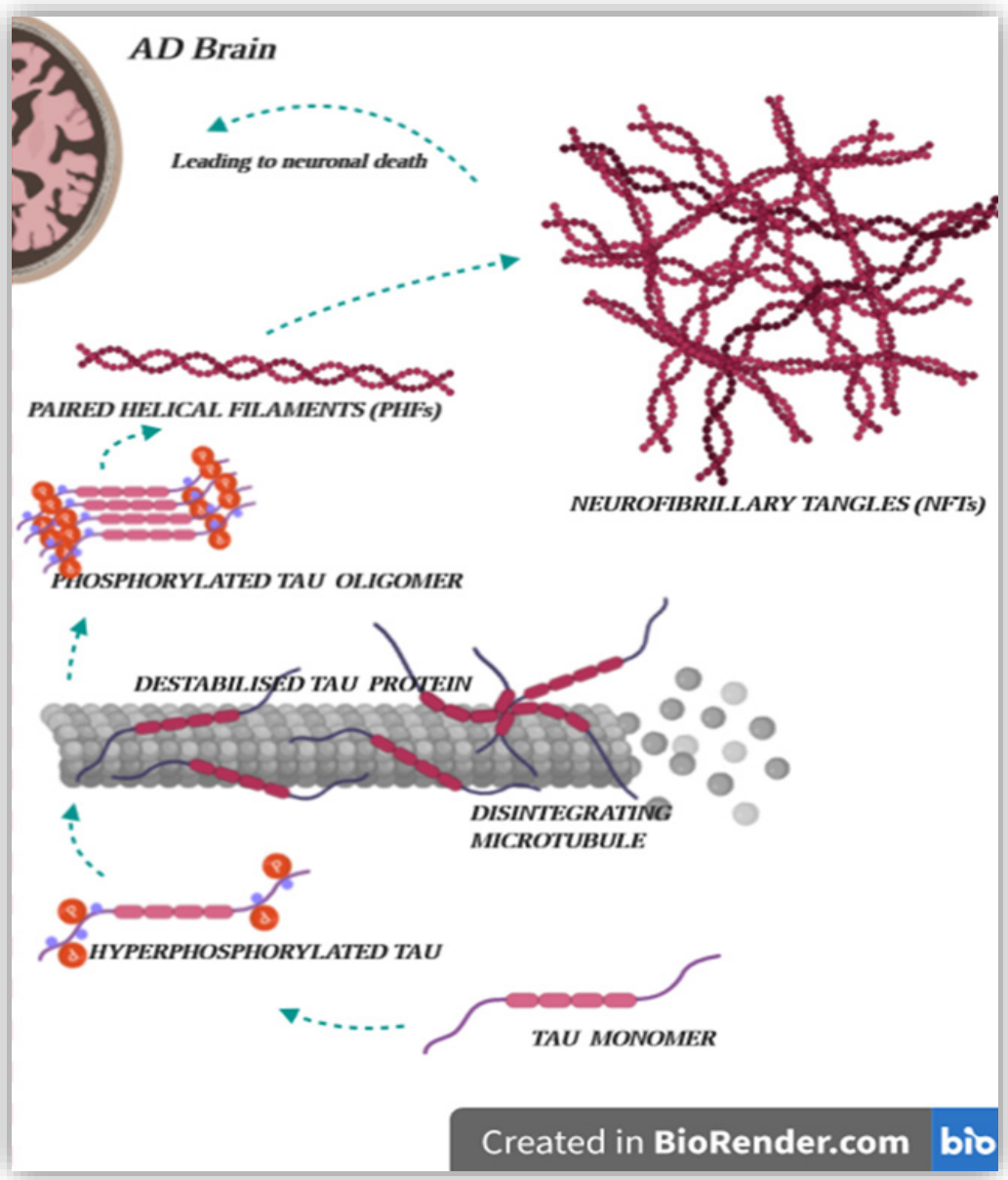

Figure 1.4: A schematic representation of formation of Neurofibrillary tangles in AD. Tau is hypothesised to cause neurodegeneration by becoming hyperphosphorylated which reduces its function of binding to microtubules thereby destabilising them. Abnormally phosphorylated tau misfolds to form aggregate prone dimers, trimers and larger species called oligomers which in turn accumulates to form larger species like PHFs and NFTs. Axonal transport is disrupted leading to impaired synaptic functions and eventually death of the neuron. Created with BioRender.com

Hyperphosphorylation of tau is not just a result of decreased phosphatase activity but also a combinatorial effect of increased activity of not only ERK1/2 but also p70 S6 kinase (Pei *et al.*, 2003). Downregulation of phosphatases such as protein phosphatases PP1, PP2A and PP2B have also been associated with AD. Decreased levels of PP1 and PP2A along with an increase in the levels of PP2A inhibitors are seen in AD (Tanimukai, Grundke-Iqbal and Iqbal, 2005).

To conclude, there are a number of kinases and phosphatases directly implicated in abnormal phosphorylation of tau, thereby contributing to pathogenesis of the disease. There is enough evidence to support the link between AD-associated hyperphosphorylation of tau and the overall effect created by an imbalance due to decreased phosphatase activity and increased kinase activity seen in various studies (Stoothoff and Johnson, 2005).

1.12 Tau and Abeta in AD

For a long time, senile plaques and NFTs were considered the primary cause of AD. However, studies have now shown that soluble forms of Aβ and tau independently are more damaging to the health of neurons rather than plaques and tangles (Haass and Selkoe, 2007). The amyloid hypothesis was the predominating theory for decades which stated changes in Aβ initiate a cascade of pathological events, including hyperphosphorylation of tau thereby leading to formation of NFTs in AD (Hardy and Higgins, 1992) (Hyman, 2011). Although Aβ peptides have been primarily found in senile plaques, there is increasing evidence showing that the unstable Aβ oligomers, rather than Aβ fibrils, are more neurotoxic (Sengupta, Nilson and Kayed, 2016). Aβ oligomers lead to disrupted functioning of ion channels by elevating abnormal levels of extracellular glutamate levels and subsequent NMDAR (N-methyl-D-aspartic acid receptor) mediated excitotoxity. Aβ oligomers also disrupt intracellular calcium homeostasis, mitochondrial dysfunction, and causes oxidative damage by generation of reactive oxygen species (ROS), thereby leading to neuronal apoptosis and synaptic loss (Benilova and De Strooper, 2013). Given that over the years all clinical trials targeting Aβ have failed, the focus of the underlying cause shifted from Aβ to tau. In recent years, there have been an increasing number of studies showing that the origin and spread of tau (rather than Aβ) correlates better with Braak and Braak stages and the progress of the symptoms of the disease over time. It has been hypothesized that abnormal/misfolded tau starts to accumulate in small number of cells and then propagates from region to region in an ordered fashion to indicate prion like manner of spread across specific regions of the brain as the disease progresses over time. Studies have shown in both cultured cells and mice models that abnormal tau converts normal protein to the seed competent type (Clavaguera *et al.*, 2009), (Frost, Jacks and Diamond, 2009), (Hasegawa, 2016) (Nonaka *et al.*, 2010), (Lasagna-Reeves *et al.*, 2012), (Goedert and Spillantini, 2017). This has led to the speculation that different conformers of tau exist, and they contribute differentially to the different pathologies seen across tauopathies (Kaufman *et al.*, 2016). However, the exact mechanism of tau propagation is not yet clear. Studies have shown that a reduction in endogenous tau levels protects against cognitive deficits

seen in AD model (Leroy *et al.*, 2012) (Roberson *et al.*, 2007). However, studies have also reported negative effects of reducing endogenous tau levels especially with cognitive and motor functions as age progresses (Lei *et al.*, 2014). Hence, targeting tau for treatment options would require not just a deep knowledge about the physiological roles of tau and its isoforms but also of its absence, especially its consequence in development and ageing. Pathological Aβ and tau cause neuroinflammation marked by gliosis, proliferation and activation of microglia, another hallmark seen in AD, while glial cells, through a feedback mechanism, regulate Aβ and tau pathology. Oligomeric Aβ can stimulate microglial proliferation and activation (Jin and Yamashita, 2016) which could possibly be the reason for dispersal of tau seeds through the neural networks in the brain. TREM2 is a receptor abundantly expressed in microglia and has been identified as a risk factor of AD. Although there are quite a few studies showing the influence of Aβ on tau and vice versa, unfortunately we do not yet have a clear understanding of the mechanism underlying the pathology.

1.13 Current AD Models

In order to understand, study and recapitulate the pathological conditions and progression of AD, several different *in vitro* and *in vivo* models have been generated. Transgenic animal models are those that have been genetically modified to either express, or inhibit expression of, a particular gene or set of genes, so that the organism acquires the ability to display the underlying pathophysiological aspects and behaviour related to a condition or disease of interest. These models mostly include rodents like mice, rats, invertebrates like Drosophila melanogaster, Caenorhabditis elegans and other vertebrates like zebrafish. Moreover, there are a variety of *in vitro* models of AD. These are either fixed brain slices from human post-mortem brains, primary cells derived from human tissue explants or cells modelled by gene modification or addition of synthetic compounds which ultimately recapitulate some aspects of the disease.

Discussed below are the key features of some of the AD models (both *in vivo* and *in vitro*), keeping in mind each of them has their own advantages and disadvantages.

1.14 In vivo models

Animal models are one of the prime research tools used for studying the underlying mechanism and finding new treatments for AD. These are genetically engineered to replace the animal form of a specific gene of interest with the human form so that they serve as a better platform to study the human nature of the disease. Although the majority of AD cases are sporadic, most of the models used to study the underlying mechanism of AD are based on FAD mutations. For decades, we have studied the various aspects of AD using FAD models, unfortunately the underlying cause of SAD is still unclear. However, despite differences in their aetiologies and mean age of onset, both SAD and FAD have common pathophysiology and clinical features. Studies have shown no difference in the pattern of distribution of various features, including neuritic plaques and NFTs, ratio of neuronal loss to plaques and NFTs, MRI or PET scans (Duara *et al.*, 1993; Lippa *et al.*, 1996) Application of these models provides great insight into the underlying mechanisms and pathology of the disease. However, they fail to completely recapitulate every aspect of the disease. An ideal AD model would be a system that recapitulates the human form of the disease and develops the entire spectra of clinical and pathological changes, including amyloid plaques, neurofibrillary tangles, synaptic dysfunction, gliosis, axon degeneration, neuron death, cognitive failure and behavioural deficits.

For the past decades, mouse models for FAD were established with a single or multiple APP FAD or PSEN FAD mutations. However, the majority of AD cases are sporadic (with no established SAD mutations) whereas FAD accounts for only a minority of AD cases. Except for the age of onset, there seems to be a similarity in the neuropathological and clinical features of the disease. Hence, most of the models developed are either targeting specific mutation of interest or downstream events that are similar in both cases.

1.14.1 Transgenic mouse models

The mouse models overexpressing the human APP (hAPP) gene are the most commonly used transgenic mouse model for studying AD. These mice develop amyloid pathology, cognitive deficits, and synaptotoxicity but fail to exhibit neuronal loss-(Hall and Roberson, 2012a). There are a number of hAPP transgenic mouse lines depending on the mutations they express. PDAPP is an example of a transgenic line which carries a mutation on the γ-secretase cleavage site (V717F). This was one of the earliest transgenic AD models developed which showed age-dependent extracellular amyloid beta deposition, neuritic plaques, dystrophic neuropathy, gliosis and synaptic dysfunction (Games *et al.*, 1995). Tg2576 is a model developed by Karen

Hsiao which overexpresses hAPP (isoform 695) with the Swedish mutation K670N/M671L. It is a double mutation where two amino acids lysine (K) and methionine (M) are substituted with arginine (N) and leucine (L) (Mullan *et al.*, 1992). Similar to the PDAPP this model also shows age-dependent accumulation of Aβ, plaque formation, memory and behavioural deficits with a rise in ratio of Aβ(1-42) over Aβ(1-40) (Hsiao *et al.*, 1996; Westerman *et al.*, 2002) The APP23 transgenic mouse line is another model used to study AD. It uses the long isoform 751 amino acid form of APP and has a 7-fold overexpression of APP. These mouse lines are widely used to study inflammation in AD.

Studies have shown an increase in Aβ42 species with no change in the Aβ40 species in both PSEN1 and PSEN2 FAD mutant transgenic mouse models, thereby increasing the Aβ42/ Aβ40 ratio as seen in the disease (Duff *et al.*, 1996; Citron *et al.*, 1997; Wen *et al.*, 2004) This effect is seen with the mutant PSENs and not with overexpression of wild type (Duff *et al.*, 1996). However, unlike mutant APP transgenic mice, studies on PSEN transgenic mice showed a lack of plaque pathology in the brain. One of the possible reasons would be the decrease in the ability to aggregate due to difference in sequence of Aβ between the species (Dyrks *et al.*, 1993). In order to accentuate the formation of plaque pathology, some studies have also explored the effects of expressing multiple PSEN1- FAD mutations. In cases where PSEN1-FAD mutations are overexpressed or APP-FAD mutant mice are crossbred with PSEN1-FAD mutant or PSEN1 knock in mice, there is an increase in the Aβ42/ Aβ40 ratio along with plaque deposition seen much earlier than individual APP-FAD mutant or PSEN1-FAD mutant mice or chimeric APP mutant PSEN1 wild type mice (Borchelt *et al.*, 1997; Citron *et al.*, 1997; Holcomb *et al.*, 1998; Lamb *et al.*, 1999; McGowan *et al.*, 1999; Dewachter *et al.*, 2000). This indicates that the prescence of PSEN1 FAD mutation increases the generation of Aβ42 levels and accelerates the formation and deposition of plaques in APP FAD transgenic mice models. Although these manipulations show some features of the disease, cognitive impairment due to neuronal loss is rarely seen. However, a study where a PSEN1 FAD mutation was combined with multiple APP-FAD mutations, such that a 5xFAD mutant mice carrying three different APP FAD mutations and two PS1 FAD mutations has been generated (Oakley *et al.*, 2006). In this model, the Aβ42 levels in the brain reach very high levels rapidly, with intraneuronal accumulation of Aβ42 as early as 1.5months. Amyloid deposition starts as early as 2 months, these mice have memory deficits seen with a decrease in synaptic markers and loss of pyramidal neurons in the cortex. This model shows rapid formation of amyloid pathology

which demonstrates an intraneuronal Aβ42 dependent neurodegeneration, plaque formation along with memory impairment in the AD mice models.

In humans there are six isoforms of Tau, while in mice there are only three. Recently in an attempt to seek better mouse models to study the disease, a mouse model was developed by Takaomi Saido and Takashi Saito which expresses all 6 human isoforms (Saito *et al.*, 2019). Saito and Saido's group reported a new mouse model with wild-type human tau knock-in wherein the preliminary data suggested that when these mice were crossed with APP knock-in mice, hyperphosphorylation of tau with insoluble forms and subsequent neuronal death occur. This mouse model could provide a platform to study aspects of human tau especially since all the APP knock-in and models overexpressing human APP lack tau neuropathology and neurodegeneration, an important feature of AD.

Researchers have also transplanted human neurons into mouse brains that mimic some of the hallmarks of the disease. This model was generated by the joint efforts of Pierre Vanderhaeghen and Bart De Strooper (Espuny-Camacho *et al.*, 2017). They found that when compared to mouse neurons, human neurons are more sensitive to amyloid plaques. They found the Pluripotent Stem Cell-derived precursor cortical neuronal cells differentiate and integrate *in vivo* and express 3R/4R forms of Tau with abnormal phosphorylation and neurodegeneration. Despite these efforts, none of the models have been able to recapitulate Aβ-induced NFTs or neurodegeneration as seen in AD patients.

With years of research, we now know that rodent Aβ differs from human Aβ as it fails to develop fibrils, one of the critical phenomena seen in AD, thereby not completely replicating key pathophysiological aspect of the disease. However, the current research is now more inclined towards humanised models wherein a human based platform is preferred over other species. This has led to interest in making transgenic animal models with human proteins - tau and Aβ as well as use of human induced pluripotent stem cells (hiPSC) and human embryonic stem cells (hESC) for developing *in vitro* models.

1.14.2 Other in vivo models used

In addition to the transgenic animal models, which have provided an exceptional tool in understanding the underlying aspects of the disease, there are some non-transgenic "natural" wild-type animal species, which could serve as excellent models to study some aspects of the

disease and also serve as better models for drug target testing plaque -like deposits are found in dolphins (Gunn-Moore *et al.*, 2018), polar bears (Davies *et al.*, 1988), cats (Chambers *et al.*, 2015) and dogs (Wegiel, Henryk and Soltysiak, 1998) but is rarely found in mice and rats. Primates like lemurs (Bons *et al.*, 2006) and aged chimpanzees (Rosen *et al.*, 2008) are some of the best models to study AD, as these animals show age-related brain pathophysiology as seen in AD. Some, but not all, primates show AD- like-taupathy, a phenotype that is rarely seen in rodent models. However, their high cost, maintenance-especially with their longer lifespan, availability and animal ethics are some of the reasons why they are not widely used by laboratories to study AD.

1.14.2.1 Non-human primates

Non- human primates are best characterised for AD neuropathophysiology which closely mimics humans. These animals, due to their proximity to human biology including anatomy, physiology, cognitive function, sequence homology, social behavioural complexity and immunology, deliver a vast advantage in studying AD. They have a large brain size which makes it easier for imaging, cerebral spinal fluid (CSF) collection and complete sequence homology with human APP (Selkoe *et al.*, 1987; Price *et al.*, 1991) Due to their long life span a few studies have observed AD pathology in apes including chimpanzee, gorillas and orangutans. Formation of amyloid plaques as a result of Aβ accumulation is observed in aged apes. However, tau pathology is quite rare in apes. Despite the 100% and 95 % of sequence homology between human and chimpanzee or gorilla tau respectively, the ageing apes do not show typical tau associates neuronal loss or NFTs (Gearing *et al.*, 1997), but that could be attributed to the use of antibodies with higher specificity. In aged gorillas, baboons and macaques the presence of Alz-50, MC-1 and AT8 positive cells scattered along the borders of the cortex have been observed (Härtig *et al.*, 2000; Kiatipattanasakul *et al.*, 2000; Schultz *et al.*, 2000) Furthermore, the memory decline is more age-related than extensive lapse as observed in AD.

Octodon degu (O.degu), a hystricomorph belonging to the family Octodontidae, is a native to central Chille. O.degu are closely related to guinea pigs and known to naturally develop AD associated pathology as they age. Their average life span ranges around 5 to 8 years. O.degu are considered as non-engineered-sporadic AD models. They have a high sequence homology with the human Aβ. Since studies have found O.degu develop intracellular and extracellular Aβ accumulation and plaques, as well as intracellular tau accumulation, astrocytosis, synaptic

changes and memory impairment related to higher levels of oligomers, O.degu is considered a promising model to study AD (Braidy *et al.*, 2015; Deacon *et al.*, 2015) However, some studies suggest that O.degus born and bred in captivity do not necessarily develop amyloid accumulation or tangle formation as well as extensive neuronal loss and microglial activation to the extent as seen in AD (Steffen *et al.*, 2016).

In conclusion, animal models have given deep insight into the mechanism of the disease, unfortunately they have failed to translate to clinical trials. This is mainly because of the differences between animal and human nervous systems, which render them not the best candidates to study a complex ageing disease like AD. For instance, there is a difference in structure as well as protein expression profile in rodents when compared to humans. Also, the relatively short life span of animal models does not allow them to completely develop the pathophysiology of AD. These could be some of the reasons why promising AD clinical trials have repeatedly failed over the past years.

1.15 In vitro Models

In vitro disease models for AD include human fixed brain sections from AD patients, cell lines used to engineer the disease like such as neuroblastomas, pheochromocytoma cells, primary cell lines derived from rodents and, in some cases, humans. In recent times, embryonic stem cells and human induced pluripotent cells have been used to create disease models; either by taking skin cells from diseased patients or transfecting cells with genes which are associated with AD. The major genes associated with AD and which have been widely used to develop in vitro models are APP, PSEN1, PSEN2 and APOE 4, as they play a major role in mimicking the development and progression of pathogenesis in humans.

1.15.1 Brain tissue

Ex vivo fixed/frozen brain sections mounted on slides, suitable for immunohistochemistry and in situ hybridisation assays are a great tool to identify cellular location of proteins or genes in tissues. Fixed/frozen brain tissue could be used for other applications such as in situ hybridisation DNA and RNA studies. The general practise at the brain banks are to section one hemisphere while freeze the other hemisphere. Braak and braak in their study in 1991 demonstrated different staging of AD-related neuropathology over different hemispheres of the brain using brain sections typically reflecting the progress of the disease based on expansion of the lesions (Braak and Braak, 1991). A recent study used fixed brain sections from a transgenic mouse AD model with double APP mutation on the APP gene and a single PSEN 1

mutation. This study combined micro-Fourier transform infrared imaging, Raman Spectrometry and immunofluorescence to show the co-localisation of astrocytic processes with the rich lipid layer that surrounds plaques which is seen in post-mortem AD brains, thereby adding evidence correlating astrogliosis to the biochemical changes occurring around plaque formation in AD (Palombo *et al.*, 2018). Studies with brain sections have provided a strong foundation in understanding certain aspects of the disease. However, the use of brain tissue comes with its own set of limitations. For instance, all the information collected from the different studies are all stage specific (at the time of death) and thus are not progressive. It limits our understanding of the early on-biochemical changes that leads/furthers the disease progression. The quality of frozen tissue is another major challenge in using human brain tissue. Age, gender, agonal status described as abnormal or strained breathing in the final moments of death, cause of death, associated disease, post-mortem interval (usually no more than 72 hours), duration of time in the fixative and any pre-death medications all play a major role when it comes to determining the quality of tissue which could be critical for specific studies that rely on integrity of biological molecules post-mortem (Gomez-Nicola and Boche, 2015). Fresh frozen tissues are prone to degradation and therefore become tedious to work with especially for transcriptomic studies since RNA degrades faster than proteins. Furthermore, the use of human brain for research in the UK is regulated by the Human Tissue Authority (HTA) and brain banks require HTA ethical approval to use human tissue for specific projects. Since this is a strict requirement the approval and availability of human tissues for a certain project could be considered a limitation.

1.15.2 Cell Lines and primary cultures

Cell lines and primary cultures provide for a simpler and more economic means to study certain aspects of neurodegenerative diseases like AD. Primary neuronal cultures from brain explants either from humans or animal models, provide a good platform to study certain aspects of the disease, such as the effect of certain substances/ agents on the nerve cells. There are plenty of studies reported with testing effects of Aβ in various forms on primary neurons. Synthetic Aβ treated cultured hippocampal neurons from rats at embryonic stage day18 showed neurotoxic effects at higher concentrations on mature neurons and neurotrophic to undifferentiated neurons (Yankner, Duffy and Kirschner, 1990). Studies have reported use of primary neurons to study pathological changes involved in AD including inflammation, enzyme kinetics and signalling pathways. However, since these cells cannot be cultured for long term and due to the issues revolving around the availability of human brain tissue, a vast variety of studies

cannot be carried out on these cells. Hence, they are limited in vitro models for AD, and mostly used for short-term studies.

One of the most commonly used neuronal cell lines to study AD are SH-SY5Y. SH-SY5Y is a human neuroblastoma cell line derived from metastatic bone-marrow biopsy. SH-SY5Y has been used to generate a number of neurodegenerative models as it is a good model for expressing neuron specific markers with functional synaptic structures and axonal transport (Agholme L FAU - Lindstrom *et al.*, 2010). SH-SY5Y can express mature neuron specific proteins like NeuN, β III tubulin and synaptic protein Sv2, which is prerequisite for a good AD model. This cell line has been used to study the underlying mechanism of AD (Jämsä *et al.*, 2004) as well as for drug discovery studies (Yan *et al.*, 1994; Li *et al.*, 1996; El-Agnaf *et al.*, 2000). However, SH-SY5Y is a cancerous cell line and the various interactions with the oncogenes interrupts the complete recapitulation of the cellular and molecular mechanism of the disease (Yan *et al.*, 1994).

Rat hippocampal cells are another example of cells used to study AD. The advantage of using these primary cells is it provides a specific subtype of cells, in this case hippocampal cells, which are some of the primary cells affected in AD. There are 2 advantages to using rat hippocampal cells, they can be controlled; either to proliferate rapidly or differentiate into specified cell type when exposed to growth factors without further proliferation. These hippocampal cells are derived from embryonic rats and made immortal by retroviral transduction using oncogenic alleles which belong to the simian40 large tumors. These cells express markers of neurons and glia- Neurofilament protein and GFAP (glial fibrillary acid protein) respectively (Eves *et al.*, 1992). Hippocampal cells are important for learning and cognition and since these cells are affected in AD they are widely used to study pathogenesis. These are better candidates than neuroblastoma cells, lack the different and aberrant cell signalling in the cancerous cells forming malignant tumours, and lack lineage specificity. However, since they are derived from rodents they are not the best candidates since they lack receptors for human Aβ peptides (Carolindah *et al.*, 2013). For instance, a study used PC-12 cells to identify the exact secretary cleavage site $Lys^{16}Leu^{17}$ in APP. They used conditioned media from non-transfected PC-12 cultured cells which were differentiated to neuronal phenotype using a nerve growth factor (NGF) to purify secreted APP (Anderson *et al.*, 1991).

PC12 are cells derived from the rat adrenal gland with pheochromocytoma. PC12 cells are used widely to study the toxicity of Aβ oligomers in vitro (Yankner *et al.*, 1989; Yan *et al.*, 1996)

and its effect on cell physiology (Guo *et al.*, 1996). These cells are not generally used for modelling or studying the underlying mechanism of the disease but rather to study oligomer formation or aggregation of Aβ peptides in the disease (Weidemann *et al.*, 1989; Wang *et al.*, 2000).

1.15.3 Stem cells

With the discovery and advent of stem cell technology, more and more researchers have used it as a model to study various neurodegenerative diseases. Stem cells are defined as the unique population of cells that are unspecialized and able to self-renew and give rise to different specialized cell types through a process called differentiation. This can happen when specific signal cues are introduced from the microenvironment in which they reside, called the niche. Pluripotent stem cells are an inexhaustible source of undifferentiated cells with their unique regenerative ability to differentiate into any mature cell-type of the three lineages-ectoderm, endoderm and mesoderm. They are found in developing embryos, foetuses and in adult tissues including the brain. Stem cells are quite sensitive to the signals received from their niche and, depending on these cues, either self-renew or differentiate to maintain normal turnover of cells in the respective organs. However, the proliferation ability varies between different tissue systems. For instance, the blood, skin and intestinal stem population have higher rate of division as compared to the other organ systems in the body.

What makes them inexhaustible is their property to self-renew either through symmetric or asymmetric division. Both daughter cells could either maintain their stem cell identity identical to the mother cell through mitosis or stem cells can divide to give rise to differentiated progeny while simultaneously maintaining the stem cell pool in the niche (Horvitz and Herskowitz, 1992). This kind of division is called “asymmetric division”. Asymmetric division is a critical process by which cellular components are inherited unequally by the daughter cells during mitosis. When a stem cell divides asymmetrically one of the daughters -stem/progenitor cell acquires a copy identical to the mother cell, retaining the ability to self-renew and differentiate when necessary and a second daughter cell becomes more specialized/differentiated thus beginning the process of differentiation. Thus, asymmetric differentiation is critical to ensure balance between maintaining the stem/progenitor cell pool and generation of functional differentiated cell types. However, there is evidence that stem cells also divide symmetrically (Morrison and Kimble, 2006). Symmetric cell division has been shown in both vertebrates and invertebrates. Stem cells have known to divide symmetrically for self-renewal (Shahriyari and Komarova, 2013). However, the ability to divide symmetrically is retained to replenish the

stem cell pool in case of injury or disease. The fate decision to stay quiescent or enter cell cycle division either via symmetric or asymmetric division is a very critical one and is made stochastically, but in a tightly regulated fashion. Given these unique features, stem cells can serve as important research tools in studying neurodegenerative diseases.

There are different classifications of stem cells. Based on their different potency they are classified as – totipotent, pluripotent, multipotent, oligopotent or unipotent. Stem cells that have the ability to differentiate into all cell types and develop into an entire organism are defined as totipotent stem cells. The classic example of totipotent stem cells are the zygote cells, formed during the fertilization of the egg. Totipotent cells are cells that can generate extra-embryonic placental cells and the entire embryo during development (Condic, 2013). Pluripotent cells that form the embryo are essentially progenies of totipotent cells that generate cell types of all three germ layers but cannot generate the extra-embryonic cells. The most common example is the inner cell mass (ICM) of the blastula which is formed by pluripotent cells from which ESCs (Kaufman and Evans, 1981) and teratocarcinomas (Stevens, 1970) are derived . Stem cells with a limited potency to differentiate are termed multipotent stem cells. Tissue specific stem cells such as haematopoietic stem cells (HSC) (Spangrude, Heimfeld and Weissman, 1988) and mesenchymal stem cells are classic examples of multipotent stem cells. These stem cells are essentially lineage-restricted stem cells that differentiate into only a few terminally differentiated cell types. HSCs gives rise to all lineages of the blood system (Weissman, Anderson and Gage, 2001). Lastly, unipotent stem cells are cells which can only differentiate into a single cell-type while still having the ability to self-renew. For example muscle progenitor stem cells called myosatellite cells are unipotent stem cells (Muaro, 1961; Konigsberg, Lipton and Konigsberg, 1975).

Based on their source of origin, stem cells are classified as – foetal stem cells, embryonic stem cells, and tissue-specific stem cells. Human foetal stem cells are those derived from clinically aborted foetuses. Human embryonic stem cells are those derived from 5-7 days old blastocysts. Tissue-Specific stem cells, also called the somatic/ adult stem cells, are more specialized in terms of potency than ESCs. They differentiate into different types of cells in the specific tissue /organ of residence. For instance, haematopoietic stem cells are found in the bone marrow and are the blood-forming stem cells. They also give rise to platelets. Mesenchymal stem cells, also called stromal stem cells, can differentiate into osteocytes, chondrocytes and adipocytes.

1.15.3.1 Embryonic stem cells and AD

Embryonic stem cells (ESCs) are derived from the pluripotent ICM of the blastocysts (day5-7) which have the ability to differentiate into cells of the three lineages -endo,-meso and ectoderm (Evans and Kaufman, 1981; Martin, 1981) (Fig 1.5). Since their first extraction, human ESCs have shown great potential that could be used as a tool to study and treat a variety of diseases, such as Parkinson's disease, AD and Spinal cord Injury. Due to their source of origin, ESCs pose critical ethical controversies (Lo and Parham, 2009). Also, transplantation of undifferentiated ESCs form teratomas and are at greater risk of rejection for transplantation in patients (Nussbaum *et al.*, 2007). However, differentiated derivatives from ESCs are less likely to be rejected (Drukker *et al.*, 2006).

In recent years defined protocols have been established in differentiating embryonic stem cells to neurons and also glial cells (Gerrard, Rodgers and Cui, 2005; Dottori and Pera, 2008) Many researchers have exploited ESCs to study AD at the biochemical and molecular level, either by over-expression of human tau (Mertens *et al.*, 2013) and APP genes (Abe *et al.*, 2003) or over-expression of a single or multiple mutations responsible for AD (Honda *et al.*, 2016).

Efforts are also being made to compensate for neuron loss in the CNS by externally stimulating the endogenous stem cell pools or by using transplanted genetically modified stem cells into sites in the brain which can then migrate and integrate into site of damage/ loss.

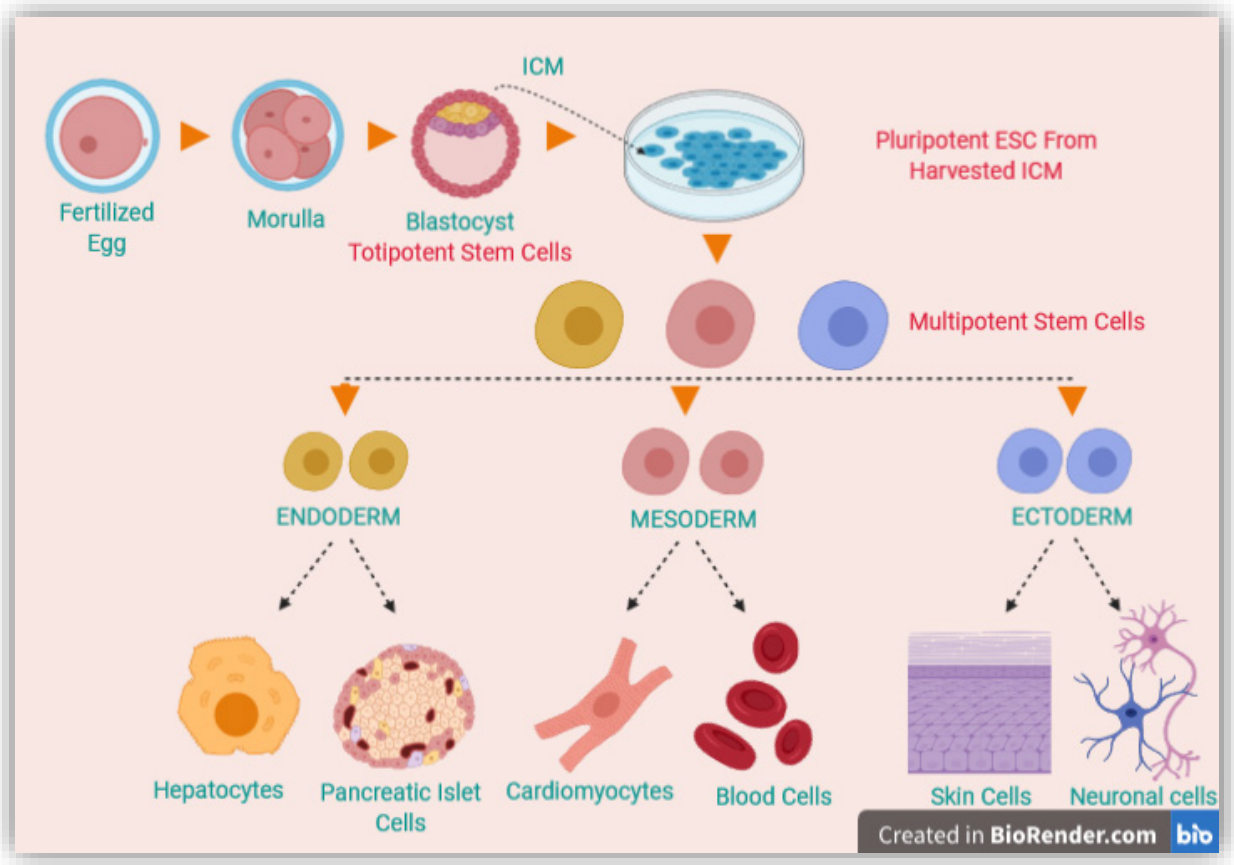

Figure 1.5: Human Embryonic stem cells from fertilization to culture and differentiation into the 3 germ lineages. Created with BioRender.com

1.15.3.2 Induced Pluripotent Stem Cells (iPSCs)

Induced Pluripotent Stem Cells, as the name suggests, are not a naturally occurring source of stem cells, but rather are induced from somatic cells to de-differentiate into pluripotent embryonic like-stem cells. The discovery of iPSCs in the year 2006 by Yamanaka and his group was an important breakthrough in the field of research. iPSC technology was the result of developing an alternate approach to generate stem cells without any ethical and clinical concerns. They have shown how cell-fate of a differentiated cell type (for e.g.: Skin cells or blood cells) can be altered merely by the exogenous expression of 4 key transcription factors – Oct3/4, Sox2, c-Myc and Klf4 (Takahashi and Yamanaka, 2006). Like ESCs, iPSCs are cells that can be differentiated into any cell type of the three germ layers under proper conditions. This research tool has particularly benefitted studies in neuroscience by supplying not just a surplus of neuronal cell subpopulations that were previously inaccessible, but also by making available disease/patient specific cells which are very valuable. A number of protocols of differentiation of ESCs to neurons and glia have been established (Fraichard *et al.*, 1995; Okabe

et al., 1996; Gottlieb and Huettner, 1999).With the advent of iPSCs these protocols were optimized and used for differentiation of iPSCs. iPSCs make a better option than neuronal cell lines or embryonic stem cells for disease modelling. Over the years iPSCs have been used to model a number of genetic diseases like Gaucher's disease (GD) type III, Duchene (DMD) and Becker muscular dystrophy (BMD), and Parkinson's disease (PD), Huntington's disease (HD), Down syndrome and Juvenile-onset type 1 diabetes mellitus (Das and Pal, 2010).

1.15.3.3 Advantages and Disadvantages of iPSCs over other Stem Cells

1.15.3.3.1 Advantages

- Developed from somatic cells like skin or blood, hence bypasses the need to destroy embryos and oocytes (Takahashi and Yamanaka, 2006).
- No immune rejection reaction when transplanted as patients own cells used to create iPSCs (Yamanaka, 2010).
- It is now possible to develop iPSCs with virus free constructs thereby rendering iPSCs usable for transplantation treatments (Okita *et al.*, 2008, 2011; Stadtfeld *et al.*, 2008; Junying *et al.*, 2009).
- It overcomes some of the limitations of the other available sources like animal models and cell-based models (Dragunow, 2008), such as long term viable cultures, high throughput assays for drug discovery.
- Regenerative medicine provides one of the best tools to study human growth and developmental stages. Comprehensive understanding of diseases right from developmental stage.
- Provides platform to find cures/cell-replacement treatments as well as better alternative to test millions of potential drug targets.
- Beneficial to neuroscience since previously unavailable and limited sources of human brain cells now can be made available on a large scale.
- iPSCs make it possible to model Sporadic forms of diseases like AD (Hossini *et al.*, 2015; Ochalek *et al.*, 2017; Lin *et al.*, 2018).

1.15.3.3.2 Disadvantages

- iPSCs differentiate into different neuronal subtypes with decreased efficiency and increased variation (Hu *et al.*, 2010).
- Lack of standardised protocols used to generate the iPSC lines.
- Epigenetic modifications used to create the cell lines may be retained by the cell even after differentiation.
- Donor to donor variations may cause phenotype variation in different cell lines.
- Difficult to age these cell lines in order to generate an AD phenotype in lab settings.

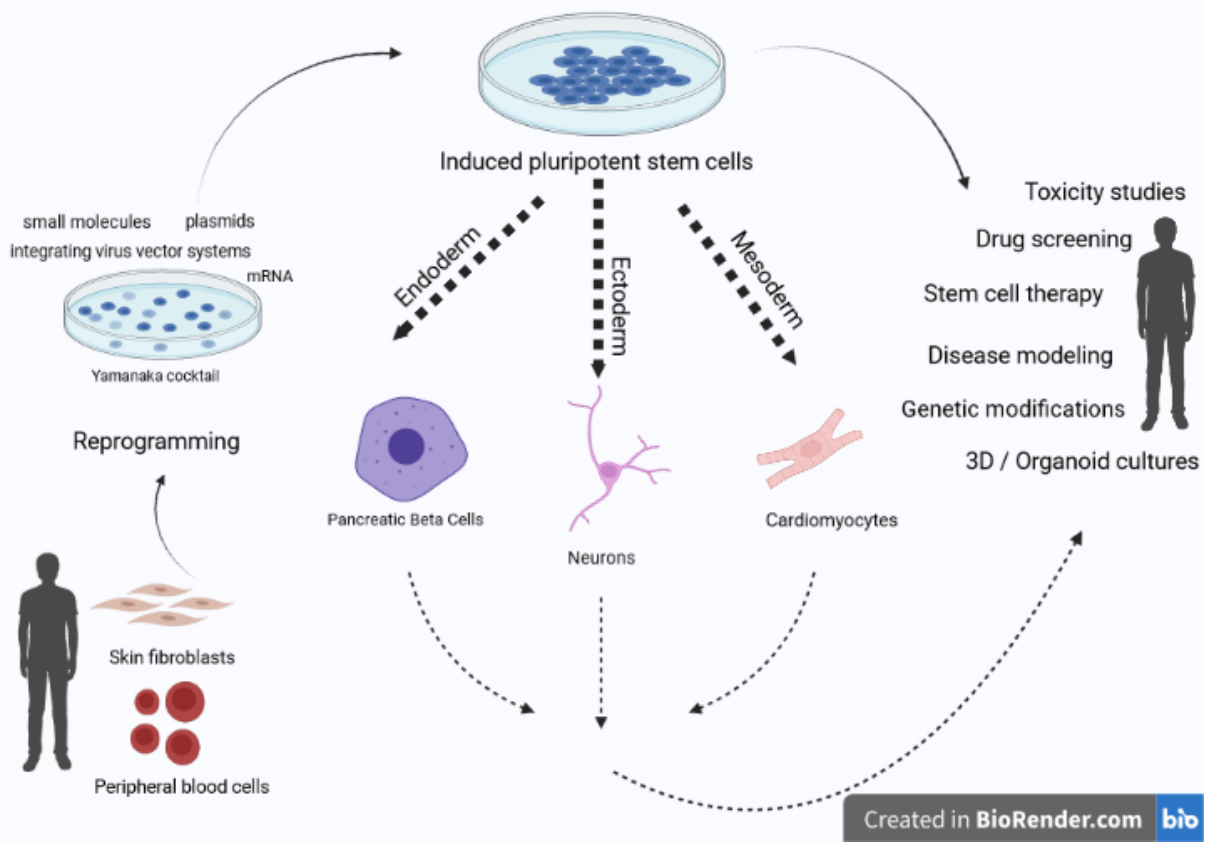

Figure 1.6 : Schematic showing generation of iPSCs and its various clinical application. Non-invasively accessible somatic cells such as blood cells and skin cells could be reprogrammed into iPSCs by the introduction of 4 transcription factors Sox2, Oct3/4, c-Myc and Klf4 using tools like viral vectors or integration free plasmids. These iPSCs with or without genetic defects could be corrected or manipulated using techniques like CRISPR, Transcription activator-like effector nucleases (TALENs) and zinc finger nucleases. These iPSC either edited or non-edited could be differentiated into different cell types belonging to the Ectoderm, Endoderm or Mesoderm. These differentiated cell types could further be used for Cell replacement therapy, modelling a disease or for high-throughput and drug discovery studies. Adapted from Diecke et al 2014. Created in BioRender.com.

1.16 Need for Human-based neurodegenerative models

Due to the inaccessibility of the human brain, most of the knowledge regarding the neurodegenerative diseases is either from post-mortem brain tissues or animal models modified to express FAD mutations. Although post-mortem analysis gives an in-depth knowledge about the pathology of the disease, unfortunately it is limited to the terminal stages of the disease. There are biochemical and molecular changes happening in the human brain at least 15-20 years before the clinical manifestation of the disease. Limited availability of resources is one of the major restrictions in modelling and drug discovery for neurodegenerative diseases. Hence animal models have been extensively used to understand the underlying mechanisms of

diseases and to screen drugs. Animal models have been able to replicate AD phenotypes but only to a certain extent. However, due to the major differences in species and especially due to the differences between the human and rodent nervous system, it is relatively impossible to create an exact replica of the disease in animals, thereby leading to conflict in observation seen across various models and failure to translate into successful clinical trials costing enormous amounts of money and efforts in the past decade. Some of the major issues identified are:

- Structural differences as well as differences in the molecular composition of the nervous system.
- Shorter life span in animals induced with human forms of the gene expression could be inadequate time for the complete development of disease phenotype seen in humans, especially in cases of age-related disease like AD. For instance, symptoms related to AD in majority of the cases occur around or after 65 years which when compared to the lifespan of rodents (around two years) seems to be insufficient time to develop some pathology.
- There are substantial differences in the expression of proteins in both systems. For instance, the adult murine brain expresses three isoforms of tau having 4R binding repeats with either no (0N), one (1N) or two (2N) N-terminal inserts whereas the human adult brain expresses all the 6 isoforms of tau (McMillan *et al.*, 2008).
- All models created either by overexpression of a mutation/gene of interest or by insertion of a combination of different mutations in order to force the disease phenotype may lead to conditions which are not pathophysiologically relevant.

These could be some of the reasons why drugs that have shown promising results on animal models have failed to rescue cognitive decline in clinical trials (Green *et al.*, 2009; Doody *et al.*, 2013, 2014; Salloway *et al.*, 2014) Most of our understanding of disease associated-inflammatory response and behavioural studies come from such animal models. Thus, it becomes crucial not just to develop relevant human based models but also to validate the findings from post-mortem brain, animal models and other *in vitro* models in human based models.

The only sources of live human tissue to study a neurodegenerative disease like AD currently are either the post-mortem brain or the surplus of brain tissue saved after a Neurosurgery

(healthy tissue sometimes gets dissected and normally then discarded while making incisions to reach a tumour or during resective surgeries to treat epilepsy). These tissues are live and can be kept in cultures only for a few days with electrophysiologically active cells. However, these cells do have some limitations depending on the delay post-mortem and collection method. The other sources of brain tissue would be the large brain banks created to supply sections or brain samples post-mortem from demented and non-demented patients. However, these cells are fixed and would provide us with information regarding only the terminal stages of the disease and little information regarding the early cellular or biochemical changes occurring during the initial stages underlying the very cause of the disease.

1.17 iPSCs for modelling AD

Different cell types can now be generated from iPSCs using defined growth factors and exposure times which help direct differentiation of neural progenitors to a specified cell fate. In order to study/model a neurodegenerative disease, defined protocols are essential to generate cell types involved in the disease. The protocol established by Shi et al in 2012 is one of the most followed protocols for cortical neural differentiation (Shi *et al.*, 2012a; Shi, Kirwan and Livesey, 2012) This protocol employs a step wise differentiation of human stem cells to progenitor cells and cortical cells induced by retinoid signalling, proceeding into cortical neurogenesis followed by terminal maturation giving synaptically functional cells. This system generates all types of projection neurons of the cortex thereby mimicking in vivo developmental stages.

Several research groups have shown differentiation of AD patient derived iPSCs to functional neurons. Most of these lines have been developed from patients with FAD mutations. For instance, in the study by Yagi et al (2011)-one of the first groups to model FAD mutations using iPSCs, iPSCs generated from fibroblasts with the PSEN1 mutation L246E and the PSEN2 mutation N141I showed increased levels of Aβ42 secreted in media with an increased ratio of Aβ42/Aβ40 compared to non-AD controls, thereby recapitulating one of the hallmarks of AD (Yagi *et al.*, 2011).

In the study by Israel et al (2012), synaptically functional neurons derived from iPSCs generated from FAD (duplicate APP gene) and sporadic patients (APOE) showed an increase in Aβ40, phospho-Tau (Thr231) and αGSK3β compared to neurons derived from individuals without AD. β–secretase and γ-secretase reduced Aβ secretions of all cell types including

control lines. β–secretase reduced levels of αGSK3β and p-tau/total tau in SAD and APP lines. However, γ-secretase had no effect on levels of αGSK3β and p-tau/total tau levels across cell lines (Israel *et al.*, 2012)

In the study by Muratore et al (2014), iPSCs were generated from fibroblasts from a father and daughter pair with the London FAD APP V717I mutation. Even though the mutation lies near the γ-secretase cleavage site, an increase in the cleavage activity of β–secretase was seen, eventually leading to an increase in levels of Aβ42 and Aβ38 over the differentiation period, along with an increase in the Aβ42/Aβ40 ratio. There was an increase in the levels of tau as early as 26 days with an increase of phospho- Tau in 100 days of culture (Muratore *et al.*, 2014).

The studies described above show that over the years of research it has been possible to not just generate mature and functional neurons from patient-derived iPSCs but also to generate cells which address not all but some key aspects of the disease phenotype. These protocols could be further explored and modified for 3D cultures for improving differentiation, maturation and function of neurons so that they provide a more physiological microenvironment for the development of the disease phenotype.

1.18 3D Cultures

3D cultures could be described as culture of cells, within pre-defined three-dimensional supporting matrices or scaffolds to create a system which mimics the tissue or organ specific microenvironment. 3D cultures are a more accurate way of representing cells in their natural microenvironment. In recent years, research on 3D cultures has received more impetus. Research is being carried out to develop 3D cultures for a more physiological microenvironment to better facilitate growth and differentiation as well as pathology development in human cells. This could largely bring down the use of animal cells for culture assays. However, this technique has a long way to go in terms of defining the conditions and characteristics for specific cell types depending on its intended application.

1.19 2D vs 3D

1.19.1 Limitations of 2D cultures

A traditional 2D culture system involves the plating of cells directly onto rigid (artificial) substrate generally made of glass or plastic which may or may not be coated with solutions that mimic one or a few components of the extracellular matrix (ECM), either for better adhesion,

proliferation or differentiation. Studies have shown that cells are sensitive to their physical environment and which influence morphology, phenotype and adhesion depending on the substrate stiffness *in vitro* (Dityatev and Schachner, 2003; Gerardo *et al.*, 2019). This mirrors what is seen *in vivo*. For instance, the brain is a much softer tissue than the bone and thus engineering culture systems for osteoblasts require a much stiffer and rigid culture substrate than that required by neural stem cells. There are many studies that show neural stem cells proliferate and differentiate better in softer 3D cultures conditions compared to the much stiffer 2D culture conditions (Chowdhury *et al.*, 2010; Marchini, Favoino and Gelain, 2020) Adult stem cells reside in unique niches that with different cues from the microenvironment influence cells towards proliferation or differentiation. The optimal stiffness for proliferation is around 3.5kPa and for differentiation to neurons is <1 kPa (Leipzig and Shoichet, 2009). This shows NSCs differentiate better on softer matrices. One of the reasons why *in vitro* culture models fail to faithfully recapitulate the diseased phenotype could be that cells do not completely mature in 2D cultures. The previously detailed iPSC studies were all 2D based cultures which showed functional and mature neurons and an increase in Aβ pathology which is considered as an early change in AD but failed to show any late-stage effects like plaques and tangles in the cultures. This could be due to the absence of a 3D microenvironment in the appropriate matrix which alters the dynamic process occurring *in vivo*. 2D cultures allow cells to interact mostly in just two dimensions which is not an accurate representation of how cells behave during development, interaction, homeostasis or injury. One of the major drawbacks of 2D cultures in modelling neurodegenerative disease like AD is its lack of three-dimensional cellular compartmentalisation. This is required for allowing the accumulation and deposition of pathogenic protein conformers for the development of plaques and tangles which are typical disease phenotypes. The possibility of pathogenic protein build up is lost in 2D as it is cleared away with regular media changes to maintain cells *in vitro*.

1.19.2 Advantages of 3D cultures

The relation between a stem cell and its niche plays an important role in specification of cell fate (Rompolas, Mesa and Greco, 2013). Unlike 2D cultures, cells are surrounded by other cells in 3D, thereby providing better spatial organisation and increasing surface area for cells to grow, migrate, and extend neurites thereby increasing the chances of cell-cell interactions and formation of strong cellular networks. Matrices made of physiologically relevant material, in this case laminin, hyaluronic acid and collagen which are encapsulated into hydrogels not just provide relatively closer stiffness but also provide binding motifs which makes intricate

networks with cell-cell and cell-ECM interactions in such 3D structures. For instance, Matrigel provides a brain -like ECM which is rich in a variety of proteins such as laminin, entactin, collagen and heparin sulphate proteoglycans. Scaffolds/matrices could be customized as per the research requirement. There is evidence that 3D cultures mimic the *in vivo* microenvironment and accelerate neuronal differentiation and synapse formation (Ortinau *et al.*, 2010; Liedmann, Rolfs and Frech, 2012; Cheng *et al.*, 2013) Differentiation in 3D aids the maturation of cells and increases the expression of mature neuronal markers as opposed to 2D cultures (Choi *et al.*, 2014a). A 3D culture system allows for deposition of these proteins in the surrounding matrix even with regular media changes.

1.19.3 Limitations of 3D cultures

Some of the major drawbacks of using 3D cultures to study neuronal systems are the lack of blood brain barrier, the lack of flow and interaction of both blood and cerebrospinal fluid and the total absence of the immune system. Spheroids are relatively larger cultures and affect the diffusion of nutrients and oxygen leading to hypoxic and necrotic centres. However, some of the disadvantages of 3D cultures outweigh that of 2D and 3D cultures are an unprecedented choice to use as a tool to model neurodegenerative diseases like AD. Microfluidics systems are being developed to compensate for the lack of continuous supply of nutrients and removal of waste. However, the lack of a blood brain barrier may slow down the translation of high throughput drug studies to clinical outcomes. 3D cultures are not particularly easy to work with as compared to their 2D counterpart when it comes to cell access for electrophysiological studies. Although it may depend on the research question being asked and the type of disease being modelled, 3D cultures have a long way to go in terms of having a better understanding of the interaction of cells with ECM and other components in their niche and developing standardised protocols for iPSC reprogramming and differentiation for different cell types.

1.20 AD-3D Culture models

In recent years different research groups have tried to develop *in vitro* 3D models for differentiating neurons. Here I include some such studies with a focus on AD. For instance, in the Zhang et al (2014) study, the 3D neural culture system was coupled with mechanotransduction to improve culture models of AD. They have created this model by differentiating human iPSC derived Neural-epithelial cells from healthy individuals in self-assembling peptide hydrogels called RADA-16. Healthy cells were used to standardize the model so that in the future AD specific iPSCs could be used. The 3D cultures showed elevated

levels of phospho-PAK (P-21-activated kinase) and cytoskeletal proteins such as Debrin and lower levels of Cofilin compared to 2D iPSCs, which are characteristic in late-stage AD brains. On exposure to Aβ oligomers there was a redistribution of phospho-PAK from nuclear and cytosolic locations to submembraneous regions, which resembles an AD brain. Delocalization of debrin was also seen on exposure to Aβ oligomers (Zhang *et al.*, 2014).

Choi et al in 2014, established a 3D culture system where human neural precursor cells (ReN cells) were transfected with mutant APP -K670N/M17L, with V717I or APP-V717I with PSEN1 △E9. The immortalised cell lines producing a high amount of pathogenic Aβ were differentiated in Matrigel to form a 3D culture system. A thick 3D culture system was used for biochemical analysis and thin 3D culture system was used for immunofluorescence Although not a physiologically relevant model on account of overexpression, the 3D culture system has shown evidence for the first time of extracellular deposition of Aβ. This has never been shown in 2D cultures possibly because of the dispersion of Aβ into culture media preventing any accumulation. The cultures showed Aβ expression 1000-fold higher than physiological levels and 17-fold increase in Aβ40 and Aβ42 levels in APP/PSEN1 cultures with a 5-fold increase in Aβ42/40 ratio in PSEN1 cells. At the RNA level the authors showed by PCR equal ratios of 3R:4R in their control cells, equivalent to adult physiological ratios. However, this ratio or the presence of 4R tau at the protein level has not been shown. There was a significant increase in the Phospho-tau AT8 and PHF1 levels in the FAD cells. Cultures showed the presence of aggregated tau in the somatodendritic compartment and showed the presence of sarkosyl-insoluble filamentous structures. β-secretase and γ-secretase inhibitors have shown a decrease in both Aβ deposition and tauopathy; these findings were validated against 2D cultures and confirmed that these were attributed to the 3D culture method (Choi *et al.*, 2014a).

In 2016 Raja et al (2016) created a human brain organoid system from iPSCs derived from AD patients with FAD mutations and healthy controls (Kadoshima *et al.*, 2013). Two cell lines with a duplication in the APP gene, one with PSEN 1 mutation M146I and one with PSEN 1 mutation A264E along with two healthy control lines were used. The neurons in the organoids mature at 60days *in vitro* and form denser MAP2 structures at day 90 *in vitro* The 3D brain organoids with FAD mutations have shown pathological changes including Aβ aggregation and tau hyperphosphorylation. The model showed a progressive increase in number and size of Aβ aggregates at days 60 and 90 post plating. They also showed increased tau phosphorylation in FAD lines compared to control at Ser394 or Thr181 residues at 90 days,

but no difference was seen at 60 days post plating, unlike Aβ which showed more aggregates compared to controls at both 60- and 90-days post plating.

Due to the lack of oxygen and nutrient penetration in deeper layers, the underlying cells show necrosis which stain positive for secondary antibodies alone. Thus, the analysis was restricted to the superficial 250μm of tissues. The 3D brain organoids showed a decrease in the accumulation of disease associated phenotype with beta and gamma secretase inhibitors treatment (Raja *et al.*, 2016).

In 2016, Lee et al created a 3D neuro-spheroid model utilizing iPSCs derived from the blood of five advanced sporadic AD patients. This study is the first to generate a sporadic AD 3D model. However, no control lines or FAD lines were included in the study. The cultures showed expression of both neurons and astrocytes, however the exact time around which the cells start showing the mature phenotype is unclear The 3D floating spheroid cultures showed increase in amyloidogenesis and were treated with BACE1/ γ-secretase inhibitor Compound E. Interestingly, 2D cultures showed greater reduction in Aβ40 and Aβ42 as compared to 3D cultures with one of the four cell lines showing no significant difference with the treatments. Proteomic analysis showed that there was reduced levels of APP in the 4 lines and could be the reason why the inhibitors showed less efficacy in the one AD line with no significant decrease in the Aβ levels (Lee *et al.*, 2016).

Although there are very few studies based on sAD patient derived iPSC 3D models, they are able to recapitulate certain key events of the neurodegenerative disease pathology. This provides evidence that this approach gives an added advantage over 2D culture models. These studies provide promising results towards the goal to develop a potential tool for human based *in vitro* disease models that could possibly give more in-depth knowledge into the mechanism of disease development and also provide human specific platforms for targeted drug discoveries which have failed over the past decades in clinical trials.

Thus, there is enough evidence to show that the 3D cultures can truly be a more practical and beneficial approach than 2D cultures especially in modelling a neurodegenerative, age-related pathology like AD.

The overarching aim of this study is to develop a physiologically relevant human 3D neural culture system to generate a heterogenous population of complex neural structures mimicking the cortex tissue with mature and functional neurons. This critical and reliable system would recapitulate physiological events in the brain and be held as a gold standard not just to

investigate but also possibly be a reliable platform for drug testing for neurodegenerative diseases like AD. In order to develop this clinically relevant model, iPSC-derived from patients with three PSEN1 mutations will be compared against age-matched controls. iPSCs technology is an unparalleled method to develop relevant phenotypes without the need to overexpress mutations or force AD-phenotype by combining expression of different FAD mutations which is not physiological. The autosomal dominant FAD-PSEN1 mutations are the most commonly occurring and most commonly studied FAD mutations. Thus, the findings from the 3D cultures could be validated with existing information. In this study, a novel differentiation protocol using a combination of specific growth factors has been developed and optimized to generate a complex heterogenous population of mature neurons including excitatory and inhibitory neurons along with glial cells to encourage the differentiation and function of these neurons *in vitro.* 3D culture rather than spheroid or organoid method of culture was chosen. This was to obtain a controlled and directed differentiation system rather than a system which generates random-unspecified neural regions with necrotic centres. Also, 3D cultures have more uniform sizes. By combining two cutting edge techniques- the iPSC technology and -the 3D culture system to develop a directed differentiation technique, this study aims to analyse some early and late-stage biochemical aspects of the age-related neurodegenerative pathology AD.

1.21 Research Hypotheses

We hypothesize that a human 3D iPSC culture model will recapitulate the *in vivo* phenotype, neuronal maturation and neuronal network formation with synapse formation and presence of both excitatory and inhibitory neurons *in vitro*.

We hypothesize that the mature neurons will express the adult 4R tau isoform along with MAP2 and B3 tubulin and either VGLUT1 (glutamatergic neurons) or GAD65/67 (GABAergic neurons).

We also hypothesize that AD pathological characteristics like presence of Aβ oligomers and pathological Tau will be recapitulated in iPSC-derived 3D cultures from AD patients with PSEN1 mutations as compared to age-matched healthy individuals.

1.22 Research Aims and Objectives

To test the above research hypotheses, we will aim:

Aim 1: Optimization and reproducibility of the previously established human 3D culture model.

Objective A: To optimize the differentiation protocol of iPSC-derived human neural model: human foetal Neural Stem Cells (hfNSCs) previously established in the lab will be differentiated *in vitro* in 2D using different concentrations of Retinoic Acid (RA) to determine the best concentration that:

-generates cells with healthy morphology and highest cell survival over a period of 8 weeks *in vitro*

-generates optimal levels of mature neurons expressing MAP2 over a period of 8 weeks *in vitro*

-generates cultures with fewest Nestin positive neural progenitor/stem cells over a period of 8 weeks *in vitro*

-generates a healthy proportion of astrocytes expressing GFAP- 8 weeks post differentiation *in vitro*.

Objective B: To standardize each assay used to characterize the 3D cultures as well as to assess the reproducibility of the differentiation protocol - Neural Precursor cells (NPCs) derived from three iPSCs lines of AD patients with PSEN1 mutations L286V, A246E and M146L and from two iPSC of healthy individuals will be used.

Conventional 2D protocols will be adapted to the 3D cultures to make them efficient for quantification analysis. An array of markers will be used with the following techniques -

-Immunofluorescence - MAP2, Nestin, GFAP, B3-Tubulin, Synapsin 1, VGLUT 1, GAD65/67.

-Western Blotting assays - detection of total tau and its isomers.

-In order to determine the reproducibility of the differentiation protocol

- the standardised techniques such as Immunofluorescence and Western Blotting (following results from above aims) will be simultaneously used.

-The presence of specific tau isoforms will be analysed to indicate the stage of neuronal development.

- the expression of PHF1 in the cultures will be analysed to detect pathological changes is 3D cultures.

Aim 2: To compare the 3D culture with the traditional 2D culture to determine the most efficient neural differentiation method.

In order to validate the neural differentiation efficiency of the 3D cultures and compare with the 2D cultures: NPCs -derived from three iPSCs of AD patients with PSEN1 mutations L286V, A246E and M146L and from two iPSC of healthy individuals, differentiated in 3D cultures will be compared to the same cell lines in 2D cultures keeping constant the culture conditions for a period of 6 weeks post differentiation.

-To analyse neuronal differentiation over time: Quantification of different markers expressed in 3D cultures at week 0, -6 and -12 post differentiation *in vitro*- MAP2, Nestin, GFAP, B3-Tubulin

-To compare 2D with 3D cultures- Characterisation and quantification of the different cell phenotypes will be done using an array of markers namely

- Immunofluorescence - MAP2, Nestin, GFAP, B3-Tubulin - week 0, week 6

-Western Blotting assay- total Tau.

Aim 3: To analyse changes in the disease associated protein tau implicated in AD pathogenesis in the human 3D culture model.

To analyse the early-stage pathogenesis of AD in the 3D cultures: NPCs derived from three iPSCs of AD patients with PSEN1 mutations L286V, A246E and M146L and from two healthy individuals, differentiated in 3D cultures, will be investigated at different time points for:

- difference in the expression of total tau AD vs control cell lines at early time points
- difference in aggregation of tau in AD vs control cell lines at early time points
- difference in expression of 3R Tau isoform in AD vs control cell lines
- difference in expression of 4R Tau isoform in AD vs control cell lines
- difference in phosphorylated tau in AD vs control cell lines

Chapter 2 – Human Neural 3D culture - Optimization and Validation of 3D Culture method

2.1 Introduction

Alzheimer's disease is an age-related neurological disease with a very complex pathology which is still not fully understood and unfortunately has no cure. The only treatments available are symptomatic. This complex nature of the disease along with the lack of relevant models to study the complexity of the disease has impacted the development of effective treatments. Furthermore, the lack of relevant models does not just affect the treatments for terminal patients but also forces the scientific community to rely heavily on *in vitro* and *in vivo* models which fail to recapitulate faithfully the pathology of the disease leading to abundant misleading information which only distances us further from our ultimate goal. There is an evident need for a reliable and reproducible *in vitro* human model to study the pathology of diseases like AD. The field of stem cells and developmental biology has come a long way in the 14 years after the invention of iPSC. This development in stem cell technology along with the advent of 3D cultures together gives hope to a promising human based *in vitro* model in the future which will help bridge the gap between the known and the unknown. There are many challenges that need to be addressed to reach this goal. Hence, it is important to critically assess all aspects while developing such an *in vitro* model.

To study a neurodegenerative disease like AD, cortical neurons are the most relevant subtype to use. There are various studies using the dual smad inhibition method to differentiate pluripotent stem cells whether ESCs or iPSCs into cortical cell types. The primary aim of these differentiation protocols is to direct differentiation into all three of the cortical stem and progenitor cells – 1. neuroepithelial ventricular zone cells being the primary stem progenitor population of the cerebral cortex, 2. Basal progenitor cells and 3. Outer radial glial cells (oRG) found *in vivo* and without which there is incomplete replication of corticogenesis *in vitro* (Chambers *et al.*, 2009; Shi *et al.*, 2012b). To reproduce the microenvironment and the signalling cues *in vitro* the differentiation protocols closely follow the *in vivo* neuronal development. Patterning of the neural induced stem cells with morphogens and small molecules influence the differentiation into specific-neuron subtypes. These differentiation protocols aim at generating functional synaptic networks of cortical cell types *in vitro.* Such electrophysiologically active neurons are considered mature neurons. A summary of such

growth factors and neurotrophic factors used by various studies in their differentiation protocol to generate specific subtypes *in vitro* is described in figure 2.1. For the differentiation of iPSC derived NSCs in this project we used the following growth factors:

Retinoic Acid

Retinoic Acid (RA) is a vitamin A (Retinol) metabolite. It is a morphogen that plays an important role in cell growth, differentiation and organogenesis (Chambon, 1996). It plays a vital role in the patterning of the neural plate and neural tube in early embryos as well as axon regeneration in adults (Maden, 2007). In early embryos a concentration gradient dependent patterning/specification of cell fate is observed. A higher concentration of RA is found in the hindbrain and spinal cord as the concentration decreases towards the anterior region. This is an increasing pattern in the anterior–posterior axis in the neural plate in a developing embryo. Similarly, RA plays a vital role in the dorso-ventral axis of neural tube. It works in harmony with sonic hedgehog (SHH), fibroblast growth factor (FGF) and bone morphogenetic protein (BMP) to determine the fates of sensory, inter neurons and motor neurons (Dhara and Stice, 2008).

Cell types	Protocols	Results	References
Astrocytes	cAMP (1 μM)	S100ß+ (6 weeks), GFAP+ (12 weeks)	[22]
	BDNF & GDNF (20 ng/ml)	GFAP+ (19% at 8 weeks)	[104]
	CNTF, FBS (10%)		[110]
	BDNF & NT3 (20 ng/ml)	GFAP+	[102]
	BDNF (10 ng/ml), SHH (200 ng/ml), GDNF (10 ng/ml), IGF (10 ng/ml), CNTF (10 ng/ml), FBS (1%), FGF1/2 (50 ng/ml)	GLT1+ GLAST+	[111]
	CNTF (5 ng/ml), BMP2 (10 ng/ml), heregulin (10 ng/ml)	~70% GFAP+ (5 weeks)	[112]
Oligodendrocytes	T3, PDGF-AA, IGF1, NT3	O4+ (16 weeks)	[22]
	BDNF& GDNF (20 ng/ml)	OLIG2+ , CNPase+, NogoA+ , BMP+ (42%) and myelinating-like processes (8 weeks)	[104]
	PDGF-AA (5 ng/ml), IGF-1 (5 ng/ml), NT3 (5 ng/ml), BDNF (10 ng/ml)	20–40% CD140a+, 5–10% O4+ (21 weeks)	[113]
	all-trans RA (100 nM) followed by SHH agonist SAG (1 μM)	44–70% O4+ (11 weeks)	[114]

Cell types	Protocols	Results	References
Neurons	Retinoic acid(100 nM), SHH (100 ng/ml), cAMP, (1 μM) cultured on laminin substrate	TUJ1+, HOXC8+ (6 weeks)	[22]
	BDNF & GDNF (20 ng/ml)	TUJ1+, VGlut+, SYN+ (8 weeks)	[104]
	Growth factor removal, immunopanning using NCAM.	MAP2+ (90%), Voltage gated Na+ & K+ currents and TTX sensitivity (8 weeks)	[115]
	FGF8, PMA and AA on matrigel, followed by BDNF, GDNF & TGF-ß3 (10 ng/ml), AA (200 μM), & cAMP (500 μM).	TUJ1+, evoked APs & TTX sensitivity (4 weeks)	[92]
	FBS (10%) on a gelatin substrate	TUJ1+, SYN+ (2 weeks)	[91]
Cortical neurons	Growth factor removal on laminin substrate	MAP2+, PSD95+. SYN+, VGlut1+, Tbr1+, Ctip2+ Evoked APs	[12]
	BDNF & GDNF (10 ng/ml) on laminin substrate	MAP2+, SYN+, Tbr1+, Brn2+, Ctip2+ (4 weeks)	[110]
	BDNF & NT3 (20 ng/ml)	NeuN+, MAP2+	[102]

Figure 2.1: Cell type-specific methods for differentiation of human iPSC-derived NPCs (Siney et al., 2018)

Sonic Hedgehog

SHH is implicated in embryonic development. It plays a vital role in cell growth, cell specialization, and morphogenesis / body pattern formation. SHH is essential factor that influences the forebrain development. SHH is also implicated in the formation of right and left hemispheres of the brain. It also plays a major role in the development of eyes. SHH plays a minimal role in maintenance of stem cell pluripotency and proliferation of stem cells (Wu *et al.*, 2010). but plays an important role in differentiation of human embryonic stem cells towards the neuroectoderm lineage. With RA dependent differentiation SHH is highly activated. Also exogenous administration of the protein leads to increase in expression of the Neuroectoderm markers Nestin, Sox1, MAP2, MSI1 and MSX1 (Wu *et al.*, 2010).

Brain-derived Neurotrophic Growth Factor

Brain-derived Neurotrophic Growth Factor (BDNF) is a member of the Neurotrophins superfamily (Leibrock *et al.*, 1989). BDNF is implicated in the survival and differentiation of certain neuronal subpopulations both in central and peripheral nervous system (Minichiello *et al.*, 1999). Neural crest cells, placode derived sensory neurons, dopaminergic neurons in substantia nigra, basal forebrain cholinergic neurons, hippocampal neurons, cerebellar granule cells and retinal ganglion cells are some of the neural cells sensitive to BDNF (Korsching, 1993). A recent study has shown the implication of BDNF in therapeutic intervention of AD. Overexpression of BDNF shows neuroprotective effects in vitro against β amyloid induced toxicity in NSCs. BDNF-NSCs-derived neurons engrafted animal models showed cognitive recovery (Wu *et al.*, 2016). A similar study showed implication of BDNF in the recovery of motor function form Huntington's disease by combining cell replacement and BDNF administration as a therapeutic approach for Huntington's disease (Wu *et al.*, 2016).

Glial cell line derived neurotrophic factor

Glial cell line derived neurotrophic factor (GDNF) as the name suggests is a neurotrophic factor. It belongs to the tumour growth-factor beta (TGFβ) superfamily. It is well known for its potent neuroprotective effects against several neuronal insults. It was found to be 75 times more potent than the other neurotrophins for promoting survival of rat motor neurons in culture (Henderson *et al.*, 1994). It acts as a trophic factor to promote survival of dying neurons in the peripheral nervous system. In vivo GDNF rescues apoptosis and prevents death of facial motor neurons from axotomy due to deprivation of target- derived survival factors (Henderson *et al.*, 1994). GDNF was shown to promote survival and the differentiation to dopaminergic neurons

both *in vivo* and *in vitro* (Lin *et al.*, 1993; Granholm *et al.*, 2000). It also seems to promote recovery of degenerating neurons from harmful toxins (Aoi *et al.*, 2000). GDNF pre-treatment has also shown to enhance survival of grafted neural stem cells in a Parkinson's disease rat model post transplantation (Wang *et al.*, 2011).

Cyclic Adenosine Monophosphate

Cyclic Adenosine Monophosphate (cAMP), was the first ever second messenger to be discovered by Earl Wilbur Sutherland Jr. and colleagues in 1957 (Sutherland and Rall, 1958). cAMP is a second messenger to G-protein coupled receptors. Second messengers are small intracellular signalling molecules that convert extracellular signals (first messengers) received on cell surface receptors to a cascade of intracellular signalling events mediated by second messengers to trigger physiological cellular functions like proliferation, differentiation, migration, survival or apoptosis. cAMP plays a vital role in cell differentiation and proliferation and depending on cell types seems to have opposite effect (Schmitt and Stork, 2002). cAMP promotes neuronal functions like synaptic plasticity and memory formation (Inda *et al.*, 2017). The downstream activation of cAMP responsive element binding protein (CREB) is a key step in neuronal differentiation (Stachowiak *et al.*, 2003). cAMP induces neuronal phenotypes in PC-12 (Ginty, Bonni and Greenberg, 1994) and neuroblastoma cells (Beyer and Karolczak, 2000). On the other-hand inhibition of cAMP leads to inhibition of neurite growth (Beyer and Karolczak, 2000; White *et al.*, 2000)

Insulin-like growth factor 1

Insulin-like growth factor 1 (IGF 1) originally was called somatomedin C. It is a peptide hormone which is a major regulator of pre- and postnatal growth. It is involved in proliferation and function of nearly every cell, tissue and organ in the body. IGF 1 is mainly synthesized in the liver but is also seen locally in many tissues. It is a major regulator of differentiation of NSCs to neurons (Brooker *et al.*, 2000). During Central Nervous System development and adult neurogenesis, signalling through the IGF 1 receptor (IGF 1-IR) regulates proliferation and survival of neural progenitors as well as differentiation and maturation of neurons (Beck *et al.*, 1995; Cheng *et al.*, 2001; Russo *et al.*, 2005; Fernandez and Torres-Alemán, 2012; O'Kusky and Ye, 2012) It also imparts neuroprotection through two pathways – the mitogen-activated protein kinase (MAPK) pathway and phosphatidylinositol 3-kinase/Akt pathway (Zaka *et al.*, 2005; Otaegi *et al.*, 2006; Hodge, D'Ercole and O'Kusky, 2007; Alagappan *et al.*, 2014). IGF 1 is also known to promote differentiation and maturation of neural progenitors to

oligodendrocytes which produces myelin (Carson *et al.*, 1993; Ye, Carson and D'Ercole, 1995; Hsieh *et al.*, 2004). Moreover, IGF 1 stimulates proliferation and differentiation of astrocytes under both physiological conditions and injury (Ye, Carson and D'Ercole, 1995; Cao *et al.*, 2003; Ye *et al.*, 2004)

These growth factors were used with the intention of differentiating the specified hfNSCs into a heterogenous population of cortical neural culture consisting largely of mature cortical neurons expressing MAP2 and the 4R Tau isoform with subtypes such as excitatory neurons (glutamatergic) and inhibitory (GABAergic) neurons, approximately 20% of astrocytes and oligodendrocytes (to a lesser extent). The factors were also used for maintenance of neural long term cultures, improving the survival and accelerating neuronal maturation *in vitro.* Thus, this protocol of differentiation was used to recapitulate relevant neural cell types to model neurodegenerative disease like AD *in vitro.*

Disclaimer: The formulation of the differentiation protocol was a project undertaken by Dr. Elodie Siney under Dr. Sandrine Willaime-Morawek and Dr. Amrit Mudher, prior to my PhD project. The main aim of her project was to develop an in vitro protocol to differentiate iPSC derived human neural stem cells into mature neurons and astrocytes. Since formulating a protocol on iPSC derived cells would have been rather expensive, human fetal derived neural stem cells (derived from aborted foetuses collected from the Princes Ann Hospital and established by Dr. Elodie herself) were used several times to develop the protocol. Once the results were satisfactory it was used on a patient derived iPSC neural precursor cell line -HAD2 (L286V) from Axol Biosciences. Some of the aims of my project were -to optimize the differentiation protocol to ensure the conversion of almost all neural precursor cells to mature neurons and astrocytes in culture as well as to validate the preliminary results from this pilot project to assess if the results were replicable on other cell lines,- to standardize each marker for the different techniques used for the characterisation such as Western Blotting and Immunofluorescence of the 3D cultures so as to be able to use the culture for quantification analysis. Lastly once the 3D model was standardised and validated, to analyse any early changes in AD-associated pathological changes seen in these cultures.

2.2 Aims

The major aim of this chapter can be broadly classified into:

Aim 1: Optimization and reproducibility of the previously established human 3D culture model.

Objective A: To optimize the differentiation protocol of iPSC-derived human neural model: human foetal Neural Stem Cells (hfNSCs) previously established in the lab will be differentiated *in vitro* in 2D using different concentrations of Retinoic Acid (RA) to determine the best concentration that:

-generates cells with healthy morphology and highest cell survival at 8 weeks *in vitro*

-generates optimal levels of mature neurons expressing MAP2 over a period of 8 weeks *in vitro*

-generates cultures with fewest Nestin positive neural progenitor/stem cells over a period of 8 weeks *in vitro*

-generates a healthy proportion of astrocytes expressing GFAP- 8 weeks post differentiation *in vitro*.

Objective B: To standardize each assay used to characterize the 3D cultures as well as to assess the reproducibility of the differentiation protocol - Neural Precursor cells (NPCs) derived from three iPSCs lines of AD patients with PSEN1 mutations L286V, A246E and M146L and from two iPSC of healthy individuals will be used. Conventional 2D protocols will be adapted to the 3D cultures to make them efficient for quantification analysis. An array of markers will be used with the following techniques -

-Immunofluorescence - MAP2, Nestin, GFAP, B3-Tubulin, Synapsin 1, VGLUT 1, GAD65/67.

-Western Blotting assays - detection of total tau and its isomers.

-In order to determine the reproducibility of the differentiation protocol

- the standardised techniques such as Western Blotting and Immunofluorescence staining (following results from above aims) will be simultaneously used.
-The presence of specific tau isoforms will be analysed to indicate the stage of neuronal development.
- the expression of PHF1 in the cultures will be analysed to detect pathological changes is 3D cultures.

Note: In order to explain the detailed methods and techniques used in these experiments: the two different objectives of this chapter, the method, results and discussion sections will be presented separately.

2.3 Part A – Optimization of the differentiation protocol

To test the functionality of the cells, electrophysiology was performed by Dr. Mariana Vargas-Caballero on 3D cultures – hAD2 -12 weeks post differentiation previously prepared by Dr. Elodie Siney in 2015. There is evidence of some action potentials in these cultures at 12 weeks. However, this was not seen consistently in all our cultures (data not shown). Although, the cultures showed features of maturing neural cultures as expected, one of the main concerns was the expression of high levels of $Nestin^{+}$ cells at 12 weeks post differentiation This is an indication that some of the cells in the 3D cultures were still in an undifferentiated state. This finding corresponded to the low signals of action potentials seen during electrophysiology. Hence it was highly important that the differentiation and maturation protocol was optimized before it was validated across the expensive iPSC cell lines. In this section of the chapter, by increasing the RA concentration (from the previously used 0.1µM) we expected to see not just an increase in the number of differentiated neurons but also an increase in the number of astrocytes and a corresponding decrease in the number of $Nestin^{+}$ cells at the end of 8 weeks *in vitro*. To achieve this quickly and efficiently while using least possible cells and expensive resources, hfNSCs previously established in the lab (more details in methods section) will be used to differentiate *in vitro* using 2D cultures. This would allow to answer the question using more experimental parameters and timepoints for optimal outcome.

2.3.1 Methods

2.3.1.1 Cell Culture

Human foetal neural stem cells (hfNSCs) lines previously derived from aborted foetuses by Dr. Elodie Siney were used for optimization of the neuronal differentiation protocol. The neural tissue was provided by the Royal South Hants Hospital in accordance with Southampton and West Hampshire local research ethics committee (REC296/00). For optimization of neuronal differentiation protocol, 2D culture was thought to be a fast, cost-effective and efficient method. For plating cells in 2D, cells were seeded on Matrigel coated coverslips in a 24well plate dish. Based on previous experiments, four different concentrations of RA - 0.1µM, 0.5µM, 1µM and 2µM were used in order to determine which concentration efficiently differentiates most of the neural stem cells resulting in the adequate proportion of mature neurons and astrocytes in vitro. Three different vials were used a few weeks apart for the cultures. Each vial was used to set-up n=1 for the experiment.

2.3.1.1.1 Thawing and expansion of hfNSCs

Vials of hfNSCs were extracted from liquid nitrogen and quickly transferred to a water bath (37°C). Once the cells were defrosted (about 90%) they were rapidly transferred into prewarmed Axol Neural Maintenance Media (ANM media) (Table 2.1) and collected in a 15ml falcon tube. Cells were centrifuged at 200g for 5 minutes. The supernatant was slowly discarded, and cells were transferred to fresh pre-warmed ANM media and plated in in a T25 flask (for each vial). Cells were placed in the incubator with 5% CO2 at 37°C. ANM media was supplemented with EGF (PeproTech, UK.) and FGF (PeproTech, UK.) for optimal stem cell proliferation. ANM media was partially changed every second day. Once the cells were adequately confluent (70-80% confluent), they were passaged.

Axol Neural Maintenance Media	
Components	**Final Concentration**
Axol Neural Basal Media (ax0013b)	1x
Axol Supplement (ax0031a)	1.5% (v/v)
EGF (PeproTech, AF-100-15)	100µg/ul
FGF (PeproTech,100-18B)	50µg/ul
Heparin (Sigma Aldrich, H3149-10KU)	10µg/ul
Antibiotic-Antimycotic solution (Sigma Aldrich, A6964-100x)	1x

Table 2.1: List of components used in Axol Neural Maintenance Media and their respective concentrations.

2.3.1.1.2 Routine passaging

For plating cells, media from the flasks was discarded. Cells were washed with 1xPBS without Ca-Mg (Gibco, UK.) and detached using prewarmed- 3ml of Accutase (Sigma Aldrich, UK.) for 5 minutes in the incubator (5% CO2 at 37°C). Detached cells were then diluted in 15ml of ANM media without the factors and collected in a 15ml falcon tube. Cells were centrifuged at 200g for 5 minutes. The supernatant was discarded, and the pellet was gently resuspended in 1ml of fresh prewarmed ANM media. Cells were quantified using trypan blue exclusion cell count method. For counting live cells, trypan blue (Sigma Aldrich, UK.) was used to manually count cells in a haemocytometer. All viable cells present within each of the 4 (wbc) outer chambers were manually counted. 10µl of cell suspension was mixed with 10µl of trypan blue and 10µl of this was placed in the Neubauer chamber. The viable cell count was calculated using the following equation: Viable cells per ml = Average cell count x 2 (dilution factor) x

10^4 (volume of chamber). The cells were suspended in appropriate amount of respective medium, depending on the cell concentration needed for the particular experiment.

2.3.1.1.3 Seeding for the experiment in 2D cultures

Matrigel -Growth Factor Reduced (Corning 354230) was gradually thawed overnight at 4°C to avoid jellification. Autoclaved and pre-sterilised coverslips were used for coating with Matrigel 24 hours prior to plating cells in 24 well plate and placed in the incubator (5% CO2 at 37°C For plating this experiment in 2D (ref section 2.3.1.1.2), 6000 cells were seeded evenly in 100µl of media per well over the Matrigel coated coverslips in the 24 well plate and placed in the incubator for 2 hours. Once the cells have settled for 2 hours, another 100µl of media is added gently over each well. 24 hours after incubation, respective cells are induced with four different concentrations of RA (Sigma Aldrich R2625) except the control group.

2.3.1.1.4 Differentiation of hfNSCs

Four days post RA treatment cells (except the control group) were supplemented with Axol Neural Induction Media (ANI media) supplemented with Sonic Hedge Hog (SHH, PeproTech,100-45) at 100ng/ml concentration along with the respective concentration of RA - 0.1µM, 0.5µM, 1µM and 2µM (Table 2.2).

Axol Neural Induction Media	
Components	**Final Concentration**
Axol Neural Basal Media (ax0013b)	1x
Axol Supplement, (ax0031a)	1.5% v/v
Retinoic Acid (Sigma Aldrich, R2625)	0.1µM, 0.5µM, 1µM or 2µM
Sonic Hedge Hog (PeproTech,100-45)	100ng/ml
Antibiotic-Antimycotic solution (Sigma Aldrich, A6964-100x)	1x

Table 2.2: List of components used in Axol Neural Induction Media and their respective concentrations.

14 days after induction, treated cells were maintained in ANI media, cells were supplemented with a cocktail of growth factors 0.01mg/ml Brain Derived Neurotrophic Factor (BDNF, PeproTech, 450-02), 0.01mg/ml Glial cell line Derived Neurotrophic factor (GDNF, PeproTech, 450-10), 1mg/ml cyclic Adenosine Monophosphate (cAMP, Sigma Aldrich, A9501), 0.01mg/ml Insulin-like Growth Factor (IGF-1, PeproTech, 100-11B.) (Table 2.3) to promote neural cell differentiation for the next 8 weeks *in vitro*. Partial media was changed every day.

Axol Neural Differentiation Media	
Components	**Concentration**
Axol Neural Basal Media(ax0013b))	1x
Axol Supplement (ax0031a)	1.5% v/v
BDNF (PeproTech, 450-02)	0.01mg/ml
GDNF (PeproTech, 450-10)	0.01 mg/ml
Camp (Sigma Aldrich, A9501	1mg/ml
IGF-1 (PeproTech, 100-11B.)	0.01mg/ml
Antibiotic-Antimycotic solution (Sigma Aldrich, A6964-100x),	1x

Table 2.3: List of components used in Axol Neural Differentiation Media and their respective concentrations.

2.3.1.2 Immunofluorescence assay

In order to determine the proportion of mature and immature neurons/ undifferentiated cells, cells were co-stained for MAP2 and Nestin. In order to determine the proportion of astrocytes in culture cells were stained with GFAP co-stained with Nestin. For the two different stainings separate lab-standardised protocols were used. Although the overall method for the staining is the same, different buffers were used for the two protocols. The details of the different buffers used namely - permeabilization buffer, blocking buffer and the wash buffers have been explained in tables 2.4 and 2.5 for MAP2- Nestin and GFAP-Nestin respectively.

For staining the 2D culture-coverslips were rinsed with 1 x PBS (Merk, UK.) to remove any media and fixed in 4% PFA (Faculty of Medicine, SGH) for 15 minutes at room temperature, followed by three rinses in 1 x PBS and stored at 4°C in PBS until used for staining. The coverslips were permeabilized using PBST for 20 minutes. Blocking was done using PBST with 10% donkey serum (Sigma Aldrich, UK.) for an hour followed by incubation with primary antibodies made in blocking buffer (Table 2.6) overnight at 4°C. Further, these coverslips were washed with PBST three times for 5 minutes each. The coverslips were then incubated with fluorescently labelled secondary antibodies (Fig 2.6) in blocking buffer for 2 hours at 37°C followed by three washes with PBST for 5 minutes each and counterstaining with DAPI (Sigma Aldrich, UK.) at a concentration of 2 µg/mL in permeabilization buffer for 15 minutes. Final

washes (3x) with PBST for 5 minutes each was given before sealing with anti-fade agent Mowiol (Biomedical Imaging Unit, SGH) to prevent quenching of fluorescence.

Although, the cultures were set up a few weeks apart from each other, immunofluorescence staining for all coverslips for each stain was performed at the same time.

BUFFERS	COMPOSITION
Permeabilization Buffer (PBST)	PBS with 0.2 % Triton-X100 (Sigma Aldrich, UK.)
Blocking Buffer	PBST with 10% donkey serum (Sigma Aldrich, UK.)
Wash Buffer	PBST
Primary Antibody Solution	MAP2 (1:200) and Nestin (1:200) diluted in Blocking Buffer
Secondary Antibody Solution	488-antiRabbit (1:200) and 568-anti Mouse (1:200) dissolved in Blocking Buffer
DAPI	2 µg/ml in (1: 500) dilution in PBST

Table 2.4: List of buffers used for staining with MAP2 and Nestin

BUFFERS	COMPOSITION
Permeabilization Buffer (PBST)	PBS with 1% Triton-X100 (Sigma Aldrich, UK.)
Blocking Buffer	PBST with 10% donkey serum (Sigma Aldrich, UK.)
Wash Buffer	PBST
Primary Antibody Solution	GFAP (1:200) and Nestin (1:200) diluted in Blocking Buffer
Secondary Antibody Solution	488-anti Rabbit and 568-anti Mouse (1:200) antibody diluted in Blocking Buffer
DAPI	2 µg/ml in (1: 500) dilution in PBST

Table 2.5: List of buffers used for staining with GFAP-Nestin

	Antibody	Species raised in	Catalogue number	Company	Dilution
Primary Antibodies	Nestin	Mouse	MAB5326	Millipore	1:200
	MAP2	Rabbit	4542	Cell Signalling	1:200
	GFAP	Rabbit	ZO334	Dako Cytomation	1:200
Secondary Antibodies	488 Alexa Fluor	Donkey	A21206	Invitrogen	1:200
	568 Alexa Fluor	Donkey	A11057	Invitrogen	1:200

Table 2.6: List and details of antibodies for used for immunofluorescence

2.3.1.2.1 Confocal Imaging

Images were taken using Confocal Laser Scanning Microscope TCS SPS8. DAPI was excited with 405nm solid state laser, AF488 was excited with 488 line of argon laser and AF568 was excited with 561nm solid state laser. Sequential imaging of DAPI and AF568 followed by AF488 was performed to avoid spectral bleed-through of DAPI into AF488 channel. A negative control (secondary only) slide was always used for each set of stains, thereby setting a threshold for autofluorescence and non- specific binding. Confocal settings for imaging – gain, offset, pinhole and laser intensity remained constant across a particular wavelength for same experiment for comparison. Leica Application Suite X (Las X Industries, Inc) was used to process the confocal images.

For these experiments, images were taken at 20x magnification. Three different coverslips were used per condition for each time point for statistical analysis. Five different areas per coverslip were analysed. A negative control (secondary only) slide was always used for each set of stains. Confocal settings for imaging remained constant across a particular stain for comparison and quantification. Leica Application Suite X (Las X Industries, Inc) was used to process the confocal images.

2.3.1.2.2 Statistical analysis

All positive cells were manually counted using ImageJ software (NIH). All values are presented as the mean ± standard error of the mean. To compare differences between the groups, statistical analysis was performed using GraphPad Prism ver. 8 (GraphPad software, Inc). Graphs for plots were also generated using GraphPad Prism software Graphs for plots were also generated using GraphPad Prism software. A non-parametric Kruskal Wallis test with Dunn's correction was used for statistical analysis on all data sets.

2.3.2 Results

2.3.2.1 Cell culture

During the expansion phase the cells had a fibroblast like morphology with large flat elongated cells with processes extending outwards from the cell body, as seen in figure 2.2.A. These cells had a slow to moderate division rate with a passage required within a week of plating. Cells at passage 3 were used for the experiments.

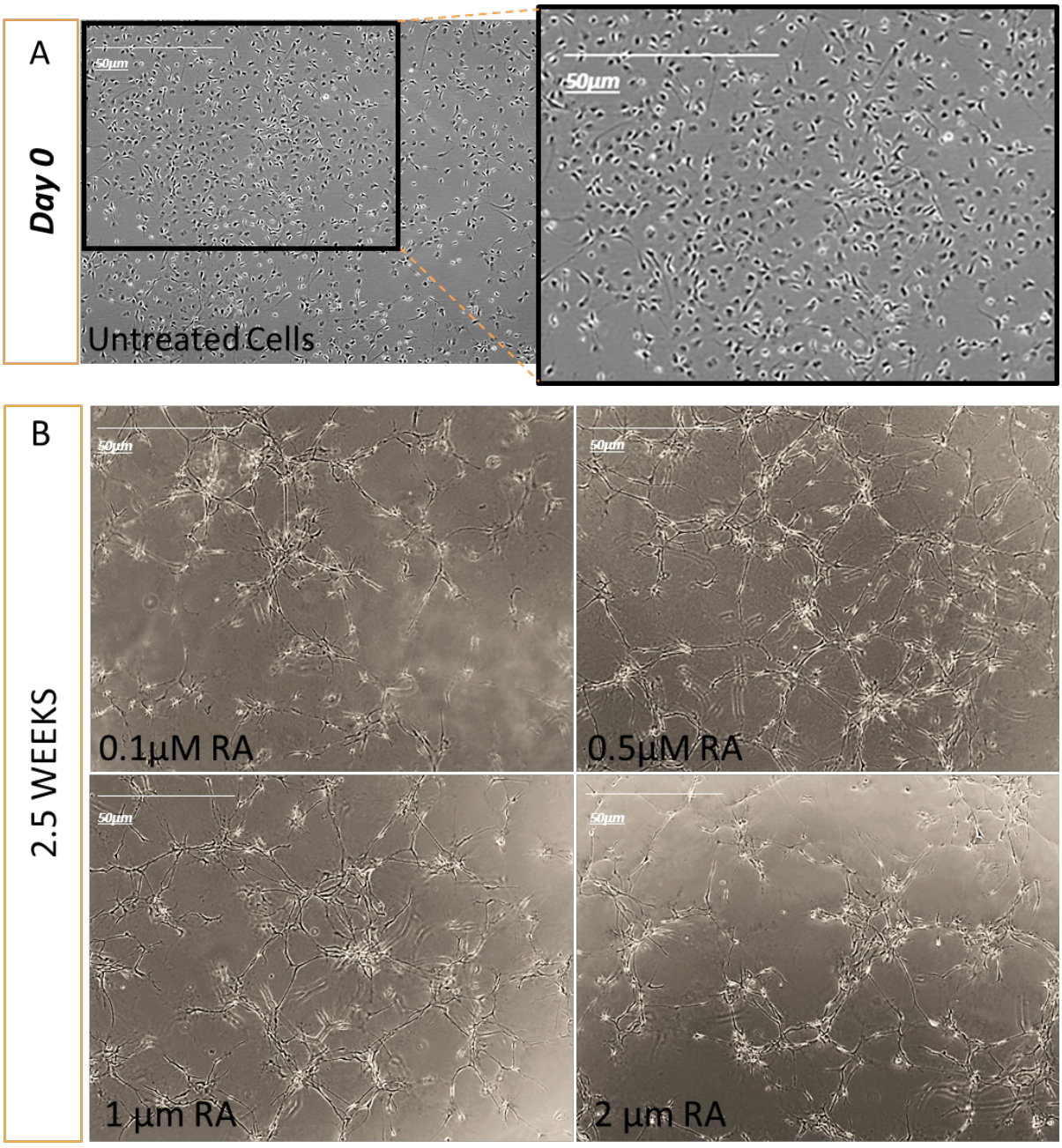

Figure 2.2: A. Morphology of human foetal stem cells at day 0 after plating in 2D cultures. B. Light microscopy images of cells treated with different concentrations of RA (0.1,0.5,1 and 2µM) at 2.5 weeks post differentiation at 10x magnification in 2D cultures. (Scale-50µm).

After 2 weeks of neural induction, the cells stop proliferating. 2.5weeks after induction the cells lose their fibroblast like morphology and become more elongated having neurite like morphology as seen in figure2.2. B. However, there is not much difference in phenotype between the different treated cultures at this early timepoint. All the cells look like they have transitioned from the initial fibroblast like morphology to cells with multiple projections all reaching out in an intricate network like formation.

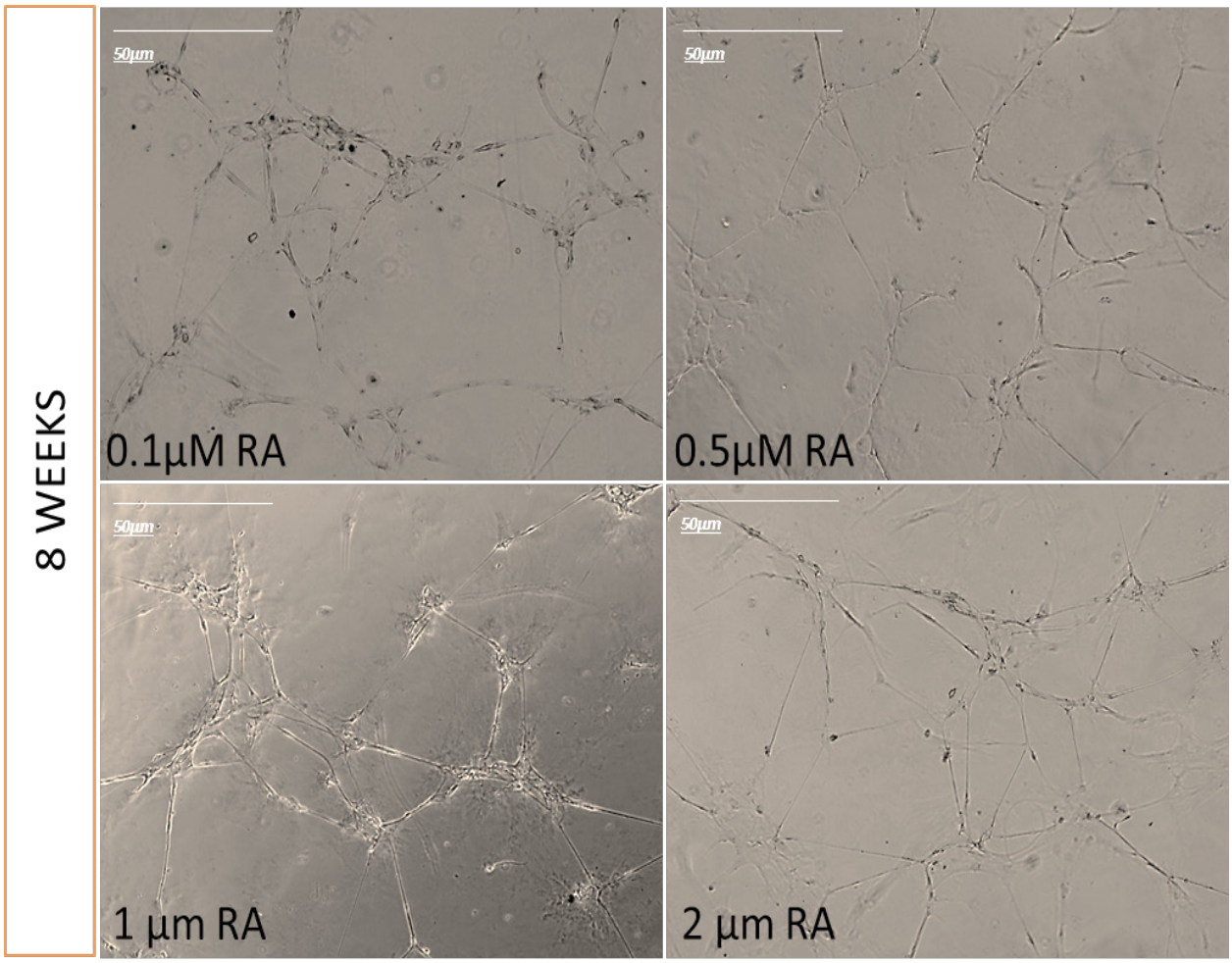

Figure 2.3: Light microscopy images of human foetal Neural Stem Cells at 8 weeks post differentiation in vitro, differentiated using different concentrations of RA (0.1,0.5,1 and 2µM) in 2D cultures at 10x magnification (scale bar 50µm).

As the cells continued differentiation over 8 weeks there is a difference in the cell number and morphology across different treatments. After 8 weeks of differentiation, the number of cells seemed to be decreasing with higher RA concentrations indicating more cell death. Also, the morphology of cells treated with 2µM RA appeared unhealthy compared to the rest of the treated cultures at 8 weeks timepoint (Fig 2.3).

2.3.2.2 Four different populations of cells observed during early stages of differentiation *in vitro*

The primary aim of the experiments described in this chapter was to show that by regulating the RA concentrations early during differentiation, the proportion of Nestin+ NSCs can be reduced over time with most of the cells being pushed towards a mature phenotype with adequate proportion of astrocytes to support the neurons in the culture. Cells at different timepoints – day 1, 2.5 weeks and 8 weeks were stained with Nestin and MAP2 to find the proportion of neural stem cells and neurons in the cultures as they differentiated over 8 weeks post differentiation (Fig 2.4). On analysis, four different populations were observed in these cultures - $Nestin^{+}MAP2^{-}$, $Nestin^{+}MAP2^{+}$, $Nestin^{-}MAP2^{+}$ and $Nestin^{-}MAP2^{-}$ cells. The four different populations of cells were counted manually depending on the presence of the markers mentioned above. There is a visible difference in the number of $Nestin^{+}MAP2^{-}$ cells and $Nestin^{-}MAP2^{+}$ between the day 0 cells as compared to the cells at different timepoints. Cells seems to have undergone fewer rounds of proliferation since the day of plating and then remained constant after induction.

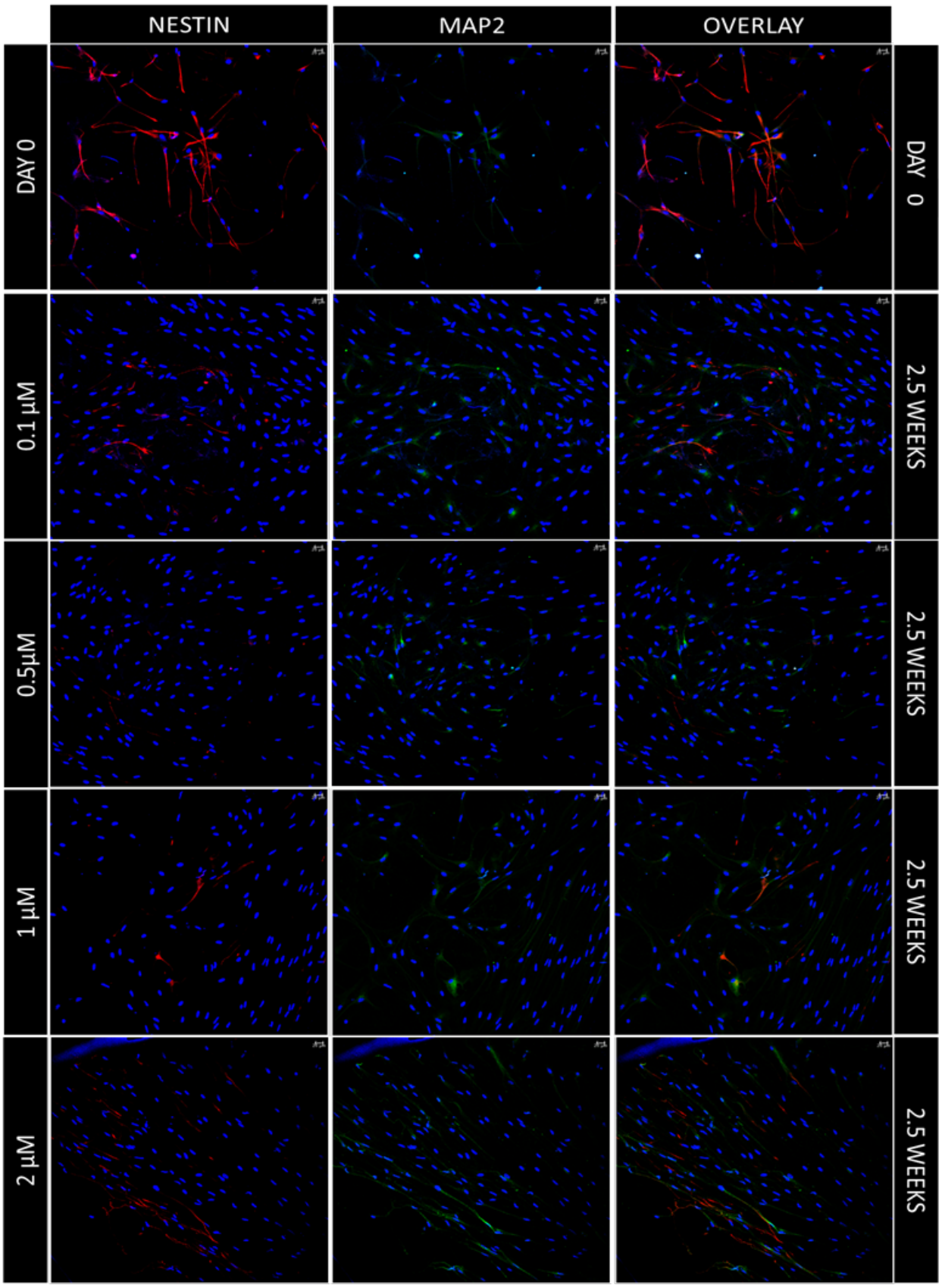

Figure 2.4: Immunofluorescence images of Nestin (red) and MAP2 (green) expression seen in foetal Neural Stem Cells in 2D cultures at 20x magnification under confocal microscope (scale bar 20 µm), counterstained with DAPI (blue, at different timepoints day 0- and 2.5-weeks post differentiation. (n=3)

2.3.2.3 RA induces neuronal differentiation of NSCs *in vitro*

The percent positive cells of the four different population of cells - Nestin^{+}Map2^{-}, Nestin^{+}Map2^{+}, Nestin^{-}Map2^{+} and Nestin^{-}Map2^{-} cells, normalize against the total number of cells (dapi) was analysed at 2.5 weeks post differentiation in 2D cultures of hfNSCs. Untreated cells at day 0 showed a higher number of Nestin^{+}Map2^{-} (Fig 2.5. A) and lower levels of Nestin^{-} Map2^{+}cells (Fig 2.5. B). At 2.5 weeks, with different concentrations of RA there was no significant change among the different treated cells.

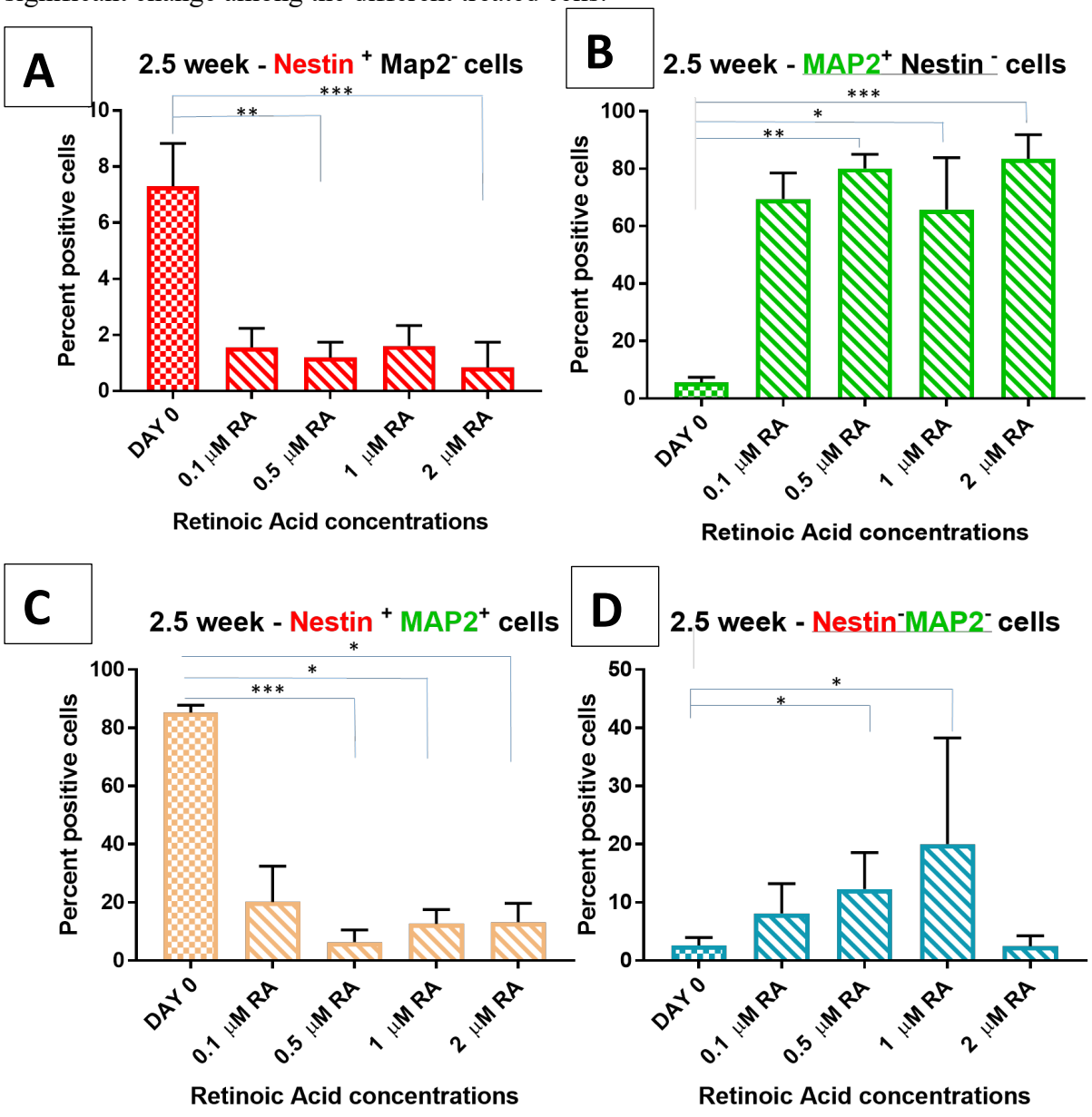

Figure 2.5: Analysis of the immunofluorescence staining of MAP2 and Nestin at 2.5 weeks post differentiation in 2D hfNSC cultures (n=3). Four different population of cells – A. Nestin^{+}MAP2- B. Nestin -Map2^{+}, C. Nestin^{+}Map2^{+}and D. Nestin^{-}Map2^{-} cells were analysed against control (day 0) hfNSCs. All values were normalised against total number of cells (dapi). A non-parametric Kruskal Wallis test

with Dunn's correction was used for statistical analysis on all data sets. *p<0.05, ** p<0.01, *** p<0.001.

However, there are significant differences in the number of $Nestin^{+}Map2^{-}$ cells between control and 0.5µM a well as 2µM RA concentrations. This shows that with an increase in the RA concentration the number of $Nestin^{+}$ cells decreases with time along with an increase in the number of $MAP2^{+}Nestin^{-}$ cells. There was a significant decrease in the number of $MAP2^{+}Nestin^{+}$ cells between day 0 cells and 2.5-week-old cells especially 0.5µM RA treated cells (Fig 2.5.C). There is also a difference in the number of $Nestin^{-}MAP2^{-}$ cells between day0 and 2.5week treated cells (Fig 2.5.D).

2.3.2.4 Higher concentrations of RA toxic to cells *in vitro*

An increase in RA concentration in the early stages of differentiation seems to have a distinct effect on the differentiation and survival of neurons at later stages of differentiation. At 8 weeks post differentiation there seems to be an increase in the number of $Nestin^{-}$Map2+ cells with a gradual decrease in the number of $Nestin^{+}Map2^{-}$ cells (Fig 2.6). Cells treated with higher concentrations show altered morphology. The cells treated with 1 and 2µM RA not only look sparse but also show senescent phenotype with overall enlarge flattened but irregular shaped cells. This indicates higher concentrations of RA are toxic to the cells, however this effect is more prominent in the 2µM RA treated cells. Cells treated with 2µM RA appear to have enlarged and sparsely spaced cells with a decrease in total cell number. However, there is no obvious decrease in the number of cells in 1µM RA treated cells.

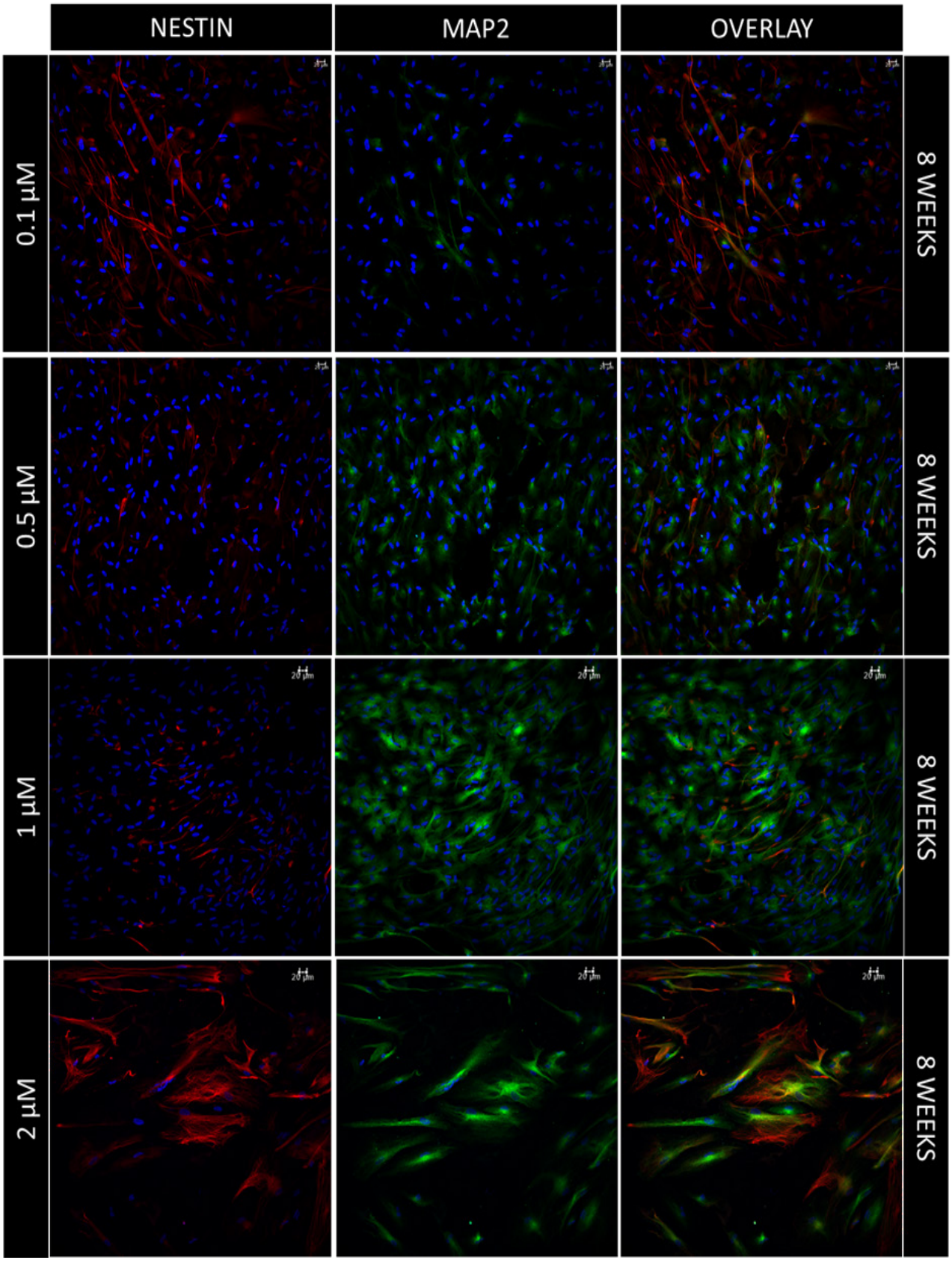

Figure 2.6.: Immunofluorescence images of Nestin (red) and MAP2 (green) expression seen in foetal Neural Stem Cells in 2D cultures at 20x magnification under confocal microscope (scale bar 20 µm), counterstained with DAPI (blue), at 8 weeks post differentiation.

2.3.2.5 Number of Nestin+ cells decrease with increase in RA concentration

The percent positive cells of the four different population of cells - $Nestin^{+}MAP2^{-}$, $Nestin^{+}MAP2^{+}$, $MAP2^{+}$ $Nestin^{-}$ and $Nestin^{-}MAP2^{-}$ cells, normalized against the total number of cells (DAPI) was analysed at 8 weeks post differentiation in 2D cultures of hfNSCs.

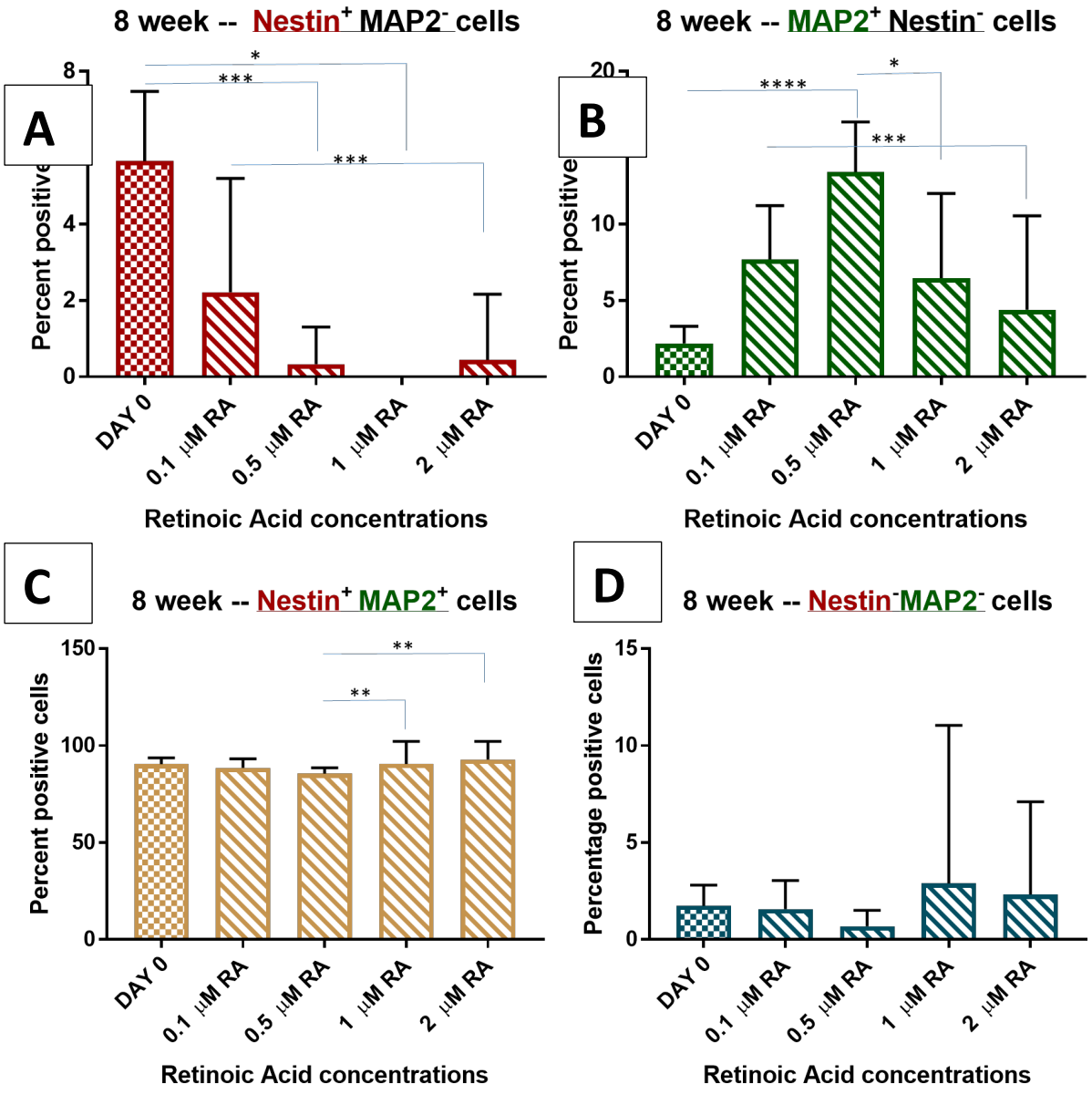

Figure 2.7: Analysis of the immunofluorescence staining of MAP2 and Nestin at 8 weeks post differentiation in 2D hfNSC cultures (n=3). The percent positive cells of each of the four different population of cells -A. $Nestin^{+}Map2^{-}$, B. $Map2^{+}Nestin^{-}$, C. $Nestin^{+}Map2^{+}$ and D. $Nestin^{-}Map2^{-}$ cells were analysed against control (time 0) hf NSCs. A non-parametric Kruskal Wallis test with Dunn's correction was used for statistical analysis on all data sets. *p<0.05, ** p<0.01, *** p<0.001.

An increase in RA concentration significantly reduced the number of Nestin^{+} cells at 8 weeks post differentiation. At 8 weeks post differentiation, the number of Nestin^{+} cells have significantly decreased since day 0 (Fig 2.7. A) the lowest being 1µM RA and 0.5µM RA treated cells with less than 1% of cells being positive for Nestin. The number of MAP2^{+} cells have significantly increased from day 0 (Fig 2.7. B) the highest numbers seen in cells treated with 0.5µM RA, approximately 13% cells in culture. There is an increase in the number of MAP2^{+} cells at lower concentrations whereas the number decreases at higher concentrations of 1 and 2µM RA. One possible reason for this could be attributed to the toxicity of RA at higher concentrations. The best concentration of RA to differentiate the hfNSCs at 8 weeks was found to be 0.5µM RA giving the highest number of MAP2^{+}Nestin $^{-}$ cells and lowest number of Nestin^{+} MAP2^{-} cells.

2.3.2.6 RA influences the proportion of Astrocytes in the neural cultures *in vitro*

In order to determine the proportion of astrocytes (GFAP+ only cells) at 8 weeks post differentiation in the cultures, cells were dual stained for GFAP and Nestin. Similar to the previous markers, on analysis, four different populations were observed in the cultures- GFAP^{-} Nestin^{+}, GFAP^{+} Nestin^{+}, GFAP^{+} Nestin^{-} and GFAP^{-} Nestin^{-} cells (Fig 2.8). Each cell population type was counted (manually) and normalized against total number of cells (DAPI). The percent positive cells were analysed for the different concentrations at 8 weeks post differentiation. At 8 weeks post differentiation, GFAP^{+} Nestin^{-} cells had a typical astrocytic phenotype, wherein the cells looked star shaped with long processes and multiple branches. However, compared to the other treated cells, the cells treated with 2µM RA looked unhealthy as seen previously. Visibly there were more GFAP^{+} Nestin^{-} cells in 0.5µM RA treated cells.

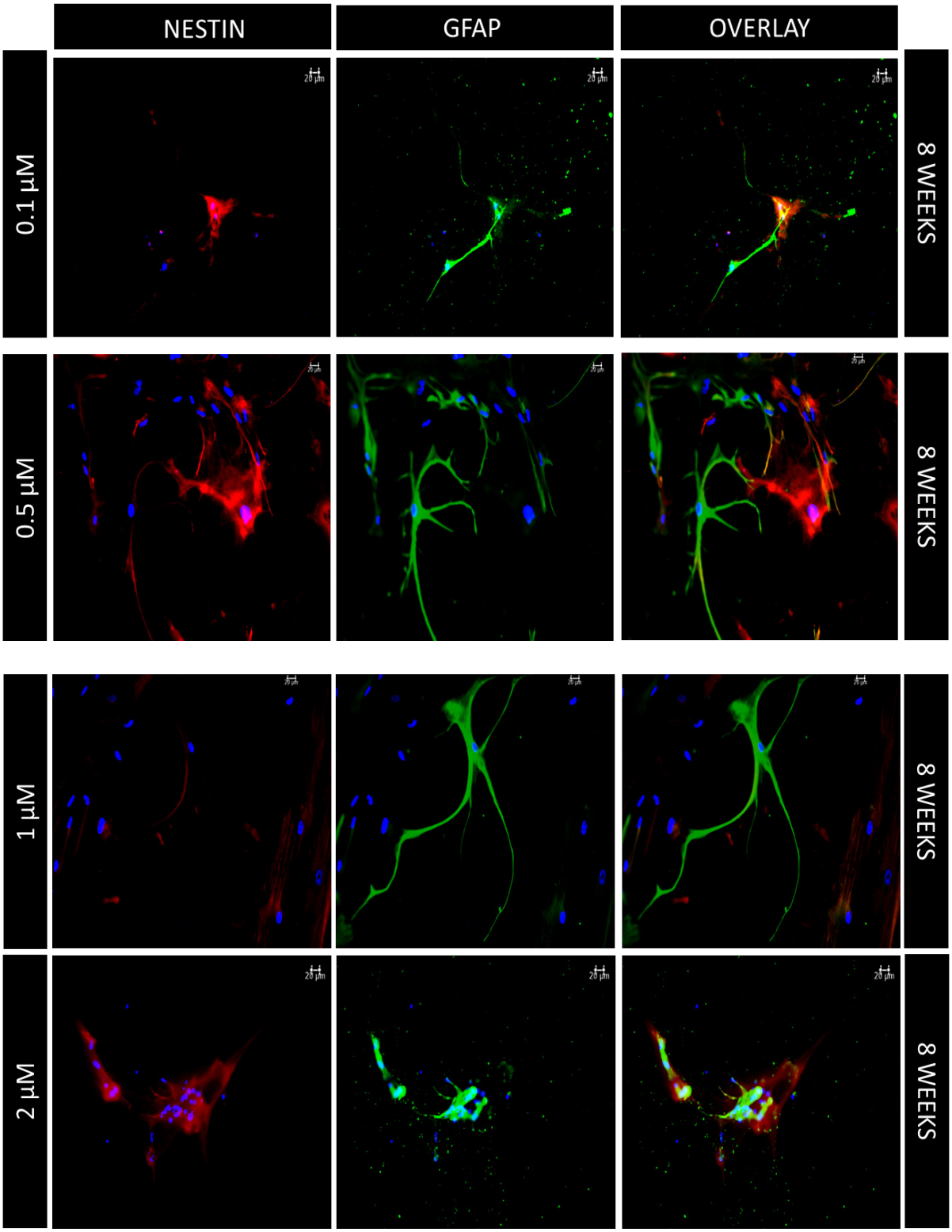

Figure 2.8: Immunofluorescence images of Nestin (red) and GFAP (green) expression seen in hfNSCs in 2D cultures at 20x magnification under confocal microscope (scale bar 20 µm), counterstained with Dapi (blue), at 8 weeks post differentiation.

There is a significant increase in the number of GFAP$^+$ Nestin$^-$ cells in the 0.5µM RA treated cells compared to the other treated cells (Fig 2.9. A). There are approximately 25% of cells in culture expressing GFAP$^+$ cells when treated with 0.5µM RA at 8 weeks post differentiation. As seen previously there is a population of cells expressing both GFAP and Nestin, however there is no significant difference between the different treated cells.

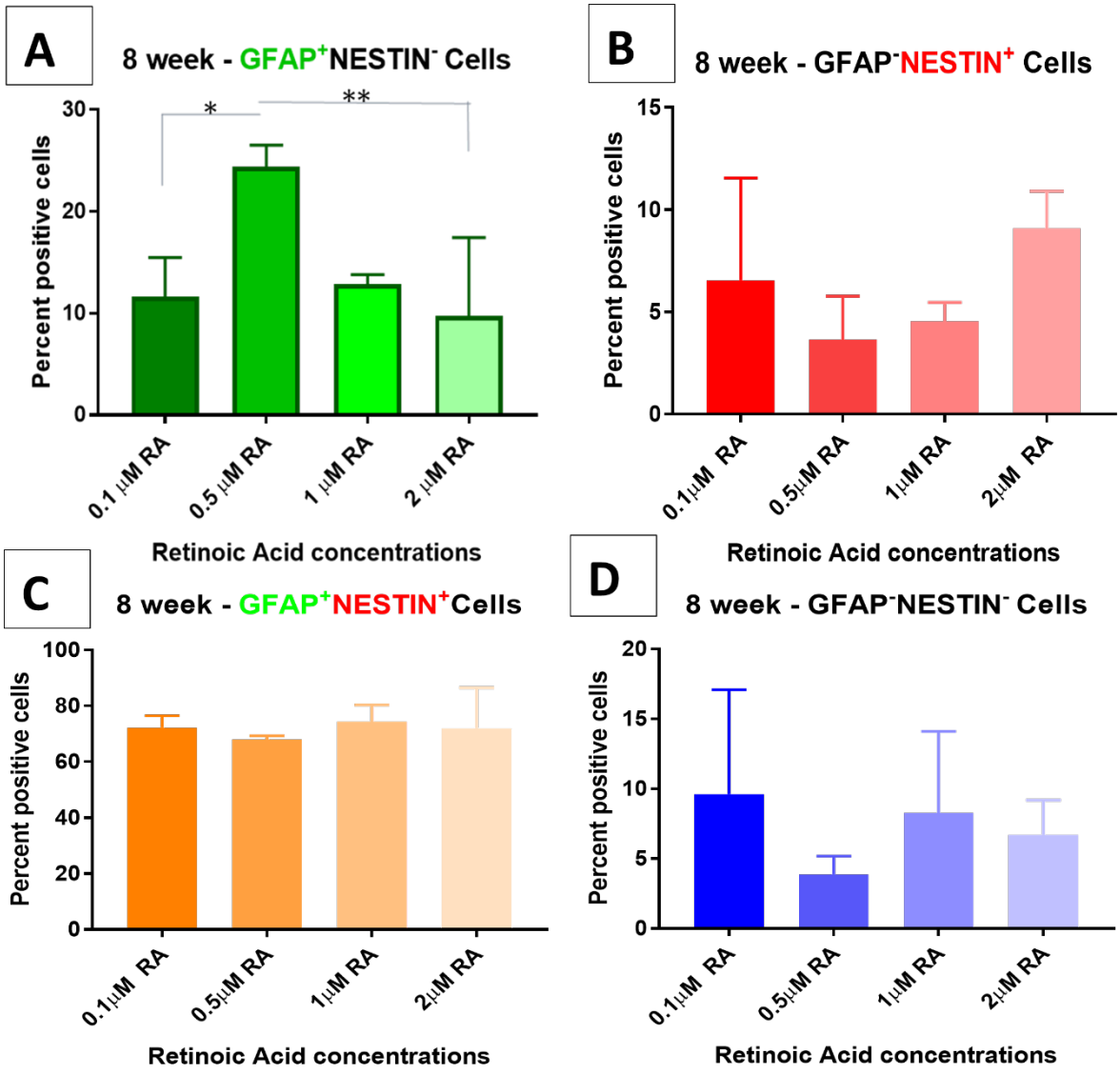

Figure 2.9: Analysis of the immunofluorescence staining of GFAP and Nestin at 8 weeks post differentiation in 2D hfNSC cultures (n=3). The percentage positive cells of each of the four different population of cells –A. GFAP$^+$ Nestin$^-$, B. GFAP$^-$Nestin$^+$ C. GFAP$^+$Nestin$^+$, and D. GFAP$^-$ Nestin$^-$ cells were analysed. A non-parametric Kruskal Wallis test with Dunn's correction was used for statistical analysis on all data sets. *p<0.05, ** p<0.01, *** p<0.001.

2.3.3 Discussion

The primary aim of this experiment was to optimize the neural differentiation protocol by selecting the most efficient dose of RA for induction of neural and glial differentiation *in vitro.*

2.3.3.1 RA induces neural and glial differentiation

There is enough experimental evidence supporting the role of endogenous retinoids in the anterior/posterior development of the central axis of the body in vertebrates in a dose gradient way (Blumberg, 1997; Ross *et al.*, 2000; Rhinn and Dollé, 2012) . Very high doses or low doses both seem to have a harmful effect on foetal development, and it seems a balance of retinoids is of absolute importance during gestation (Means and Gudas, 1995). There is plenty of evidence supporting the fact that RA induces post-mitotic neural phenotypes in various stem cells *in vitro*, hence implying that RA is key in flipping from proliferation to differentiation state. RA is a lipophilic molecule with small molecular weight (300Da) and is a metabolite of vitamin A. Cellular RA binding protein2 (CRABP2) is a transporter involved in transporting RA from the cytoplasm to the nucleus initiating a cascade of events facilitating neural differentiation (Delva *et al.*, 1999). In the nucleus RA binds to the RA receptors RARα, β or γ. These RARs bind to one of the retinoid X receptors RXRs - RXRα, β or γ to form a heterodimer complex which when bound to DNA initiates transcription of RA primary response genes (Niederreither and Dollé, 2008). RA is known to increase Pax 6 expression which is known to promote neural differentiation (Gajović *et al.*, 1998). By promoting the degradation of SMAD1, RA antagonizes BMP and SMAD signalling thereby facilitating neural differentiation (Sheng *et al.*, 2010)

RA induces Embryonic stem cells/iPSCs to differentiate intro different neural cell phenotypes like neurons, astrocytes and oligodendrocytes ((Bain *et al.*, 1995; Maden, 2007). There is evidence pointing to the ability of RA to promote astroglial differentiation (Asano *et al.*, 2009). There are studies proving that RA is a potent inducer of (Jang *et al.*, 2004; Herrera *et al.*, 2009; Herrera, Chen and Schubert, 2010) Moreover, the astrocytic differentiation is specifically regulated by the receptor activated. RARα is described to promote astrocytic and oligodendrocytic differentiation while RARβ is more specific for a neuronal pathway.

2.3.3.2 Higher doses of RA cause cellular senescence

In this Chapter-Part A, the results show that RA works in a concentration and time dependent manner. NSCs treated with different concentrations of RA for the initial 14 days of differentiation generates a population of cells with four different cell types which differ in proportion depending on the RA concentration used. However, by the end of 8 weeks of differentiation an altered morphology is seen with signs of unhealthy cells in the samples with higher doses of RA. There are reports stating that RA has the ability to inhibit cell proliferation and cause cellular senescence (Park, Lim and Jang, 2011; Ma *et al.*, 2018). In fact, this property of retinoids is now being explored as treatment measures for certain cancers (Chen *et al.*, 2006). Reports show that retinoids do not only inhibit cell proliferation (Crowe, Kim and Chandraratna, 2003) but also cause cellular senescence in pre-malignant mammary lesions and tumours (Shilkaitis, Green and Christov, 2015). This is in line with what we see in our cultures. In this experiment, the cells treated with 1 and 2µM RA eventually start showing signs of senescence and death, which goes to prove that these higher concentrations are not the best suited concentrations for differentiation of NSCs *in vitro* in our experiments.

2.3.3.3 0.5µM is the optimum concentration of RA for neural and glial differentiation *in vitro*

As seen with these experiments, using different concentrations at different timepoints it was evident that 0.5µM of RA would be the best concentration for efficient differentiation of NSC to neuronal and glial cells. At 2.5 weeks post differentiation there is a significant decrease in the percentage of $Nestin^+$ cells and a significant increase in the percentage of $MAP2^+$ cells in the cells treated with 0.5 µM of RA. At 8 weeks post differentiation there is a significant decrease in the percentage of $Nestin^+$ cells and a significant increase in the $MAP2^+$ cells in both 0.5 and 1 µM of RA. At 8 weeks post differentiation the cells treated with 0.5 µM of RA shows the highest increase in the percent of $GFAP^+$ cells. Also, at 8 weeks post differentiation, the cells might be progressing towards senescence which is not evident yet for cells treated with1 µM, but this could be clarified by keeping the cells for longer to see if their condition worsens. Therefore, taking into account all these results, 0.5µM of RA was considered the best concentration for efficiently differentiating NSCs to post-mitotic neurons and astrocytes.

There are studies which use RA as a neural induction agent in the range of 0.5µM to 1 µM. For instance, in the Tao-Tan et al 2015 study, they use a 0.5 µM RA concentration to differentiate NSCs derived from rat spinal cord for 14 days. They show that RA promotes neuronal differentiation to generate functional mature neurons and the growth of cellular dendrites (Tan

et al., 2015). The Kothapalli et al 2013 study compares different concentration of RA for ESC differentiation and show that 0.5µM RA promotes neurons as well as astrocytes and oligodendrocytes in the cultures whereas 1 µM RA promotes more the neuronal fate but not so much the glial fates. 1 µM RA was observed to be supressing both the astrocytes and the oligodendrocyte numbers (Kothapalli and Kamm, 2013).

A large number of cells express both $GFAP^{+}Nestin^{+}$ at 8 weeks post differentiation which is an indication that cells are still immature and in a state of transition. This combined with the fact that GFAP is not an absolute marker for astrocytes but also a marker of radial glial cells, the $GFAP^{+}$ $Nestin^{-}$ cells seen in the cultures may not be purely astrocytes. They could be indicative of a population of neuronal progenitor cell type. Using markers more specific for astrocytes like S100β or aquaporin 4 may be more informative regarding the presence of astrocytes in these cultures. Similarly, to determine the presence of neural progenitor stem cells an array of markers could be used namely- SOX1, SOX2, Doublecortin/DCX, vimentin etc. To determine quiescent neural progenitor stem cell population any of the above markers with an absence of Ki67 (proliferation marker) would be more informative.

In conclusion, we have achieved our aim to optimize the differentiation protocol which generates cells with healthy morphology for long term cultures, which generates optimal levels of mature neurons expressing MAP2 with fewest Nestin positive neural progenitor stem cells and a healthy proportion of astrocytes expressing GFAP over a period of 8 weeks post differentiation *in vitro* in the 2D cultures.

2.3.4 Future Work

This was a pilot experiment to optimize the most efficient dose of RA to get the optimum number of neurons and astrocytes in culture. The same experimental design could be used to study the effect of different RA concentrations on the number of oligodendrocytes in the cultures at different timepoints.

Since there were some senescent cells seen at the end of 8 weeks with the higher concentrations of RA, cell viability assays such as the MTT (3-[4,5-dimethylthiazole-2-yl]-2,5-diphenyltetrazolium bromide) test, could confirm the toxic effects of different concentrations of RA *in vitro.* Moreover, some IF staining for markers for senescence such as p53 and p21 could be used to confirm cellular senescence and cell death at higher doses of RA.

2.4 Part B- Standardization and Validation of 3D cultures

This part of the chapter focuses on validation of the human 3D neural culture method using different cell lines derived from iPSCs of AD patients with PSEN1 mutation L286V, A246E and M146L compared against cell lines derived from iPSCs of two healthy adult individuals. This part of the chapter will also focus on the standardization of the different techniques such as Immunofluorescence and Western Blot used to characterize the 3D cultures from the above mentioned iPSC derived cell lines.

2.4.1 Methods

2.4.1.1 Cell Culture

The iPSC derived Neural Stem Cell (NSC) lines from AD patients (hAD2, hAD3 and hAD4) and healthy adult individuals (hN8 and hN9) were obtained from Axol Biosciences (Table 2.7). The cell lines with the AD-PSEN1 mutaions were specifically selected as these 3 were some of the most commonly studied mutations in both in vitro and in vivo studies. This would provide a broader sense of understanding and information to compare and contrast with the effects seen in our 3D cultures.

Cell Lines from Axol Biosciences			
CONTROL CELL LINES	**hN8 (ax0018)**	**hN9 (ax0019)**	
CELL TYPE	iPSCs derived NSCs from healthy individual	iPSCs derived NSCs from healthy individual	
SEX	Male	Female	
AGE of collection	74 years	64 years	
AD CELL LINES	**hAD2 (ax0112)**	**hAD3 (ax0113)**	**hAD4 (ax0114)**
MUTATION	**PSEN1- L286V**	**PSEN1- M146L**	**PSEN1- A246E**
CELL TYPE	iPSCs derived NSCs from AD patient	iPSCs derived NSCs from AD patient	iPSCs derived NSCs from AD patient
SEX	Female	Male	Female
AGE (collection)	38 years	53 years	31 years
AGE (onset)	Onset at 39 years of age	Unknown	Onset at 45 years of age

Table 2.7: Details of iPSC derived NSC from Axol Biosciences Skin fibroblasts had been used to generate iPSCs by using integration free episomes to deliver specific regulatory factors and differentiated into NPC using defined conditioned Media (Axolbio, no date).

2.4.1.1.1 Thawing and Expansion of iPSC-Derived Neural Stem Cells

The cells were thawed using the same method as described in Chapter 2 Part B sectin 2.3.1.1.1…. with minor modifications. The composition of the modified ANM media used for this experiment is described in the table below (Table 2.8). Axol cells were thawed and expanded in Sure Bond coated flasks. SureBond (1000x, Axol Bioscience-ax0041), a coating solution for optimal surface adherence and growth, was slowly defrosted at 4°C two days prior to thawing cells, to prevent jellification. SureBond was diluted (5µl/ml) in 10ml of sterile PBS without Ca-Mg (Gibco,10010023) to coat T75 culture flasks one day prior to plating cells. Two vials of each cell line containing 1.5 million cells were extracted from liquid nitrogen and rapidly thawed. Post thawing Axol cells were resuspended in modified ANM media supplemented with Sure Boost and incubated at 5% CO2 at 37°C. SureBoost (1000x, Axol Biosciences-ax0045), a supplement provided with the cells for maximum viability after

thawing. After two hours of incubation the media was replaced with fresh ANM media supplemented with FGF2 (20ng/ml) for 6 days for optimal cell growth and proliferation.

Axol Neural Maintenance Media	
Components	**Concentration**
Axol Neural Basal Media (ax0031b)	1x
Axol Supplement (ax0031a)	1.5%v/v
Antibiotic-Antimycotic solution (Sigma Aldrich, A5955)-100x	1x

Table 2.8: Details of Axol Neural Maintenance Media used for this section of experiments.

2.4.1.1.2 Seeding for 3D Cultures

On day 6, cells were processed using the same method as described previously (section 2.3.1.1.2) with the exception of Accutase. . Axol Unlock (1x, Axol Biosciences-ax0044) was added to the cells for five minutes at 37°C in the incubator for the cells to detach. For 1ml of Unlock 4 times volume of media was used to stop reaction and collect cells. For seeding in 3D cultures, cells were plated on ice, in an 8 well-Lab-Tek chamber slide (Lab-Tek system, Nunc-177445) in 3D Plating Media (Table 2.9) at a density of 2 x 10^6/ml per well with RA at a concentration of 100ng/ml supplemented with Matrigel (Corning, 354230,) at a ratio of 1:15 v/v, which is then left in the incubator to form a gel at 37°C to eventually form 3D cultures. An extra 200µl of modified ANM media (Table 2.8) was added two hours after the cultures were plated.

3D Plating Media	
Components	**Final Concentration**
Axol Neural Basal Media (ax0031b)	1x
Axol Supplement (ax0031a)	1.5%
Retinoic Acid (Sigma Aldrich, R2625)	0.1µM
Antibiotic-Antimycotic solution (Sigma Aldrich, A5955)- 100X	1x

Table 2.9: Details of 3D Plating Media.

2.4.1.1.1 Differentiation of iPSC-Derived NSC to neurons in 3D cultures

The differentiation protocol followed for the 3D cultures is as described previously (section 2.3.1.1.4) For Induction media (refer Table 2.9) 100ng of RA was used. For Neural Differentiation media refer Table 2.3. Media was changed every other day for 3 weeks followed by everyday up to 18 weeks *in vitro*.

For all the experiments, results and discussions hence forth, timepoints are described in weeks. The cells were harvested at the end of the respective week for each timepoint, except week 0 where the cells were grown for a day and harvested next day before growth factors were added. The following is a table (Table 2.10) describing the corresponding days in cultures for reach timepoint:

Weeks Post Differentiation	Days Post Differentiation
Week 0	Day 0- next day after plating
Week 6	Day 42
Week 12	Day 84
Week 18	Day 126

Table 2.10: Timepoints in weeks and days post differentiation

A schematic representation of the method used to expand and differentiate these cells along with their timepoints is described in Figure 2.10.

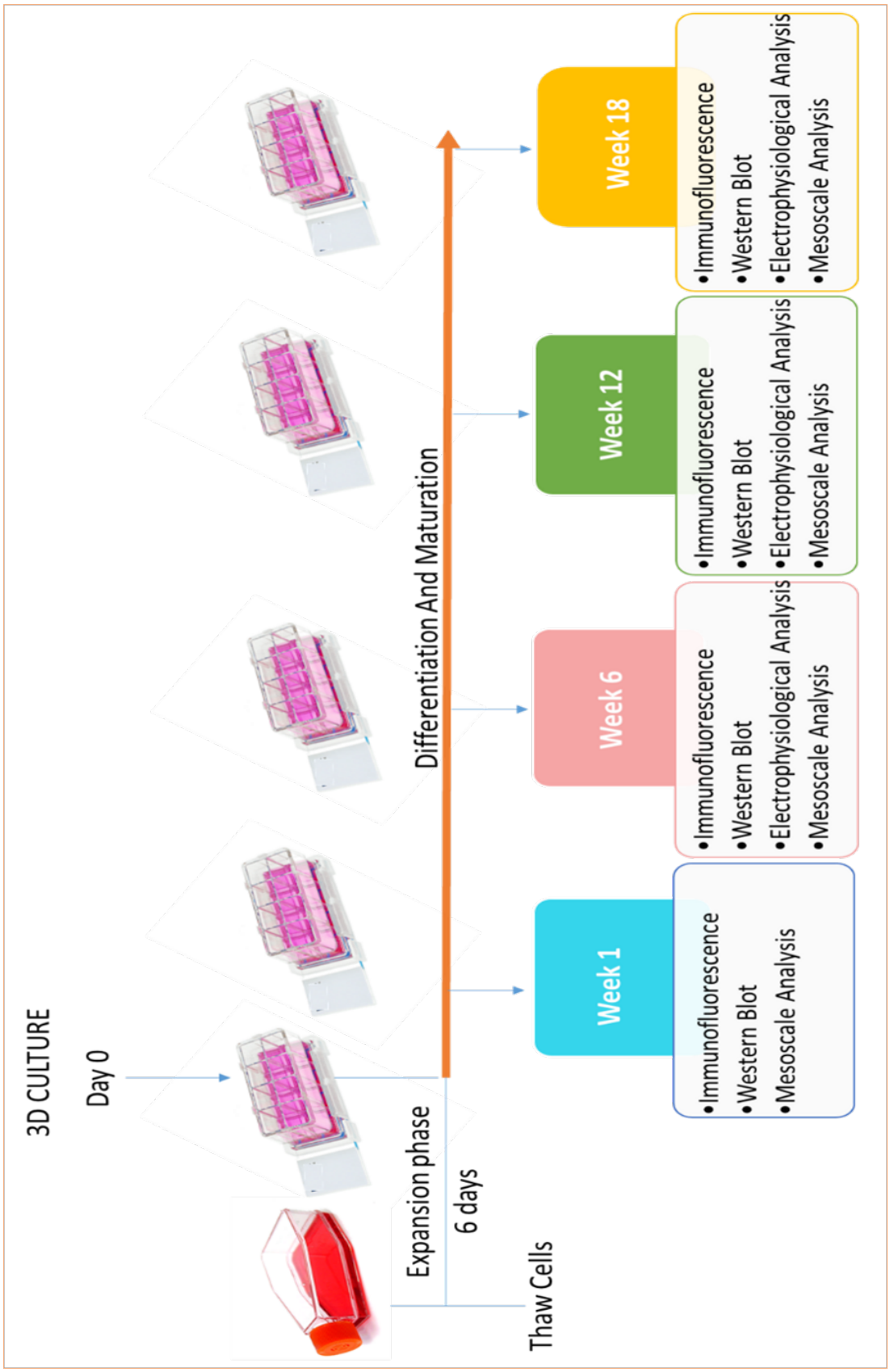

Figure 2.10: Schematic representation of the differentiation protocol. Cells are thawed and expanded for 6 days in flasks following which cells are seeded in 3D and supplemented with growth factors to over a period of 12 to 18 weeks in vitro for differentiation into neurons and astrocytes. At timepoints -day1, week 6, week 12 and week 18 cells are harvested to perform different assays such as Western Blotting and Immunofluorescence.

2.4.1.2 Standardization of Immunofluorescence for 3D cultures

In order to standardize and adapt the technique to immunostain 3D cultures a few different samples were used. During the pilot study of this project Dr. Elodie Siney had used iPSC-derived human Neural Stem Cells hAD2 (Axol Biosciences) for 3D culture as a preliminary study. These cultures were differentiated, fixed and cryo-sectioned according to the protocols described in this chapter-section. These cultures were not just used to practice cryo-sectioning but further utilised to standardise various markers for IF staining. These cultures/sections are hence referred as 3D culture-2015. In order to optimize IF staining in the 3D cultures, the primary antibody was tested on a positive control prior to cultured cells. Mouse brain section was used as a positive control for MAP2, GFAP, B3-TUBULIN, SYNAPSIN, GAD 65/67 and VGLUT 1. For Nestin, cultured hfNSCs (details in section 2.3.1.1) were used. Sections from 26-week-old female Mf1 (outbred) mice brain were harvested and fixed in 4% PFA overnight at 4°C and later embedded in OCT to section 14µm thick slices in a cryostat. Only after primary antibodies were tested against positive controls were, they used to standardize the 3D-IF stains using either sections from the old 3D culture-2015 or the batch of 3D cultures described in the methods section of this chapter-section. For standardisation of each marker, a step-wise trial and modification basis was adopted. Different buffers were tried one at a time to determine the best working protocol for each stain. For all the IF stains, optimizations were made to the staining protocols as required only after assessing the trial images as shown in the results section below.

2.4.1.2.1 Sample Preparation – 3D cryo-section

The 3D cultures were fixed in 4% PFA (Faculty of Medicine, SGH) for 24 hours at 4°C, rinsed three times in 1xPBS and stored at 4°C in 30% sucrose (Sigma Aldrich, UK.) solution. The 3D cultures were then embedded in Optimal Cutting Temperature (O.C.T) embedding medium over dry ice. Cultures were first immersed in blue coloured O.C.T and then in clear O.C.T to demarcate between the cells and the frozen O.C.T. Frozen O.C.T cultures were sectioned at 14 micrometres thickness using a S35 microtome Blade (Cell Path, JDA-0100-00A) on a cryostat. Sections were transferred onto SuperFrost slides (Thermo fisher, UK.) Slides were left overnight at room temperature to dry and later stored at -20°C.

2.4.1.2.2 Protocol Optimization for GFAP immunofluorescence

The sections were defrosted and dried at 37°C for 30 minutes. For optimization the sections were permeabilized using PBST (PBS with 0.2% or 1% Triton-X100, Sigma Aldrich, UK.) for 20 minutes. Blocking was done using PBST with 10% donkey serum (Sigma Aldrich, UK.), for an hour followed by incubation with primary antibodies made up in blocking buffer (Table 2.11) overnight at 4°C. Further, these sections were washed with PBST three times for 5 minutes each. The sections were then incubated with fluorescently labelled secondary antibodies in blocking buffer for 2 hours at 37°C followed by three washes with PBST for 5 minutes each and counterstaining with DAPI (Sigma Aldrich, UK.) at a concentration of 2 µg/ml in permeabilization buffer for 15 minutes. Final washes (3x) with PBST for 5 minutes each was given before sealing with anti-fade agent Mowiol (Biomedical imaging Unit, SGH) to prevent quenching of fluorescence.

BUFFERS	COMPOSITION
Permeabilization Buffer (PBST)	PBS with 0.2% or 1% Triton-X100 (Sigma Aldrich, UK.)
Blocking Buffer	PBST with 10% donkey serum (Sigma Aldrich, UK.)
Wash Buffer	PBST
Primary Antibody Solution	GFAP antibody (1:200) dissolved in Blocking Buffer
Secondary Antibody Solution	488-anti (1:200) Rabbit antibody (raised in donkey) dissolved in Blocking Buffer
DAPI (Sigma Aldrich, UK.)	2 µg/ml (1 in 500) in PBST

Table 2.11 : Composition of Buffers used for GFAP immunostaining.

2.4.1.2.3 Protocol Optimization for MAP2 and NESTIN immunofluorescence

The sections were dried at 37°C for 30 minutes. For optimization, the sections were permeabilized using PBST (PBS with 0.1% or 0.2 % Triton-X100) for 20 minutes. Blocking was done using PBS with 10% donkey serum (Sigma Aldrich, UK.), 0.1% or 0.2% Triton-X100 (Sigma Aldrich, UK.) for an hour followed by incubation with primary antibodies made up in blocking buffer (Table 2.12) overnight at 4°C. Further, these sections were washed with 0.1% or 0.2% PBST three times for 5 minutes each. The sections were then incubated with fluorescently labelled secondary antibodies in blocking buffer for 2 hours at 37°C followed by three washes with 0.1% or 0.2% PBST for 5 minutes each and counterstaining with DAPI

(Sigma Aldrich, UK.) at a concentration of 2 µg/mL in permeabilization buffer for 15 minutes. Final washes (3x) with 0.1% or 0.2% PBST for 5 minutes each was given before sealing with anti-fade agent Mowiol (Biomedical imaging Unit, SGH) to prevent quenching of fluorescence.

BUFFERS	COMPOSITION
Permeabilization Buffer (PBST)	PBS with 0.1% or 0.2 % Triton-X100 (Sigma Aldrich, UK.)
Blocking Buffer	PBST with 10% donkey serum (Sigma Aldrich, UK.)
Wash Buffer	PBST
Primary Antibody Solution	MAP2 (1:200) and Nestin (1:200) antibodies dissolved in Blocking Buffer
Secondary Antibody Solution	488-anti (1:200) Rabbit (raised in donkey) and 568-anti (1:200) Mouse (raised in donkey) antibodies dissolved in Blocking Buffer
DAPI (Sigma Aldrich, UK.)	2 µg/ml (1 in 500) in PBST

Table 2.12: Composition of Buffers used for Map2 and Nestin immunostaining.

2.4.1.2.4 Protocol Optimization B3-TUBULIN immunofluorescence

The sections were dried at 37°C for 30 minutes. For optimization, the sections were permeabilized using PBST (PBS with 0.2 % or 1% Triton-X100) for 20 minutes. Blocking was done using PBS with 10% donkey serum (Sigma Aldrich, UK.), 0.2% or 1% Triton-X100 (Sigma Aldrich, UK.) for an hour followed by incubation with primary antibodies made up in blocking buffer overnight at 4°C. Further, these sections were washed with 0.2% or 1% PBST three times for 5 minutes each. The sections were then incubated with fluorescently labelled secondary antibodies in blocking buffer for 2 hours at 37°C followed by three washes with 0.2% or 1% PBST for 5 minutes each and counterstaining with DAPI (Sigma Aldrich, UK.) at a concentration of 2 µg/mL in permeabilization buffer for 15 minutes. Final washes (3x) with 0.2% or 1% PBST for 5 minutes each was given before sealing with anti-fade agent Mowiol (Biomedical imaging Unit, SGH) to prevent quenching of fluorescence.

For the optimization based on company (primary antibody) recommendations, the sections were dried at 37°C for 30 minutes and were permeabilized and blocked with 1% Triton-X100 (Sigma Aldrich, UK.), 4% donkey serum (Sigma Aldrich, UK.), 1% BSA (Sigma Aldrich, UK.) and 0.3M glycine (Fisher Bioreagents, UK) for 1 hour 30 minutes. This was followed by incubation with primary antibodies (Table 2.13) overnight at 4°C. Further, these sections were washed

with 1% PBST three times for 5 minutes each. The sections were then incubated with fluorescently labelled secondary antibodies in blocking buffer for 2 hours at 37°C followed by three washes with 1% PBST for 5 minutes each and counterstaining with DAPI (Sigma Aldrich, UK.) at a concentration of 2 µg/mL in permeabilization buffer for 15 minutes. Final washes (3x) with 1% PBST for 5 minutes each was given before sealing with anti-fade agent Mowiol (Biomedical imaging Unit, SGH) to prevent quenching of fluorescence.

BUFFERS	COMPOSITION
Permeabilization Buffer (PBST)	PBS with 1 % Triton-X100 (Sigma Aldrich, UK.)
Blocking Buffer	PBST with 4% donkey serum (Sigma Aldrich, UK.), 1% BSA (Sigma Aldrich, UK.) and 0.3M glycine (Fisher Bioreagents, UK.)
Wash Buffer	PBST
Primary Antibody Solution	B3-Tubulin (1:200) dissolved in Blocking Buffer
Secondary Antibody Solution	488-anti (1:200) Mouse (raised in donkey) dissolved in Blocking Buffer 568-anti (1:200) Mouse (raised in donkey) dissolved in Blocking Buffer
DAPI (Sigma Aldrich, UK.)	2 µg/ml (1 in 500) in PBST

Table 2.13: Composition of Buffers used for B3-Tubulin immunostaining.

2.4.1.2.5 Protocol Optimization for Synapsin 1 immunofluorescence

The sections were dried at 37°C for 30 minutes. For optimization, the sections were permeabilized using PBST (PBS with 0.1% or 0.2 % Triton-X100) for 20 minutes. Blocking was done using PBS with 10% donkey serum (Sigma Aldrich, UK.), 0.1% or 0.2% Triton-X100 (Sigma Aldrich, UK.) for an hour followed by incubation with primary antibodies made up in blocking buffer (Table 2.14) overnight at 4°C. Further, these sections were washed with 0.1% or 0.2% PBST three times for 5 minutes each. The sections were then incubated with fluorescently labelled secondary antibodies in blocking buffer for 2 hours at 37°C followed by three washes with 0.1% or 0.2% PBST for 5 minutes each and counterstaining with DAPI (Sigma Aldrich, UK.) at a concentration of 2 µg/mL in permeabilization buffer for 15 minutes. Final washes (3x) with 0.1% or 0.2% PBST for 5 minutes each was given before sealing with anti-fade agent Mowiol (Biomedical imaging Unit, SGH) to prevent quenching of fluorescence.

BUFFERS	COMPOSITION
Permeabilization Buffer (PBST)	PBS with 0.1 or 0.2 % Triton-X100 (Sigma Aldrich, UK.)
Blocking Buffer	PBST with 10% donkey serum (Sigma Aldrich, UK.)
Wash Buffer	PBST
Primary Antibody Solution	Synapsin 1 (1:200) dissolved in Blocking Buffer
Secondary Antibody Solution	488-anti (1:200) Rabbit (raised in donkey) dissolved in Blocking Buffer or 568-anti (1:200) Rabbit (raised in donkey) dissolved in Blocking Buffer
DAPI (Sigma Aldrich, UK.)	2 µg/ml (1 in 500) in PBST

Table 2.14: Composition of Buffers used for SYNAPSIN 1 immunostaining.

2.4.1.2.6 Protocol Optimization for VGLUT 1 and GAD 65/67 immunofluorescence

The mouse brain sections were dried at 37°C for 30 minutes. For optimization, the sections were permeabilized using PBST (PBS with 0.2 % or 1% Triton-X100) for 20 minutes. Blocking was done using PBS with 10% donkey serum (Sigma Aldrich, UK.), 0.2% or 1% Triton-X100 (Sigma Aldrich, UK.) for an hour followed by incubation with primary antibodies made up in blocking buffer overnight at 4°C. Further, these sections were washed with 0.2% PBST three times for 5 minutes each. The sections were then incubated with fluorescently labelled secondary antibodies in blocking buffer for 2 hours at 37°C followed by three washes with 0.2% PBST for 5 minutes each and counterstaining with DAPI (Sigma Aldrich, UK.) at a concentration of 2 µg/mL in permeabilization buffer for 15 minutes. Final washes (3x) with 0.2% PBST for 5 minutes each was given before sealing with anti-fade agent Mowiol (Biomedical imaging Unit, SGH) to prevent quenching of fluorescence.

The 3D culture sections were dried at 37°C for 30 minutes. They were permeabilized and blocked with 1% Triton-X100 (Sigma Aldrich, UK.), 4% donkey serum (Sigma Aldrich, UK.), 1% BSA (Sigma Aldrich, UK.) and 0.3M glycine (Fisher Bioreagents, UK) for 1 hour 30 minutes (Table 2.15). This was followed by incubation with primary antibodies overnight at 4°C. Further, these sections were washed with 1% PBST three times for 5 minutes each. The sections were then incubated with fluorescently labelled secondary antibodies in blocking buffer for 2 hours at 37°C followed by three washes with 1% PBST for 5 minutes each and counterstaining with DAPI (Sigma Aldrich, UK.) at a concentration of 2 µg/mL in permeabilization buffer for

15 minutes. Final washes (3x) with 1% PBST for 5 minutes each was given before sealing with anti-fade agent Mowiol (Biomedical imaging Unit, SGH) to prevent quenching of fluorescence.

BUFFERS	COMPOSITION
Permeabilization Buffer (PBST)	PBS with 1 % Triton-X100 (Sigma Aldrich, UK.)
Blocking Buffer	PBST with 4% donkey serum (Sigma Aldrich, UK.), 1% BSA (Sigma Aldrich, UK.) and 0.3M glycine (Fisher Bioreagents, UK.)
Wash Buffer	PBST
Primary Antibody Solution	*VGLUT1 (1:200)* dissolved in Blocking Buffer. *GAD65/67* (1:200) dissolved in Blocking Buffer
Secondary Antibody Solution	488-anti (1:200) Rabbit (raised in donkey) dissolved in Blocking Buffer
DAPI (Sigma Aldrich, UK.)	2 µg/ml (1 in 500) in PBST

Table 2.15: Composition of Buffers used for VGLUT1 and GAD65/67 immunostaining.

Below is the list of details for all the Antibodies used for immunofluorescence experiments (Table 2.16)

	Antibody	Species raised in	Catalogue number	Company	Dilution
Primary Antibodies	**Nestin**	Mouse	MAB5326	Millipore	1:200
	MAP2	Rabbit	4542	Cell Signalling	1:200
	GFAP	Rabbit	ZO334	Dako Cytomation	1:200
	B3-TUBULIN	Mouse	801202	Biolegend	1:200
	Synapsin 1	Rabbit	ab8	Abcam	1:200
	VGLUT1	Rabbit	135303	Synaptic systems	1:200
	GAD 65/67	Rabbit	G5163	Merck	1:200
Secondary Antibodies	**488 Alexa Fluor**	Donkey	A21206	Invitrogen	1:200
	568 Alexa Fluor	Donkey	A11057	Invitrogen	1:200

Table 2.16: List of antibodies used for Immunofluorescence

Once the antibodies were standardized on the old 3D Cultures sections (2015-Dr. Elodie Siney), the standardized staining protocols were used on the entire set of 5 cells line (Table2.7) cultured to check for replicability. However, all cell line-sections were not stained for all the antibodies standardized in this chapter. Only MAP2 and Nestin were used for all the cell lines, since the aim of this experiment was also to check if there is optimal differentiation as expected in the 3D cultures. For MAP2 and Nestin, sections from all cell lines were stained in parallel.

2.4.1.2.7 Confocal Imaging

For details on confocal imaging refer Chapter 2-Part A (section 2.3.1.2), images were captured in Confocal Laser Scanning Microscope (Leica TCS SPS8, Leica Microsystems, UK.) at 63 x magnification using a glycerol immersion objective. The z-stack were kept constant at 1µm for all experiments. The data from multiple z-stacks were compressed into single images by obtaining the maximum projection of the stack. Since we did not need these images for quantitative analysis, only two to three frames per slide were taken. Leica Application Suite X (Las X Industries, Inc) was used to process the confocal images

2.4.1.3 Standardization of Western Blotting for 3D cultures

The general protocol for WB was followed as per protocols previously standardized by the Mudher laboratory for detection of tau protein. The samples were first tested alongside drosophila fly samples and human foetal neural stem cells samples before they were tested on the expensive iPSC- derived human neural 3D cultures.

2.4.1.3.1 Sample Preparation for Western Blot – Total Lysate.

The 3D cultures (4 wells) were homogenised in 100µl TBS extraction buffer (Table 2.17) with plastic pestle. To prevent any protein degradation activity by endogenous proteases, Halts protease and phosphatase cocktail (Roche, UK.) was added to the buffer. A small volume (50µl) of the lysate was separated and stored at -80°C, the rest was further processed for fractionation.

2.4.1.3.2 Sample Preparation for Western Blot – Lysate Fractionation

The protein solubility assay was adopted from a previous protocol for fly samples (Cowan *et al.*, 2015). Three consecutive fractions (S1, S2 and S3) were recovered from each sample processed. S1 represents the cytosolic compartment, S2 represents the membrane bound compartment and S3 represents the insoluble fraction. 3D cultures (4 wells pooled) were lysed using the TBST/SDS/Urea extraction method. To prevent any protein degradation activity by endogenous proteases, Halts protease and phosphatase inhibitor cocktail (Roche, UK.) was added to each buffer. The samples were collected in 100 µl of TBS/Lysis Buffer (Table 2.17).

The cells were homogenized at 4°C in 100 µl TBS Lysis buffer (Table 2.17) in Beckman's eppendorf tubes (Beckman Coulter, UK, 357448) with plastic pestle. The lysate was then ultra-centrifuged at 186,000g for 2 hours at 4°C. The supernatant (S1-TBS soluble fraction) was stored at -80°C. The pellet was resuspended in 100 µl of 5% SDS/TBS buffer (Table 2.17) and rehomogenised. The lysate was then ultra-centrifuged at 186,000g for 2 hours at 25°C. The supernatant (S2- SDS-soluble fraction) was stored at -80°C. The subsequent pellet was resuspended in 100 µl SDS buffer (Table 2.17) and ultra-centrifuged at 186,000g for 1 hour at 25°C. Since this was a wash spin, the supernatant was discarded and the pellet rehomogenised in UREA buffer (Table 2.17) and agitated for 12-18 hours at room temperature to resuspend in buffer. Once the lysate (S3-SDS insoluble) dissolves completely, it is suspended in equal volumes of 2 x Loading Buffer (LB) and boiled for 5 min at 95°C. S3 fraction was then stored at -80°C.

EXTRACTION BUFFERS	COMPONENTS	FINAL CONCENTRATION
TBS BUFFER	Tris-HCl pH 7.4	50 mM
	NaCl	175 mM
	HALTS Cocktail	1X
SDS BUFFER	Tris-HCl pH 7.4	50 mM
	NaCl	175 mM
	SDS	5%
	HALTS Cocktail	1x
UREA BUFFER	Tris-HCl pH 7.4	50 mM
	NaCl	175 mM
	UREA	8 M
	SDS	8%
	HALTS Cocktail	1x

Table 2.17: Composition of reagents used for protein lysis.

2.4.1.3.3 Casting 10% Poly Acrylamide Gels (PAGE)

To pour gels, washed and cleaned glass plates (1.5mm) were wiped with 70% ethanol and set up using the gel casting apparatus. Once the apparatus is secured, the following (Table 2.18) recipe was used to pour the resolving gel.

RESOLVING GEL (2 X 1.5mm)	10%
dH20 (ml)	8
1.5M Tris (HCl) pH8.8 (ml)	5.2
10% SDS (ul)	200
Protogel (ml)	6.8
10% APS (ul)	100
TEMED (ul)	20

Table 2.18: Recipe for pouring Resolving Gel

The Ammonium persulphate (APS) and the TEMED are the polymerising agents which were added just before mixing and pouring the solution. Distilled water was used to top up the gel solution to avoid air-bubbles. The gel was left to set for 45 minutes.

Once the resolving gel was set, water was discarded and the following recipe (Table 2.19) was used to prepare and pour the stacking gel ensuring there are no air bubbles. The 10 well comb (1.5mm) was placed and the gel allowed to set for 20 minutes.

STACKING GEL	1x 1.5mm	2x 1.5mm	3x 1.5mm	4x 1.5mm	5x 1.5mm
dH20 (ml)	2.4	4.8	7.2	9.6	12
0.5M Tris (HCl), pH6.8 (ml)	1	2	3	4	5
Protogel (ml)	0.52	1.04	1.56	2.08	2.6
10% SDS (ul)	80	160	240	320	400
10% APS (ul)	40	80	120	160	200
TEMED (ul)	10	20	30	40	50

Table 2.19: Recipe for pouring 5% Stacking Gel

2.4.1.3.4 Western Blot

To standardise WB, a dummy blot for some drosophila-lysates positive ($Elav^{0N3R}$) and negative for tau protein (Oregan R) were run. These fly lysates were prepared by Dr. Megan Sealey. For the 3D cultures, the technique of WB was followed as per the protocols already standardised in the Mudher Lab. For total protein blots, 10 µl of sample and 10 µl of loading dye (2xSDS dye) were resolved in a 10% polyacrylamide gel. To analyse the presence of the protein Tau, protein fractions (10 µl protein fraction and 10 µl loading dye-2xSDS dye) S1, S2 and S3 were resolved in a 10% polyacrylamide gel. For the WB technique, PAGE electrophoresis was run at 120V until the pre-stained ladder (Page Ruler Plus Prestained Protein Ladder,2619, Thermo Scientific) was completely resolved on the gel. Proteins were then transferred onto a nitrocellulose membrane at 60V for 1:30 hours (Table 2.20). These blots were then blocked with 5% BSA in 0.5% tween-TBS solution (Table 2.20). The blots were incubated overnight in primary antibodies, made up in blocking buffer (Table 2.21) at 4°C on a shaker. After incubation these blots were washed three times for 5 minutes each with 0.5% tween TBS before incubation with secondary antibodies made in blocking buffer (Table 2.21) for 1hr at room temperature. The secondary antibodies were made up in blocking buffer at 1:20,000. The blots were washed with 0.5% tween-TBS for 5 minutes each time changing solution and rinsing with distilled water. The blots were scanned using the Licor Imaging System with Odyssey software to detect the signals.

BUFFERS	COMPONENTS	VOLUMES (ml) for 1L	FINAL CONCENTRATION
RUNNING BUFFER	Laemmli Buffer (10x)	100	1x
	Distilled Water	900	1x
TRANSFER BUFFER	Laemmli Buffer (10x)	100	1x
	Methanol	200	20%
	Distilled Water	700	1x
WASH BUFFER	TBS (10X)	100	1x
	Tween-20	5	0.5%
	Distilled Water	900	1x
BLOCKING BUFFER	Wash Buffer	100	1x
	Bovine Serum Albumin	5g	0.5%

Table 2.20: Recipes for different buffers used for WB

	Antibody	CATALOG #	Company	Concentration
Primary Antibody	**Dako Tau**	A0024	Dako	1:10000
	PhF1	Gift from Peter Davis	ALZFORUM	1:1000
	RD3	05-803	Millipore	1:1000
	RD4	05-804	Millipore	1:1000
	GAPDH	ab9485	Abcam	1:5000
	B-Actin	ab8224	Abcam	1:5000
Secondary Antibody	**goat anti-rabbit (800)**	926-32211	Licor	1:20000
	goat anti-mouse (680)	926-68070	Licor	1:20000

Table 2.21: List of Antibodies used for Western Blot.

2.5 Results

2.5.1.1 Morphology of cells in 3D cultures

In order to characterize the 3D cultures, the morphology of these cultures at different time points during the differentiation and maturation phase was first observed. The cells undergo different phases of morphological changes as they progressed during their differentiation in 3D cultures, starting from day 0 with visual changes until 6 weeks post 3D plating. Beyond this the cells (all cell lines) would form a round ball, which was optically dense and could not be properly observed under a light microscope. However, no differences in morphology between control and AD cell lines were observed. Thus, to describe the morphological changes in all the 3D cultures, hN8 has been shown as a representative culture. Initially, during the expansion phase, cells appear to have two different types of morphology in the 2D cultures. Most appear to have a fibroblast-like morphology (flat with elongated tapering edged spindle shaped cells), while a few appear to have spherical morphology (Fig 2.11). By day 6, cultures become 90-100% confluent.

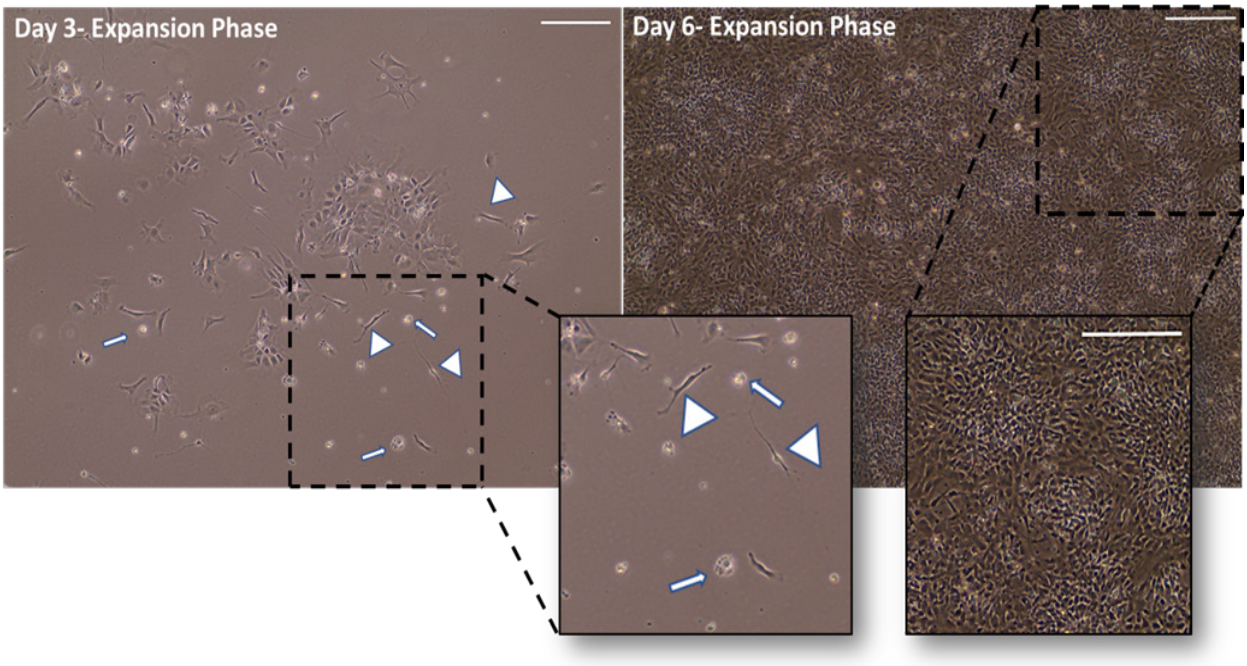

Figure 2.11: Morphology of iPSC derived NPC in 2D during the expansion phase – day 3 and 6. Light microscopy images of NPCs plated on Sure Bond for expansion in 2D till day 6 (Scale-20µm). The white arrows show cells with round morphology whereas the white arrowheads show fibroblast like cells. (n=1)

On day 6, the cells are seeded in 3D using Matrigel to allow differentiation and facilitate long-term maturation. All cells initially appear spherical post seeding in 3D cultures (Fig2.12), until a few days later where cells seem to become more elongated and, having neurites, make connections within the 3D cultures (Fig 2.13) and the walls of the chamber slides (Fig 2.14A).

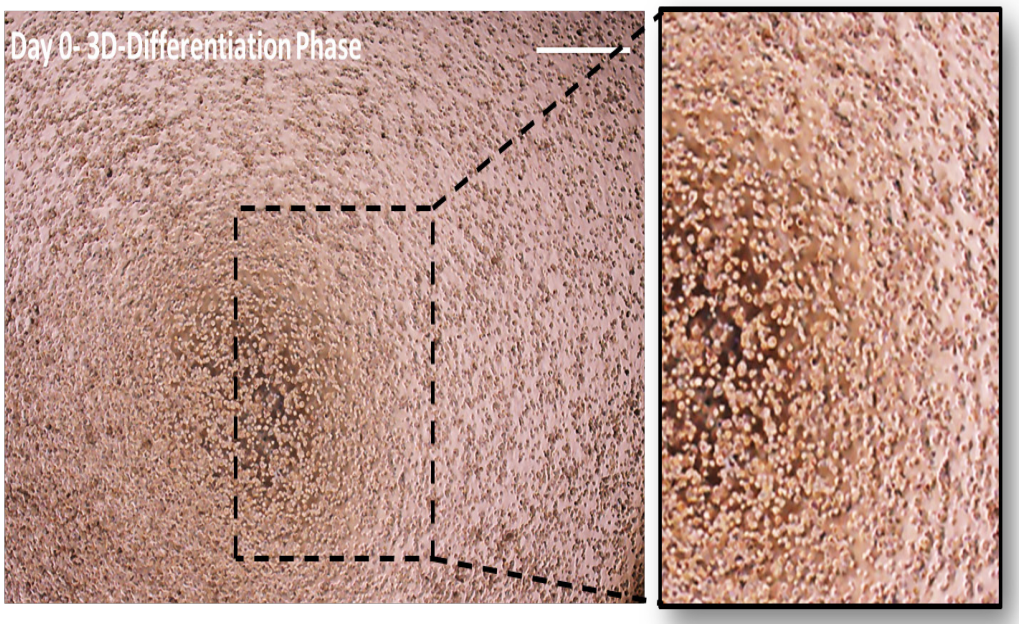

Figure 2.12: Morphology of iPSC derived NPC (hN8) in 3D during the initial stages of differentiation phase - day 0-3D culture. The cells appear spherical in morphology and are evenly suspended in Matrigel. Light microscopy images of NPCs after they were plated in Matrigel for differentiation in 3D (Scale-20µm) (n=1).

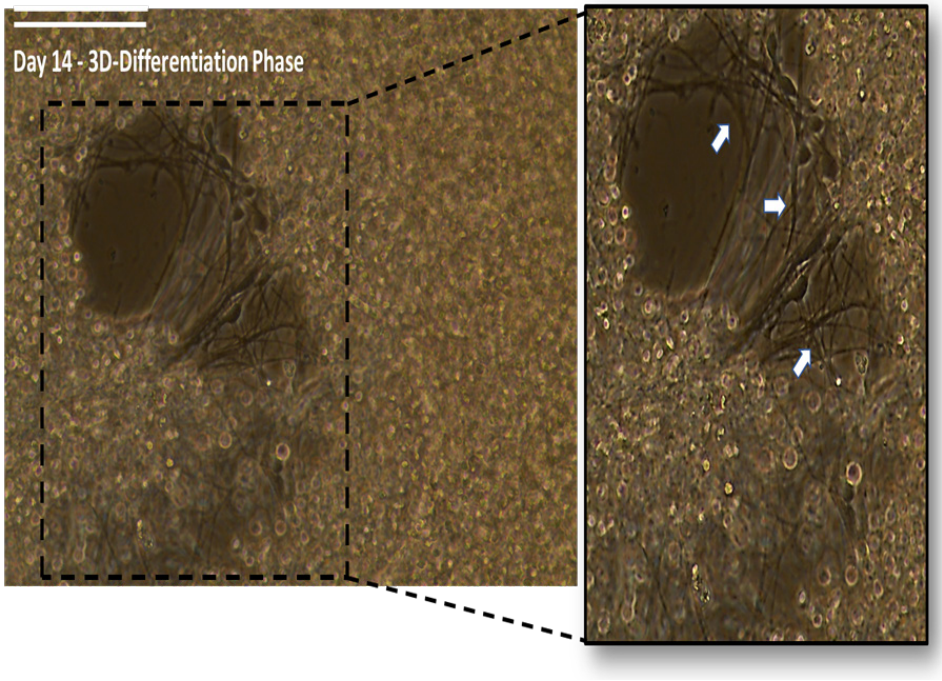

Figure 2.13: Morphology of iPSC derived 3D cultures (hN8) during the early stages of differentiation phase – week 2. Light microscopy images of cells forming neural like extensions and forming connections within layers of 3D (40x-magnification -Scale-10µm) (n=1).

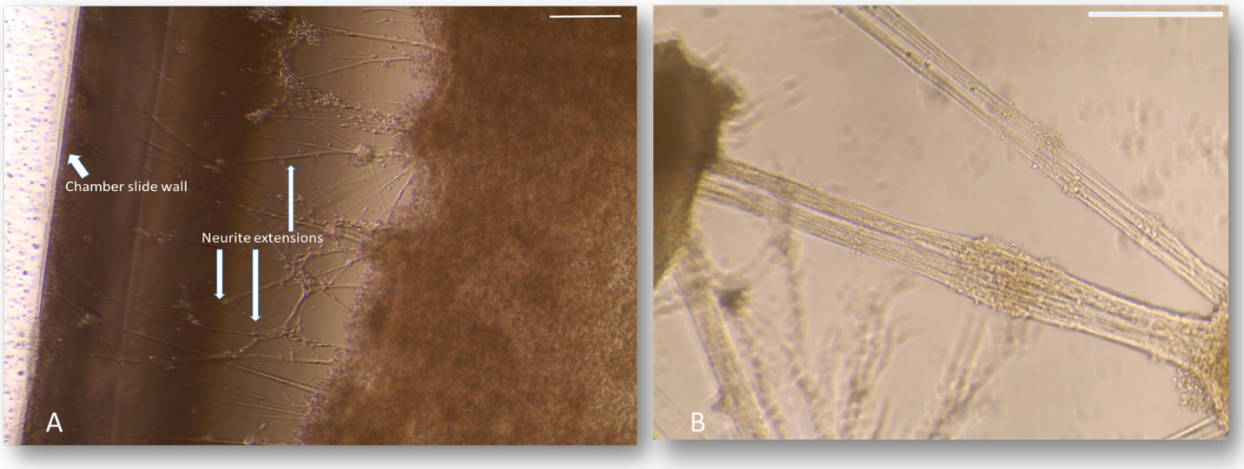

Figure 2.14:A: Morphology of cultures in 3D (hN8) during the early stages of differentiation phase-day 15. Light microscopy images of formation of long neurites between cell mass and the walls of chamber slides (Scale- 20µm). B: Morphology of cultures in 3D (hN8) during the differentiation phase- week 6. Light microscopy images of formation of long neural like extensions between cells (Scale-10µm).

By weeks 3 and 4, these neurite-like extensions elongate further and form denser and thicker connections between the cells and surrounding walls of the chamber slides. This could be because the matrix is being replaced by the matrix secreted by the cells as time progresses and the cells are looking for new points of contact.

By the end of 5- 6 weeks, cells come together and rearrange themselves, condensing in the middle and forming a self-organising sheet of cells having elongated connections with surrounding walls eventually detaching from the sides and base of the chamber slides (Fig 2.14B -2.15).

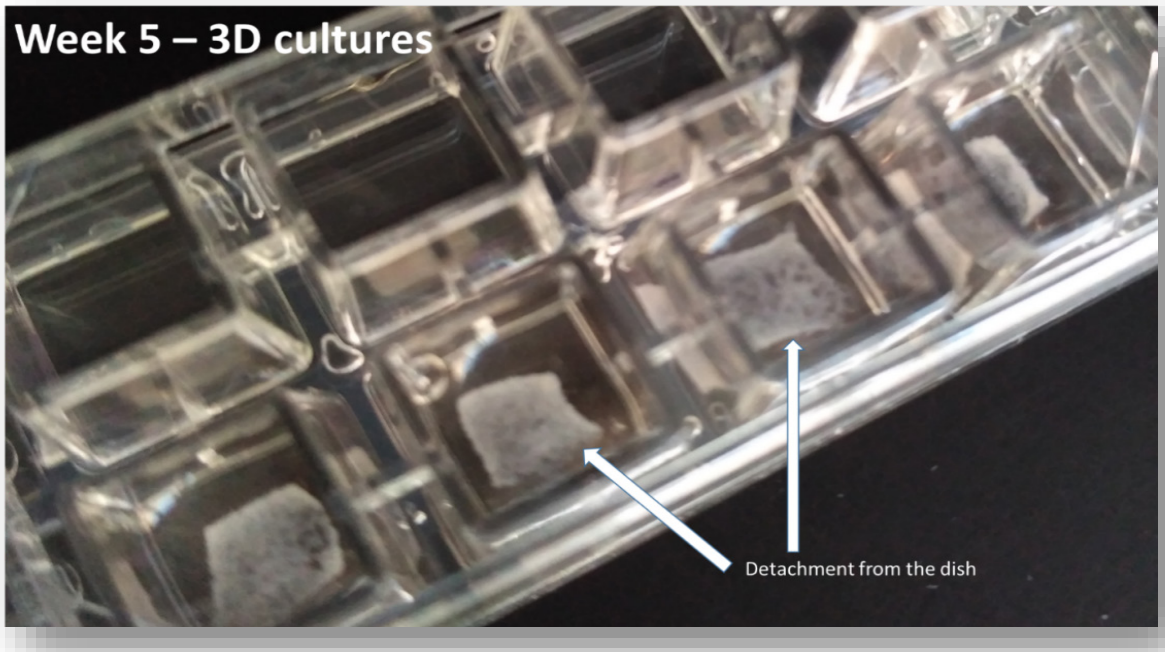

Figure 2.15: Image of 3D cultures in chamber slides , self-organising and detaching from the walls of the culture dish- week 5 (n=1).

These extensions are lost by 6-7 weeks post 3D plating and the cell sheet starts to float freely in the media. These sheets then curl up to form free floating ball-like structures (Fig 2.16)

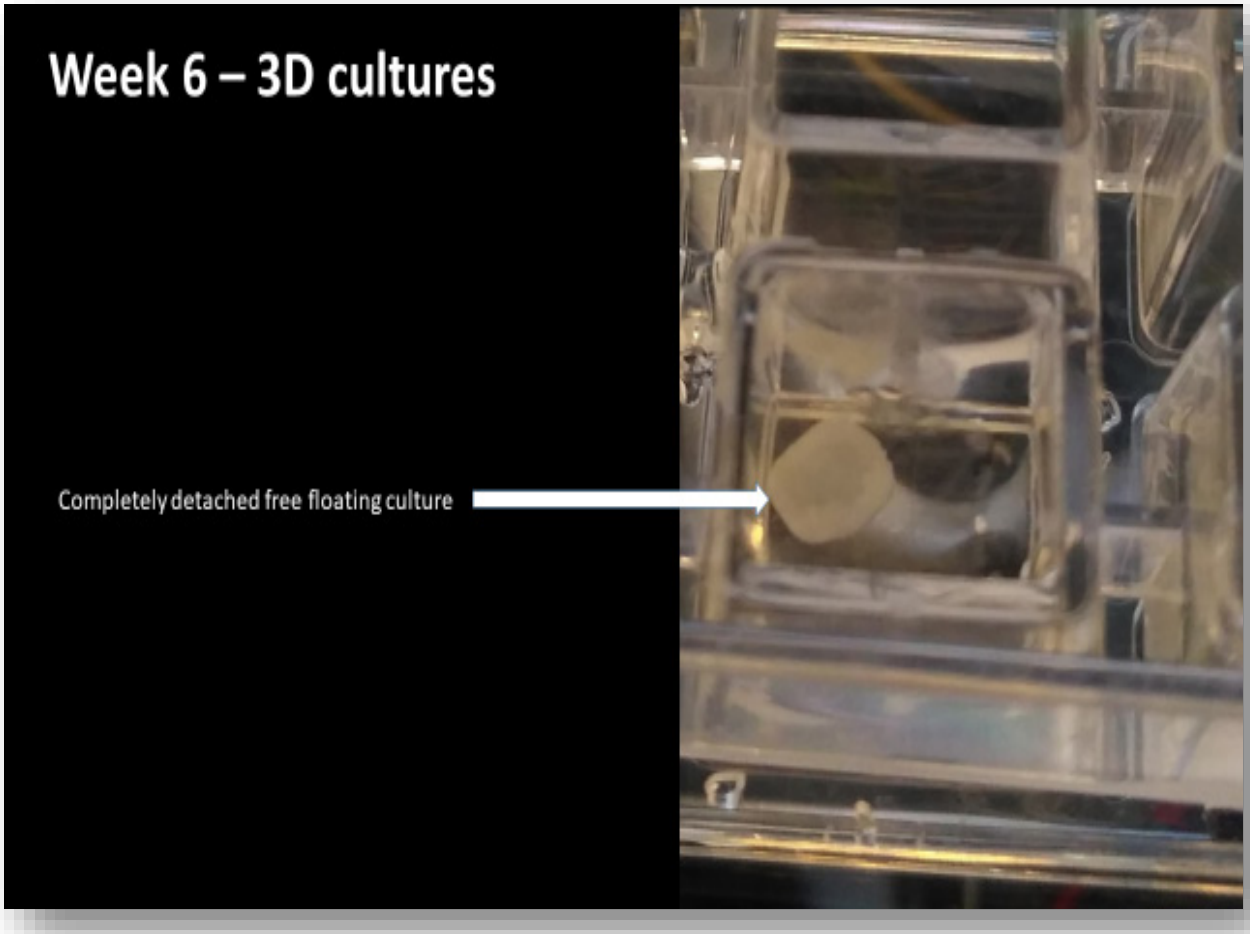

Figure 2.16: Image of 3D cultures in chamber slides , self-organising and detaching from the walls of the culture dish- week 5 (n=1).

Once the cell mass form this ball-like structure, it is difficult to further image them under a light microscope and obtain a clear picture. All 3D cultures were maintained in culture for up to 12 weeks; except hAD2 and hAD3 which were maintained for up to 18 weeks. Due to a shortage of cells, not all cells could be cultured till 18 weeks post differentiation *in vitro.*

2.5.1.2 Immunofluorescence for characterisation of the 3D cultures

To optimize the protocol for immunofluorescence for each antibody that would be used for the 3D cultures, we used 3D culture sections that were previously fixed from an experiment performed by Dr. Elodie Siney in 2015 (3D culture-2015). Since the 3D cultures and cell lines used were very expensive and we had a small sample size, it was crucial to use the existing samples for standardization. These are hAD2 cells cultured in 3D for a period of 18 weeks and are named as "3D Cultures-2015" (for convenience of naming samples). Once the staining methods were standardized on 3D cultures-2015, they were used for immunostaining my first set of 3D Cultures. Later, these protocols were adopted for the 2D cultures as well.

2.5.1.2.1 Standardisation of MAP2 immunofluorescence staining

Adult mouse brain sections were used as positive control for standardizing the antibody for immunostaining cultures. Triton-X100 0.2% was used as a standard for all buffers in immunofluorescence of the mouse brain sections (Fig 2.17 A). This was mainly to test if the antibody worked in a sample which is supposed to have the protein of interest, in this case MAP2, but not to optimize the staining in a mouse brain section, since all our samples are either human 2D or 3D cultures. Once the antibody was tested on the mouse brain sections, the antibody was used to stain human iPSC-derived 3D cultures. A stepwise method for trial and assessment was used to determine the best conditions for staining 3D cultures using MAP2 Ab. These stainings shown in Fig 2.17 were not done at the same time but rather sequentially to arrive at the best protocol for 3D. For permeabilization and subsequent washes, 0.1% Triton-X100 was used as a starting percentage (Fig 2.17 B). Since the antibody did not stain the structures clearly and distinctly, the strength of the permeabilization buffer was increased for better penetration of the antibody into the 3D cultures. The Triton X-100 percentage for permeabilization and subsequent washes was increased to 0.2% (Fig 2.17 C). A simple fluorescence microscope could not capture the clear distinct structures of 14-micron thick sections, as seen in figure 2.17.C, hence all imaging of 3D cultures was done using SP8, Leica Confocal Laser Scanning Microscope. Clear and distinct neurite extensions were seen in cultures when permeabilized with 0.2% Triton-X100 at 63x magnification – glycerol (Fig 2.17 D). A secondary only staining was used while staining each sample, as a negative control for immunofluorescence staining technique.

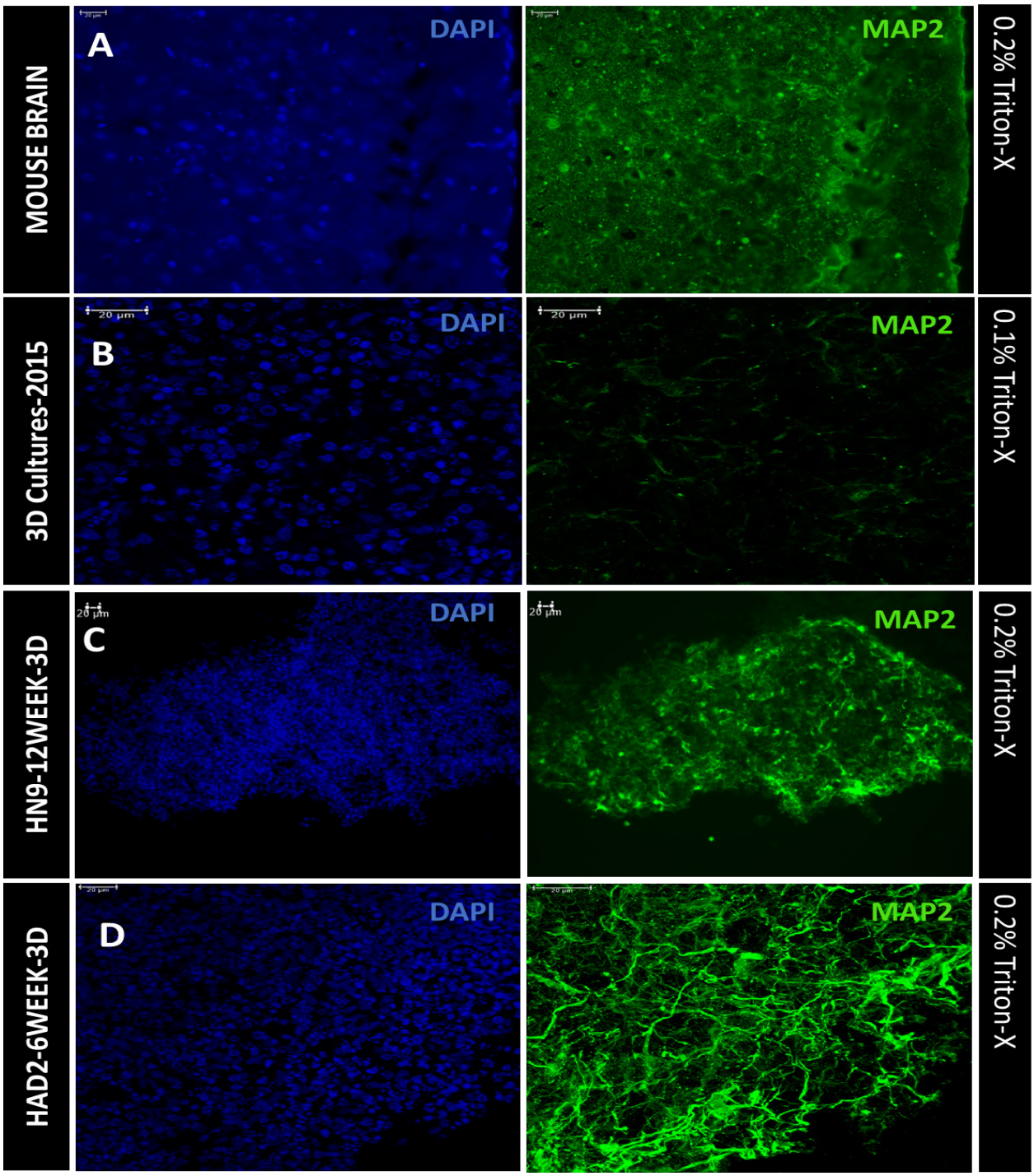

Figure 2.17: Immunofluorescence images of different samples stained to standardize neuronal marker MAP2 (green) and nuclear stain DAPI (blue)- (Scale bar = 20 µm). A. Immunofluorescence images of adult mouse brain section permeabilized with 0.2% triton-X100 (40X magnification). B. Confocal images of 3D-hAD2-18week post differentiation cultures permeabilized with 0.1% triton-X100 (63X magnification glycerol). C. Confocal images of hN9-3D cultures-12week post differentiation permeabilized with 0.2% triton-X100 (20X magnification). D. Confocal images of hAD2-6weeks post differentiation 3D cultures permeabilized with 0.2% triton-X100 (63X magnification glycerol) (n=1).

After considering the IF images from the different staining conditions used to optimize the MAP2 antibody for IF staining, the following conditions (Table 2.22) were finalised for MAP2 staining:

BUFFERS	COMPOSITION
Permeabilization Buffer (PBST)	PBS with 0.2 % Triton-X100
Blocking Buffer	PBST with 10% donkey serum
Wash Buffer	PBST
Primary Antibody Solution	MAP2 (1:200) diluted in Blocking Buffer
Secondary Antibody Solution	488-anti Rabbit (1:200) dissolved in Blocking Buffer
DAPI	2 µg/ml in (1: 500) dilution in PBST

Table 2.22: Optimised List of buffers used for staining with MAP2

2.5.1.2.2 Standardisation of Nestin immunofluorescence staining

Nestin is a stem cell marker, hence week 1 human foetal NSC cultures were used as a positive control for standardizing the antibody for immunostaining cultures. 1% triton-X100 was used to permeabilize cells (Fig 2.18 A). This was done mainly to test if the antibody works in a sample which is supposed to have the protein of interest, in this case Nestin. Once the antibody was tested, the antibody was used to stain human iPSC-derived 3D cultures. A stepwise method for trial and assessment was used to determine the best conditions for staining 3D cultures using Nestin Ab. These stainings shown in fig 2.18 were not done at the same time but rather sequentially to arrive at the best protocol for 3D. For permeabilization and subsequent washes, 0.2% triton-X100 was used as a starting percentage (Fig 2.18 B). Clear and distinct cellular structures were seen in the stained images when permeabilized with 0.2% triton-X100 and imaged using the Confocal Laser Scanning Microscope at 63x magnification – glycerol (Fig 2.18 C). A secondary only staining was used while staining each sample, as a negative control for immunofluorescence staining technique.

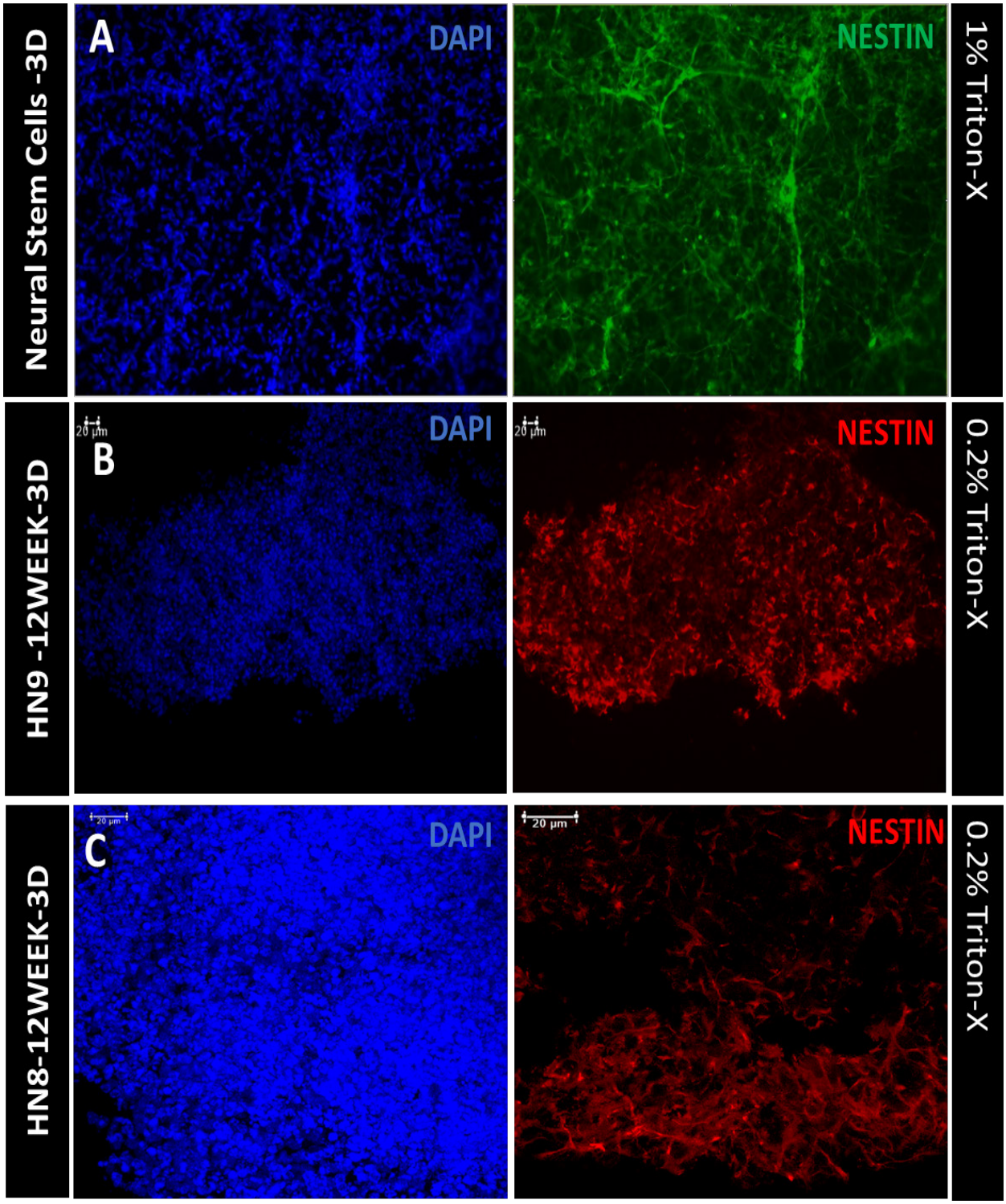

Figure 2.18: Immunofluorescence images of different samples stained to standardize stem cell marker Nestin (green/red) and nuclear stain dapi (blue)- (Scale bar = 20 µm). A. Immunofluorescence images of human foetal NSC 3D cultures permeabilized with 1% triton-X100 (40X magnification). B. Fluorescence microscope images of hN9- 12week post differentiation cultures permeabilized with 0.2% triton-X100 (20X magnification). C. Confocal images of hN8-3D cultures- 12week post differentiation permeabilized with 0.2% triton-X100 (63X magnification glycerol)(n=1).

After considering the IF images from the different staining conditions used to optimize the Nestin antibody for IF staining, the following conditions (Table2.23) were finalised for Nestin staining:

BUFFERS	COMPOSITION
Permeabilization Buffer (PBST)	PBS with 0.2 % Triton-X100
Blocking Buffer	PBST with 10% donkey serum
Wash Buffer	PBST
Primary Antibody Solution	Nestin (1:200) diluted in Blocking Buffer
Secondary Antibody Solution	568-anti Mouse (1:200) dissolved in Blocking Buffer
DAPI	2 µg/ml in (1: 500) dilution in PBST

Table 2.23: Optimised list of buffers used for staining with Nestin

2.5.1.2.3 Standardisation of GFAP immunofluorescence staining

Adult mouse brain sections were used as a positive control for standardizing the antibody for immunostaining cultures. 0.2% triton-X100 was used as a standard for all mouse brain sections (Fig 2.19 A). This was mainly to test if the antibody works in a sample which is supposed to have the protein of interest, in this case GFAP, but not to optimize the staining in a mouse brain section since all our samples are human 3D cultures. Once the antibody was tested on the mouse brain sections, the antibody was used to stain human iPSC-derived 3D cultures-2015. A stepwise method for trial and assessment was used to determine the best conditions for staining 3D cultures using GFAP Ab. These stainings shown in fig 2.19 were not done at the same time but rather sequentially to arrive at the best protocol for 3D. For permeabilization and subsequent washes, 0.2% triton-X100 was used as a starting percentage (Fig 2.19 B). Since the antibody did not stain the structures clearly and distinctly with high background noise, the triton X-100 percentage for permeabilization and subsequent washes was increased to 1% on the same cultures (Fig 2.19 C). Clear and distinct cellular structures were seen in the stained images when permeabilized with 1% triton-X100 and imaged using the SP8, Confocal Laser Scanning Microscope at 63x magnification – glycerol. A secondary only staining was used while staining each sample, as a negative control for immunofluorescence staining technique.

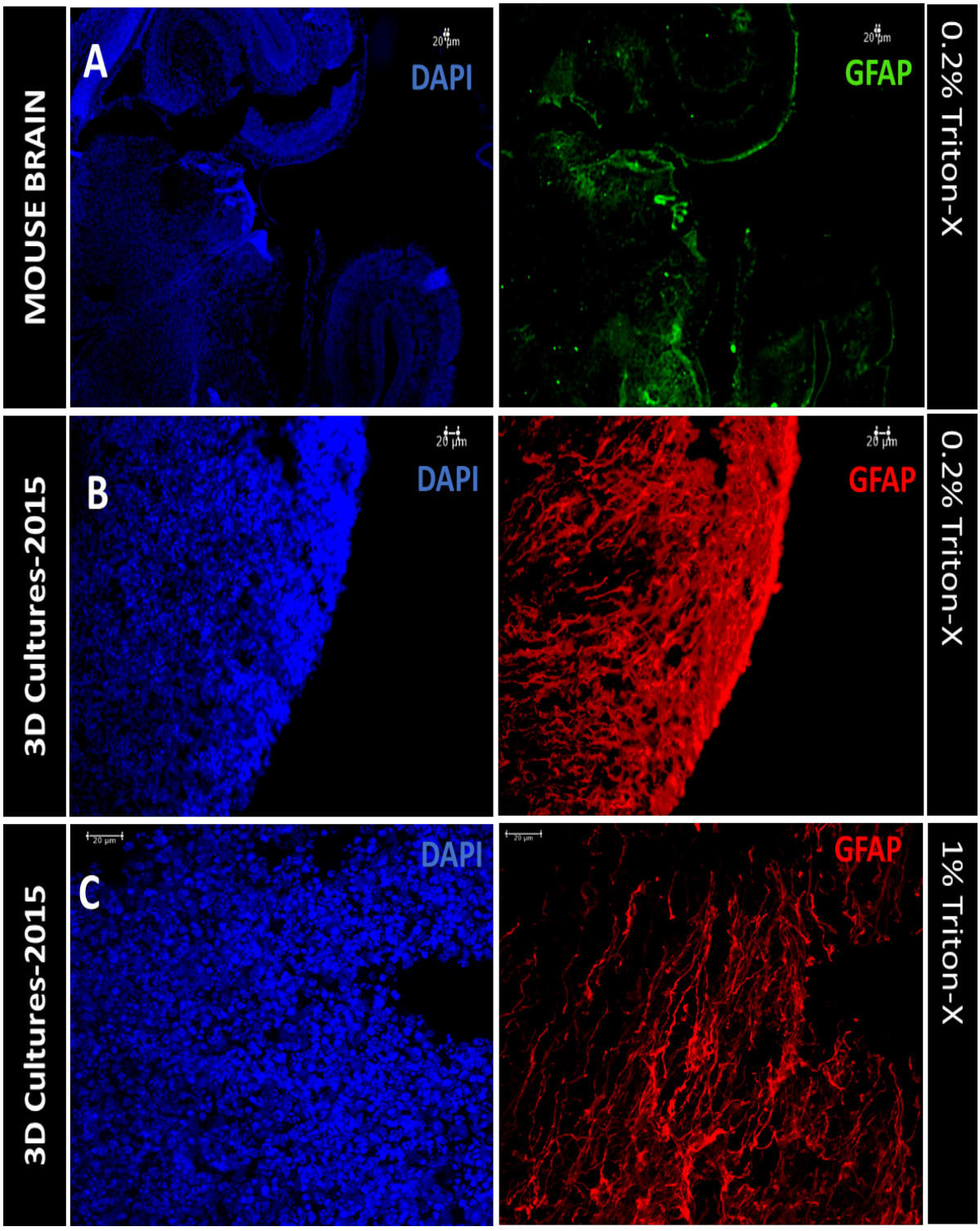

Figure 2.19: Immunofluorescence images of different samples stained to standardize astrocytic marker GFAP (green/red) and nuclear stain dapi (blue)- (Scale bar = 20 µm). A. Immunofluorescence images of adult mouse brain section permeabilized with 0.2% triton-X100 (20X magnification). B. Fluorescence microscope images of hAD2-18week post differentiation 3D cultures permeabilized with 0.2% triton-X100 (20X magnification). C. Confocal images of Had2-3D cultures-12week post differentiation permeabilized with 1% triton-X100 (20X magnification(n=1).

After considering the IF images from the different staining conditions used to optimize the GFAP antibody for IF staining, the following conditions (Table 2.24) were finalised for GFAP staining:

BUFFERS	COMPOSITION
Permeabilization Buffer (PBST)	PBS with 1% Triton-X100
Blocking Buffer	PBST with 10% donkey serum
Wash Buffer	PBST
Primary Antibody Solution	GFAP (1:200) diluted in Blocking Buffer
Secondary Antibody Solution	488-anti Rabbit antibody diluted in Blocking Buffer
DAPI	2 µg/ml in (1: 500) dilution in PBST

Table 2.24: optimised list of buffers used for staining with GFAP

2.5.1.2.4 Standardisation of B3 TUBULIN immunofluorescence staining

Adult mouse brain sections were used as a positive control for standardizing the antibody for immunostaining cultures. 0.2% triton-X100 was used as a standard for all mouse brain sections (Fig 2.20A). This was mainly to test if the antibody works in a sample which is supposed to have the protein of interest, in this case B3 Tubulin, but not to optimize the staining in a mouse brain section since all our samples are human 3D cultures. Once the antibody was tested on the mouse brain sections, the antibody was used to stain human iPSC-derived 3D cultures-2015. A stepwise method for trial and assessment was used to determine the best conditions for staining 3D cultures using B3-Tubulin Ab. These stainings shown in fig 2.20 were not done at the same time but rather sequentially to arrive at the best protocol for 3D. For permeabilization and subsequent washes 0.1% triton-X100 was used as a starting percentage (Fig 2.20.B). Since the antibody did not stain the structures clearly and distinctly with high background noise, the triton X-100 percentage for permeabilization and subsequent washes was increased to 1% (Fig 2.20.C). However, this did not give clear and distinct neural structures in 3D cultures as expected, hence changes were made according to the recommended usage of the company producing the antibody (BioLegend, Cat # 801201). The permeabilization and blocking was done using 1% triton-X100, 4% donkey serum and 1% BSA with 0.3M glycine. Clear and distinct cellular structures were seen in the stained images when permeabilized with the above-mentioned protocol and imaged using the SP8, Confocal Laser Scanning Microscope at 63x magnification – glycerol (Fig 2.20. D). A secondary only staining was used while staining each sample, as a negative control for immunofluorescence staining technique.

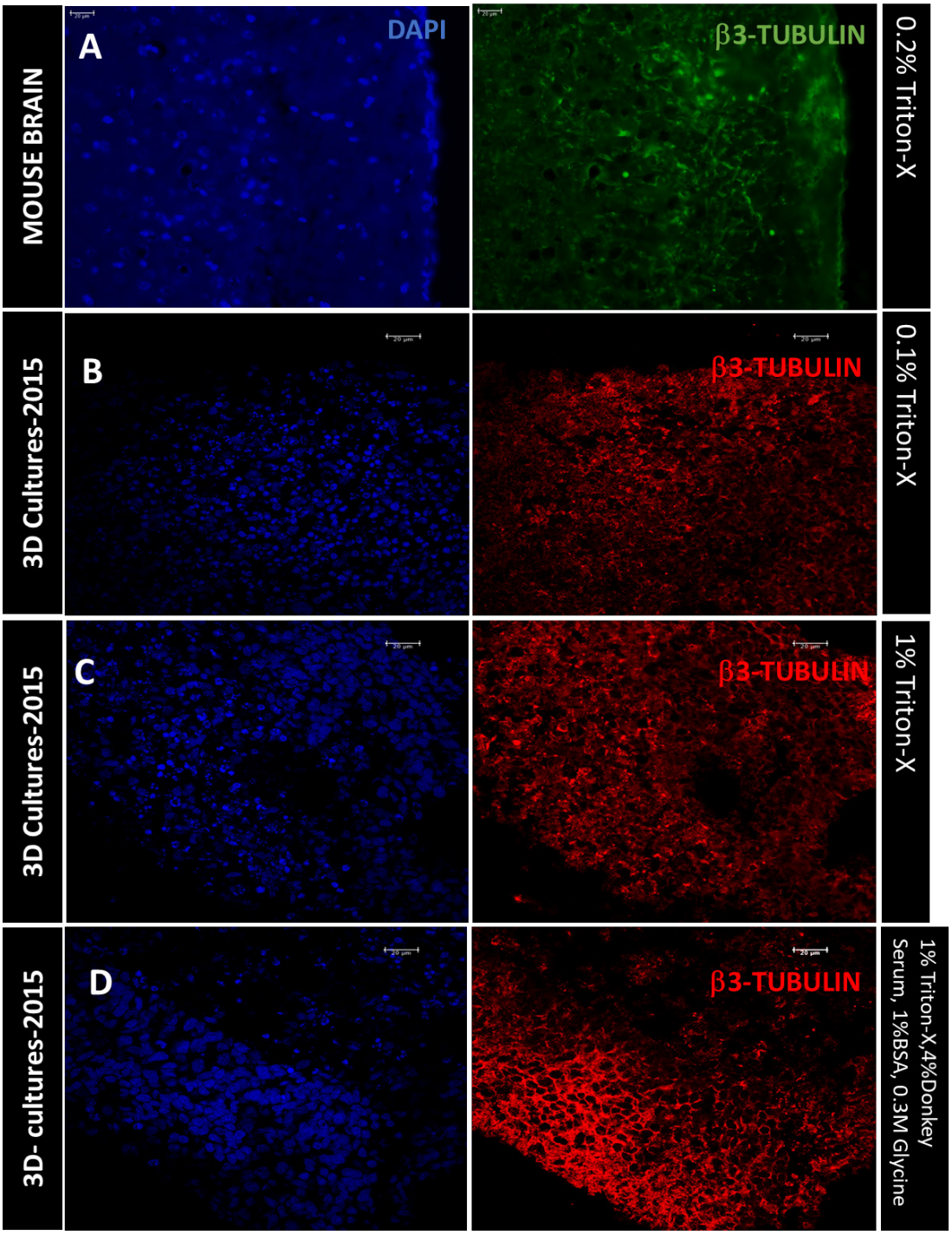

Figure 2.20: Immunofluorescence images of different samples stained to standardize neuronal marker β3-Tubuin (green/red) and nuclear stain dapi (blue)- (Scale bar = 20 µm). A. Immunofluorescence images of adult mouse brain section permeabilized with 0.2% triton-X100 (40X magnification). B. Confocal images of hAD2 18week post differentiation 3D cultures permeabilized with 0.1% triton-X100 permeabilization buffer (63X magnification glycerol). C. Confocal images hAD2 18week post differentiation 3D cultures permeabilized with 1% triton-X100 (63X magnification glycerol). D. Confocal images of hAD2 18week post differentiation 3D cultures permeabilized with 1% triton-X100, 4%donkey serum, 1%BSA and 0.3M glycine (63X magnification glycerol (n=1).).

After considering the IF images from the different staining conditions used to optimize the B3 Tubulin antibody for IF staining, the following conditions (Table 2.25) were finalised for B3 Tubulin staining:

BUFFERS	COMPOSITION
Permeabilization Buffer (PBST)	PBS with 1 % Triton-X100
Blocking Buffer	PBST- 1 % with 4% donkey serum, 1% Bovine Serum Albumin (BSA) and 0.3M glycine
Wash Buffer	PBST
Primary Antibody Solution	B3-Tubulin (1:200) dissolved in Blocking Buffer
Secondary Antibody Solution	568-anti (1:200) Mouse (raised in donkey) dissolved in Blocking Buffer
DAPI	2 µg/mL (1: 500) in PBST

Table 2.25: Optimised list of buffers used for staining with B3 Tubulin

2.5.1.2.5 Standardisation of Synapsin 1 immunofluorescence staining

Synapsin 1 is a synaptic marker found in the pre-synaptic compartment of neurons. Adult mouse brain sections were used as a positive control for standardizing the antibody for immunostaining cultures. 0.2% triton-X100 was used as a standard for all mouse brain sections (Fig 2.21 A). This was done mainly to test if the antibody works in a sample which is supposed to have the protein of interest, in this case Synapsin 1. Once the antibody was tested, the antibody was used to stain human iPSC-derived 3D cultures. A stepwise method for trial and assessment was used to determine the best conditions for staining 3D cultures using Synapsin 1 Ab. These stainings shown in Fig 2.21 were not done at the same time but rather sequentially to arrive at the best protocol for 3D. For permeabilization and subsequent washes 0.1% triton-X100 was used as a starting percentage (Fig 2.21 B). Since there was a higher background signal with no distinct structures identifiable, the permeabilization strength was increased to 0.2%. Clear and distinct cellular structures were seen in the stained sections when permeabilized with 0.2% triton-X100 and imaged using the Confocal Laser Scanning Microscope at 63x magnification – glycerol (Fig 2.21 C). A secondary only staining was used

while staining each sample, as a negative control for immunofluorescence staining technique.

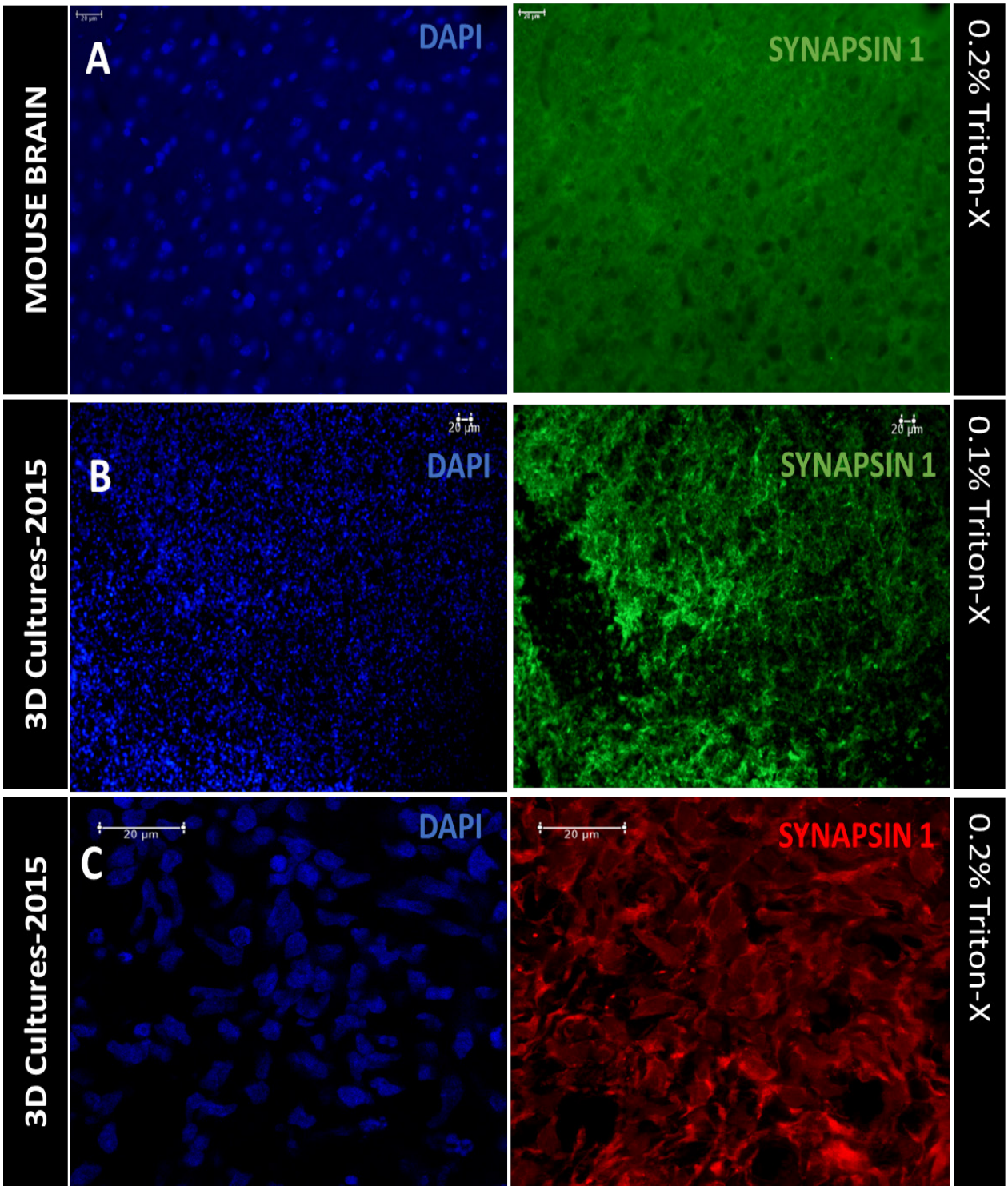

Figure 2.21: Immunofluorescence images of different samples stained to standardize synaptic marker Synapsin 1 (green/red) and nuclear stain dapi (blue)- (Scale bar = 20 µm). A. Immunofluorescence images of adult mouse brain section permeabilized with 0.2% triton-X100 (40X magnification). B. Fluorescence microscope images of hAD2-18week post differentiation 3D cultures permeabilized with 0.1% triton-X100 (40X magnification). C. Confocal images of hAD2-3D cultures-12week post differentiation permeabilized with 1% triton-X100 (63X magnification-glycerol) (n=1).

After considering the IF images from the different staining conditions used to optimize the Synapsin1 antibody for IF staining, the following conditions (Table 2.26) were finalised for Synapsin1 staining:

BUFFERS	COMPOSITION
Permeabilization Buffer (PBST)	PBS with 0.2 % Triton-X100
Blocking Buffer	PBST with 10% donkey serum
Wash Buffer	PBST
Primary Antibody Solution	Synapsin1 (1:200) diluted in Blocking Buffer
Secondary Antibody Solution	568-anti Rabbit (1:200) dissolved in Blocking Buffer
DAPI	2 µg/ml in (1: 500) dilution in PBST

Table 2.26: Optimised list of buffers used for staining with Synapsin1

2.5.1.2.6 Standardisation of VGLUT1 and GAD65/67 immunofluorescence staining

VGLUT1 is a marker for glutamatergic neuron or glutamate secreting neurons, whereas GAD65/67b is a marker for GABAergic neurons. Adult mouse brain sections were used as a positive control for standardizing both antibodies for immunostaining cultures. 0.2% triton-X100 was used as a standard for all mouse brain sections (Fig 2.22 A and C). This was done mainly to test if the antibody works in a sample which is supposed to have the protein of interest, in this case Synapsin 1. Once the antibody was tested, the antibody was used to stain human iPSC-derived 3D cultures. A stepwise method for trial and assessment was used to determine the best conditions for staining 3D cultures using VGLUT 1 and GAD65/67 Abs separately. These stainings shown in fig 2.22 were not done at the same time but rather sequentially to arrive at the best protocol for 3D. The permeabilization and blocking was done using 1% triton-X100, 4% donkey serum and 1%BSA with 0.3M glycine. Clear and distinct cellular structures were seen in the stained images when permeabilized with the above-mentioned protocol and imaged using the SP8, Confocal Laser Scanning Microscope at 63x magnification – glycerol (Fig 2.22 B and D). A secondary only staining was used while staining each sample, as a negative control for immunofluorescence staining technique.

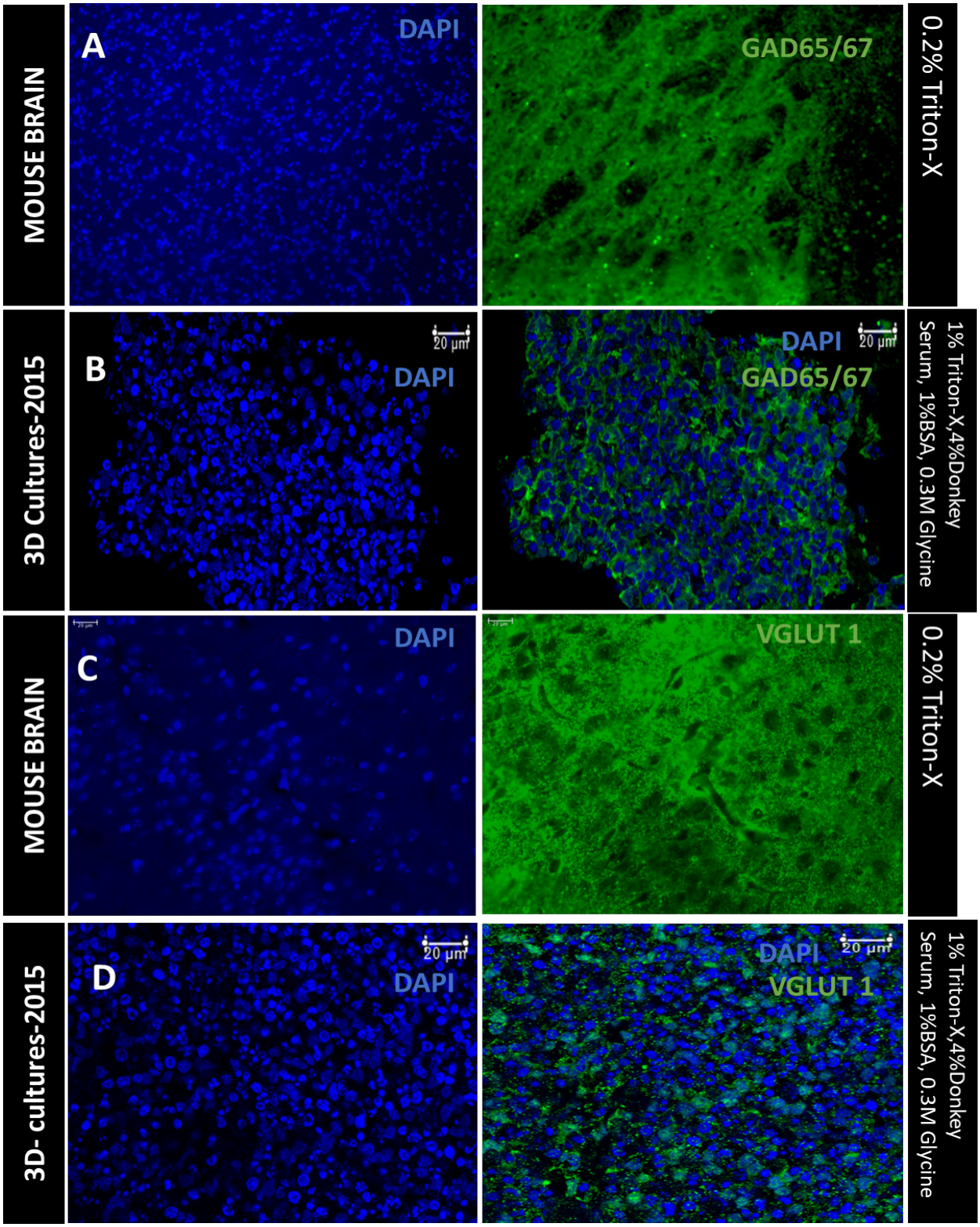

Figure 2.22: Immunofluorescence images of different samples stained to standardize synaptic marker Synapsin 1 (green/red) and nuclear stain dapi (blue)- (Scale bar = 20 µm). A and C- Immunofluorescence images of adult mouse brain section permeabilized with 0.2% triton-X100 (40X magnification). B and D- Confocal images of hAD2-18week post differentiation 3D cultures (63X magnification-glycerol) (n=1).

After considering the IF images from the different staining conditions used to optimize the GAD65/67 and VGLUT 1 antibody for IF staining. the following conditions (Table 2.27) were finalised for their staining:

BUFFERS	COMPOSITION
Permeabilization Buffer (PBST)	PBS with 1 % Triton-X100
Blocking Buffer	PBST- 1 % with 4% donkey serum, 1% Bovine Serum Albumin (BSA) and 0.3M glycine
Wash Buffer	PBST
Primary Antibody Solution	GAD65/67 (1:200) dissolved in Blocking Buffer VGLUT 1 (1:200) dissolved in Blocking Buffer
Secondary Antibody Solution	488-anti (1:200) Rabbit (raised in donkey) dissolved in Blocking Buffer
DAPI	2 µg/mL (1: 500) in PBST

Table 2.27: optimised list of buffers used for staining with GAD65/67 and VGLUT1

2.5.1.2.7 Characterisation of human iPSC-derived 3D neural Cultures.

Once the antibodies were optimized on the previous 3D cultures, immunofluorescence was performed on all five cell lines (Table 2.7). To characterize the cells in 3D cultures, immunofluorescence was performed on cryo-sectioned slides with 14-micron thick slices for time points 6 weeks, 12 weeks, and 18 weeks. Images were taken on a Leica TCS-SP8 Confocal Microscope for better resolution and to avoid issues with background staining.

As explained in the methods section above, the primary aim of this chapter was to standardize the different techniques on 3D cultures to get optimized results. Hence all cell line-sections were not stained for all the antibodies standardized in this chapter, except for MAP2 and Nestin (Fig 2.29/ 2.30/ 2.31) It was more to check if the cells had differentiated well and if the differentiation protocol required any further optimization.

To check the prescence of astrocytes GFAP was used to stain the 3D cultures. 3D cultures express GFAP at 12 weeks post 3D plating (Fig 2.23). GFAP is a type III intermediary filament that makes up the central cytoskeletal framework of the astrocytes (Eng, Ghirnikar and Lee, 2000).

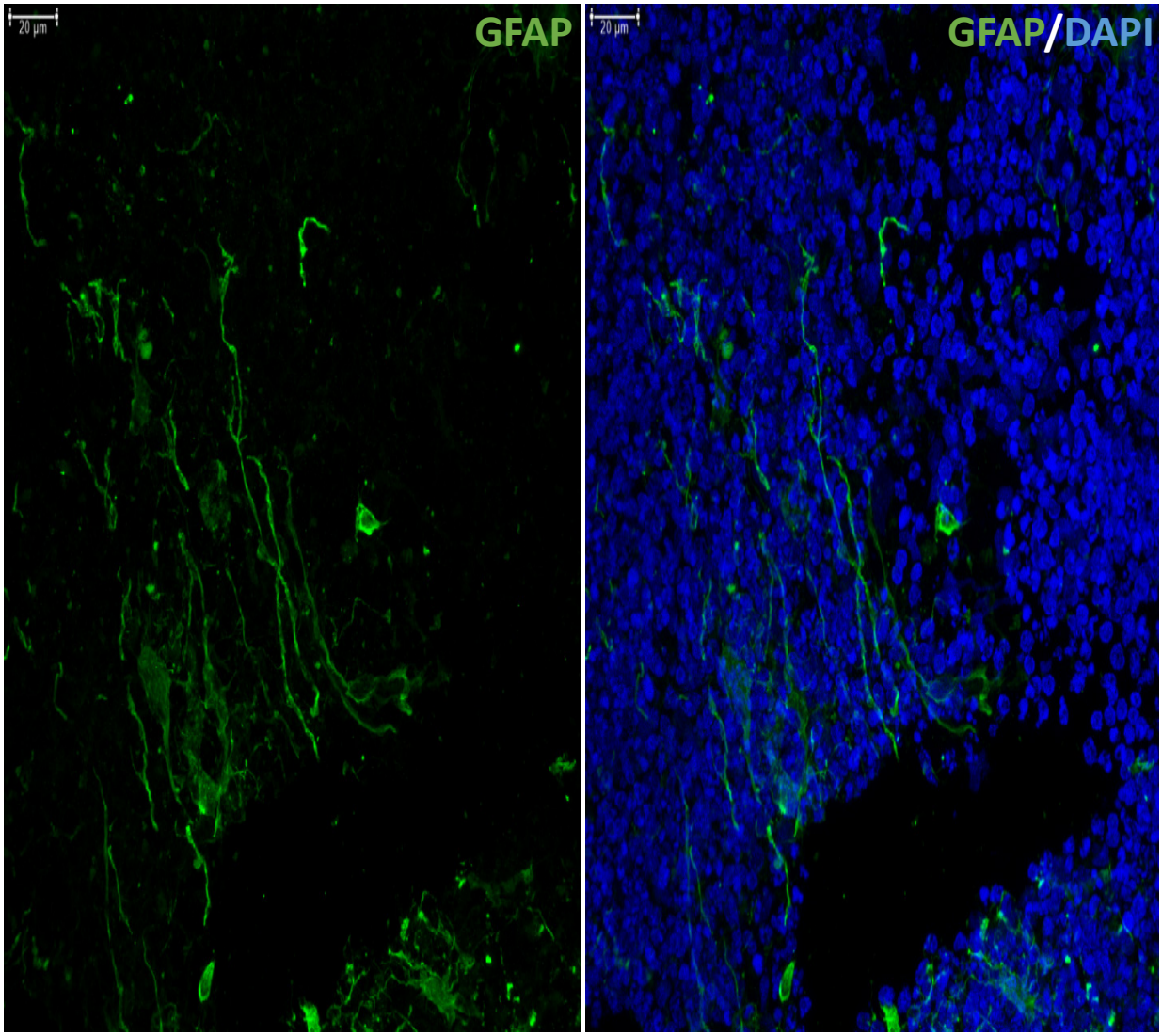

Figure 2.23: Some hN8 cells at 12 weeks post differentiation express GFAP . DAPI was used as a nuclear stain. Only a small percentage of cells express GFAP (Scale -20µm) (n=1).

GFAP expression is seen in the cytoplasmic compartment of the cells in culture and is seen in the long processes and filaments of astrocytes. In our 3D cultures, GFAP is localised to the cytoplasmic compartment extending into the filaments of the cells, an expression pattern expected in astrocyte.

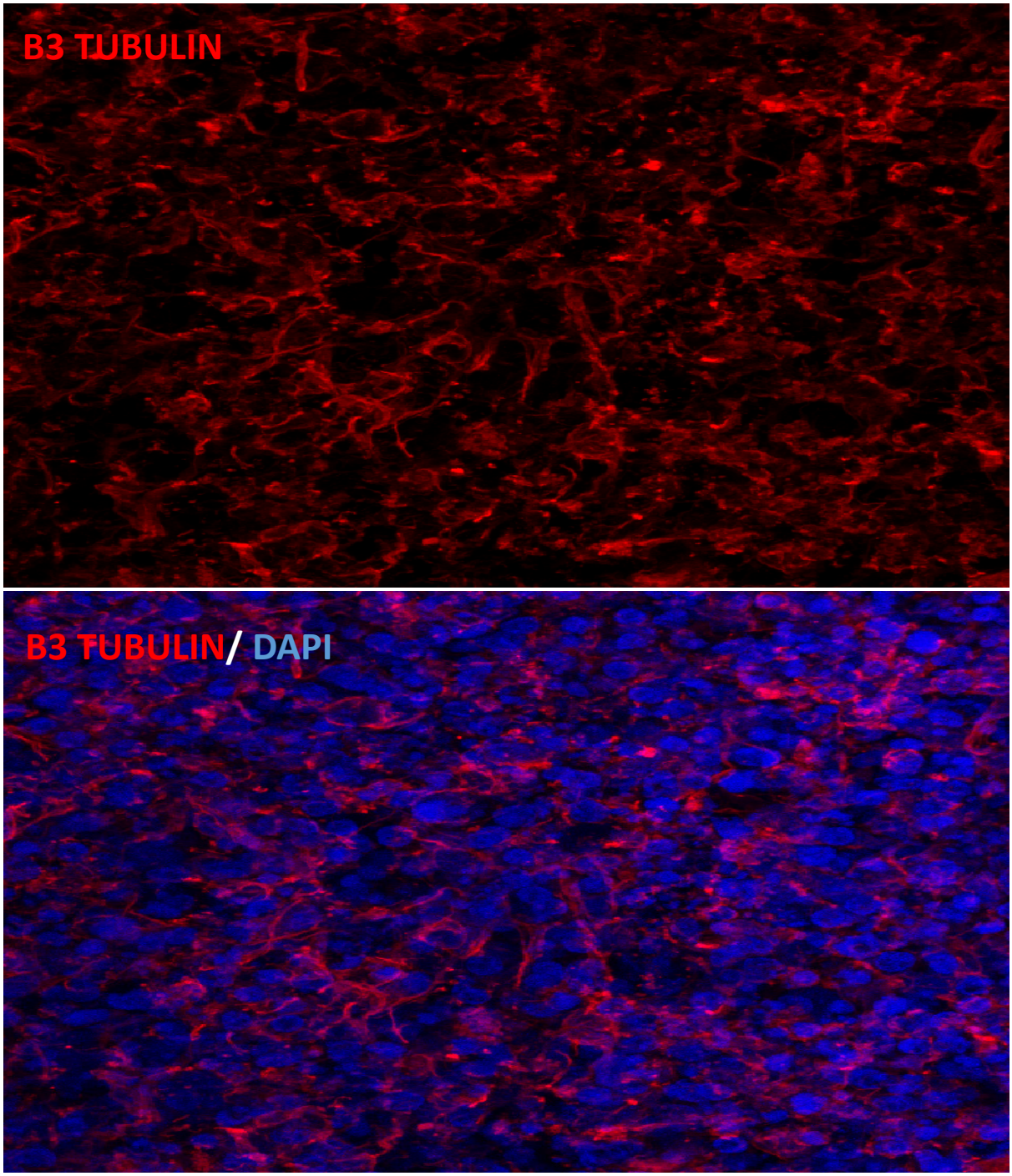

Figure 2.24: hAD2 cells at 6 weeks post differentiation express β3 tubulin (red), an early neuronal differentiation marker, and counterstained with DAPI (blue) (n=1).

β3-tubulin, an early neuronal differentiation marker, was used to observe the prescence of neurons in the culture. The majority of cells in 3D cultures express β3-tubulin as early as 6

weeks post 3D plating (Fig 2.24). β3-tubulin is a class III member of the tubulin family and plays an important role in microtubule assembly.

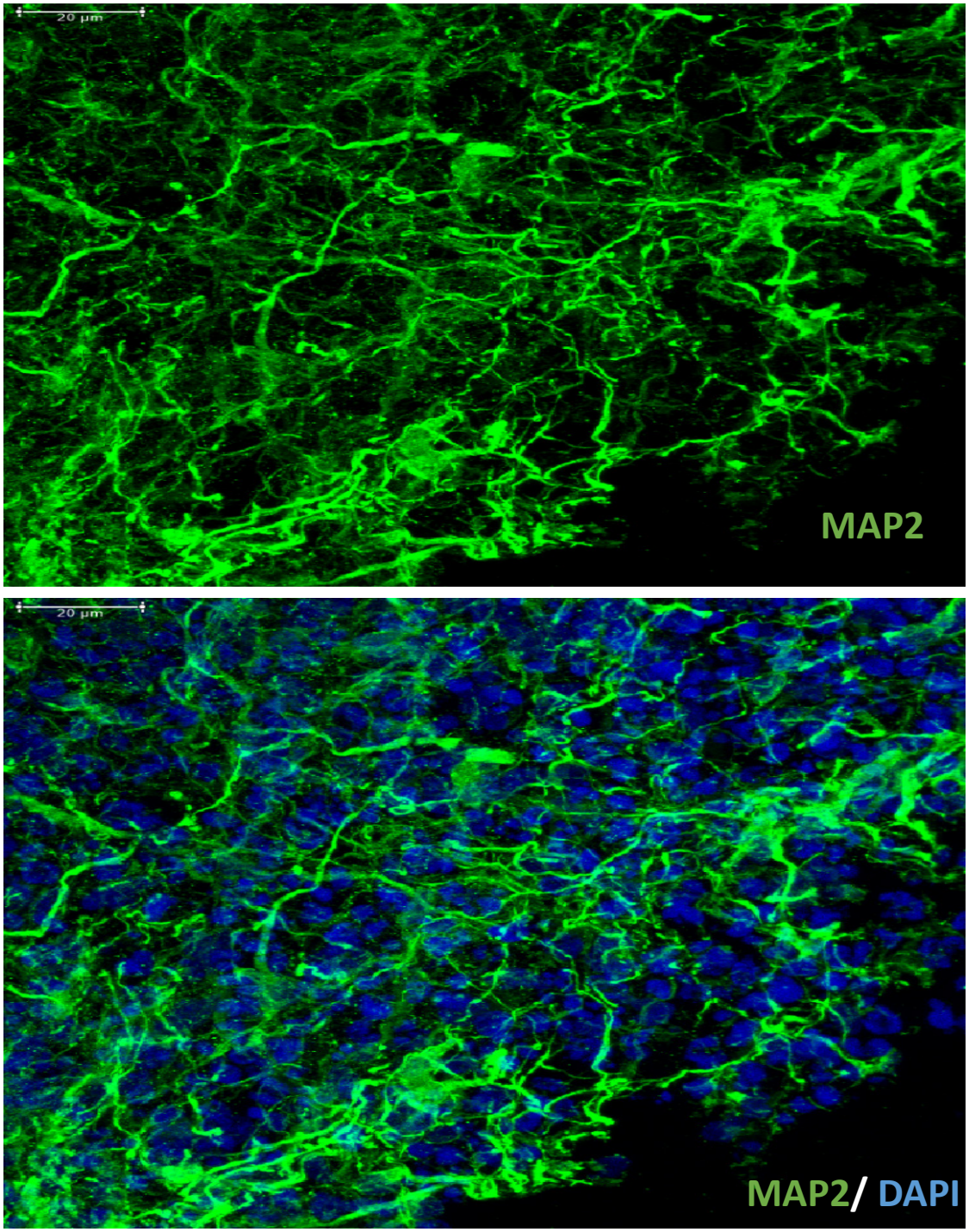

Figure 2.25: hAD2 cells at 6 weeks post differentiation express MAP2 , a late neuronal differentiation marker (n=1).

It is expressed in the cytoskeletal compartment of neurons and is seen in the long processes and cell body. As expected, 3D cultures express β3-tubulin localised in the cytoskeletal and processes of neurons

MAP2, a late neuronal differentiation marker, was seen to increase from 6 weeks to 18 weeks in culture (Fig 2.25). MAP2 is a protein found in the somatodendritic compartment of neurons (Kosik and Finch, 1987). Around 60% of cells in 3D cultures seem to express this late differentiation neuronal marker and as expected in the somatodendritic compartment.

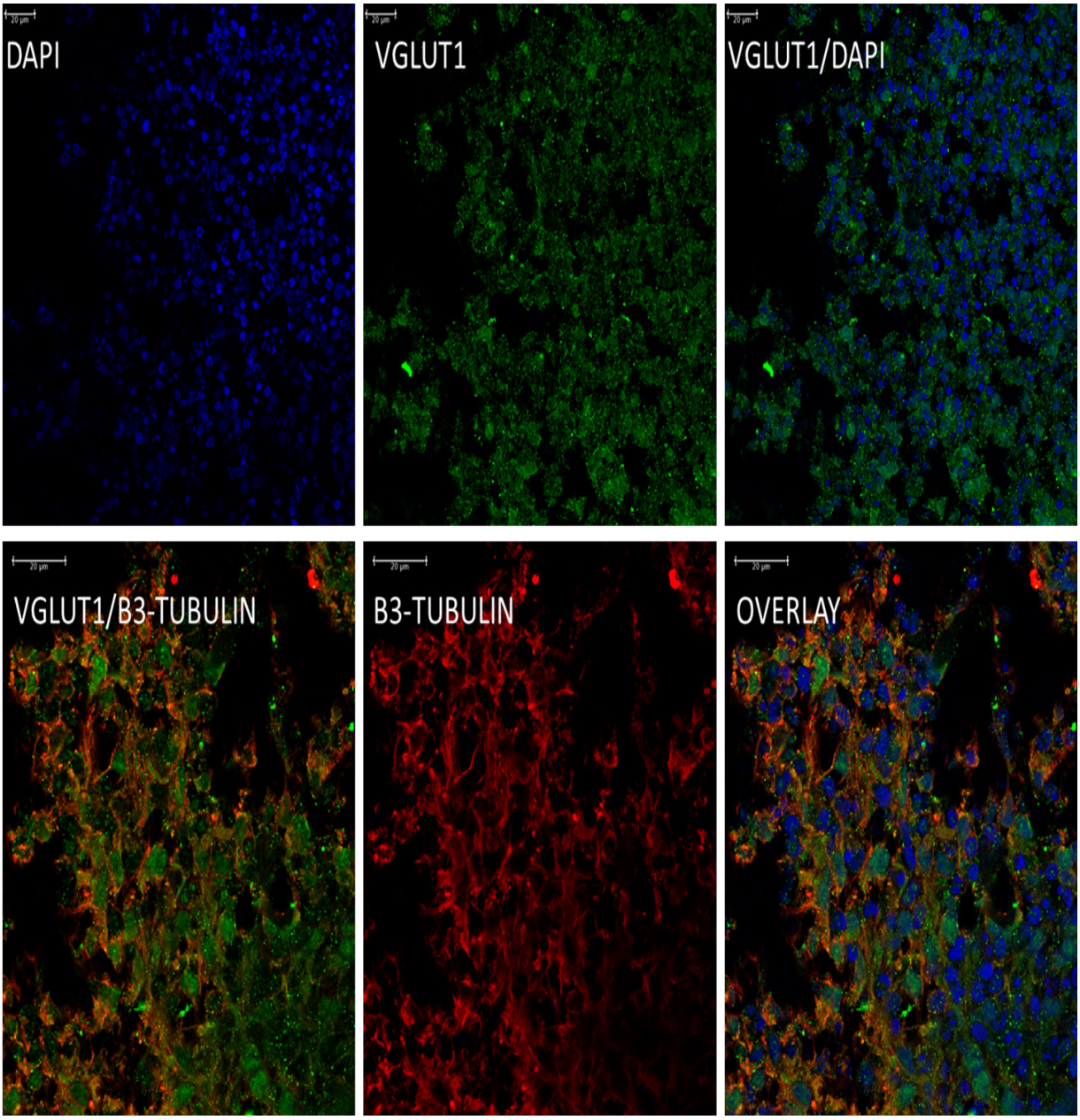

Figure 2.26: hN8 cells at 6 weeks post differentiation express VGLUT1 (green), a marker for glutamatergic neuron, and B3 Tubulin, an early-late neuronal marker, counterstained with DAPI (blue) (Scale bar= 20µm) (n=1).

VGLUT1, a glutamate transporter protein seems to be seen in majority of cells as early as 6 weeks into differentiation (Fig 2.26). VGLUT1 is a protein associated with the membranes of synaptic vesicles. VGLUT1 is found in the somatodendritic compartment as well as the axonal terminals of neurons (Herzog *et al.*, 2004). The staining however is not as per expectation and needs further optimization.

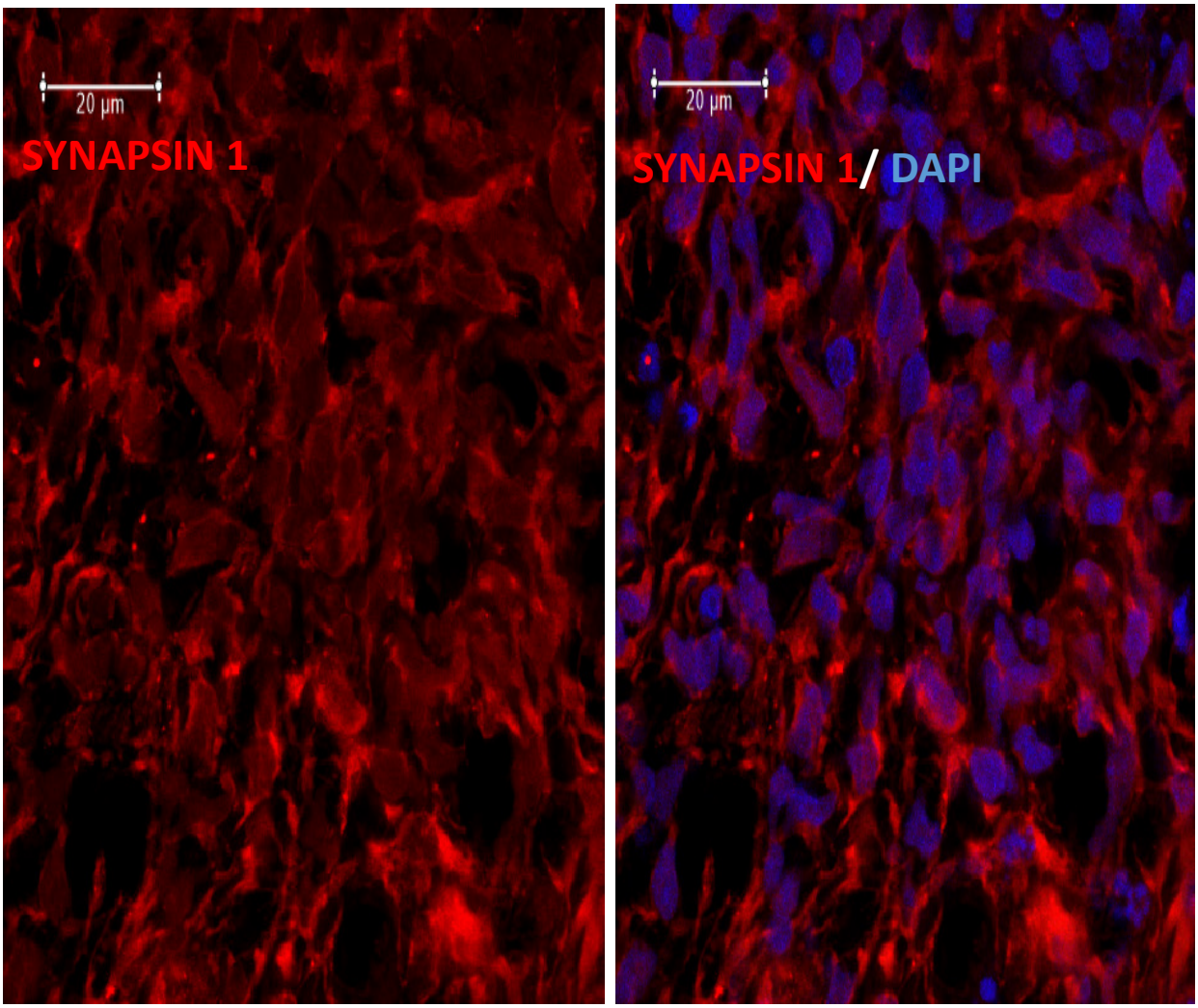

Figure 2.27: hAD2 cells at 6 weeks post differentiation express Synapsin 1 (red), a presynaptic neuronal marker, counterstained with DAPI (blue) (Scale bar= 20µm) (n=1.

Synapsin 1, a presynaptic marker, is expressed in most of the cells after 6 weeks (Fig 2.27). Synapsin 1 is found in the pre-synaptic vesicle and is seen as punctate-like expression all over the cell body and axonal terminals. However, in our staining the expression seems to occur all across the membrane. Further optimization is required for Synapsin 1 staining.

Both VGLU1 and Synapsin1 seem different to the expected pattern of staining. This could either be due to the structure of the cell in the 3D microenvironment, or the cells are not mature enough to have the proteins localised in the expected cellular compartment.

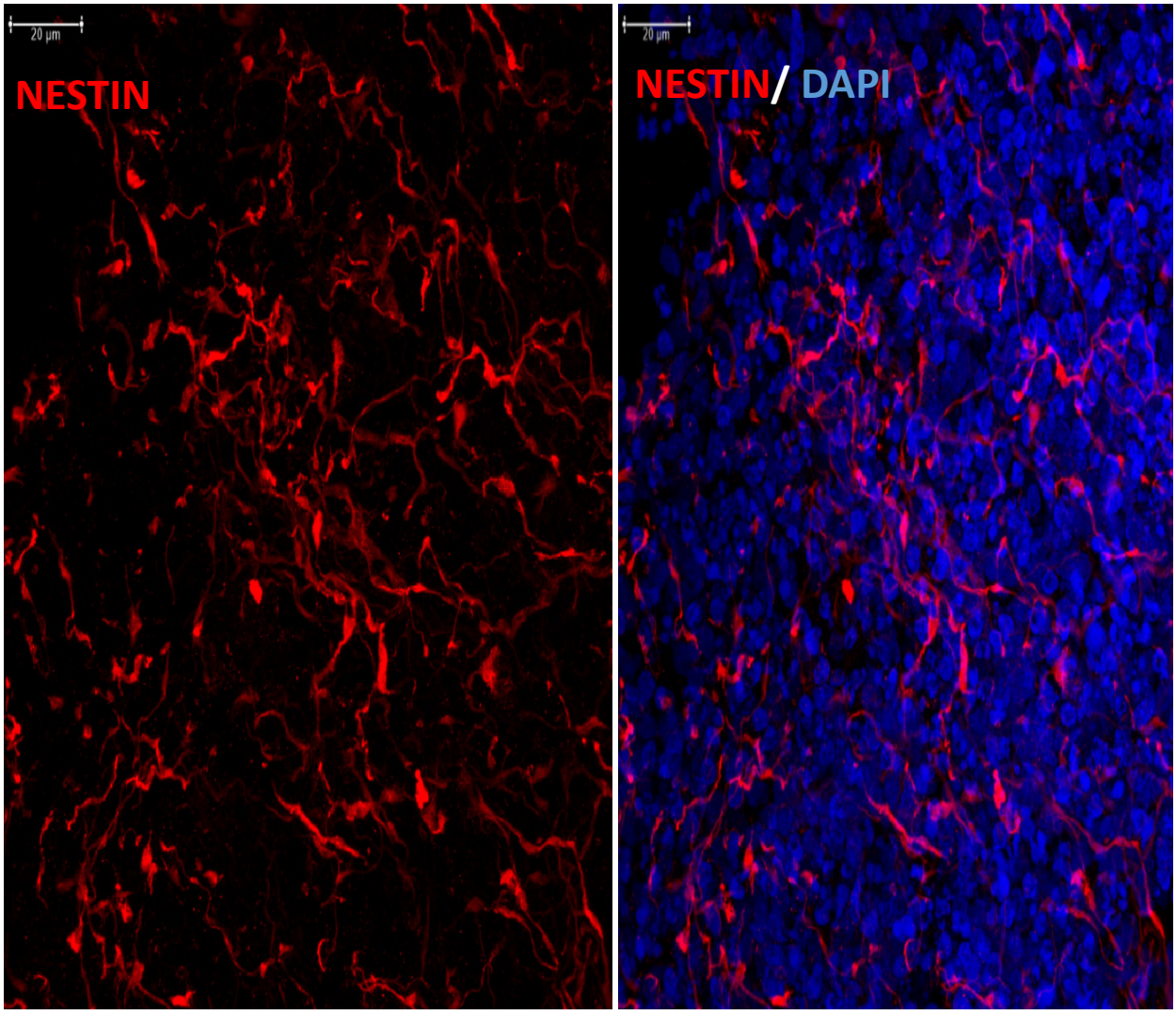

Figure 2.28: hN8 cells at 6 weeks post 3D plating express Nestin (red), a neuronal stem/ progenitor cell marker, counterstained with DAPI (blue) (Scale bar= 20µm) (n=1).

Nestin is a neural stem cell marker. It is a type VI intermediate filament protein forming a major component of cytoskeleton. Its expression is seen over the cell body and extends to the neurofilaments. Nestin expression is seen in the 3D cultures at 6 weeks as well as 12 weeks post 3D plating (Fig 2.28).

A montage of the compiled MAP2 (Fig 2.29), NESTIN (Fig 2.30) and DAPI (Fig 2.31) staining of all the cell lines reveals that by judging the number of MAP2 positive cells, there is a good amount of mature neurons, but at the same time the expression of Nestin at 12 weeks post differentiation in 3D seems a bit of a concern. The reason for expression of Nestin positive cells even at 12 weeks post 3D plating could be that not all cells have transitioned from a stem cell-like state to have completely differentiated into mature neurons. Looking back into the growth factors used for the differentiation of 3D cultures, Retinoic Acid could be one of the reasons for incomplete differentiation., which is further explained in the next chapter. Unfortunately, the samples hAD3-6week and hAD2-12week were not saved or fixed properly, thus there were no signals in their stains.

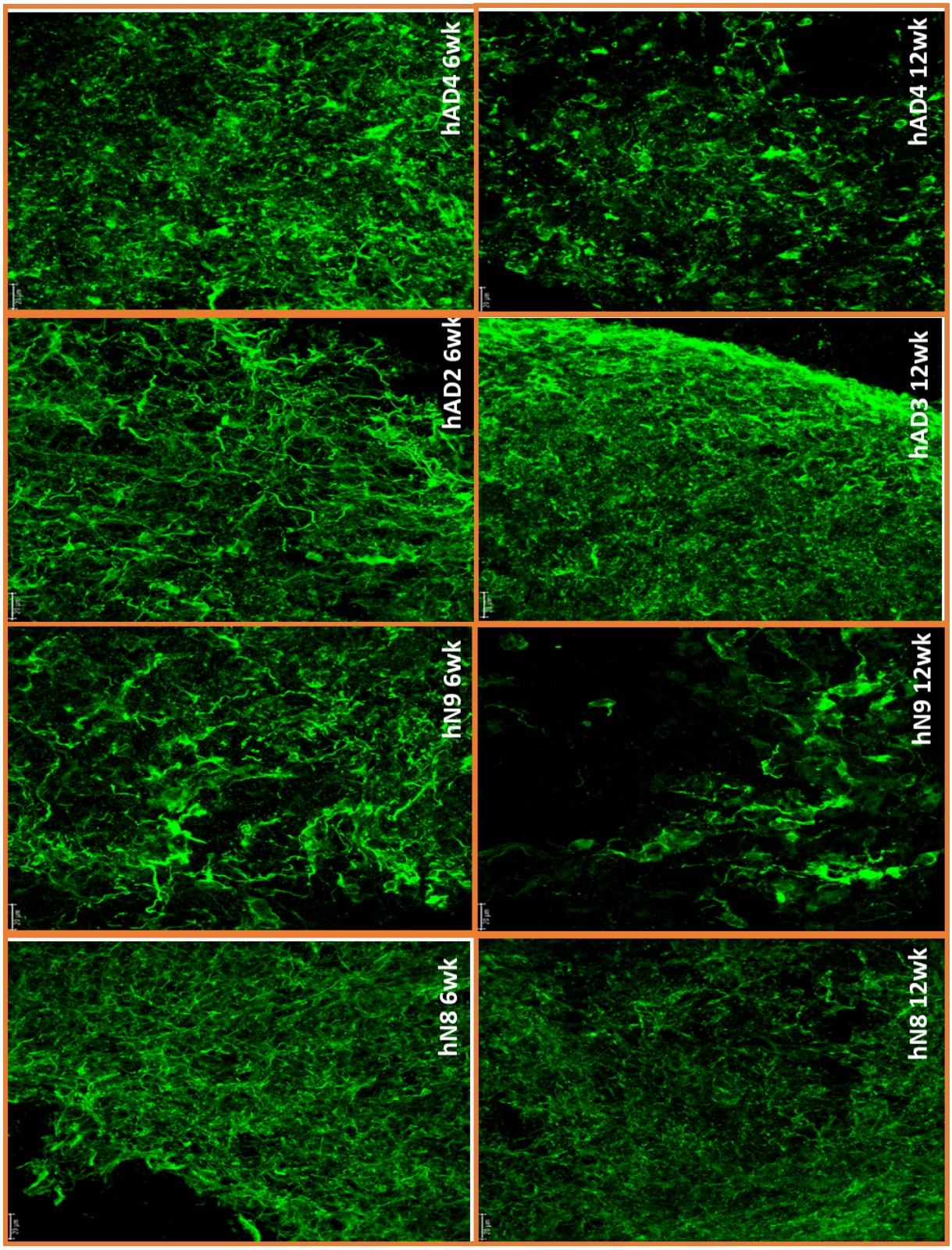

Figure 2.29: MAP2(green) expression of all five cell lines : hN8, hN9, hAD2, hAD3, and hAD4 at time points 6 weeks and 12 weeks post 3D plating (Scale bar= 20µm) (n=1).

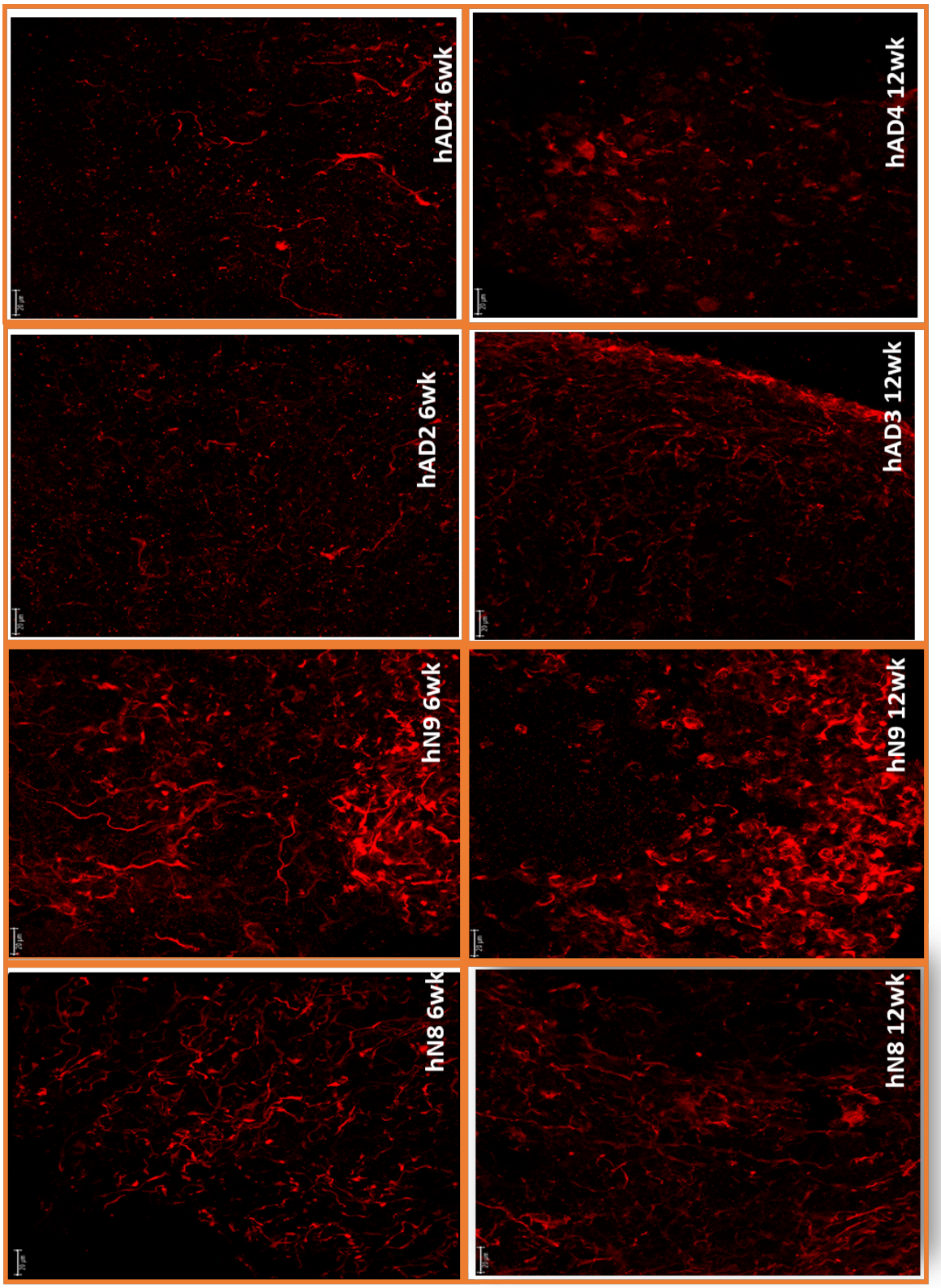

Figure 2.30: Nestin (red) expression of all five cell lines : hN8, hN9, hAD2, hAD3, and hAD4 at time points 6 weeks and 12 weeks post 3D plating (Scale bar= 20µm) (n=1).

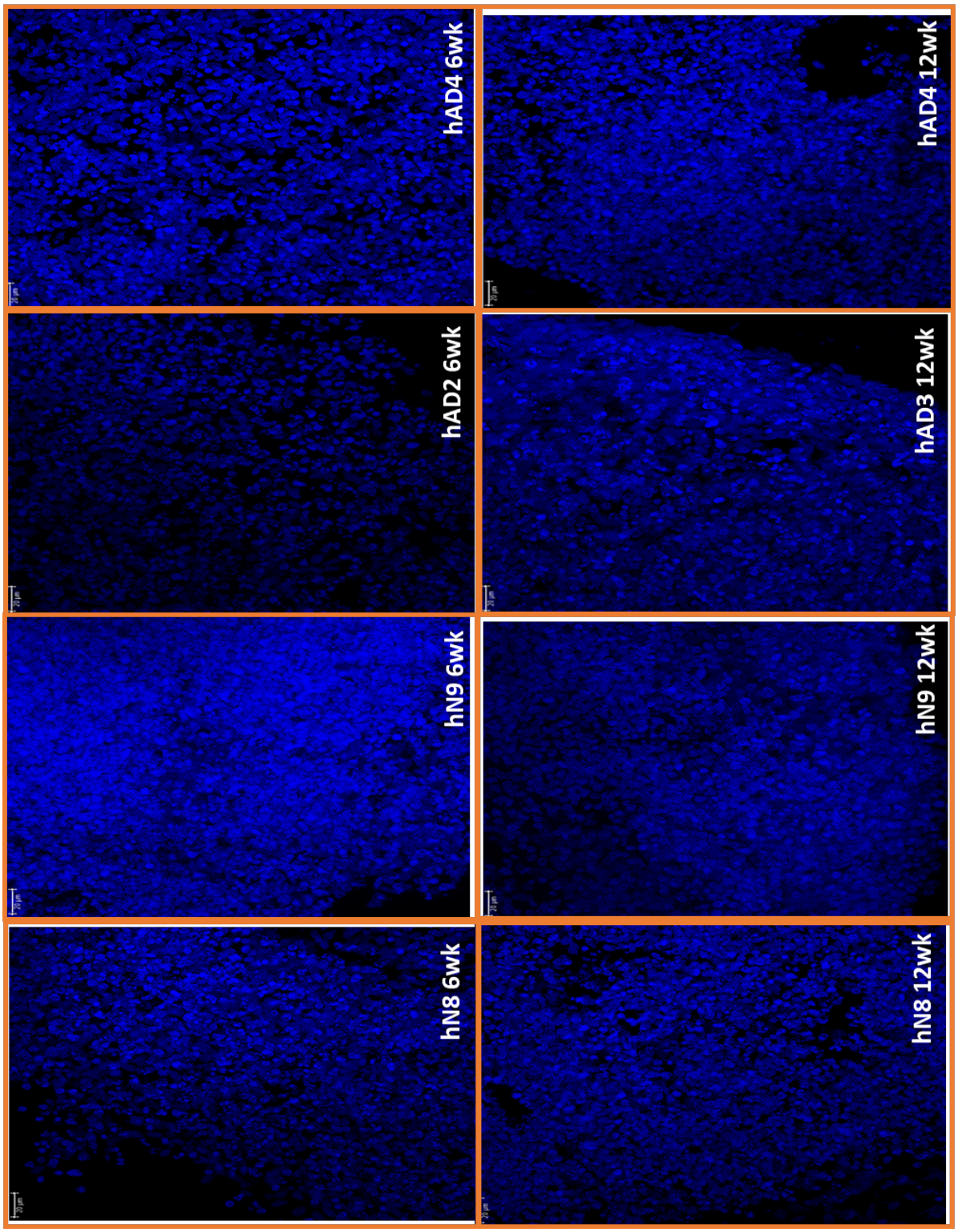

Figure 2.31: Nuclear stain DAPI (blue) of all five cell lines : hN8, hN9, hAD2, hAD3, and hAD4 at time points 6 weeks and 12 weeks post 3D plating (Scale bar= 20µm) (n=1).

2.5.1.3 Western Blot Analysis of Tau expression in the 3D cultures

Tau belongs to the MAP family of proteins, which are involved in microtubule stabilization and are abundant in neurons. Alternate splicing of the tau gene leads to expression of six different tau isoforms. The expression of tau isoforms is differentially regulated during development, with the 3R isoforms being expressed in the foetal stage and the 4R isoforms expressed in the adult stages (See section 1.9). Western blot analysis was performed to detect the expression of tau isoforms in the 3D cultures.

The total tau antibody (Dako) detects all isoforms of tau irrespective of their phosphorylation status. The molecular weight of Tau (non-phosphorylated) is 55 kDa. Detection of bands weighing more than 55kDA is an indication of the presence of phosphorylated tau. The RD3 antibody is specific for the 3R isoforms of tau with molecular weight between 45-68 kDa and 68-72 kDa when phosphorylated. The RD4 antibody is specific for 4R isoforms of tau with molecular weight between 68-72 kDa.

Western blot was performed on total lysates extracted from fly heads that were generated and homogenised by Dr. Megan Sealey. The tau negative lysates were homogenised from Oregon R Wild type fly heads and the Tau positive samples were homogenised from Elav ^{0N3R} fly heads. She kindly donated the samples for my initial experiment to practise/learn WB as a technique as well as to have 8 different samples of positive and negative controls. The samples were numbered 1 to 8 with odd numbered samples being negative and even samples being positive for tau protein (Fig 2.32).

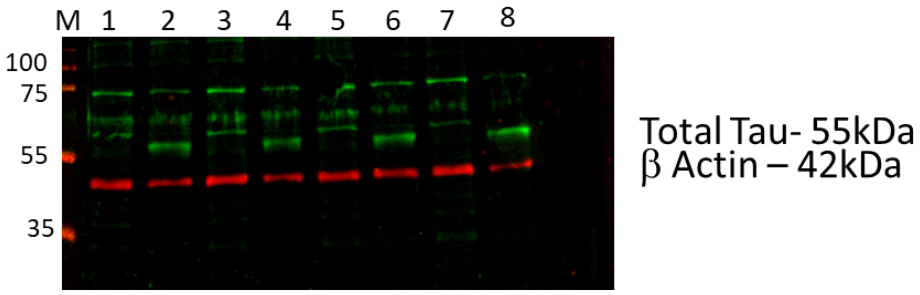

Figure 2.32: Expression of tau detected with a total tau antibody (Dako) in drosophila head lysates. Western blot was performed using Dako anti Total Tau antibody (green) and β actin (red) as housekeeping protein. M indicates molecular weight marker, with band size labelled in kDa. Tau Negative samples: 1,3,5,7 and Tau Positive samples: 2,4,6 and 8 (n=1).

Western blot analysis was performed on total lysates at week 6 post 3D plating in control hN8 and AD cell lines hAD3 and hAD4 (Fig 2.33). Since the main aim of these experiments was to standardize the western blotting technique for the 3D cultures, they were performed once on all samples. Each sample is a pool of 4 different culture wells.

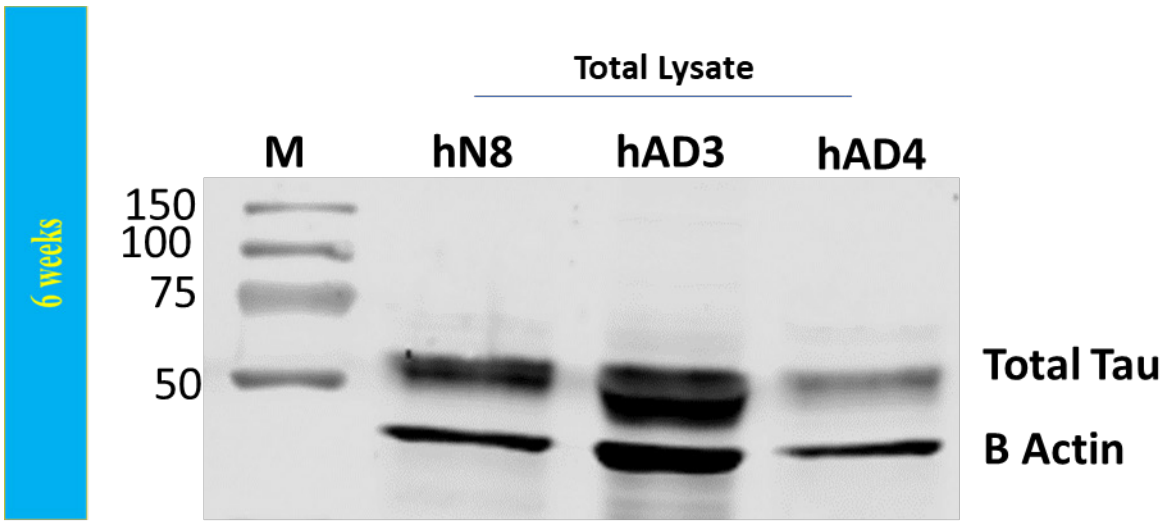

Figure 2.33: Expression of tau detected with a total tau antibody (Dako) in 3D cultures of control hN8 and AD cell lines hAD3 and hAD4 at week 6 post 3D plating. Western blot was performed using Dako anti Total Tau antibody and β actin as housekeeping protein. M indicates molecular weight marker, with band size labelled in kDa (n=1).

There is more tau expression in AD cell lines hAD3 and hAD4 (Fig 2.33) as compared to control cell line hN8 in total lysates at 6 weeks post differentiation. Although this experiment was n=1 and needs to be repeated for statistical analysis, this is an interesting preliminary result that needs to be confirmed in our 3D cultures.

All five cell lines express the protein tau in lysate fractions (S1, S2 and S3) at week 6 post 3D plating (Fig 2.34). Generally, a housekeeping protein like β-actin does not come up in all fractions and is differentially expressed in different sample fractions, as such a housekeeping protein cannot be used for normalization in case of fractionated samples.

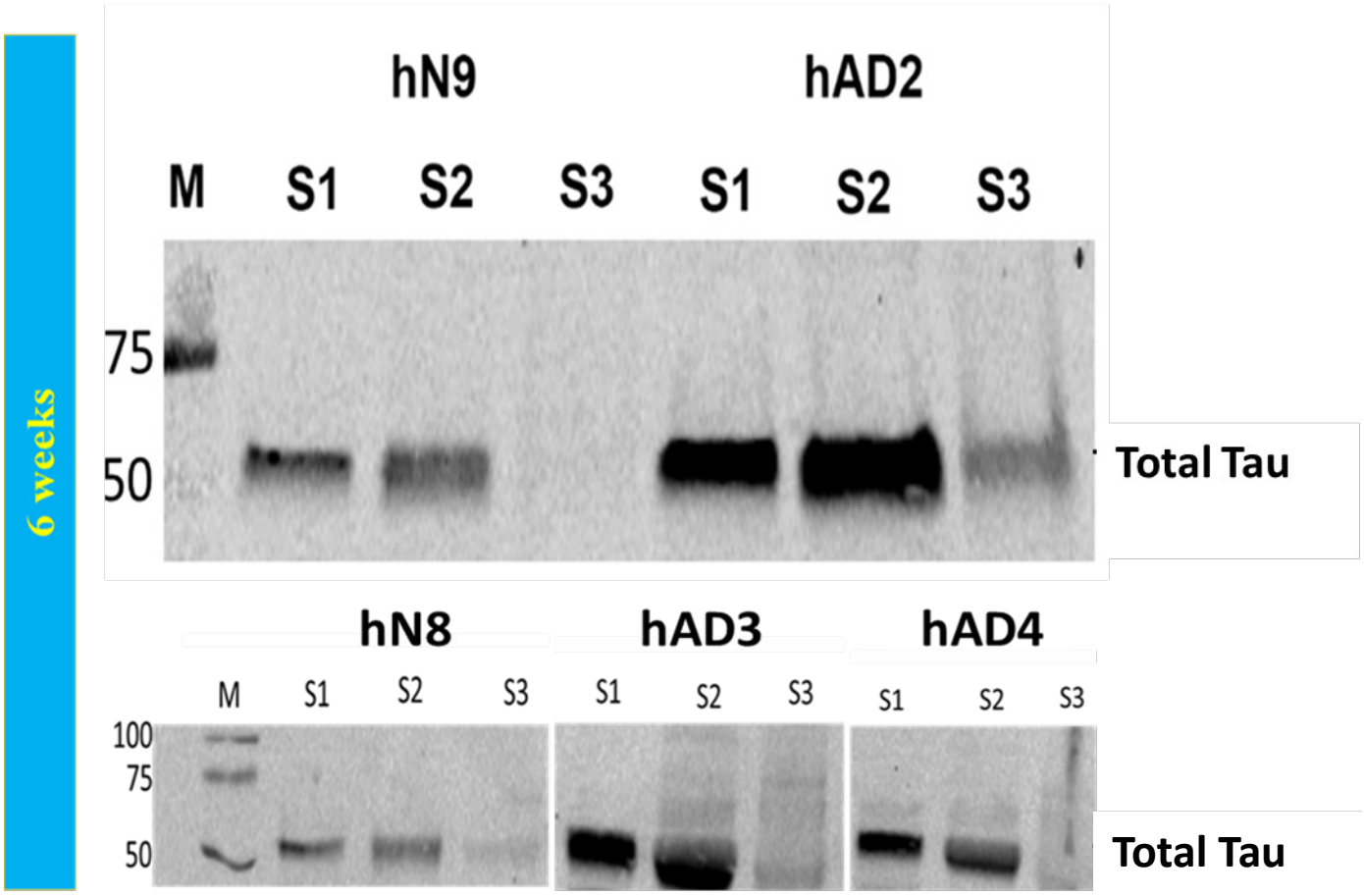

Figure 2.34: Expression of tau in 3D cultures of all five cell lines : hN8, hN9, hAD2, hAD3, and hAD4 at 6 weeks post differentiation. Western blot was performed using Dako anti Total Tau antibody. M indicates molecular weight marker, S1 (TBS soluble), S2 (SDS soluble), and S3 (Urea soluble) represent the three fractions of cell lysates (n=1).

Similarly, the AD cell lines (hAD2, hAD3, and hAD4) seem to express more of tau as compared to the control hN8 and hN9 cell lines in fractionated lysates. However, since it is difficult to have a positive or loading control in gels for lysate fractions for different time points quantification becomes an issue. Hence, all future quantifications will be done only on western blots with total lysates.

A similar pattern of tau expression is seen in all five cell lines at week 12 post 3D plating (Fig 2.35).

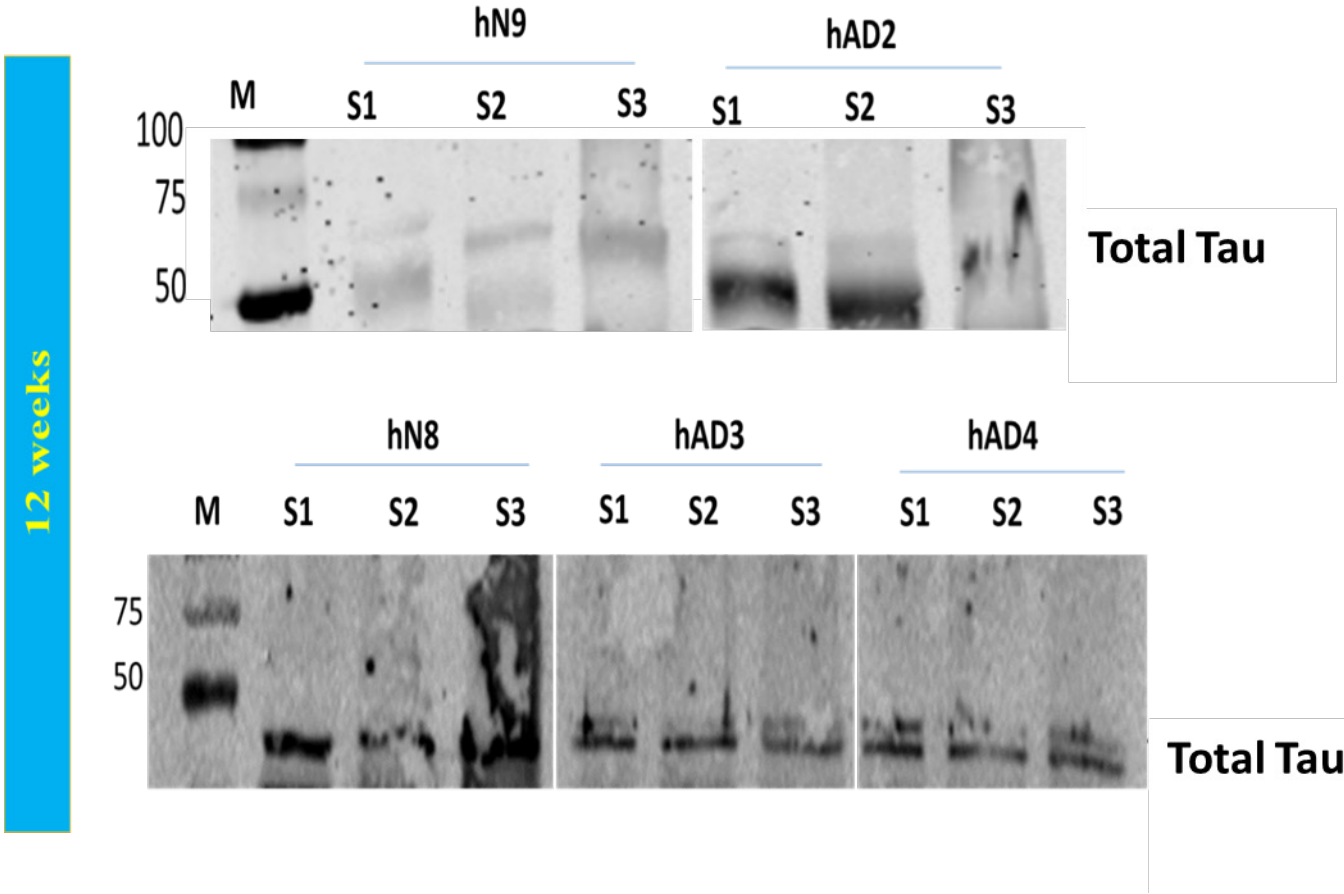

Figure 2.35: Expression of tau in 3D cultures of all five cells line : hN8, hN9, hAD2, hAD3, and hAD4 at 12 weeks post 3D plating. Western blot was performed using Dako anti Total Tau antibody. M indicates molecular weight marker, S1 (TBS soluble), S2 (SDS soluble), and S3 (Urea soluble) represent the three fractions of cell lysates (n=1).

To analyse the expression of isoforms in 3D cultures, western blot was performed to detect expression of 3R and 4R isoforms separately. Expression of 3R tau is indicative of the immature state of neurons and is detected by the RD3 anti 3R tau antibody. For clear visualization of isoforms, lysate fractions rather than total lysate were used.

3R tau expression is seen in 3D cultures of all five cell lines at 6 weeks post 3D plating (Fig 2.36). Similarly, 3R tau expression is seen at 18 weeks post 3D plating in the AD cell line hAD3 (Fig 2.39).

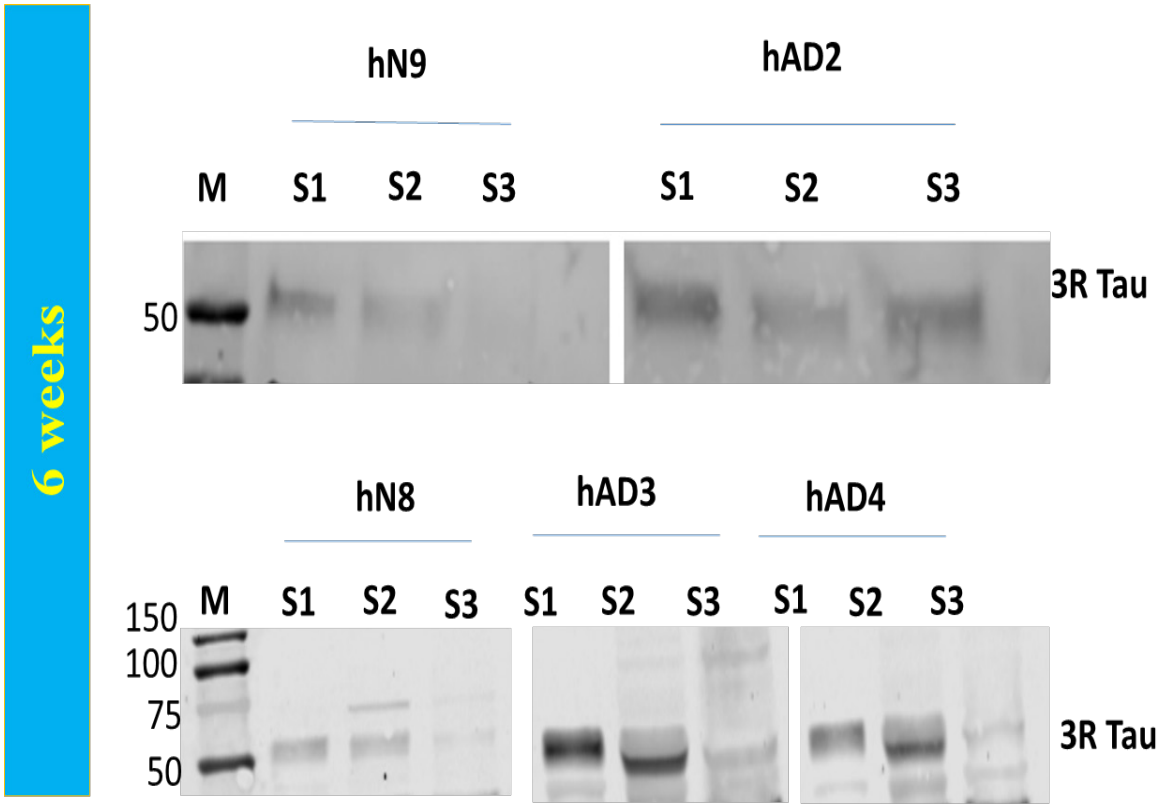

Figure 2.36: Expression of 3Repeat Tau (3R) in 3D cultures of all five cell lines: hN8, hN9, hAD2, hAD3, and hAD4 at 6 weeks post 3D plating. Western blot was performed using RD3 anti 3R Tau antibody. M indicates marker, S1 (TBS soluble), S2 (SDS soluble), and S3 (Urea soluble) represent the three fractions of cell lysates (n=1).

To analyse the maturity of neurons in 3D cultures, western blot was performed to detect the 4R tau isoform. Expression of 4R tau isoform is indicative of the mature state and is detected by RD4 anti 4R tau antibody. Since only a small percent of cells express 4R tau isoform, lysate fractions were used for better visualization of the protein.

RD4 anti 4R tau antibody expression was seen in control cell line hN8 as well as AD cell lines hAD3 and hAD4 at 6 weeks post 3D plating (Fig 2.37).

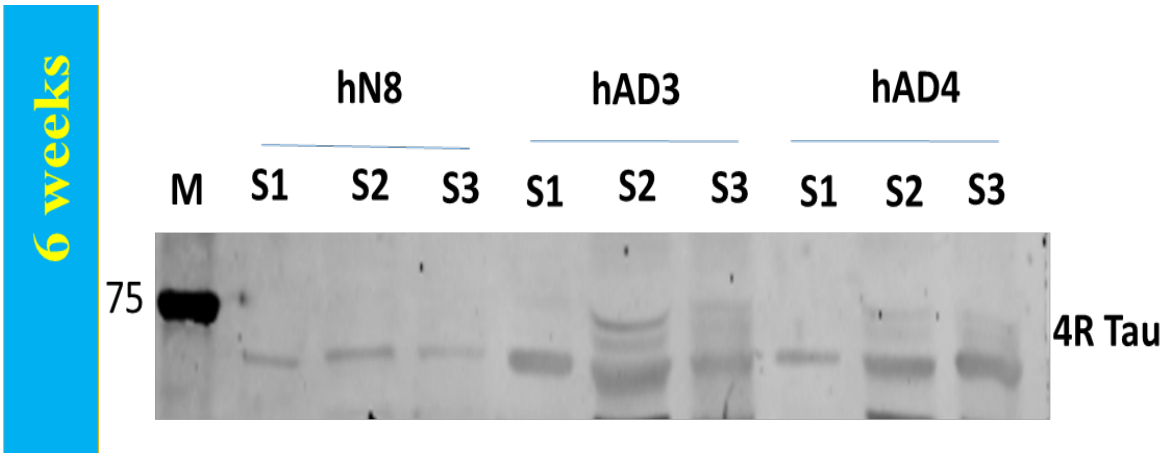

Figure 2.37: Expression of 4Repeat Tau (4R-50kDA) in 3D cultures of control hN8 and AD cell lines hAD3 and hAD4 at 6 weeks post 3D plating. Western blot was performed using RD4 anti 4R Tau antibody. M indicates marker, S1 (TBS soluble), S2 (SDS soluble), and S3 (Urea soluble) represent the three fractions of cell lysates (n=1).

RD4 anti 4R tau expression is also seen at 18 weeks post 3D plating in AD cell line hAD3 (Fig 2.39). 4R tau is expressed in the AD cell line hAD2 in the lysate fractions at 18 weeks post 3D plating (Fig 2.38). 4R Tau was observed at the expected MW (50kDA) along with other bands at higher molecular weight (approximately 60kDA). The faint expression could be attributed to the fact that only one well was used for sample lysis and fractionation. As mentioned in the methods section. (Sample preparation) 4 wells of 3D cultures were pooled for fractionation, except for the 18 weeks hAD2 sample where just one well was utilized for fractionation.

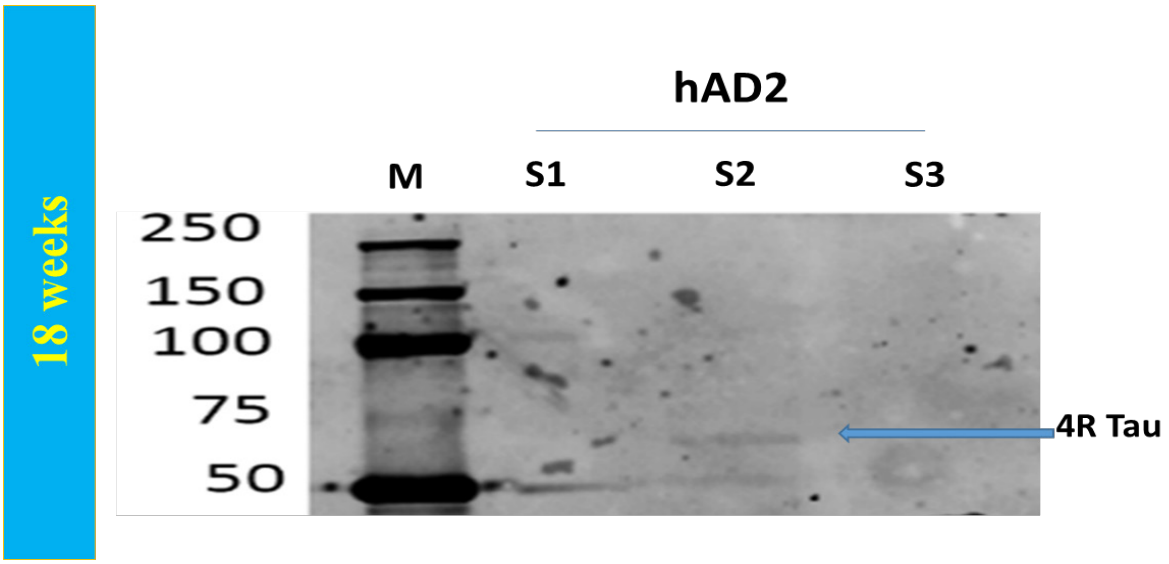

Figure 2.38: Expression of 4Repeat Tau (4R) in 3D cultures of AD cell line hAD2 at 18 weeks post 3D plating. Western blot was performed using RD4 anti 4R Tau antibody. M indicates marker, S1 (TBS soluble), S2 (SDS soluble), and S3 (Urea soluble) represent the three fractions of cell lysates.

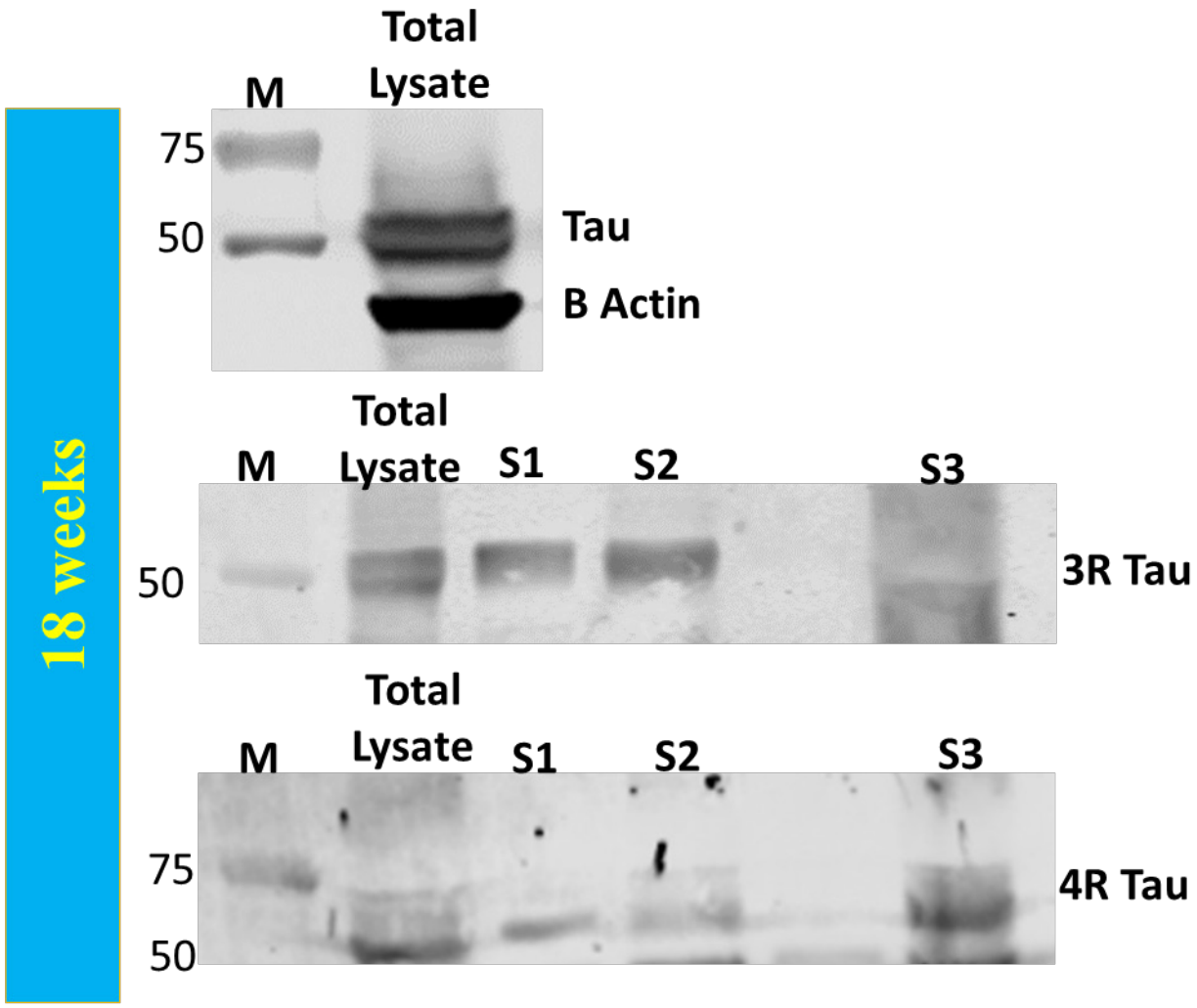

Figure 2.39: Expression of Total Tau, 3R and 4R Tau isoforms in 3D cultures of AD cell line hAD3 18 weeks post 3D plating. Western blot was performed using Dako anti Total Tau antibody, RD3 anti 3R Tau antibody and RD4 anti 4R Tau antibody, with β actin and GAPDH as housekeeping genes. M indicates marker, Input indicated total lysate, S1 (TBS soluble), S2 (SDS soluble), and S3 (Urea soluble) represent the three fractions of cell lysates (n=1).

Tau is expressed in all five cell lines. This is preliminary data suggesting that there is more tau expression in the control as compared to the AD cell lines. The 3D cultures express both 3R and 4R isoforms. 3R and 4R tau isoform expression is indicative that the cells are differentiating and maturing in the 3D cultures as expected. However, further repeats need to be performed to confirm these findings.

2.5.1.3.1 AD pathology in 3D cultures.

Hyperphosphorylation of tau is one of the key events in AD pathology. Since we were seeing expression of tau in our 3D cultures, we wanted to check if the 3D cultures showed any differences between the control and AD cell lines in the abnormal phosphorylation of tau. Western blot was optimized using PHF1 antibody to detect any hyperphosphorylated forms of tau.

PHF1 antibody detects phosphorylated Ser396/Ser404 epitopes of tau. It detects phosphorylated tau in the paired helical filaments found in Alzheimer's disease. At week 6, cultures hAD2 show light signal of PHF1 bands, whereas the control hN9 cells show very faintly detectable signal for this antibody (Fig 2.40).

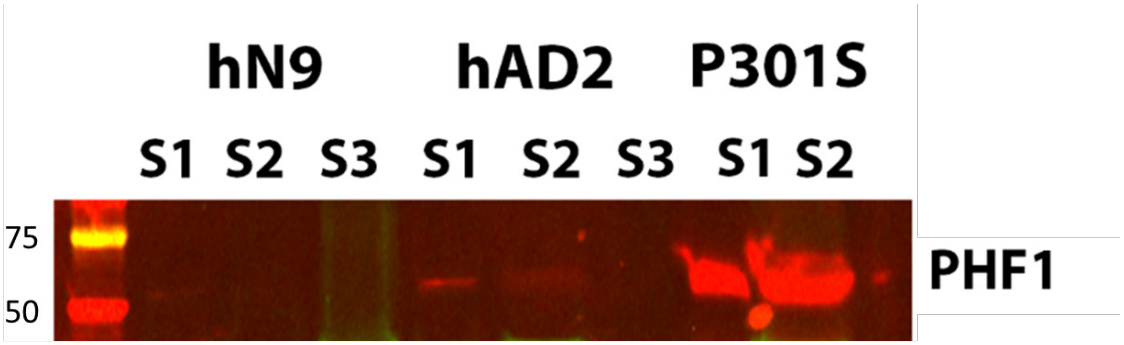

Figure 2.40: Western Blot performed to detect Phospho-tau (Ser396/Ser404) detected by anti-PHF1 antibody in hN9 control and AD cell line hAD2 cells at week 6. P301S mouse brain lysate was used as positive control (n=1).

A difference in tau pathology between the control and AD cell line is seen as early as 6 weeks post 3D plating. Though this is n=1 and needs to be shown in other cell lines, this is preliminary data suggesting that the 3D microenvironment may be conducive for the cells to develop pathological phenotype *in vitro,* similar to AD brains *in vivo,* without the need for genetic manipulation or overexpression of mutation.

2.6 Discussion

2.6.1 A Novel human *in vitro* 3D culture model to differentiate Neural Stem Cells into cortical neurons and astrocytes.

This Chapter describes a novel 3D culture system that was established using both FAD-PSEN1 cell lines and control cell lines. The FAD-PSEN 1 cell lines were bought from Axol Biosciences who had the ethical approval and the patented technique to reprogramme AD-patient skin cells to iPSC-derived NSCs. We developed a protocol to differentiate these iPSC-derived NSCs with inherent mutations and age-matched control cell lines to generate mature cortical neurons and astrocytes *in vitro.* The over-arching aim of this project was to create an *in vitro* human neural culture system which is physiologically relevant, i.e. without forcing any genetic expression of the disease-associated mutation or mutations, in order to create a pathological environment to study the cultures *in vitro.* This has unfortunately been the approach of most of the *in vitro* disease models, not just for studying AD, but also to study other neurodegenerative diseases such as Parkinson's or Huntington's disease. This approach affects the outcome of the experiments, wherein it is difficult to distinguish between effects seen due to genuine pathology over effects seen due to over-expression of the disease-associated factors. The patient iPSC derived NSCs give the major advantage of generating a physiologically relevant pathological environment *in vitro.* The effects seen in such a system will not just help to better understand the underlying mechanism of the disease pathology but will also facilitate the bench-to-bedside approach of research. This can be achieved by providing better human *in vitro* models that would help bridge the gap between translating potential drug targets into possible treatments. Dementia research has come to a crossroads where it is absolutely necessary to validate findings from the animal models and test novel treatments on human cells prior to proceeding to clinical trials.

This chapter also describes a 3D culture technique to generate cortical neurons and glia *in vitro.* Further, the detailed optimization of the different techniques that would be used to characterise the 3D cultures has been described herein. The 3D cultures gradually develop a neuronal phenotype over time, forming a large network of connections. The cultures express neural stem cell marker Nestin, early- neuronal marker B3 Tubulin, late-differentiation marker MAP2, astrocytic marker GFAP, glutamatergic marker VGLUT1, GABA-inhibitory marker GAD65/67, and presynaptic marker Synapsin 1 at 6 weeks post differentiation. The 3D cultures express Total Tau, early isoforms 3R Tau and adult-specific isoforms 4R Tau.

2.6.2 Optimised protocol for Immunofluorescence

One of the aims of our project was to quantify the proteins seen in 3D and 2D cultures such that the two factors are comparable. Whole mount immunostaining is a technique followed by most of the 3D culture / organoid groups. Whole mount staining does provide a good perspective of the overall localisation of the stained protein, however, to get a deeper understanding of the protein localisation and structures, a sectional approach will be more beneficial. The major limitation with whole mount staining is the loss of information due to issues with 100% penetration of the antibodies deep within the 3D structures. Hence, we use cryo-sections to stain rather than use whole cultures, which gives us deeper insight and also gives a platform to compare 3D cultures against their 2D counterparts.

When compared to the other published examples of B3 Tubulin staining in 3D/organoid systems, we see a similar pattern of staining, especially compared to the Marchini 2020 article (Marchini, Favoino and Gelain, 2020) article (Fig 2.41). They use 10-micron thick sections to stain their serum-free 3D culture system using hydrogel. Their 6-week *in vitro* cultures show similar staining to what we see with the B3 Tubulin staining in our 3D cultures. They seem to have used a higher concentration for most of the antibodies (1:500), hence the structures don't seem very well defined in their 3D cultures. The other possibility would be a very thick cryosection of 100 microns combined with a low permeabilization strength of buffer (0.3% Triton-x-100) and low permeabilization time of 10 mins at 4°C. Thicker sections should be fixed for a longer period of time; however, they have not mentioned the time of incubation for their 3D cultures. Similarly, in the Jakobsson et al 2017 article, we see a better structural resolution for B3 Tubulin although a lower time of fixation (10 mins) and lower concentration of permeabilization buffer (0.25% Triton-x-100) have been used. However, it could be attributed to the lower cell density (90,000 cells/cm^2) for IF experiments, giving each cell more space to have a better resolution in 3D (Jakobsson *et al.*, 2017) . With the Dingle et al 2015 article, they use a whole mount staining approach with a lower strength of permeabilization buffer (0.25% Triton-x-100) (Dingle *et al.*, 2015). This gives an idea of what B3 tubulin staining in a 3D culture with higher density would look like.

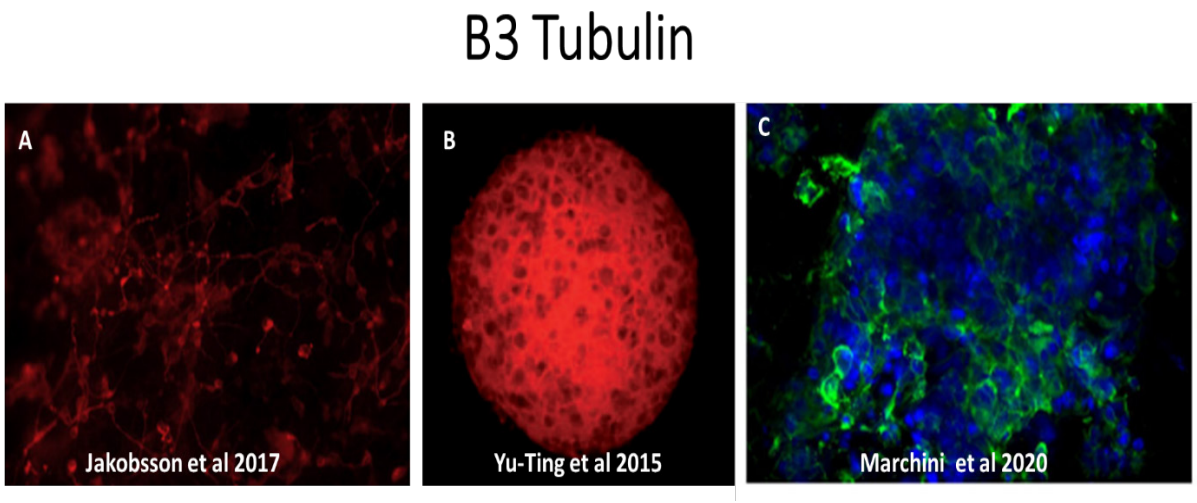

Figure 2.41: A. IF image of B3 Tubulin staining of day20 3D human neural cultures from Jakobsson et al 2017 article. B. Whole mount-immunofluorescence staining of B3 Tubulin of rat cortical spheroids at day21 in vitro. From Dingle et al 2015 article C. Immunofluorescence staining of B3 Tubulin stained human NSC cells in 3D at week 1 in vitro from Marchini et al 2020 article.

When compared to the other published 3D/organoid articles, there was a certain level of similarity in expression phenotype of MAP2, depending on certain parameters like cell density, IF processing time, buffer strength, and the thickness of the cultures used for staining (Fig 2.42). For instance, the Raja et al 2016 and Marchini et al 2020 articles show a very close resemblance to the MAP2 structures we get from staining our cultures (Raja *et al.*, 2016) (Marchini, Favoino and Gelain, 2020). The structures seen in the Jakobsson et al 2017 and Choi et al 2014 articles seem less dense and more elongated (Choi *et al.*, 2014b). This could be attributed to the low density of cells seeded for IF experiments. Both studies seem to follow two different seeding densities for their 3D cultures depending on their experiments– a high density for WB and a lower density for IF staining. Hence the structures here look more two dimensional than three dimensional. In our 3D culture experiments we make it a point not to change densities between different techniques so that comparison between different experiments is not biased based on cell densities. Hence, we keep the same cell density across all 3D experiments.

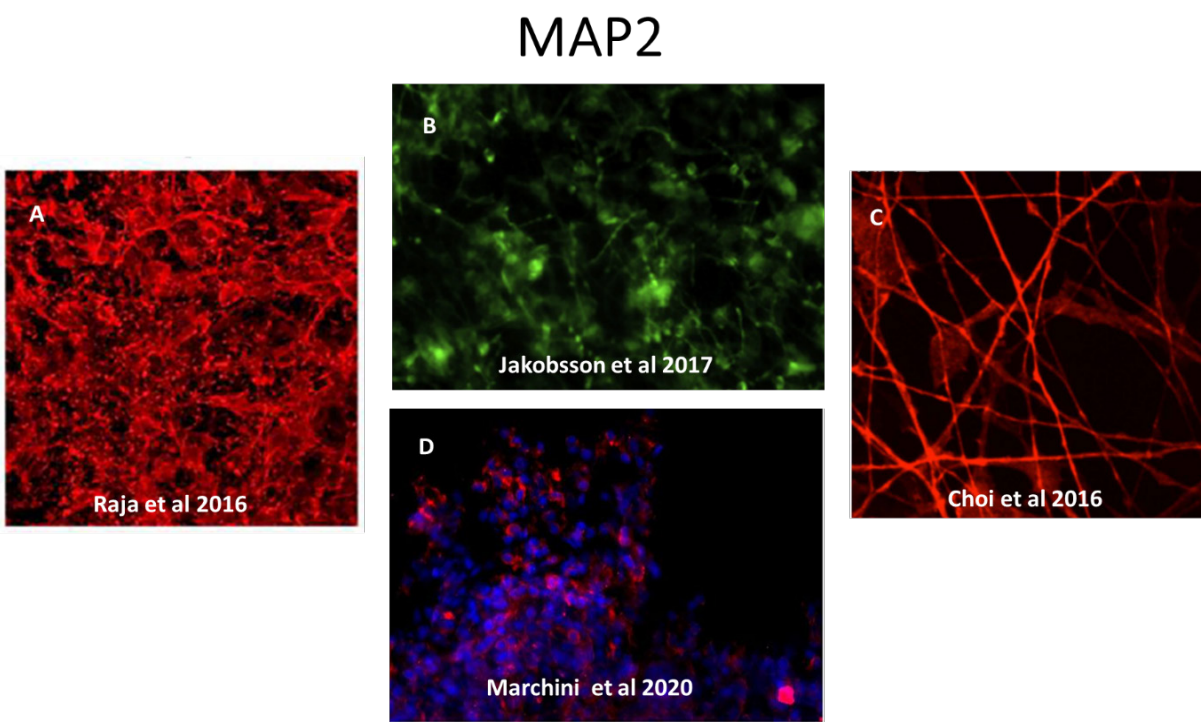

Figure 2.42: A. IF image of MAP2 staining of day90 organoid section (30micron). B. IF image of MAP2 staining of day20 3D-IF human neural cultures. C. MAP2 staining of 3D- IF cells (ReN-mCherry) at 6 weeks post differentiation. D. Immunofluorescence staining of MAP2 stained human NSC cells in 3D cultures at 1- 6 weeks in vitro.

Similarly, the Nestin expression that we see in our 3D-cultures is comparable to the other published 3D/organoid cultures (Fig 2.43). As stated before, the Jakobsson et al 2017 use a lower seeding density, which may suggest a different, almost 2D-like, Nestin phenotype in their 3D cultures (Jakobsson *et al.*, 2017). The whole mount staining in Dingle et al 2015 shows an intricate network formed by the Nestin positive cells at day 21 *in vitro* (Dingle *et al.*, 2015). These images show elongated cells, but with shorter length compared to the MAP2 or B3 Tubulin structures seen in their cultures, which reflects what we see for the Nestin expression in our 3D cultures.

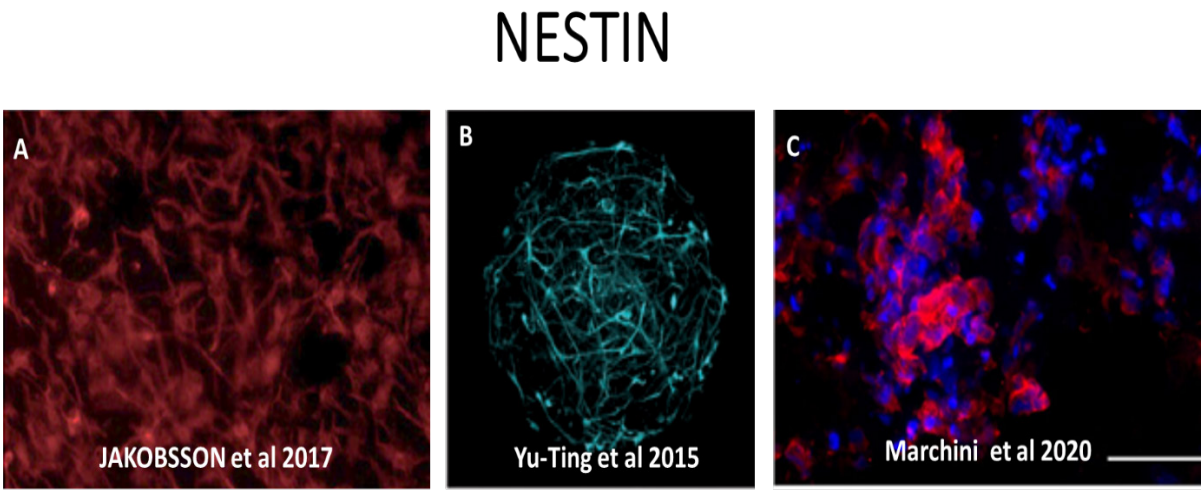

Figure 2.43: A. IF image of Nestin staining of day20 3D-IF human neural cultures . B. Whole mount-IF staining of Nestin of rat cortical spheroids at day21 in vitro. C. Immunofluorescence staining of MAP2 (red) stained human NSC cells in 3D cultures at 3 weeks in vitro.

The GFAP expression in other published articles, for instance Marchini et al 2020 and Wörsdörfer et al 2019 (Fig 2.44), resemble most to the GFAP structures we get in our 3D cultures (Wörsdörfer *et al.*, 2019; Marchini, Favoino and Gelain, 2020). However, the latter group seem to have better defined GFAP structures in their organoids. They have used 5µm paraffin sections for IF staining. On the other hand, Choi et al, dingle et al, and Jakobsson et al show astrocyte-like projections in their 3D cultures. This could be attributed to the lower seeding densities of the 3D cultures giving more room for the cells to resolve in three-dimensional space.

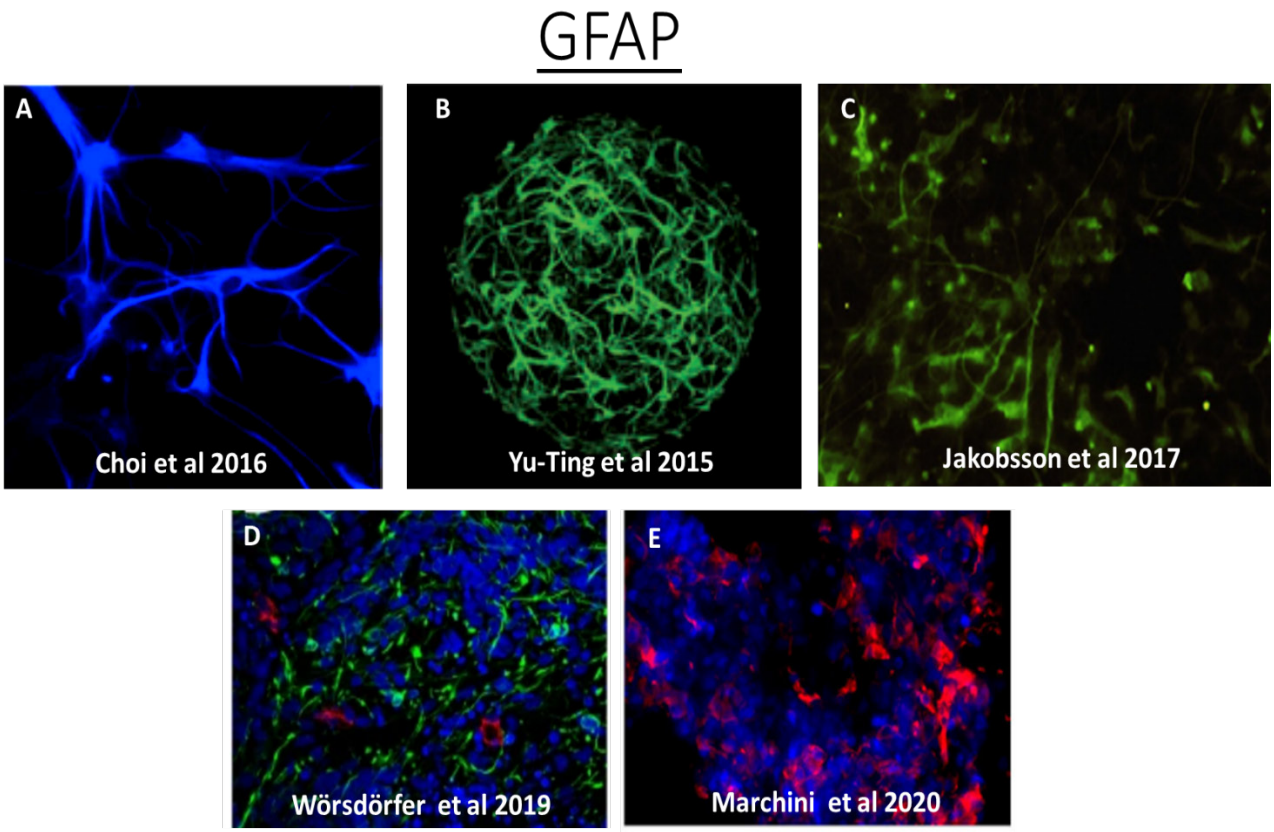

Figure 2.44: A. GFAP staining of 3D- IF cells (control) at 3 weeks . B. Whole mount-IF staining of GFAP in rat cortical spheroids at day21 in vitro. C. IF image of GFAP (green) staining of day20 3D-IF human neural cultures. D. IF images of GFAP stained organoid at day 180. E. Immunofluorescence staining of GFAP stained human NSC cells in 3D cultures at 1 week in vitro.

Given that the use of 3D cultures, organoid or spheroid cultures has become widespread the typical procedure for processing these systems are by tissue sectioning with immune-histological staining followed by confocal laser microscopy. The major downside to such process is that they are tedious and time-consuming techniques which potentially might lead to loss of tissue and valuable information while sectioning and staining especially due to improper penetration of the antibodies used. For a culture model with heterogenous population of cells wherein the 3D placement of cells plays a vital role, the information obtained from sectioning is partial and not a true representation of the entire culture. Studying the 3D cultures as a whole will give an in-depth understanding of the true nature and physiological structure that develops in such culture models. Quite a few advances have been made to improve the staining and visualization of 3D cultures. Optical tissue clearance techniques is one of the techniques developed for such tissue processing. State-of-the-art tissue clearing techniques such as CLARITY- clear lipid-exchanged acrylamide-hybridized rigid imaging/ immunostaining/ in

situ hybridization compatible tissue hYdrogel provide optically transparent and permeable but intact tissues to allow techniques like whole tissue/organ in situ hybridization, immunohistochemistry involving ab-labelling to provide complete information of such cultures in their entirety (Chung *et al.*, 2013). Not only does this give scope to improve staining protocols considerably but also makes it convenient for high-throughput studies.

Another method to optimize the clarity of the fluorescence stained images is using imaging techniques other than confocal like light sheet microscopy or selective plane illumination microscopy with faster acquisition speed, better signal to noise ratio and excellent sectional resolution (Kumar *et al.*, 2014; Power and Huisken, 2017). This also enables to visualize live dynamic changes in the subcellular level in whole organoid/3D culture systems. However, multiphoton laser scanning microscopy renders better 3D resolution in deeper tissues (Dekkers *et al.*, 2019).

2.6.3 Optimized protocol for Western Blot- Protein fractionation of 3D cultures

Tau is a protein that is implicated in AD. For years, the scientific community has been biased towards looking deep into the genetics involved around Aβ to understand the underlying pathology of AD, especially since the tau genes are not identified as one of the FAD genes directly responsible for the development of the disease but instead is a protein that is seen to be affected in the course of pathology of the disease. Unfortunately, all attempts to develop Aβ- drug-targets have either failed, or in some cases worsened, the conditions of the AD patients. Although the research around Aβ has given deep insight into the disease but studying it in isolation has not been productive. Hence, there is a paradigm shift in the research community from Aβ to Tau in the recent years.

There are two school of thoughts that surround the Tau hypothesis for AD, one being that hyperphosphorylation of tau at certain epitopes leads to the conformational change in the protein which eventually leads to its destabilisation from the microtubule assembly system disrupting the normal function of the neurons causing synaptic dysfunctions and the eventual death of the cells. The dissociation of tau from microtubules causes an increase in the cytoplasm. The free but stabilised hyperphosphorylated forms of tau facilitates assembly of filaments contributing to the formation of PHFs. The degree of severity of the disease

symptoms corresponds to the number of PHFs in the NFTs, thus implicating hyperphosphorylation of Tau in the pathology of the disease.

However, the second school of thought describes the aggregation of Tau as a protective means against the disease (Lee *et al.*, 2005). Another group came up with some compelling evidence supporting this argument such as- NFTs are also found in the viable cells in the brain towards the later stages of the disease and are present in the neurons for decades and are also present in the elderly presenting no symptoms of dementia for their entire lifetime (Castellani *et al.*, 2008). All in all it shows that the neurons can survive in the presence of NFTs with no harmful or toxic effects and thus is contradictory to the first school of thought in which just the presence of phosphorylated tau in the NFTs of AD patients is not enough evidence to implicate it in the disease.

There is enough evidence to support the fact that Tau starts its aggregation first in a few cells and then spreads from cell to cell in a prion-like manner and spreads from one brain region to another in a well-defined pattern and this distribution could correspond to the Braak and Braak stages of disease progression (Braak and Braak, 1991). Although, the exact method of transmission is yet to be confirmed, the fact that different but specific fibril species are responsible for distinct human tauopathies, it is hypothesised that different molecular conformers of aggregated tau exists (Goedert and Spillantini, 2017), which lead to distinct fibril species. The best way to study diseases wherein tau is implicated is to characterise and identify these conformers. It is considered that clinical symptoms of the disease correlates better with tau pathology rather than Aβ pathology (Joie *et al.*, 2020). There are clinical studies supporting the fact that there is an increase in the amount of total tau and phospho tau in the CSF (cerebro- spinal fluid) of AD patients (Blennow *et al.*, 1995; Lee *et al.*, 2005), thereby making tau a successful biomarker in monitoring progress of clinical symptoms and majorly as an end-point in analysing the efficacy of the of drug-treatments given to AD patients (Blennow and Hampel, 2003; Carrillo, Sanders and Katz, 2009). There are also studies suggesting the tau found in CSF is considerably different from the tau found in that of FTD- a tau mutation driven neurodegenerative disease. The increase in total and phospho tau in AD is consistent whereas it is variable in FTD patients (Mecocci *et al.*, 1998; Sjögren *et al.*, 2000).

The expression of the 4R tau isoform is considered as the sign of maturity in neurons as developmentally there is a shift in expression from the predominant 3R tau to the 4R isoform. Considering the complexity of the human brain, replicating it in a dish becomes equally

challenging. The presence of 6 isoforms of tau in the adult human brain and the protein being a prime accomplice in the ageing disease, makes the expression of all tau isoforms imperative in modelling the disease. Unfortunately, one of the major drawbacks of iPSCs are their disinclination towards ageing phenotype *in vitro* even after long term culture, making the expression of all six isoforms almost impossible in such cultures. However, efforts are being made to overcome this challenge. Most of the culture models have reported the expression of the 4R tau gene early during differentiation but unfortunately do not express enough of the protein for detection using robust techniques like western blotting. One such study has shown the increase in 4R tau transcripts using immortalised cells in 3D cultures after 7 weeks of differentiation *in vitro* (Choi *et al.*, 2014a). However, they have forced the expression of the pathology by overexpressing the driving mutation sin the cell lines. Another study using rather complex Matrigel coated alginate capsule derived cultures, have partially resolved the issue using Brain-Phys media instead of standard culture medium to show expression of all six isoforms at 25 weeks. Although the use of Brain Phys promoted the expression of all six isoforms, the higher molecular weight isoforms 2N3R and 2N4R only accounted for the 1% and 0.9% of their occurrence in the human brain (Miguel *et al.*, 2019). The expression of equimolar ratios of the 3R and 4R tau isoforms as found in the adult human brain has yet to be proven in such neural culture models and requires further efforts to achieve this goal. Another study have shown the expression of tau isoforms at the gene and the protein level after 300 days *in vitro* using engineered cerebral organoid cultures. This is one of the first report with an extensive study on tau spicing in cerebra organoids, showing acceleration in mature tau splicing pattern in 3D cultures and showing almost equimolar ratios of 3R and 4R transcripts. However, despite of 300DIV these organoids although closely but did not completely resemble that of the human brain. (Lovejoy *et al.*, 2020).

Although we see expression of 4R tau in our 3D cultures at 6 weeks and 18 weeks post differentiation, there are also some non-specific bands that are picked up by the 4R tau Ab.

In this Chapter, the western blot technique for detection of the protein Tau and its isoforms has been standardised. The method to fractionate Tau and its isoforms has also been optimized. The method for fractionation was adopted from Cowan et al 2015. The S1 fractions should contain monomers, the S2 fractions should contain monomers and oligomers and the S3 fractions contain the detergent-insoluble aggregates (Bandopadhyay, 2016).

In conclusion, we have achieved the primary aims for this section of the Chapter. We have successfully standardized IF staining for 3D cultures for markers MAP2, Nestin, GFAP and B3-Tubulin. However, Synapsin 1, VGLUT1 and GAD65/67 could be further optimized. We have successfully standardized Western Blotting technique for detection of total tau protein as well its isomers in 3D cultures. In doing so we believe the differentiation protocol is replicable when used with different cell lines. The maturation of the 3D cultures is progressing as expected and the 3D cultures show early signs of AD-pathology.

2.6.4 Summary and Future work

The main aim of this Chapter (pilot experiment) was to optimize the differentiation protocol to generate mature neurons and astrocytes *in vitro* and to establish standardised techniques to characterise these 3D cultures. Although most of the experiments were an n=1, the future work would involve having enough experimental repeats to check the reproducibility of the experiments specifically in regard to the cell lines and to statistically analyse the 3D cultures at the different timepoints. With this Chapter, the optimum concentration of 0.5µM RA was determined for all further differentiation experiments. The protocols for each antibody used for IF has been optimized to make sure all the staining is specific and there are no background noise interference since all these protocols will be utilised later to quantify the relative percentage of the cells expressing these markers in the control and AD – 3D cultures at different timepoints. Our final aim is to find any differences in these markers whether it is between different timepoints or between the controls and AD cell lines, to understand the underlying expression profile of these cells *in vitro.* With this Chapter, the protocols for WB and fractionation of the protein lysate to study the differential solubility and aggregation of protein Tau and its isoforms have also been optimized. Our future aim is to have enough experimental repeats to quantify the solubility/aggregation of Tau and its isoforms, so we have a better understating of disease progression at early and late timepoints in 3D cultures.

Chapter 3- 2D Cultures verses 3D Cultures

3.1 Introduction

Conventional *in vitro* neuronal models rely on the growth and differentiation of cells on a 2D platform predominantly made of rigid artificial substrate such as glass or polystyrene which is not an accurate representation of the *in vivo* physiological microenvironment. One of the properties of stem cells is their sensitivity towards the mechanical and chemical cues from their microenvironment. Hence, when recapitulating an *in vivo* system whether to probe into developmental biology or to model and investigate changes in neurodegenerative pathology, it becomes crucial that every aspect of the *in vitro* manipulation is considered carefully. Conventional 2D cultures have been most valuable for quick, cheap and reproducible tools to study signalling pathways, validate differentiation protocols, for co-culture studies, electrophysiological studies, migration studies and so much more. Despite their importance, they do not fully recapitulate the complex brain tissue microenvironment. This affects cell morphology, survival, proliferation, differentiation, neurite outgrowth and synaptic density (Brännvall *et al.*, 2007; Li *et al.*, 2007; Yan *et al.*, 2018)

Conventional 2D cultures are also reported to poorly recapitulate pathological conditions *in vitro.* This could be possibly because the 2D microenvironment does not accumulate pathology over time. For instance, it is reported in the Choi study that due to constant removal of the culture media the diffused Aβ prevents its aggregation in 2D cultures whereas in the 3D cultures with the same rhythm of media changes, cultures foster Aβ aggregation purely due to the 3D microenvironment (Choi *et al.*, 2014a).

3.2 Aims

Aim 2: To compare the 3D culture with the traditional 2D culture to determine the most efficient neural differentiation method.

In order to validate the neural differentiation efficiency of the 3D cultures and compare with the 2D cultures: NPCs-derived from three iPSCs of AD patients with PSEN1 mutations L286V, A246E and M146L and from two iPSC of healthy individuals, differentiated in 3D cultures will be compared to the same cell lines in 2D cultures keeping constant the culture conditions for a period of 6 weeks post differentiation.

-To analyse neuronal differentiation over time: Quantification of different markers expressed in 3D cultures at week 0, -6 and -12 post differentiation *in vitro*- MAP2, Nestin, GFAP, B3-Tubulin

-To compare 2D with 3D cultures- Characterisation and quantification of the different cell phenotypes will be done using an array of markers namely

- Immunofluorescence - MAP2, Nestin, GFAP, B3-Tubulin - week 0, week 6

-Western Blotting assay- total Tau.

3.3 Methods

3.3.1 Cell Culture

Five iPSC derived NSC – three with PSEN1 mutations hAD2, hAD3 and hAD4 (Table 2.7) were used for neuronal differentiation *in vitro* based on our optimized neural differentiation protocol (Chapter 2 part A) along with two adult control cell lines hN8 and hN9 was purchased from Axol Biosciences .All five cell lines brought from Axol Biosciences were expanded each from 2-3 different vials and cultured at different times. The experiments were set in such a way that for every cell line-cells from the same flasks cells were passaged to set up different experiments for 2D and 3D cultures to set up N=1. Such 3 sets of experiments were set up to make n=3 for comparison studies and statistical analysis. The 2D and 3D cultures formats were carefully considered keeping as many factors similar between the two formats as possible so that they are comparable using different parameters for statistical analysis. Three different timepoints week-0, week-6 and week-12 were used to analyse differences within and across cell lines over time. All comparisons between 2D and 3D cultures were done at 6 weeks post differentiation.

3.3.1.1 Thawing and expansion of iPSC derived NSCs – 2D and 3D cultures.

The method followed for thawing cells was as described in the previous Chapter 2 -Part B (section 2.3.1.1.1) with minor modifications. The details of the process is included in the flow chart (Fig 3.1). Defrosted cells were transferred to fresh pre-warmed 1x Neural Plating – XF Media (Axol Biosciences, ax0033) which was thawed 24 hours prior to thawing at 4°C. Cells are left to stabilize for 24 hours in the incubators in this media in a T-75 flask. The next day

the media is replaced with fresh pre-warmed ANM media (Table 3.1). Media is changed every second day.

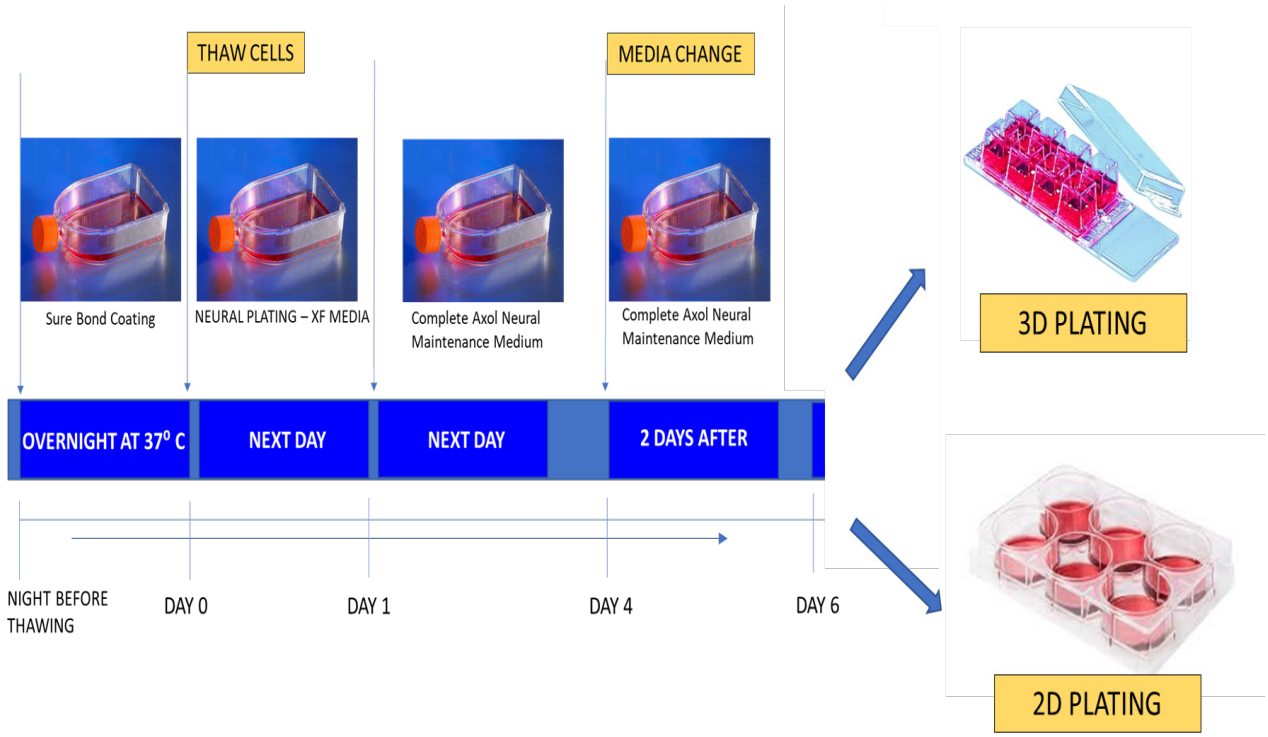

Figure 3.1: Schematic for steps involved in thawing and expansion of iPSC derived NSCs.

Axol Neural Maintenance Media	
Components	**Concentration**
Axol Neural Basal Media	1x
Axol Supplement	1.5% v/v
EGF (PeproTech, AF-100-15)	0.1mg/ml
FGF (PeproTech,100-18B)	0.05mg/ml
Antibiotic-Antimycotic solution (100x)	1x

Table 3.1: List of components used in Axol Neural Maintenance Media and their respective concentrations.

3.3.1.2 Plating for differentiation of iPSC derived NSCs – 2D culture

For plating cell lines to set up 2D culture experiments i.e. 2D-IF and 2D-WB similar method as described in Chapter 2-Part B (section 2.3.1.1.2) was used with modifications. The cell numbers for each experiment were carefully calculated to match with that of the 3D cultures so that one section (14µm) of the 3D culture would closely resemble comparable cell numbers of corresponding 2D cultures.

For plating cells in 2D cultures with subsequent immunostaining (2D-IF), autoclaved 5mm/1.5m round glass coverslips were used to coat with 0.01% solution of Poly-L-Ornithine (Sigma Aldrich- P 4957) (made in sterile filtered water) overnight followed by a coating with 50µg/ml Laminin (Sigma Aldrich-L2020) made in 1x PBS for 1 hour at 37°C in 6 well plates. We had to replace coating with Matrigel since cells did not adhere properly on the glass coverslips coated with Matrigel. For plating in 2D-IF, 6000 cells were seeded evenly per well in a 6 well dish and placed in the incubator.

For plating cells in 2D cultures with subsequent western-blot analysis (2D-WB), Matrigel (1:15) which was gradually thawed on ice to avoid jellification was used to coat the 6 well plates. As stated before, we wanted to keep the conditions as close as technically possible between the 2D and 3D cultures. Cells grown on Matrigel on a plastic surface adhere quite well. For plating in 2D-WB, 300,000 cells per well in a 6 well dish were seeded and placed in a 6 well dish.

Cells were allowed to attach at least 2 hours before supplementing with RA at a concentration of 500ng/ml.

3.3.1.3 Plating for differentiation of iPSC derived NSCs – 3D culture

For seeding in 3D culture on day 6, similar method as described in Chapter 2-Part B (2.4.1.1.2) was used with modifications. Cells were seeded at a density of 2 x 10^6/ml per well, in an 8 well-Lab-Tek chamber slide slide (Lab-Tek system, Nunc-177445). Cells were supplemented with RA a concentration of 500ng/ml.

3.3.1.4 Differentiation of iPSC derived NSCs – 2D and 3D cultures

The method used for differentiation was as described in the previous Chapter 2-PART B (2.4.11.3.). Once the 2D and 3D experiments were set up, the same differentiation protocol was followed for both formats.

3.4 Immunofluorescence assay

To compare the two culture formats keeping the variables as minimum as possible, both 2D and 3D cultures were stained using the same staining protocols (standardized in Chapter 2-PART B-2.5.1.2). In order to determine the proportion of mature and immature neurons/ undifferentiated cells, cultures were dual stained for MAP2 and Nestin. In order to determine the proportion neurons (immature and mature) B3 Tubulin was used and for astrocytes cultures GFAP was used to stain the cultures. Dapi was used to counterstain nuclei.

3.4.1.1 Sample preparation – 2D and 3D culturs

The 2D culture-coverslips were fixed in 4% PFA for 15 minutes at room temperature, rinsed three times in 1 x PBS and stored at 4°C in PBS, until used for staining-2.3.1.2.

The 3D cultures were prepared for staining using the same technique describe previously in Chapter 2 Section-part B-2.4.1.2.1

Protocols for staining was standardised for each antibody (Chapter 2-part B).

3.4.1.2 Protocol A: GFAP

For GFAP staining the protocol standardized in Chapter 2-Part B-2.5.1.2.3 was followed as explained in Table 3.2.

BUFFERS	COMPOSITION	CONDITIONS
Permeabilization Buffer (PBST)	PBS with 1% Triton-X100	20 mins at room temperature
Blocking Buffer	PBST with 10% donkey serum	1 hour at room temperature
Wash Buffer	PBST	5 mins each x 3
Primary Antibody Solution	GFAP (1:200) diluted in Blocking Buffer	Overnight at 4°C
Secondary Antibody Solution	488-anti Rabbit antibody diluted in Blocking Buffer	2 hours at room temperature
DAPI	2 µg/ml in (1: 500) dilution in PBST	15 mins at room temperature

Table 3.2: List of buffers used for staining with GFAP

3.4.1.3 Protocol B: MAP2 and NESTIN

For Nestin staining the protocol standardized in Chapter 2-Part B -2.5.1.2.1 and 2.5.1.2.2 was followed as explained in Table 3.3

BUFFERS	COMPOSITION	CONDITIONS
Permeabilization Buffer (PBST)	PBS with 0.2 % Triton-X100	20 mins at room temperature
Blocking Buffer	PBST with 10% donkey serum	1 hour at room temperature
Wash Buffer	PBST	5 mins each x 3
Primary Antibody Solution	MAP2 (1:200) and Nestin (1:200) diluted in Blocking Buffer	Overnight at 4°C
Secondary Antibody Solution	488-antiRabbit (1:200) and 568-anti Mouse (1:200) dissolved in Blocking Buffer	2 hours at room temperature
DAPI	2 µg/ml in (1: 500) dilution in PBST	15 mins at room temperature

Table 3.3: List of buffers used for staining with MAP2 and Nestin

3.4.1.4 Immunocytochemistry for B3-TUBULIN

For B3 Tubulin staining the protocol standardized in Chapter 2-Part B B – 2.5.1.2.4 was followed as explained in Table 3.4

BUFFERS	COMPOSITION	CONDITIONS
Permeabilization Buffer (PBST)	PBS with 1 % Triton-X100	1 hour 30 mins at room temperature
Blocking Buffer	PBST- 1 % with 4% donkey serum, 1% Bovine Serum Albumin (BSA) and 0.3M glycine	
Wash Buffer	PBST	5 mins each x 3
Primary Antibody Solution	B3-Tubulin (1:200) dissolved in Blocking Buffer	Overnight at 4°C
Secondary Antibody Solution	568-anti (1:200) Mouse (raised in donkey) dissolved in Blocking Buffer	2 hours at room temperature
DAPI	2 µg/mL (1: 500) in PBST	15 mins at room temperature

Table 3.4: List of buffers used for staining with B3 Tubulin

For details of the antibodies used for immunofluorescence refer Table 2.16 (Chapter 2-Part B)

4.3.2.5 Confocal Imaging and Image Analysis

All images were acquired as per the previously described method with some modifications. For 2D-IF, coverslips from three different wells (n=3) were used per cell line for each time point for statistical analysis. A minimum of three different areas per coverslip (max- five) were analysed. For 3D cultures, cryosections (14 microns) from three different 3D culture/well per cell line were used for each immunocytochemistry and for statistical analysis. A minimum of three different areas per section (max- five) were analysed.

Leica Application Suite X (Las X Industries, Inc) and ImageJ, Fiji was used to process the confocal images. In order to normalize and have a fair comparison between the 2D and 3D cultures, the densest z-stack (tiff images) was analysed in both 2D and 3D formats to measure the total surface area positive for dapi, total area positive for the 488-channel and/or the total area positive for 568-channel after thresholding in ImageJ. Each measured positive area for a given marker was then normalized against the area positive for DAPI to calculate the relative proportion of the respective marker positive cells for each channel.

3.5 Western Blotting

3.5.1.1 BCA

Pierce™ BCA Protein Assay Kit (Sigma Aldrich, 23227) was used to perform BCA on 2D and 3D cultures (1well per culture) for total protein estimation. BSA standards were prepared as per the kit to establish the standard curve. The protein concentration of each well used for western blotting was estimated using the BCA Protein Assay kit and since there were not much starting material to work with a 1:5 dilution was used (n=2) for each measurement. The OD for both the standards and the cultures were measured using a plate reader with the software Tecan, iPill. at 570nm. GraphPad Prism (GraphPad software, Inc). ver.8.4 was used to measure the unknown protein concentration of cultures against the known standard concentrations.

3.5.1.2 Sample Preparation for Western Blot – Total Lysate – 2D and 3D cultures.

2D and 3D samples for total lysates for Western Blots were prepared following the method as described in Chpater2-Part B-2.4.1.3 for each cell line one well of the 3D cultures was considered as n=1. The details of the extraction buffer used in detailed in Table 3.5.

EXTRACTION BUFFERS	COMPONENTS	FINAL CONCENTRATION
TBS BUFFER	Tris-HCl pH 7.4	50 mM
	NaCl	175 mM
	HALTS Protease and Phosphatase Cocktail Inhibitor	1X

Table 3.5: Composition of Lysis Buffer for Total lysates

The method for Western Blot for 2D and 3D cultures were followed as described in chapter 2-Part B.

The blots were stained with Total Tau (Dako- raised in rabbit) – 1:10,000 and β- Actin (raised in mouse) – 1:2,000 at 4°C overnight. Goat-anti-rabbit (800) and goat – anti -mouse (680) – 1:20,000 were used as secondary antibodies. Licor Imaging System with Odyssey software was used to detect the signals from the secondary antibodies at 680 and 800nm (Table 2.21).

3.5.1.3 Densitometry

The western blots were analysed using densitometry. This is a semi-quantitative method to measure the intensity of the bands of a given concentration of protein detected by the antibody. Licor Imaging System with Odyssey software was used to detect the signals. The scanned blots were processed in Image J software. The density of bands was calculated, and the ratio of Total tau/actin was determined.

3.6 Results

3.6.1 Expression profile of 2D cultures at week 0 *in vitro*

All the 2D and the 3D cultures were stained with the stem cell marker Nestin, neuronal marker B3 Tubulin, neuron-specific differentiation marker MAP2 and the astrocyte marker GFAP at timepoints 0-, 6- and 12-weeks post differentiation in order to get a clear understanding of the progress of differentiation of the cell lines in both 2D cultures (0, 6 weeks) and 3D cultures (0, 6 and 12 week) over time and to compare and contrast 2D and 3D cultures or control and AD cell lines.

At day1 post seeding (before any differentiation factors are added), cells plated on coverslips were used to stain for all the markers to characterise the iPSC-derived cells at week 0 timepoint (Fig 3.2). At this stage the Matrigel in 3D cultures is not stable enough to undergo cryosection, hence the 2D- 0week cultures are considered a common start point for both 2D and 3D culture formats.

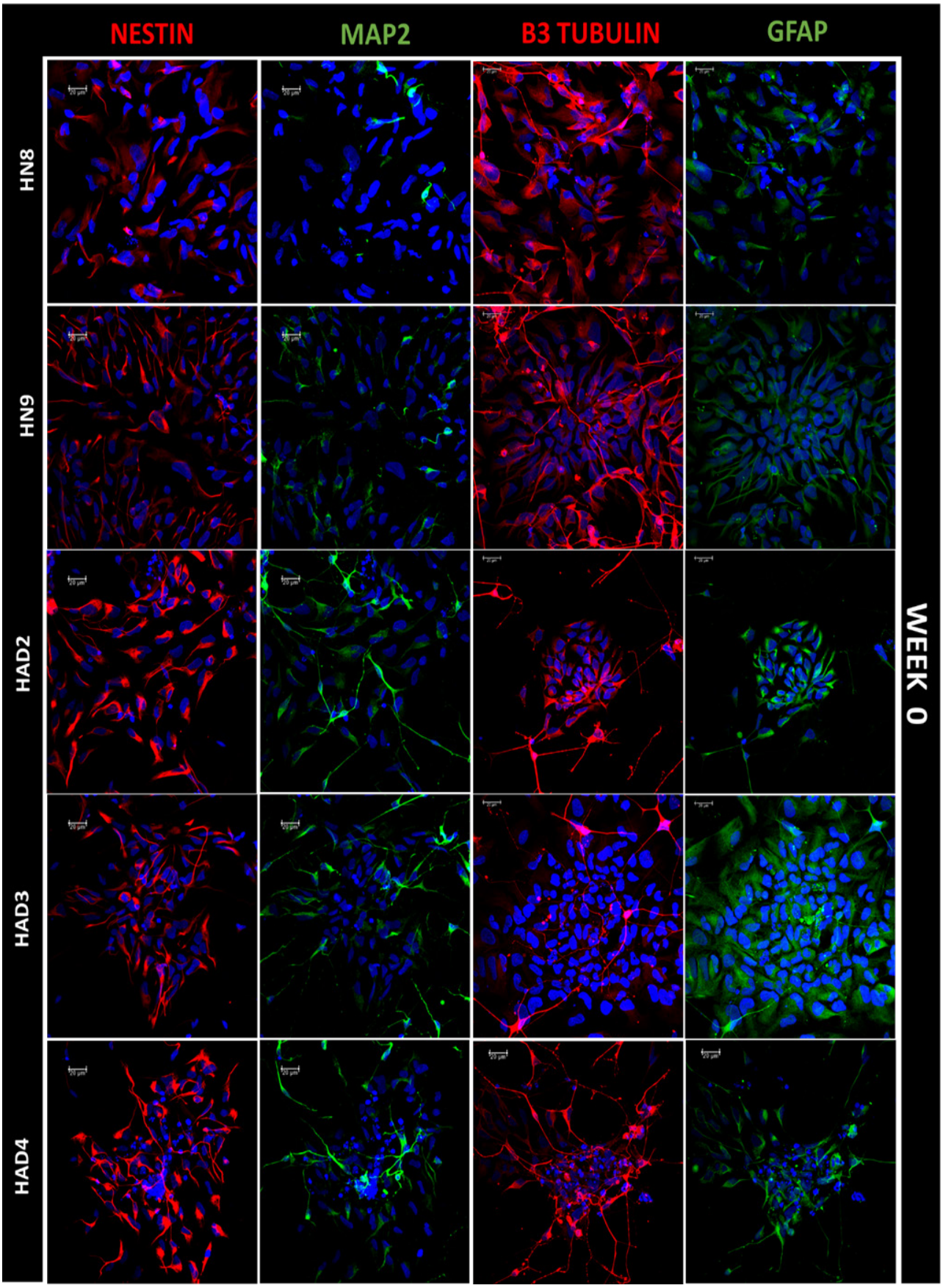

Figure 3.2: Immunofluorescence images of the week 0 (2D cultures) – IF staining for Nestin (red), Map2 (green), B3 Tubulin (red) and GFAP (green) for all 5 cell lines. The nucleus is stained blue with DAPI. (Scale bar=20µm) (n=3).

Nestin, a NSC marker is seen across all cell lines, as expected. However, there is a significant difference in the relative proportions of Nestin between the control group hN8 and AD cell line- hAD2 at week 0 timepoint. Similarly, there is a significant difference in the relative proportion of $MAP2^{+}$ cells between the control cell line hN9 and AD cell line hAD2 at week 0 timepoint. There is no significant difference across groups for the expressions of B3 Tubulin and GFAP (Fig3.3).

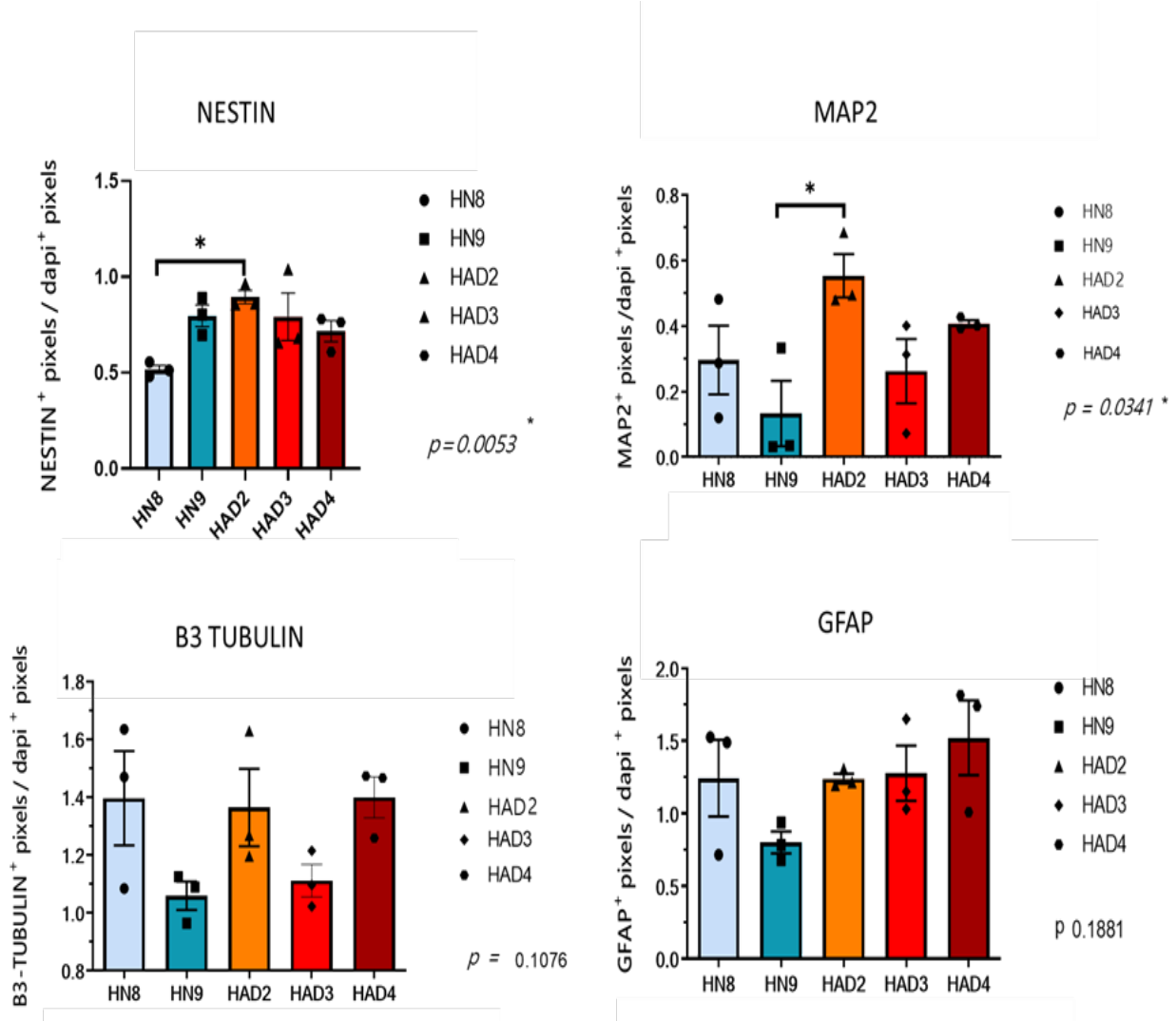

Figure 3.3: Immunofluorescence analysis of the week 0 (2D cultures) – IF staining for Nestin, Map2, B3 Tubulin and GFAP (n=3 wells, minimum of 3 images analysed per well). The data for Nestin, B3 Tubulin and GFAP were normally distributed hence One-way Anova was used for analysis with Bonferroni's multiple comparison for post-hoc test. Data for MAP2 was not normally distributed hence non-parametric Kruskal-Wallis test with Dunn's correction was used for analysis. * p<0.05.

B3 Tubulin is an early developmental neuronal marker. Its expression comes up early during the foetal developmental process and stays throughout maturity in an adult. The 2D cultures were stained with this marker to analyse the overall difference in relative proportion of neurons in the cultures between cell lines. On analysis, thereis no difference in the relative proportion of neurons between the control cell lines hN8 and hN9 at 6 weeks post differentiation in 2D cultures. However, there is a significant increase in the relative proportion of B3 Tubulin between the control cell line hN9 and AD cell line hAD3 (Fig 3.4). There seems is no significant difference between the 0 week and the 6 weeks cultures. Unfortunately, due to shortage of cells and time, no analysis could be done for hAD2 and hAD4 2D cultures.

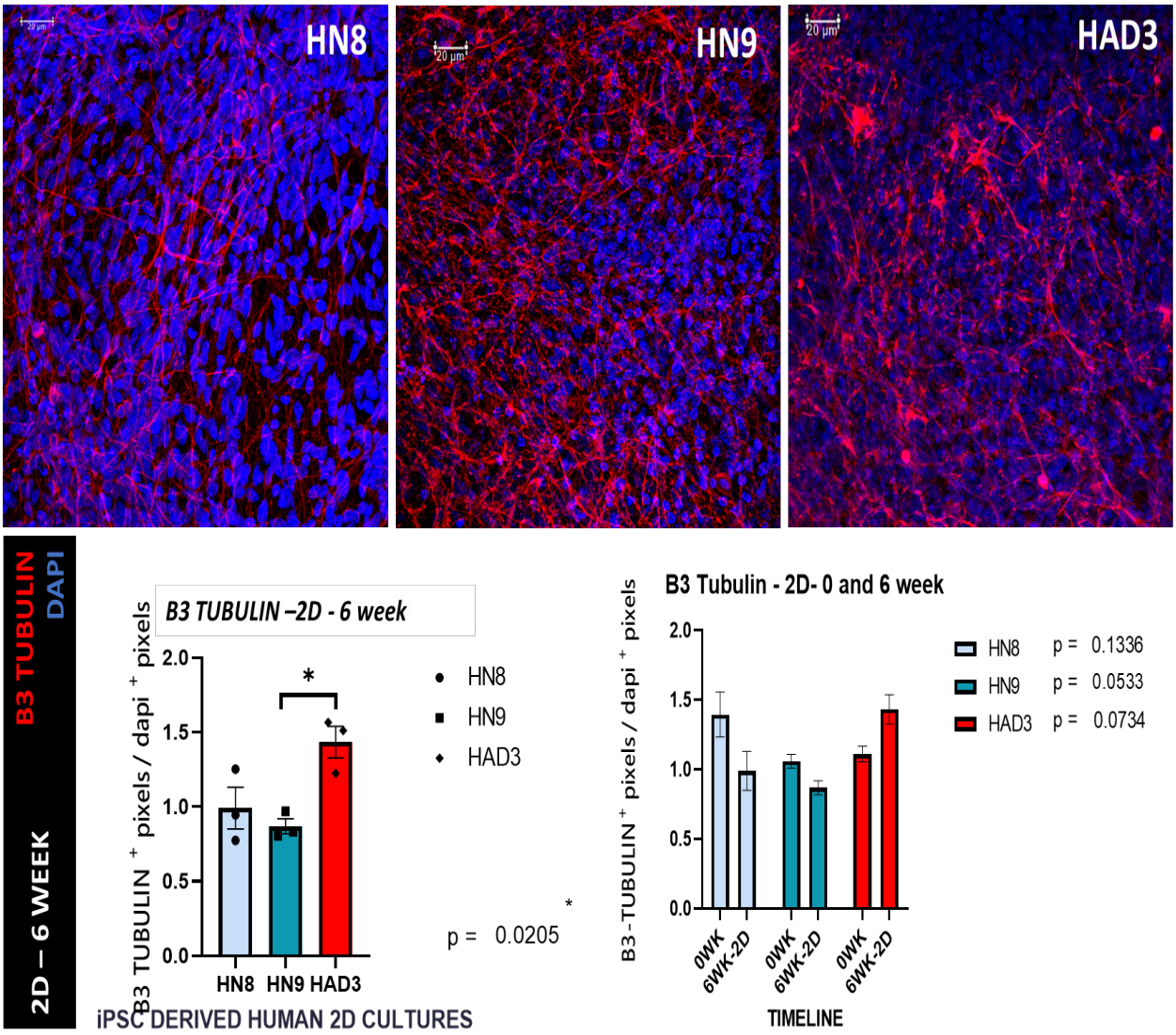

Figure 3.4: Immunofluorescence images of the week 6 (2D cultures) post differentiation – IF staining for B3 Tubulin (red) and its quantification (n=3). The nucleus is stained blue with dapi. (Scale=20µm). One-way Anova was used for analysis across cell lines at 6 weeks post differentiation since the data was normally distributed. An. unpaired t-test was used to analyse each cell line at 0- and 6-weeks post differentiation. All data were normally distributed hence the t-test with Welch's correction was used for analysis. * p<0.05.

MAP2 is a neuron specific marker seen in post-mitotic neurons. The MAP2^{+} cells appear to be staining the cytoskeletal processes and forming a wide-flattened meshwork across the cultures. On analysis, 2D cultures were found to express MAP2 at 6 weeks post differentiation (Fig 3.5). However, there is no significant difference in the relative proportions across the cell lines at 6 weeks post differentiation. When compared to the 0-week timepoint, the relative proportions of MAP2 positive cells in the 2D cultures (across cell lines) show an overall increase at 6 weeks post differentiation, however this is not a significant increase.

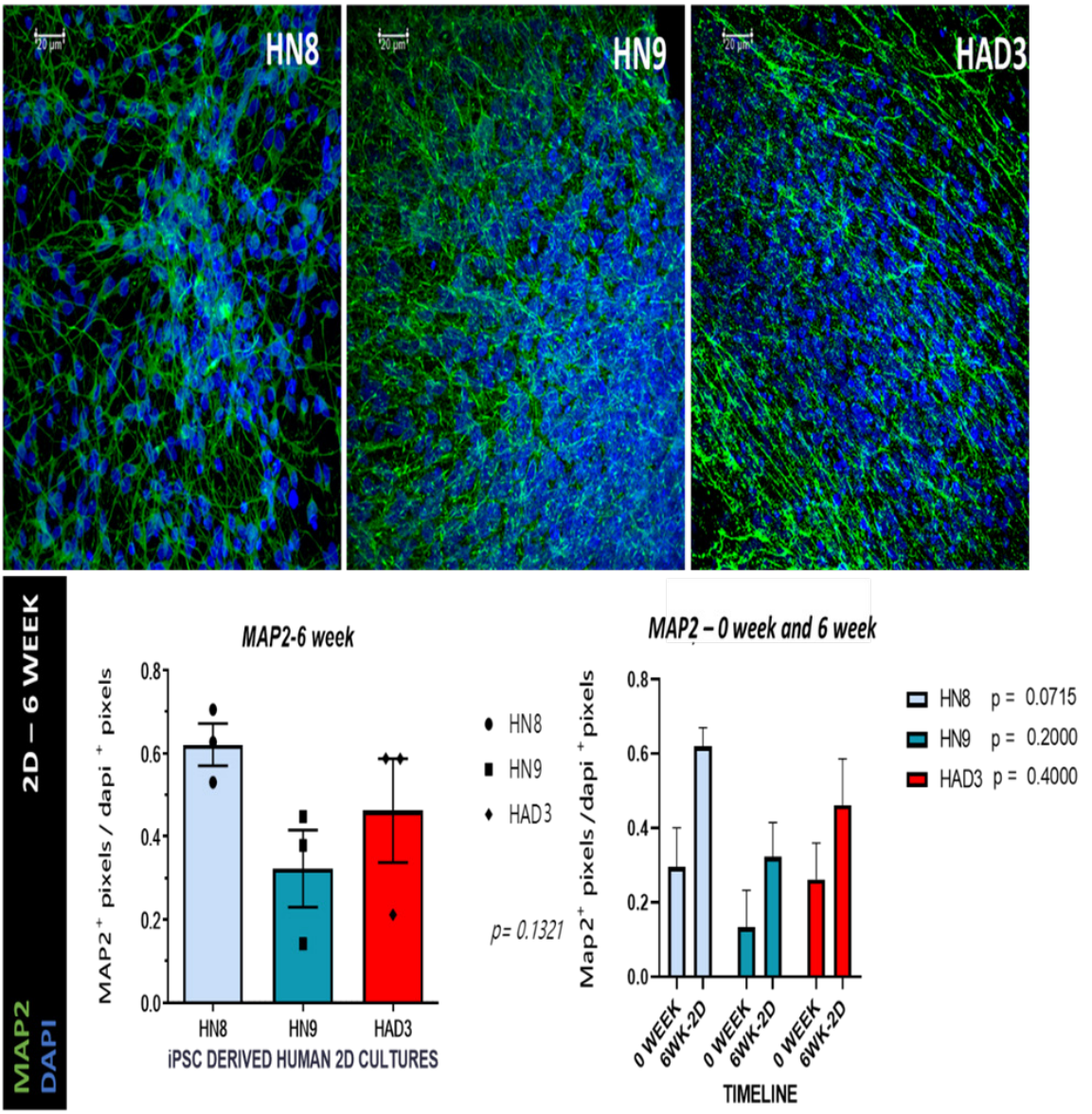

Figure 3.5: Immunofluorescence images of the week 6 (2D cultures) post differentiation – IF staining for MAP2 (green) and its analysis (comparative analysis against week 0) (n=3). The nucleus is stained blue with dapi. (Scale=20µm). The data for MAP2-2D-6week was not normally distributed hence a non-parametric Kruskal-Wallis test with Dunn's correction was performed. An unpaired – t- test was used to analyse each cell line at different timepoints. The data for HN8 was normally distributed hence a t-test with Welch's correction was performed whereas data for HN9 and HAD3 were not normally distributed hence a Mann-Whitney test was performed. * p<0.05

3.6.2 Stem cell marker decreases at 6 weeks post differentiation in 2D cultures *in vitro*

Nestin is identified as a neural stem cell marker in the developing and the adult brains. Nestin^{+} cells appear to be small flat elongated cells with staining in the cytoskeleton of the cells. On analysis, the iPSC derived NSCs (both control and AD lines) express Nestin at 6 weeks post differentiation. However, there is no significant difference across the groups at 6 weeks post differentiation. When compared to week 0, there is a significant decrease in the relative proportion of Nestin in hN9 and hAD3 at 6 weeks post differentiation, which was what we expected to see from the optimized differentiation protocol (ref Chapter 2 Part A) (Fig 3.6).

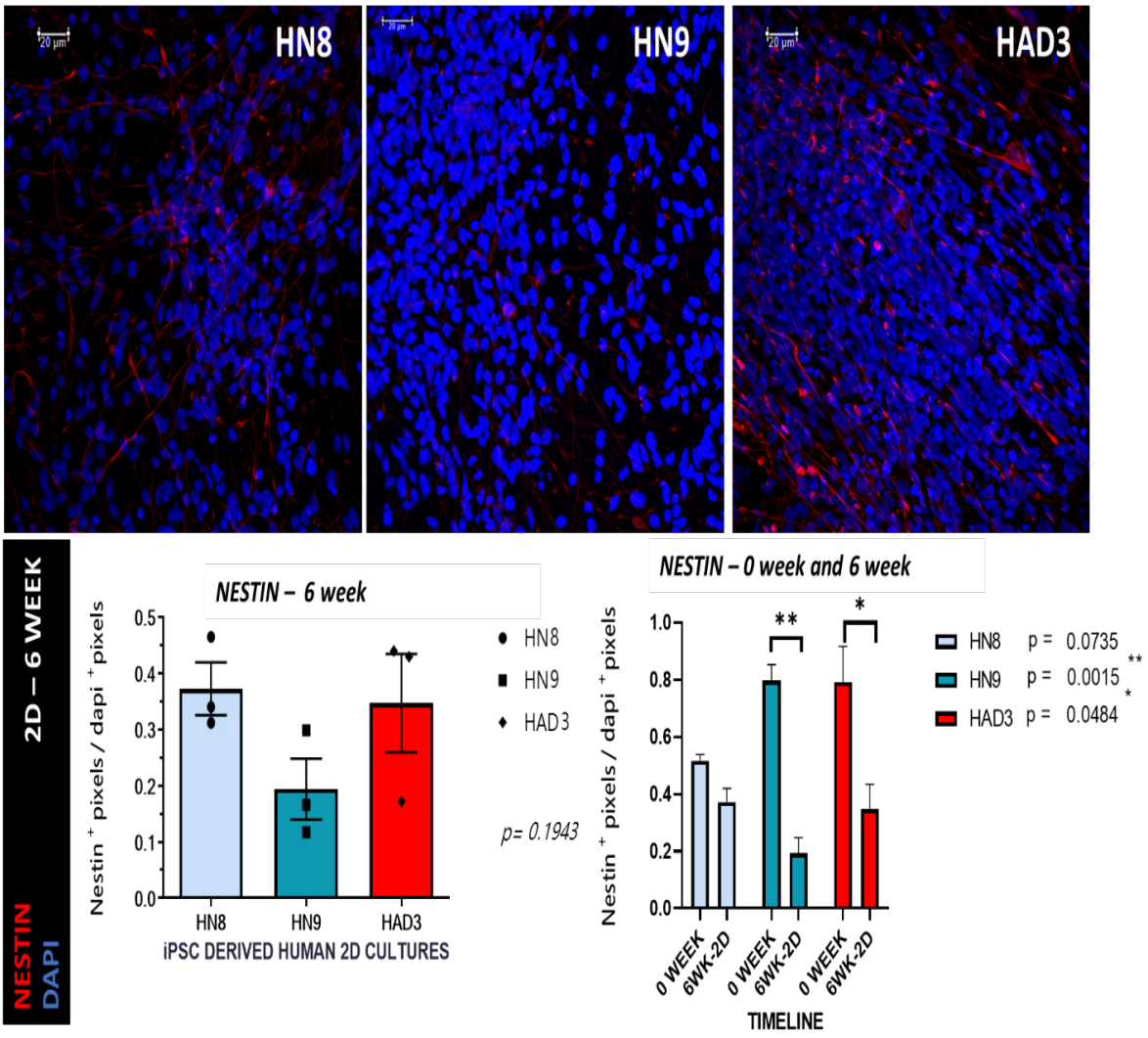

Figure 3.6: Immunofluorescence images of the week 6 (2D cultures) post differentiation – IF staining for Nestin (red) and its analysis (comparative analysis against week 0) (n=3.. The nucleus is stained blue with dapi. (Scale=20µm). One- way Anova with Bonferroni's multiple comparison post-hoc test was used for analysis across the different cell lines at 6 weeks post differentiation since the data was normally distributed. An Unpaired-t-test was performed to compare each cell line at different timepoints (0 and 6 weeks post differentiation). Since all data were normally distributed t-test was performed with Welch's correction. *p<0.05, ** p<0.01

3.6.3 2D cultures differentiate into astrocytes at 6 weeks post differentiation *in vitro*

GFAP, identified as the astrocytic marker in the CNS was used to analyse the proportion of astrocytes in culture. GFAP $^{+}$ cells appear flattened-long elongated process intertwining between cells forming a network. They don't appear to have a definitive pattern but rather are randonly distribiuted across the cultures. On analysis, there is no significant difference between the two control groups. However, there is a significant difference between the control cell line hN8 and AD- cell line hAD3 at 6 weeks post differentiation in the 2D cultures (Fig 3.7). There is a significant decrease in the proportion of GFAP positive cells in 6 week post differentiation as compared to the 0 week timepoint across cultutres. As explained before due to shortage of cells and time hAD2 and hAD4 cell lines could not be analysed.

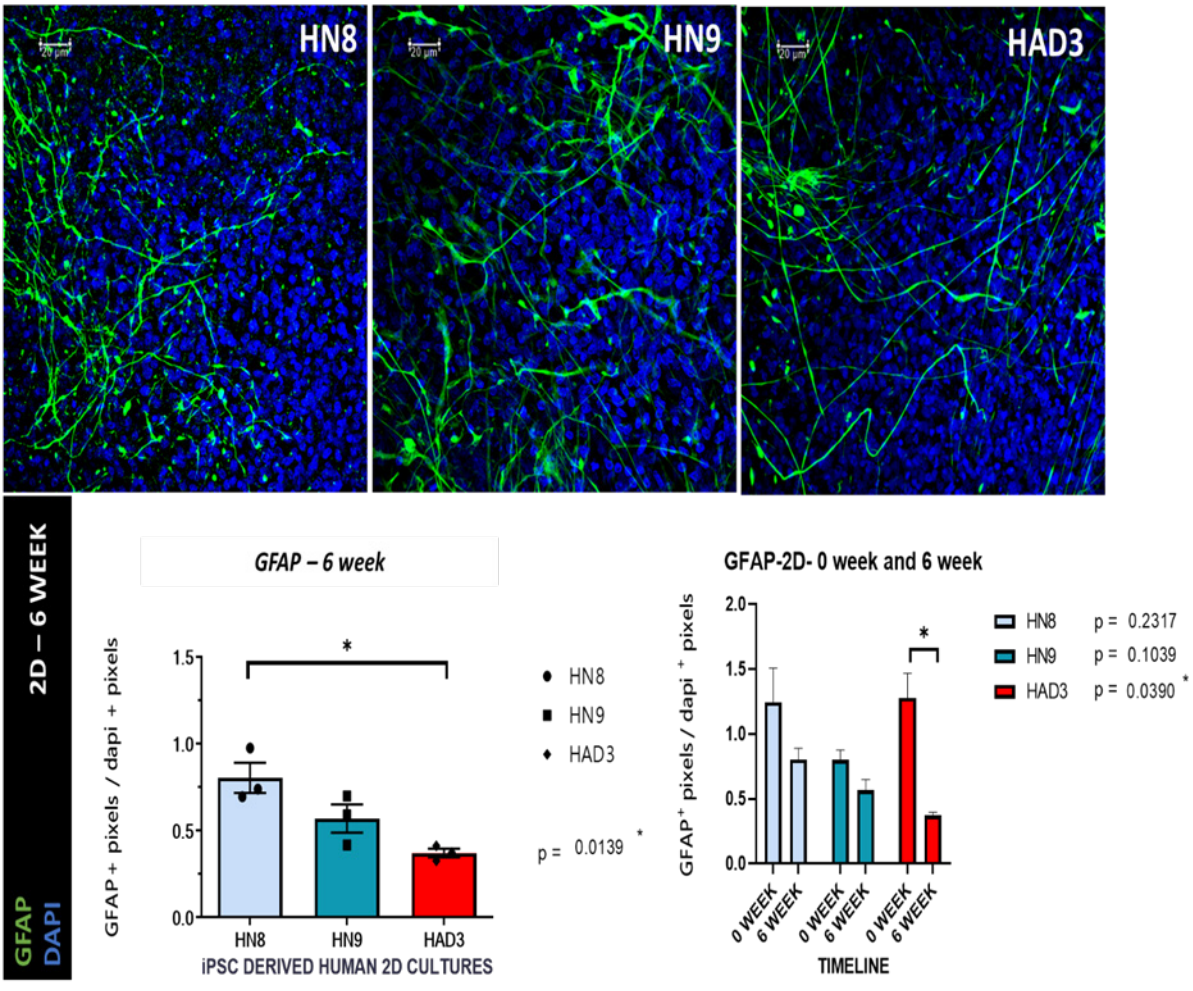

Figure 3.7: Immunofluorescence images of the week 6 (2D cultures) post differentiation – IF staining for GFAP (green) and its quantifications (n=3). The nucleus is stained blue with dapi. (Scale=20µm). One-way Anova with Bonferroni's multiple comparison post-hoc test was used to analyse the 2D-6 weeks GFAP across cell lines since the data was normally distributed. An unpaired-t-test with Welch's correction was used to compare between the 0 and the 6 weeks post differentiation-GFAP of each cell line since all the data were normally distributed. *p<0.05.

3.6.4 3D Cultures express Neuronal Markers at 6 weeks post differentiation *in vitro*

The 3D cultures at 6 weeks post diffrentiation express B3 Tubulin across all groups. B3 Tubulin appears to be present in the filaments in the cytoskeleton around the nucleus, forming a dense structurall network of filaments around the cells in the cultures. These filaments look thicker and denser than in the 2D cultures. On analysis, there is no significant difference across the cell lines at the 6 weeks timepoint for 3D cultures. Due to shortage of time hN8 could not be analysed (Fig 3.8).

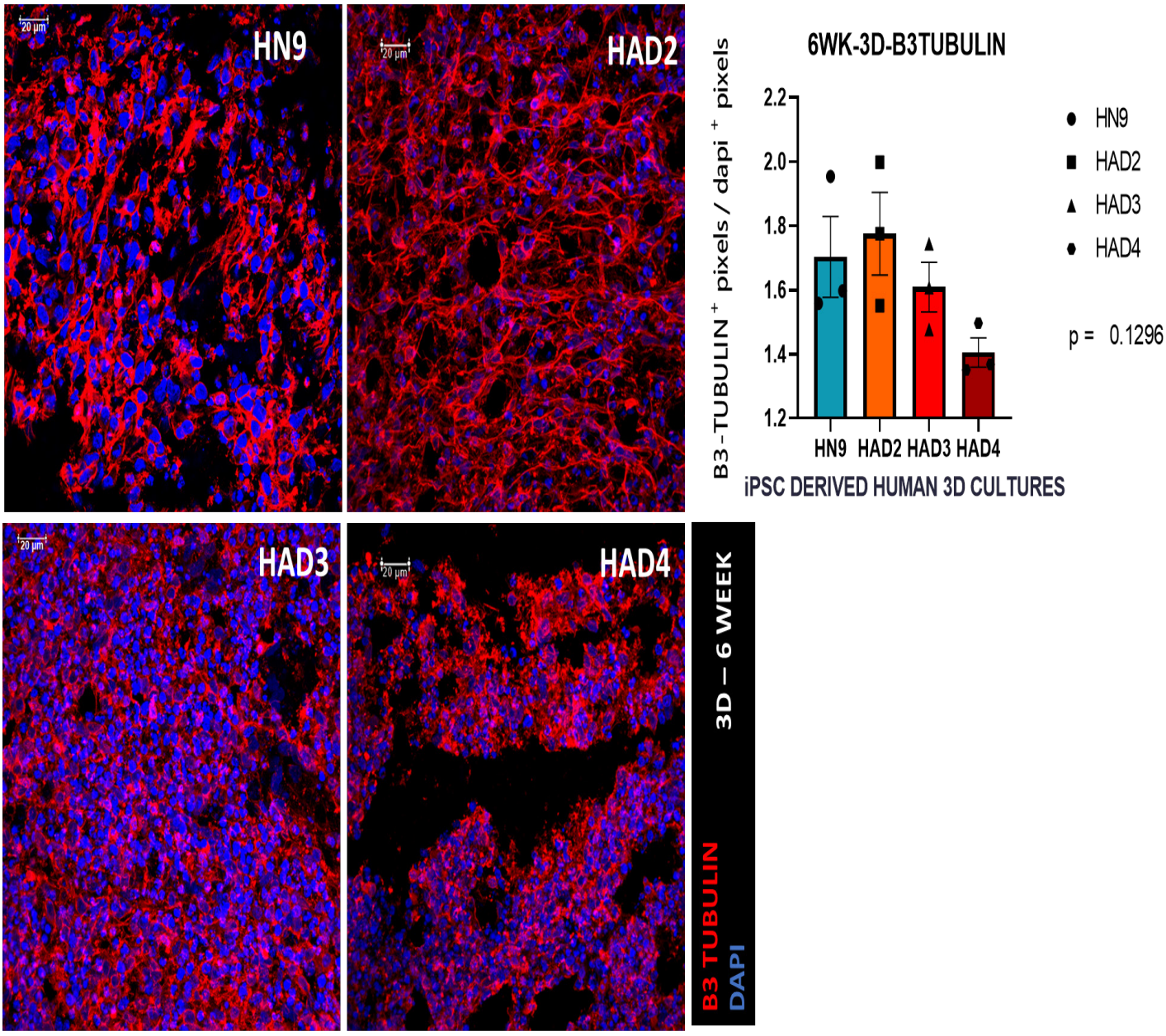

Figure 3.8: Immunofluorescence images of the week 6 (3D cultures) post differentiation – IF staining for B3 Tubulin (red) and its analysis. The nucleus is stained blue with dapi. (Scale=20µm). The data was normally distributed. One-way Anova was used for analysis with Bonferroni's multiple comparison post-hoc test.

Where B3 Tubulin is expressed by both immature and mature neurons, MAP2 is more specific for the mature post-mitotic neurons. Hence, compared to the relative proportion of B3 Tubulin across the cell lines at 6 weeks post differentiation is a smaller proportion of $MAP2^{+}$ cells. This is indication that 6 weeks post differentiation is an early time point in the *in vitro* developmental process. On analysis of the relative proportions of MAP2 in the 3D cultures at 6 weeks post differentiation there is no significant difference overall across the different cell lines except between the control line hN8 and the AD line hAD4 and between the AD lines hAD2 and hAD4 could not be analysed (Fig 3.9).

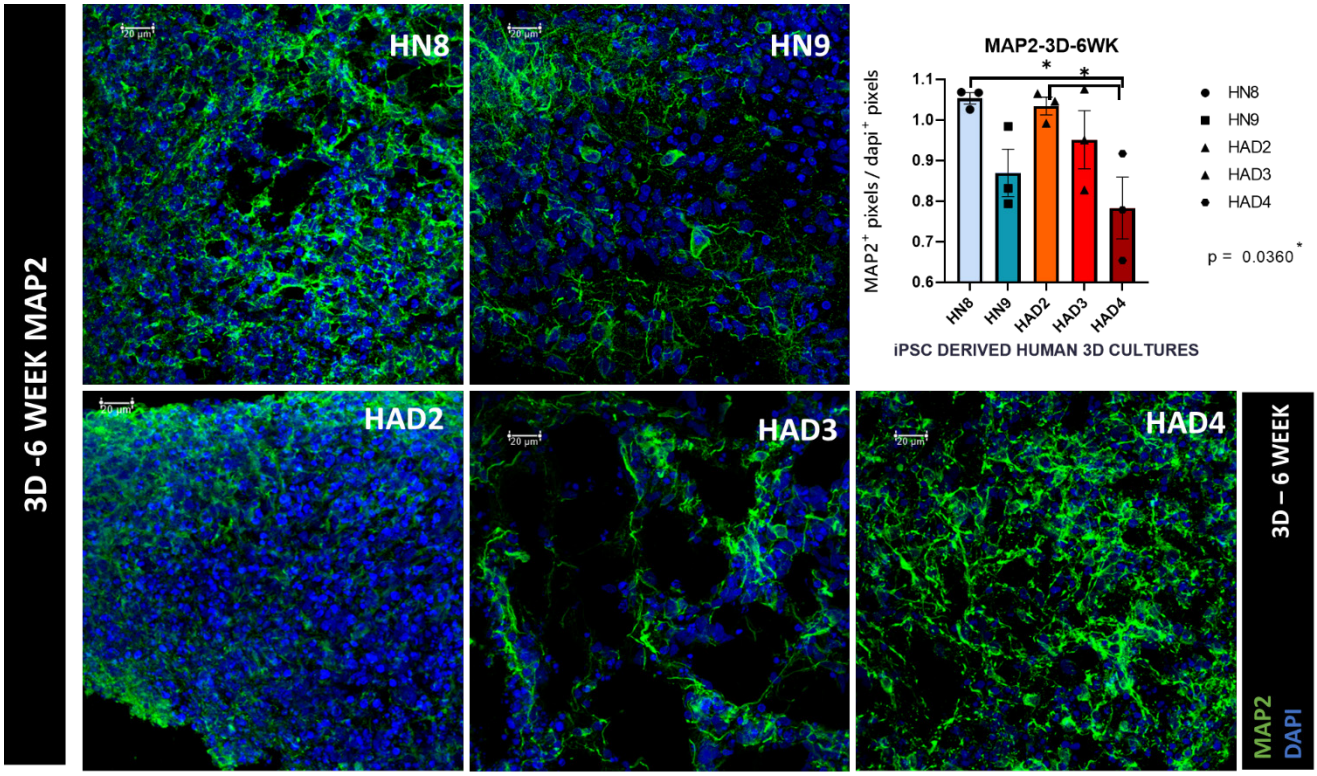

Figure 3.9: Immunofluorescence images of the week 6 (3D cultures) post differentiation – IF staining for MAP2 (green) and its analysis (n=3). The nucleus is stained blue with dapi. (Scale=20µm). Since the data was not normally distributed Kruskal-Wallis test with uncorrected Dunn's post-hoc test. was used for analysis. (Kruskal-Wallis test with Dunn's correction showed no significant difference between the groups). *p<0.05

3.6.5 Stem cell marker decreases at 6 weeks post differentiation in 3D cultures *in vitro*

Since 6 weeks post differentiation is yet an early timepoint in the differentiation process *in vitro,* Nestin expression is not entirely unexpected. Nestin staining appears filament like in 3D cultures but filaments are much smaller and less denser than the MAP2 and B3 Tubulin. On analysis there is no significant difference between the different cell lines at 6 weeks post diffrentiation except for hAD3 and hAD4 (Fig 3.10). However compared to week 0 there is a drop in the relative expression levels of Nestin at 6 weeks post differentiation (Fig 3.10).

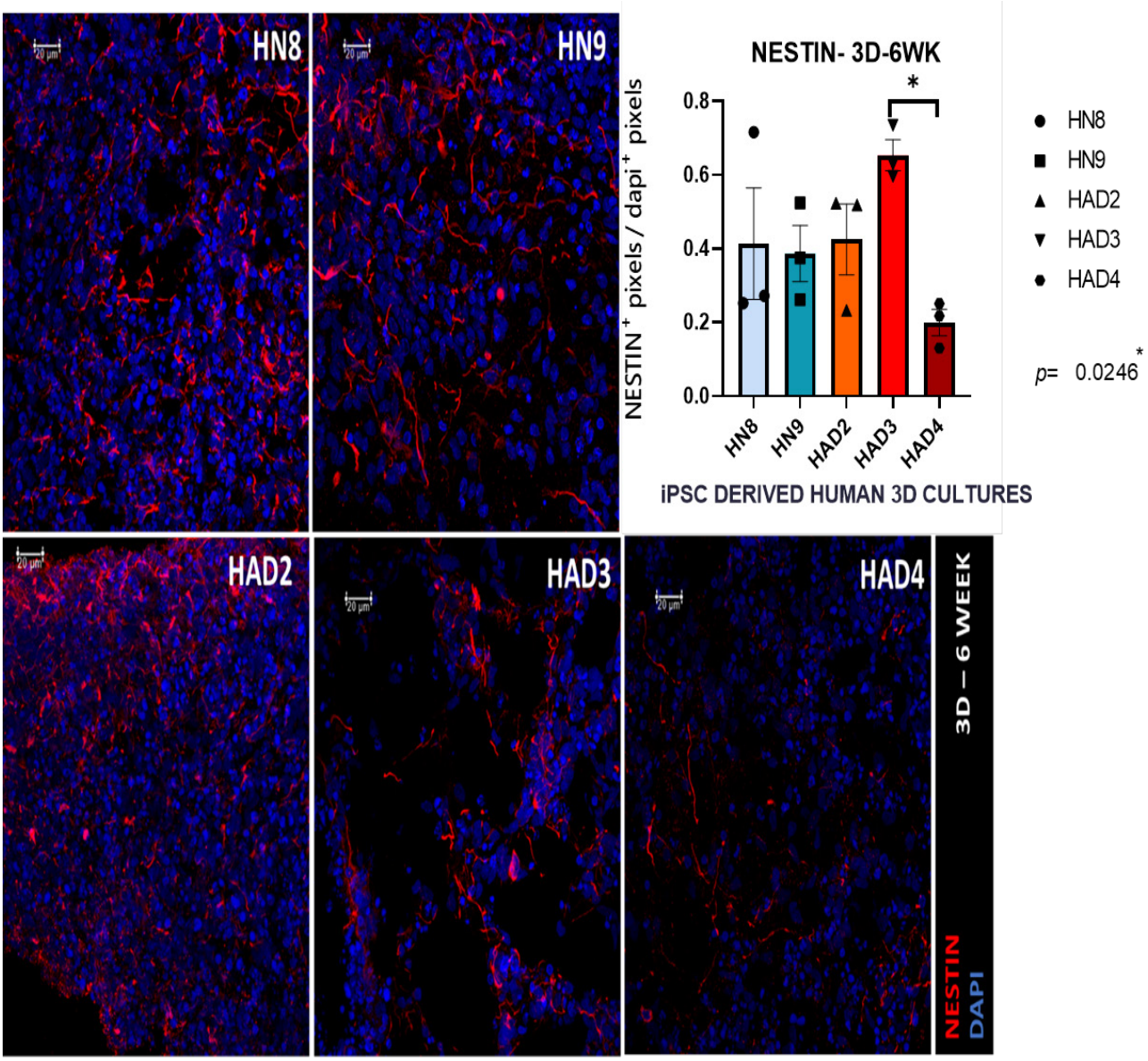

***Figure 3.10:** Immunofluorescence images of the week 6 (3D cultures) post differentiation – IF staining for Nestin (red) and its analysis. The nucleus is stained blue with dapi. (Scale=20µm). Since the data was not normally distributed Kruskal-Wallis test with Dunn's correction was used for analysis. *p<0.05*

3.6.6 3D cultures differentiate into astrocytes at 6 weeks post differentiation *in vitro*

GFAP$^+$ cells in 3D cultures appear long elongated tube like process intertwining between cells forming a network. They don't seem to have a definitive pattern but rather are randomly distributed across the cultures. On analysis, there is no significant difference across the different cell lines at 6 weeks post differentiation (Fig 3.11).

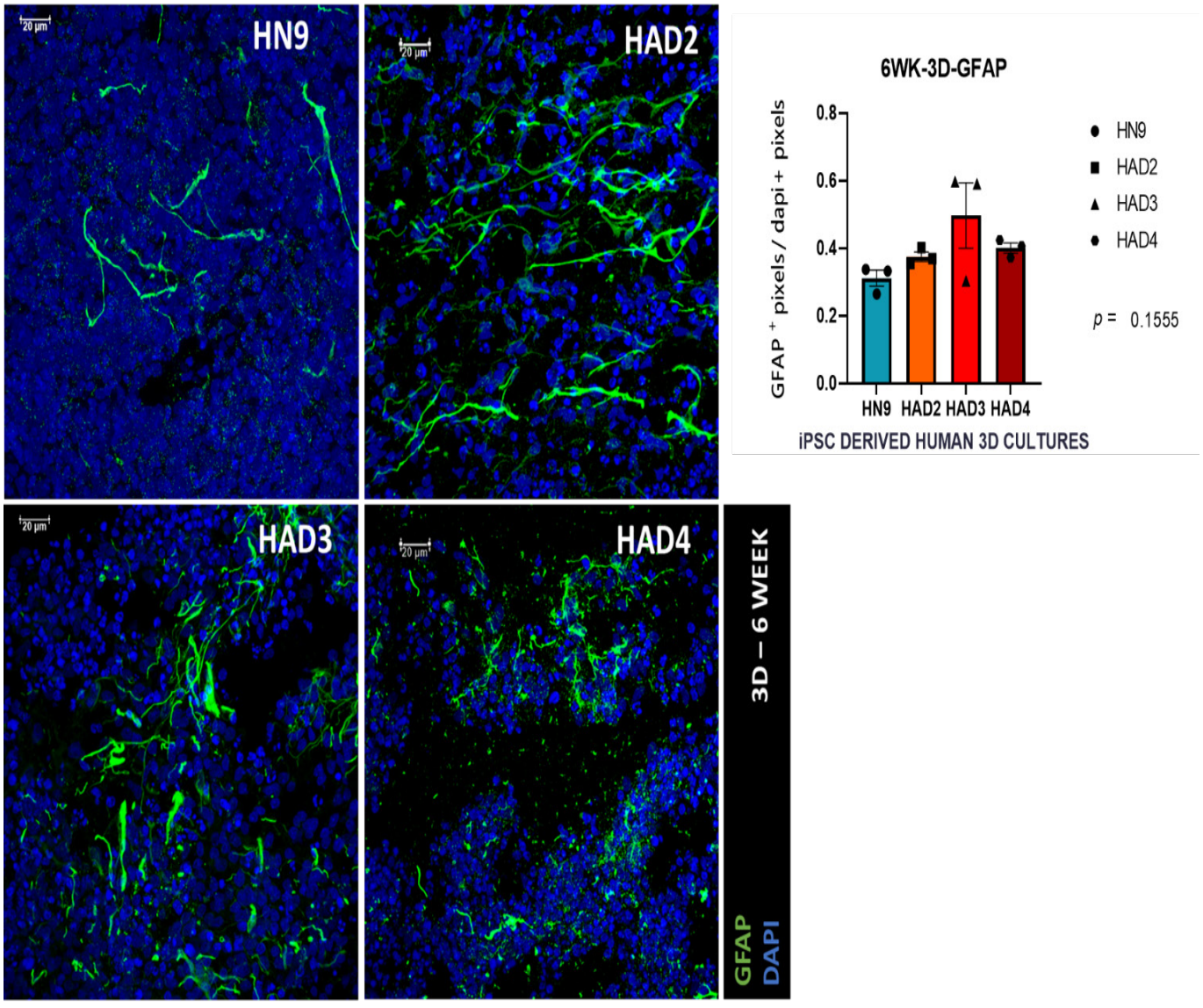

Figure 3.11: Immunofluorescence images of the week 6 (3D cultures) post differentiation – IF staining for GFAP (green) and its analysis (n=3). The nucleus is stained blue with dapi. (Scale=20µm). the data was not normally distributed. Kruskal-Wallis test with Dunn's correction was used for analysis.

3.6.7 Characterisation of 3D cultures at a later stage of differentiation *in vitro*

At 12 weeks post differentiation the 3D cultures were stained with all the above mentioned markers not just to analyse the long term progress of the diffrentiation of iPSC derived NSCs but also to check for any differences in the control and AD cell lines.

At 12 weeks post differentiation the relative proportion of B3 Tubulin of the 3D-control line hN9 and the 3D-AD lines- hAD2 and hAD3 were analysed. There is no significant difference across the different cells lines at this given timepoint (Fig 3.12).

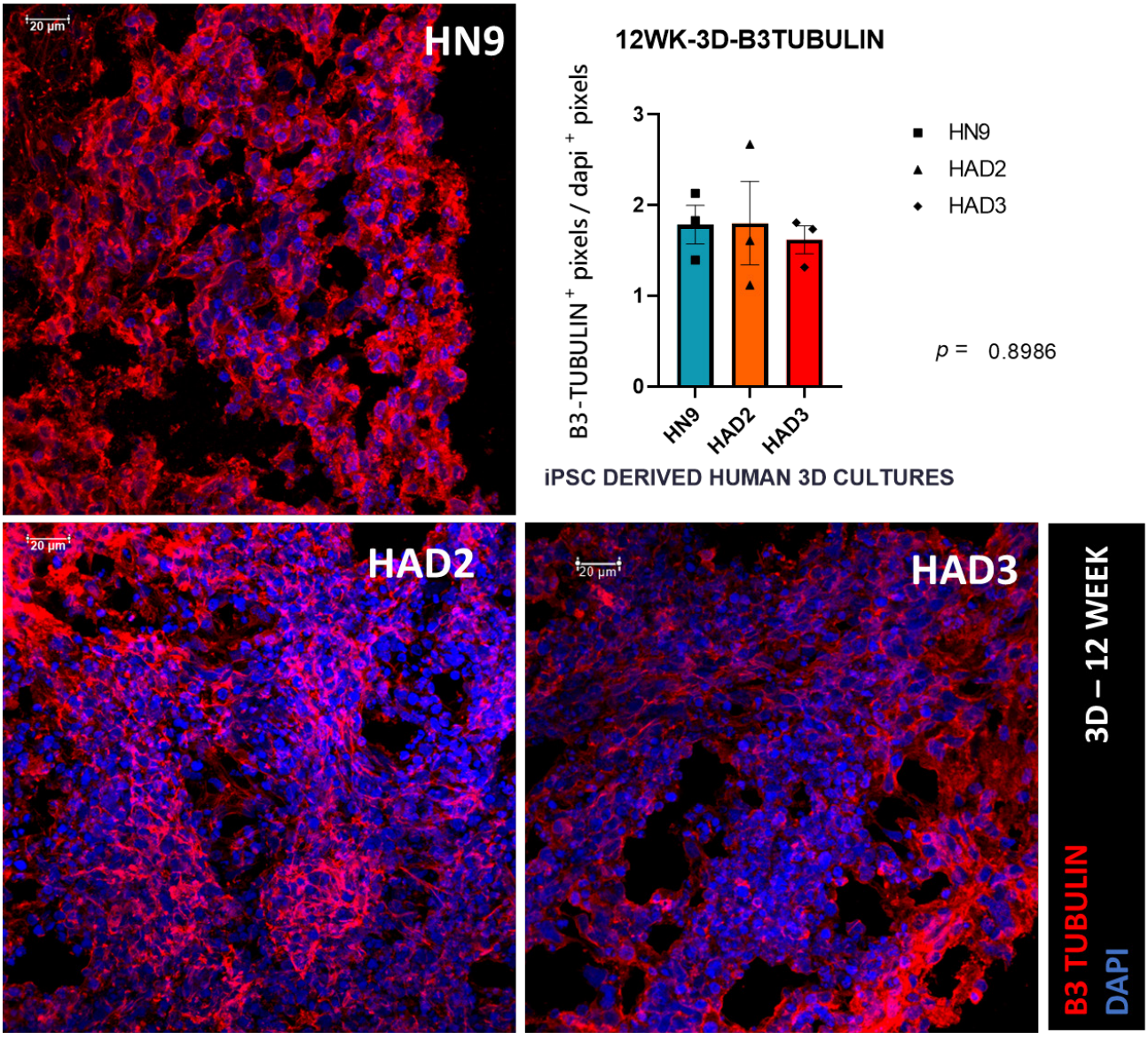

Figure 3.12: Immunofluorescence images of the week 12 (3D cultures) post differentiation IF staining for B3 Tubulin (red) and its analysis (n=3). The nucleus is stained blue with dapi. (Scale=20µm). The data was normally distributed. One-way Anova was used for analysis with Bonferroni's multiple comparison post-hoc test was performed.

There is no differences between the 3D-control groups for the relative proportions of MAP2 at 12 weeks post differentiation. However, there is a significant difference between the 3D-hAD3 and 3D-hAD4 cell lines at 12 week post differentiation (Fig 3.13).

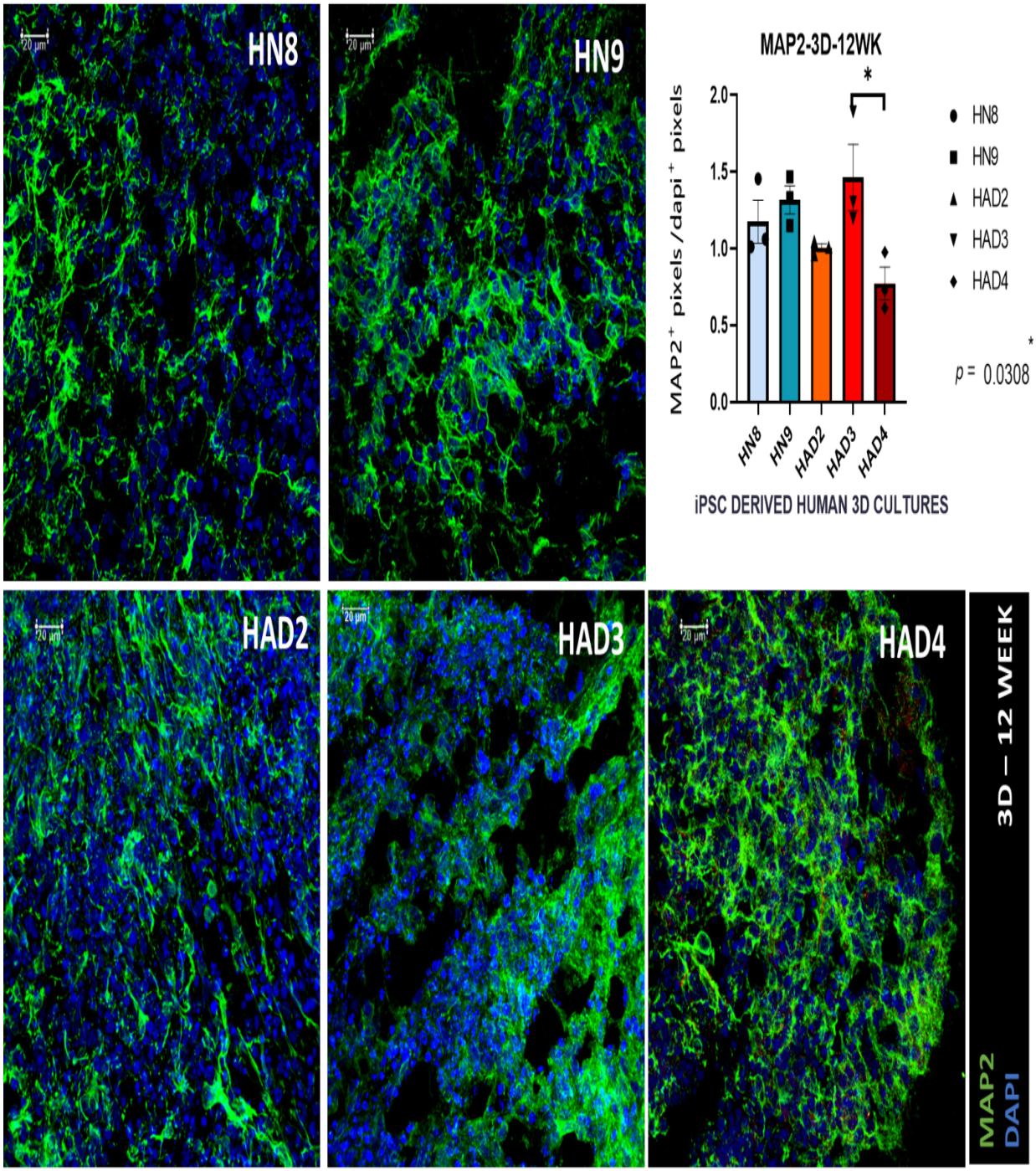

Figure 3.13: Immunofluorescence images of the week 12 (3D cultures) post differentiation – IF staining for MAP2 (green) and its analysis (n=3). The nucleus is stained blue with dapi. (Scale=20µm). The data was normally distributed. One-way Anova with Bonferroni's multiple comparison post-hoc test was used for analysis.

At 12 weeks post differntiation there is no difference between the 3D-control lines for the relative proportions of Nestin. However, there is a significant difference beween the 3D-AD cell lines hAD3 and hAD4. Similar to the MAP2 expression pattern, there is a difference in the Nestin expression levels of AD-cell lines hAD3 and hAD4 at 12 weeks post differentiation (Fig 3.14).

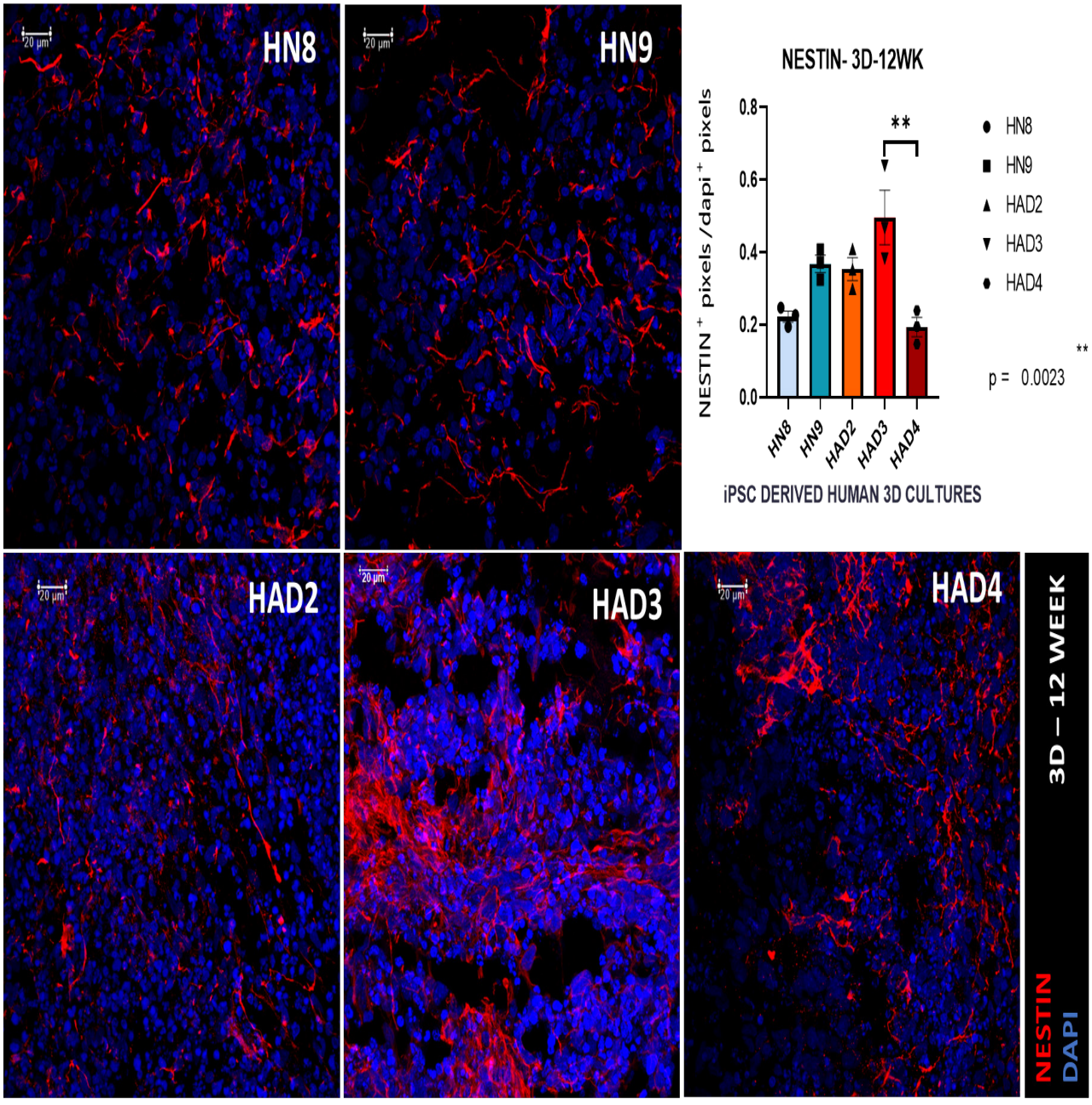

***Figure 3.14:** Immunofluorescence images of the week 6 (3D cultures) post differentiation – IF staining for Nestin (red) and its analysis (n=3). The nucleus is stained blue with dapi. (Scale=20µm). the data was normally distributed. One-way Anova with Bonferroni's multiple comparison post-hoc test was used for analysis*p<0.05, ** p<0.01*

At 12 weeks post differentiation the relative proportion of GFAP of the 3D-control line hN9 and the 3D-AD lines- hAD2 and hAD3 were analysed. There is no significant difference across the different cells lines at this given timepoint (Fig 3.15).

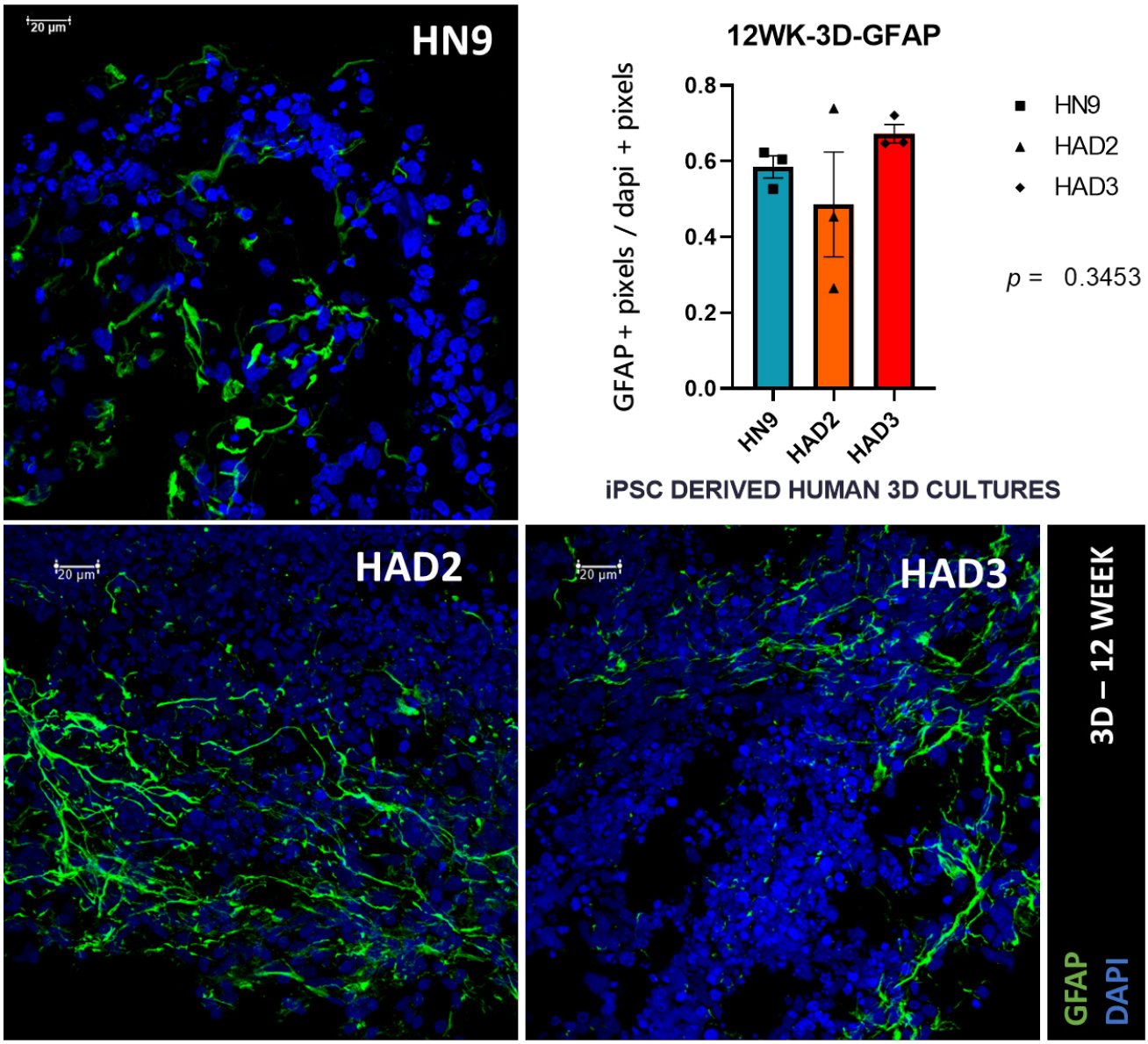

Figure 3.15: Immunofluorescence images of the week 6 (3D cultures) post differentiation – IF staining for GFAP (green) and its analysis (n=3). The nucleus is stained blue with dapi. (Scale=20µm). The data was normally distributed. One-way Anova was used for analysis with Bonferroni's multiple comparison post-hoc test was performed.

3.6.8 A time-based progression of neuronal differentiation in 3D cultures *in vitro*

In order to show a time dependent development of the 3D cultures the relative proportions of the different markers studied above for each cell line was plotted over time.

There overall trend seen in this data is an increase in the relative proportion of MAP2 from week 0 to week 12 post differentiation *in vitro* (Fig 3.16). There is no significant increase in the relative proportions of MAP2 in hN8-3D cultures overtime and hN9-3D cultures over week 0 and week 6 post differentiation. However, there is a significant increase in the relative proportions of MAP2 between week 0 and week 6 as well as week 0 and week 12 in hAD2, hAD3-3D and hAD4-3D. Similarly, in the control cell line 3D-hN9, there is a significant increase in the expression levels of MAP2 between week 0- and 12-weeks post differentiation in the 3D cultures. In both these controls the progression of MAP2 expression is as expected.

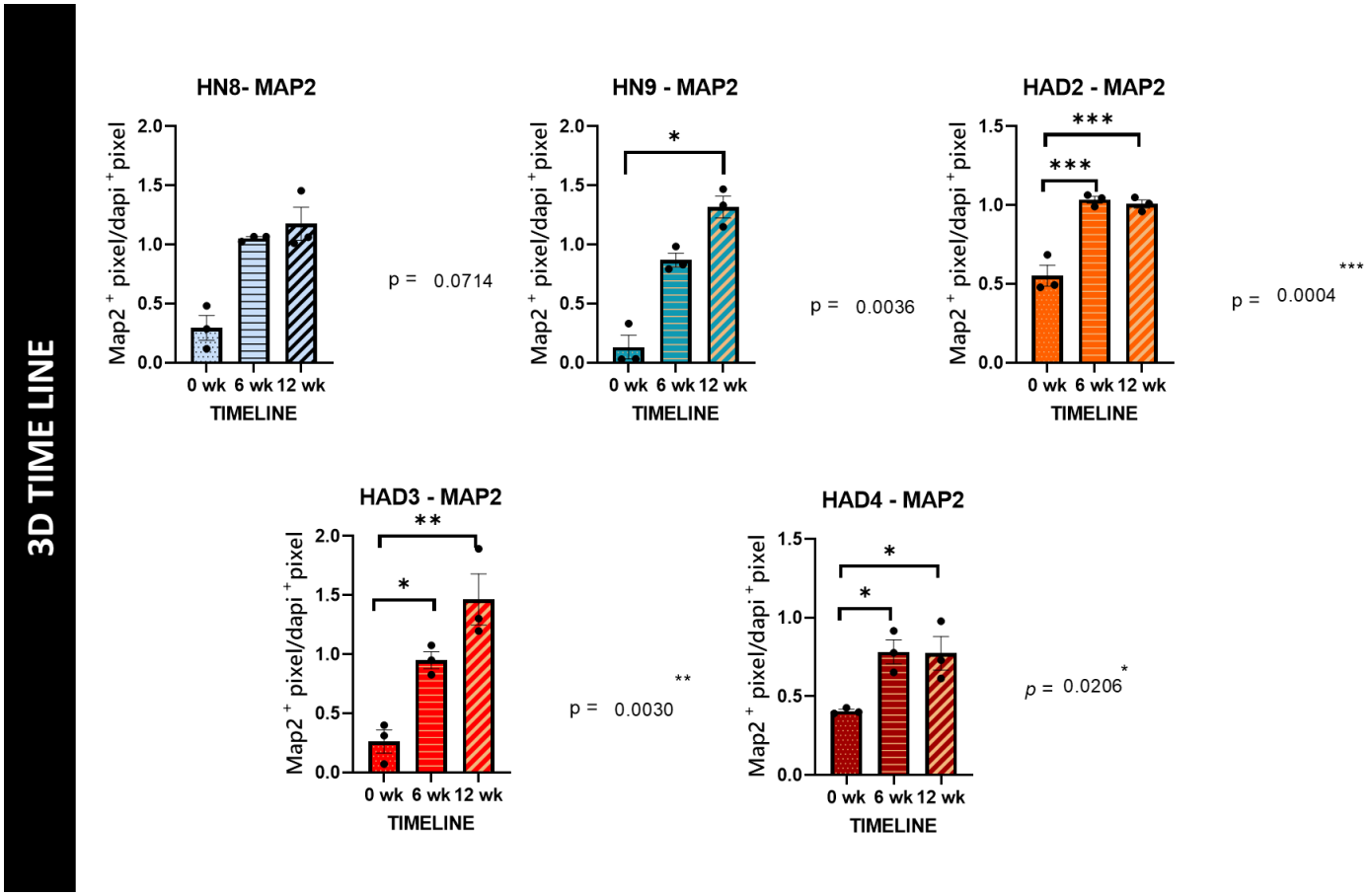

Figure 3.16: Time based analysis of the neuronal marker MAP2 observed in the 3D cultures of hN8, hN9, hAD2, hAD3 and hAD4 at timepoints 0, 6- and 12-weeks post differentiation. The data for HAD2, HAD3 and HAD4 were normally distributed hence One-way Anova with Bonferroni's multiple comparison post-hoc test was used for analysis. The data for HN8 and HN9 were not normally distributed hence the Kruskal-Wallis test with Dunn's correction was used for analysis. *p<0.05, ** p<0.01, *** p<0.001.

The AD cell lines hAD2, hAD3 and hAD4 show a similar trend in the progression from week 0 to 6wk to 12wk post differentiation. There is a significant increase in the relative proportion of MAP2 from week 0 to week 6 and week 0 to week 12 post differentiation in all the AD cell lines. This gives great confidence regarding the development of the 3D cultures whether control or AD cell line is progressing as expected with time, although it looks like there is not much difference between the 6week and 12week timepoints across the cell lines. Nevertheless, the measurements of the relative proportion of MAP2 positive cells at 18 weeks post differentiation would give an even better picture of the progress of differentiation of the 3D cultures *in vitro.*

A similar pattern is observed with the neuronal marker B3 Tubulin (Fig 3.17). There is a significant increase in the relative proportion of B3 Tubulin in the 3D-hN9 at 12-week post differentiation when compared to week 0 timepoint. Although not a statistical difference but there is a slight increase in the relative B3 Tubulin proportions in 3D-hAD2 over time. On the contrary, there is a significant increase in the relative proportions of B3 Tubulin at 6-week post differentiation and 12-week post differentiation when compared to week 0 timepoint in 3D-hAD3 cell line. However, like seen in the MAP2 progression of development in the 3D cultures there seems to be no significant difference between timepoints 6- and 12-weeks post differentiation across the cell lines.

There is a decrease in the relative proportions of GFAP across all cell lines at week 6 and 12 when compared to week 0 post differentiation (Fig 3.17). This could possibly because GFAP is not just identified as an astrocyte specific marker but also as a stem cell/ radial glial marker. At week 0 the antibody must stain mostly neural stem cells that are primed for astroglial differentiation. Hence it follows a pattern similar to the neural stem cell marker Nestin. There is a significant difference in the relative proportions of GFAP between 0-6- and 0-12-week post differentiation across cell lines 3D-hN9 and 3D-hAD3. However, unlike the other markers we have seen there seems to be an opposite effect i.e. increase in relative proportions of GFAP between timepoints 6- and 12-weeks post differentiation across cell lines. This is in line with aging, since the number of astrocytes is known to increase with age in humans.

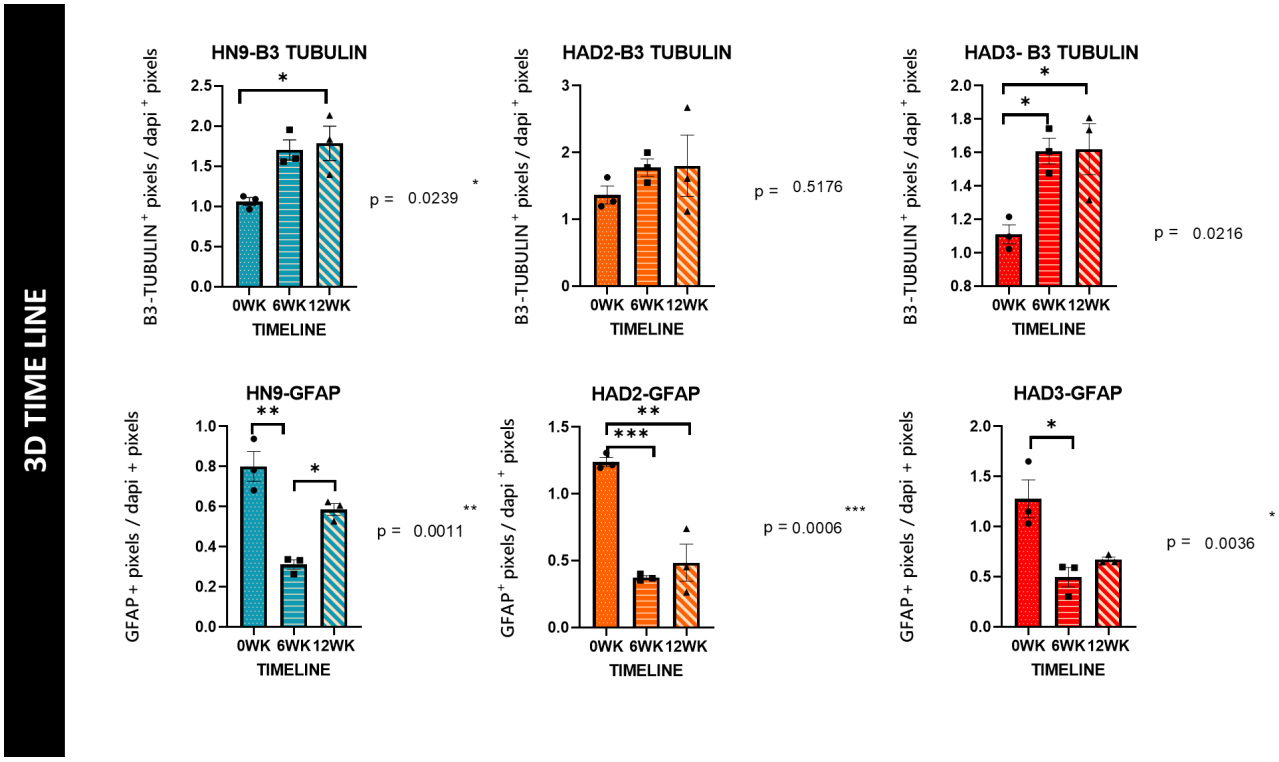

Figure 3.17: Time based analysis of the neuronal marker B3 Tubulin and GFAP observed in the 3D cultures of hN9, hAD2, hAD3 and hAD4 at timepoints 0, 6- and 12-weeks post differentiation. All the data except HAD3-GFAP were normally distributed hence One-way Anova with Bonferroni's multiple comparison post-hoc test was used for analysis. For HAD3-GFAP Kruskal-Wallis test with Dunn's correction was used for analysis. *p<0.05, ** p<0.01, *** p<0.001.

There is a gradual decrease in the expression levels of Nestin from week 0 to 6- and 12-weeks post differentiation (Fig 3.18). This is a clear indication that the optimized differentiation protocol efficiently differentiates iPSC derived NSCs to neurons and glia. Although it remains to see if a later timepoint like 18 weeks would further reduce the expression levels of Nestin across cell lines. There are quiescent stem cell niches in the adult human brain and that could possibly be what we see in these 3D cultures. 3D cultures may facilitate a small population of stem cells to remain quiescent over time *in vitro.* As seen in the figure, there is a significant decrease in the relative proportions of Nestin in the 6 week- 3D-hN9 and 3D-hAD4 cultures when compared to week 0 timepoint. There is a significant decrease in the relative proportions of Nestin in the 12 week-3D-hN9, 3D-hAD2 and 3D-hAD4 cultures when compared to week 0 timepoint. Although there is no significant difference between 6 week and 12-week post differentiation timepoints across cell lines.

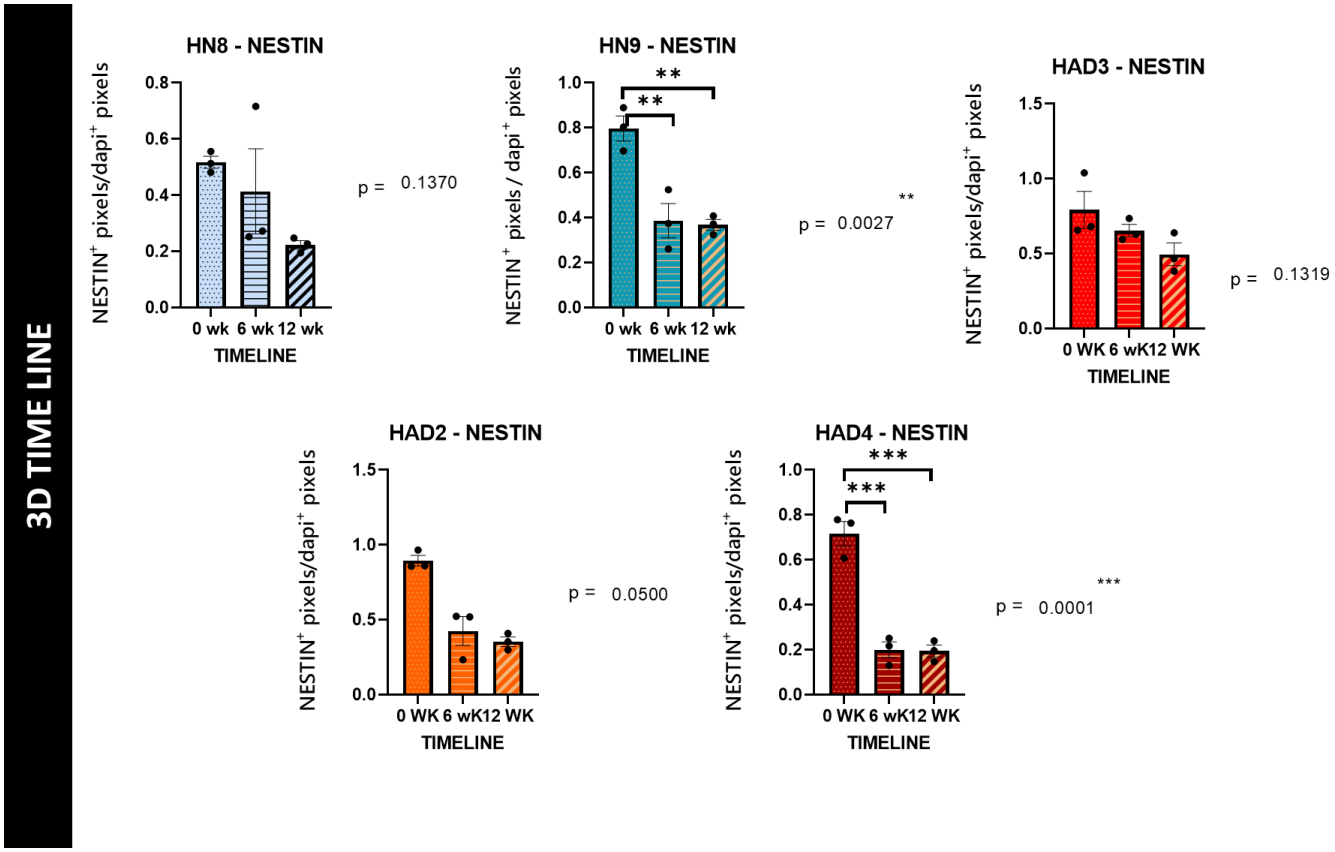

Figure 3.18: Time based analysis of the NSC marker Nestin observed in the 3D cultures of hN9, hAD2, hAD3 and hAD4 at timepoints 0, 6- and 12-weeks post differentiation. The data of HN8,HN9, HAD3 and HAD4 were normally distributed hence a One-way Anova with Bonferroni's multiple comparison post-hoc test was used for analysis. The data for HAD2 was not normally distribued and Kruskal-Wallis test with Dunn's correction was used for analysis. *p<0.05, ** p<0.01, *** p<0.001.

3.6.9 3D cultures show better Neuronal Differentiation compared to 2D Cultures at 6 weeks post differentiation *in vitro*

In order to compare and contrast the best and most efficient culture format for neuronal differentiation *in vitro,* the relative proportions of the different markers were analysed across culture types (2D and 3D).

The neuronal differentiation markers MAP2 and B3 Tubulin were compared for the same cell lines between 2D and 3D cultures (Fig 3.19). Unpaired two tailed-t test was used to analyse the difference between 2D and 3D at 6 weeks post differentiation. On analysis we observe that the relative proportions of B3 Tubulin is higher in the 3D culture compared to the 2D cultures. There is a significant increase in the relative proportion of B3 Tubulin positive cells at 6 weeks post differentiation in control 3D-hN9 cell line. Although there is no statistical difference, there

is an increase in the relative proportion of B3 Tubulin in 3D-hAD3 at 6 weeks post differentiation.

Similarly, there is a higher proportion of MAP2 in the 3D cultures as compared to the 2D cultures of the same cell lines. There is a no significant difference in the relative proportions of MAP2 positive cells in the control cell line hN8 when grown in 3D cultures rather than 2D cultures. However, there is a significant increase in the relative proportions of MAP2 in the control hN9 cell line when grown in 3D cultures. Moreover, a similar trend in (although not a significant) increase is seen in the AD cell line 3D -hAD3 at 6 weeks post differentiation.

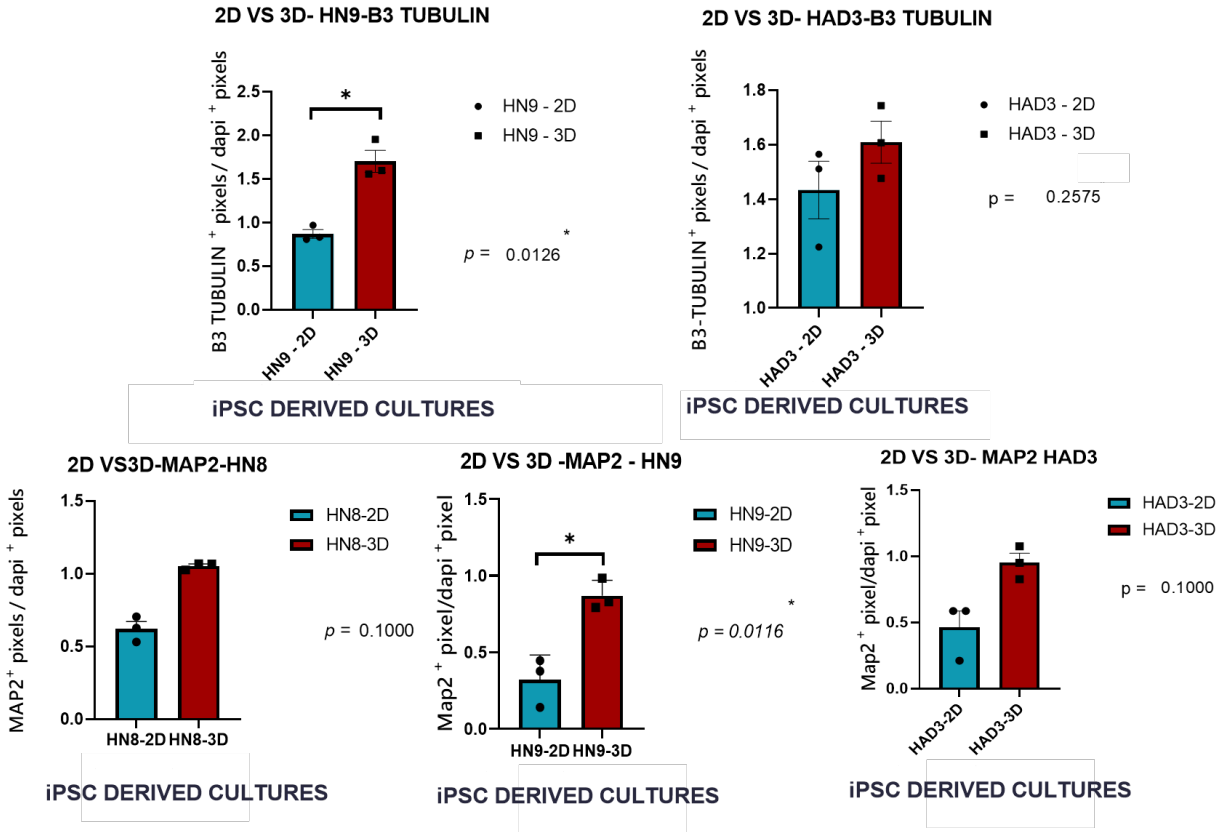

Figure 3.19: 2D (green) vs 3D (red) analysis of the neuronal markers B3 Tubulin and MAP2 at 6 weeks post differentiation (n=3). Unpaired t test was used to analyse differences between the two groups. All data except MAP2-HN8 and MAP2-HAD3 were normally distributed, hence unpaired two tailed t-test with Welch's correction was used for analysis. For MAP2-HN8 and MAP2-HAD3 Mann-Whitney test was used for analysis. *p<0.05.

The neural stem cell marker Nestin was also analysed in the same manner for the cell lines hN8, hN9 and hAD3 (Fig 3.20). Unpaired two tailed-t test was used to analyse the difference between the two groups at 6 weeks post differentiation. There is no significant difference

observed in the relative proportions of Nestin seen in the same cell line when grown in either a 2D or a 3D culture format.

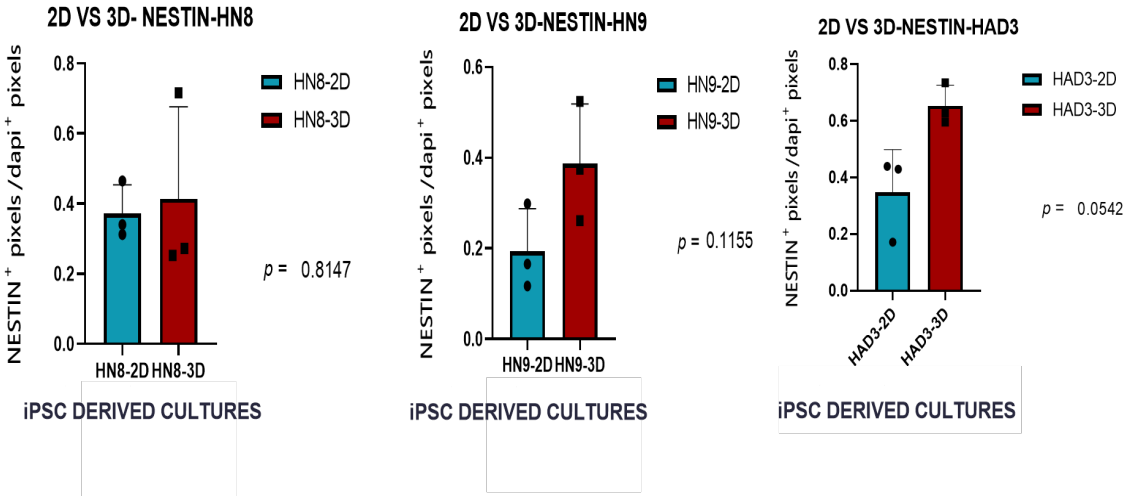

Figure 3.20: 2D (green) vs 3D (red) analysis of the neural stem cell markers Nestin at 6 weeks post differentiation (n=3). The data was normally distributed. Unpaired t test with Welch's correction was used to analyse differences between the two groups.

Similarly, there was no statistical difference observed for GFAP in the cell lines hN9 and hAD3 when grown in 3D cultures vs 2D cultures (Fig 3.21).

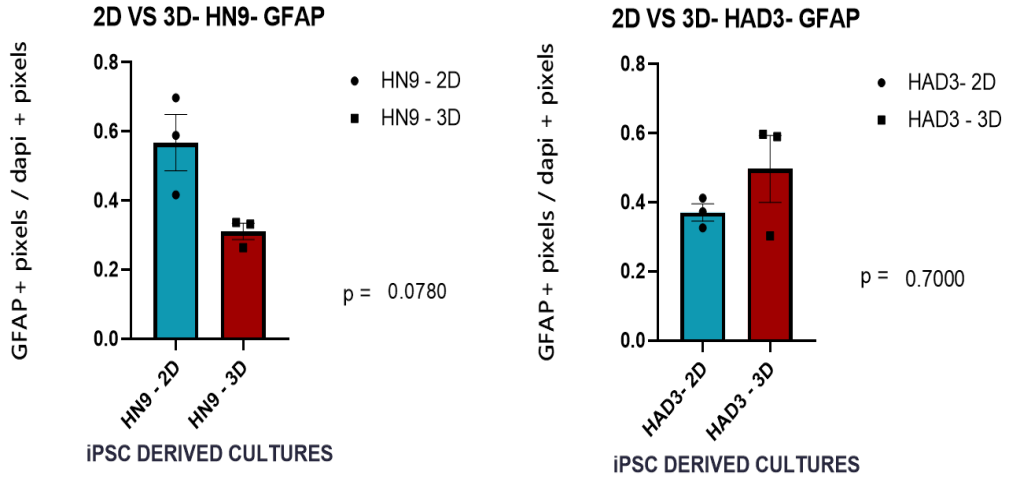

Figure 3.21: 2D (green) vs 3D (red) analysis of the astrocytic marker GFAP at 6 weeks post differentiation. the data for HN9-GFAP was normally distributed. Unpaired t test with Welch's correction was used to analyse differences between the two groups. The data for HAD3-GFAP was not normally distributed hence Mann Whitney test was used for analysis.

	HN8		HN9		HAD2		HAD3		HAD4	
NESTIN	2D	3D	2D	3D	2D	3D	2D	3D	2D	3D
0WK	*		**		**		**		**	
6WK	*	*	*	*	-	*	*	**	-	*
12WK	-	*	-	*	-	*	-	*	-	*

	HN8		HN9		HAD2		HAD		HAD4	
B3 TUBULIN	2D	3D	2D	3D	2D	3D	2D	3D	2D	3D
0WK	***		***		***		***		***	
6WK	***	-	***	***	-	***	***	***	-	***
12WK	-	-	-	***	-	***	-	***	-	-

	HN8		HN9		HAD2		HAD		HAD4	
B3 TUBULIN	2D	3D	2D	3D	2D	3D	2D	3D	2D	3D
0WK	***		***		***		***		***	
6WK	***	-	***	***	-	***	***	***	-	***
12WK	-	-	-	***	-	***	-	***	-	-

	HN8		HN9		HAD2		HAD		HAD4	
GFAP	2D	3D	2D	3D	2D	3D	2D	3D	2D	3D
0WK	*		**		***		***		***	
6WK	**	-	*	*	-	*	*	*	-	*
12WK	-	-	-	*	-	*	-	*	-	-

Table 3.6: Table summarising the 2D and 3D-IF-data for the markers - Nestin, MAP2, B3Tubulin and GFAP at timepoints week 0, -week 6 and week 12 post differentiation of the 2D and 3D cultures for each cell line namely hN8, hN9, hAD2, hAD3 and hAD4 (n=3). Each value is the ratio of the relative proportion of the Marker/DAPI. Key- *=values 0.1-0.59, **=values 0.6-0.89 and ***=values from 0.9-1.90. "-"=experiment not performed.

3.6.10 Total Tau expression at 6 weeks post differentiation *in vitro*

In order to determine the best method for cultures for *in vitro* neuronal differentiation, an analysis of Total Tau was performed between the cell lines grown in 2D and 3D culture formats. Western blot was performed to quantify any differences between the Total Tau levels in each cell line grown in 2D and 3D (Fig 3.22).

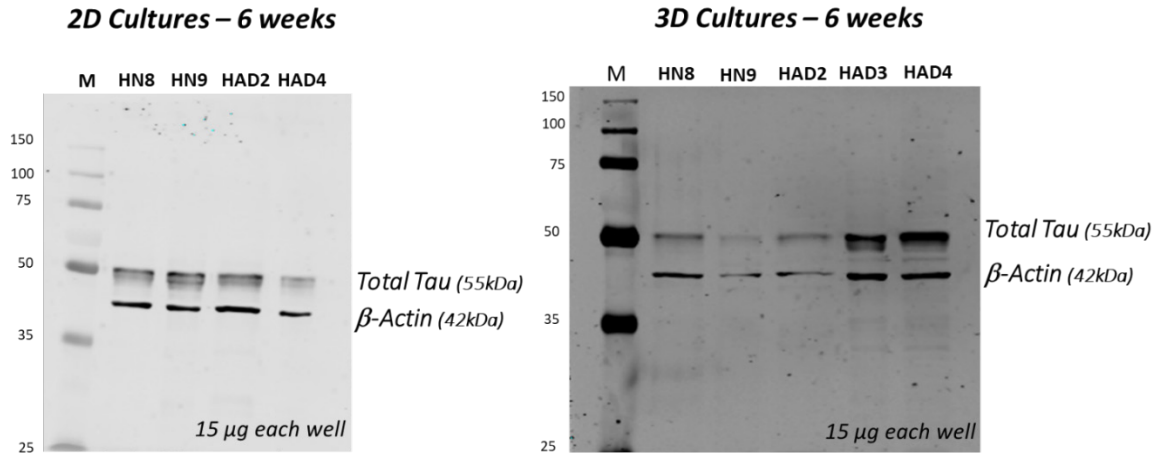

Figure 3.22: Western Blots of cell lines grown in 2D and 3D cultures at 6 weeks post differentiation. Each gel lane was loaded with 15µg of protein. The blots were stained for Total Tau (Dako) and housekeeping protein β-Actin. All Total Tau values were calculated against the loading control actin. (M=Marker)

The Total Tau/Actin values were calculated for each cell line and an unpaired- t-test was used to analyse the difference in the two groups for each cell line. There is an increase in the Total Tau levels especially in 3D-hN8, 3D-hAD2 and 3D-hAD4 cell lines when compared to their 2D cultures, although only significant for hAD4 (Fig 3.23).

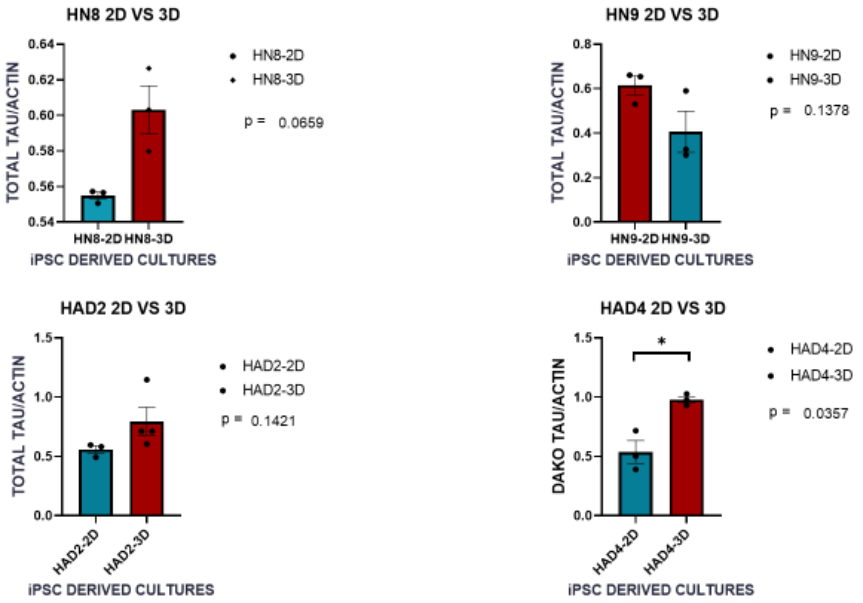

Figure 3.23: 2D (green) vs 3D (red) analysis of Total Tau at 6 weeks post differentiation. All data were normally distributed. Unpaired t test with Welch's correction was used to analyse differences between the two groups. *p<0.05

3.7 Discussion

3.7.1 Stemness - 2D vs 3D neural cultures

iPSC derived NSC express high levels of NSC marker-Nestin, at week 0 post differentiation which decreases gradually with differentiation over time in both 2D and 3D cultures. The IF analysis of Nestin in the 2D cultures shows not much of a difference between the groups at 6 weeks post differentiation but quite a significant reduction from the week 0. The IF analysis of Nestin in the 3D cultures shows a gradual decrease in the proportion of Nestin positive cells in 3D cultures over time. At 6 weeks post differentiation, although there is no significant difference in the proportion of Nestin positive cells across cell lines but there is a significantly lower proportion in 3D-hAD4 when compared to 3D-hAD3 cultures. Although not statistically significant hAD3 seems to have more Nestin positive cell population than the rest of the cell lines at 6 weeks post differentiation. Similarly, at 12 weeks post differentiation there seems to be a significant difference between 3D-hAD3 and 3D-hAD4 cultures. Compared to the other cell lines 3D-hAD3 has a higher proportion of Nestin positive cells at 12 weeks post differentiation. When the timeline of differentiation is considered Nestin expression seems to reduce in the first 6 weeks post differentiation. However, it does not decrease much further at 12 weeks post differentiation. Unfortunately, due to time restrains the 18 weeks post differentiation could not be processed and analysed, although, the information from this late timepoint would have been crucial. When the IF analysis for Nestin in the 2D cultures was compared to that in the 3D cultures at 6 weeks post differentiation, there is slightly higher proportion of Nestin positive cells in the 3D cultures. This is seen not just in the control groups hN8 and hN9 but also in the AD cell line hAD3. Hence this expression corelates to the 3D method of culturing. However, the higher proportion does not seem to be a significant difference between the 2D and the 3D cultures across groups. This shows that a small population of cells do remain undifferentiated in the 3D cultures over time *in vitro.* One possible reason would be that the 2D cultures get more exposure to the growth factors compared to the tightly compacted 3D cultures. Another explanation would be that NSCs behave like stem cells in the adult human brain where a small proportion remain silent in a niche like environment.

In the study performed by Marchini et al 2020, where they performed a similar set of experiments to characterise their HYDROSAP based 3D cultures over timepoints -day 1, -

week1 and -week 6 *in vitro*, they have shown a similar trend of expression of Nestin in their 4 different hNSC cultures over time, (Marchini, Favoino and Gelain, 2020). All the four hNSC-HYDROSAP cultures show a high proportion of Nestin at 1DIV and gradually reduce overtime. Similar to what we see in our 6week-2D and 3D cultures, they see a small population of cells positive for Nestin at 6 weeks post differentiation in all the four different hNSCs. The study claims that this property of maintaining. Stemness is attributed to the softness of the 3D-matrix, which is in line with their previous studies (Marí-Buyé and Semino, 2011; Sahab Negah *et al.*, 2017). Unfortunately, they have not grown the cells longer in culture to see if the Nestin expression reduces further or remains the same.

The same group has compared 2D cultures with 3D cultures at week1 and they see a similar increase in the expression levels of Nestin in the 3D cultures as compared to the 2D cultures. However, week 1is still a very early timepoint and show that probably the rate of differentiation is faster in 2D cultures due to the complete exposure of growth factors each cell gets as opposed to that in the 3D cultures (Marchini, Favoino and Gelain, 2020)

There are many studies showing the effect of matrix stiffness on the differentiation of stem cells. Soft substrates with less cell contractility foster the pluripotency of stem cells (Gerardo *et al.*, 2019). There is a strong correlation between stemness and intracellular contractility. The extracellular mechanical cues has an influence on the intracellular stiffness and contractility The cytoskeleton translates these mechanical signals from the ECM to the nucleus which in turn plays a vital role in influencing the shape of the cell, shape of the nucleus, size of the cell and the nucleus. This shows that factors linking the nucleus and the cytoskeletal elements play a vital role in differentiation. This could be one possible explanation to the different stages of morphological and cytoskeletal changes we see in our 3D cultures. In the initial stages, the cultures plated out in a soft Matrigel substrate express high levels of Nestin and are more stem cell like phenotype with large nucleus. As time progresses *in vitro* there are cytoskeletal changes occurring in the cultures where it looks like the cells try to become more compact and condense, trying to detach and pull away from the chamber walls trying to form a rounded 3D structure by 6 weeks post differentiation. This we suppose is a stage where the Matrigel is replaced with the cells own ECM during differentiation, replacing the soft Matrigel with something stiffer over time allowing the cells to become more contractile with rigid nucleus as they differentiate in 3D cultures. Studies show that this the stiffness of the matrix also correlates with the stiffness of the nuclei. The nuclei of the stem cells are softer and become stiffer as they become committed to a particular fate (Pajerowski *et al.*, 2007; Mazumder *et al.*, 2010).

Hence it can be agreed upon that softness directly correlates to stemness and stiffness inversely correlates to differentiation in stem cells. This could be a possible reason why we see more Nestin positive cells in our 3D cultures (softer) compared to the 2D cultures grown on a more rigid plastic surface.

3.7.2 Neural Differentiation- 2D vs 3D cultures

B3 Tubulin, an early immature neuronal marker, was observed at week 0 post differentiation and gradually increases with time in both 2D and 3D cultures. However, there is no significant change in the proportions between the cell lines at this timepoint. The IF analysis of B3 Tubulin in the 2D cultures, shows no difference between the control groups but there seems to be a significant difference in 2D cultures between the control 2D-hN9 and the AD cell line 2D-hAD3 at 6 weeks post differentiation. The IF analysis of B3 Tubulin in the 3D cultures shows a gradual increase in the proportion of B3 Tubulin positive cells in 3D cultures over time. Although there seems to be no difference between the cell lines, the proportion of B3 Tubulin positive cells in the 3D-hAD4 cells at 6 weeks post differentiation seems to be lower than the rest of the cell lines. At 12 weeks post differentiation however, a similar pattern of expression is found, there is no significant difference across the cell lines. When considering the timeline for differentiation, B3 Tubulin expression across cell lines seems to follow a similar pattern. There is a gradual increase from week 0 to week 6 post differentiation, however there is not much increased expression beyond this point at 12 weeks post differentiation. When the IF analysis for B3 Tubulin in the 2D cultures was compared to that in the 3D cultures at 6 weeks post differentiation, a higher proportion of B3 Tubulin positive cells is seen in the 3D cultures compared to the 2D cultures.

In the Marchini study, they found a similar increase from day 1 to 6 weeks in their 3D cultures *in vitro*. The increase in the percent positive B3 Tubulin cells is not drastic but a gradual one. Similarly, when they compared their 2D cultures to the 3D at week 1 *in vitro*, two out of four cell lines showed a higher percent of B3 Tubulin positive cells in 3D as compared to 2D cultures (Marchini, Favoino and Gelain, 2020).

MAP2, a late maturity marker, was seen as early as 0-week post differentiation and gradually increases with time *in vitro* in both 2D and 3D cultures. The IF analysis of MAP2 in the 2D cultures at 6 weeks post differentiation shows no difference across the groups but an increase in relative proportions when compared to 0-week post differentiation cultures. The IF analysis of MAP2 in the 3D cultures also shows an increase in MAP2 positive cells at 6 weeks post

differentiation when compared to the 0-week post differentiation cultures. However, there is a significantly higher proportion of MAP2 positive cells in the control 3D-hN8 cultures when compared to the hAD4 cells line at 6 weeks post differentiation at 12 weeks post differentiation however there seem to be no difference across the groups but a significantly higher proportion in 3D-hAD3 compared to 3D-hAD4 cell lines was observed. When the timeline of differentiation is considered there is a significant increase in the relative proportion of MAP2 positive cells between 0- and 6-weeks post differentiation but there is not much further increase at 12 weeks post differentiation across groups. In such a situation the information from 18 weeks post differentiation would be crucial to know if the proportion of MAP2 positive cells increase or plateau at this stage of differentiation, but unfortunately due to time restraints the samples could not be processed. When the IF analysis for MAP2 in the 2D cultures was compared to that in the 3D cultures at 6 weeks post differentiation, there is a significant increase in the relative proportion of MAP2 positive cells in 3D cultures across cell lines- hN9 and hAD3 as compared to the 2D cultures. This increase in the proportion of MAP2 cells is attributed to the 3D method of neural culture. This is one of the reasons why 3D cultures are more physiologically representative in supporting the NSCs to differentiate and mature *in vitro*.

In the Marchini study, they see a similar increase in percentage of MAP2 positive cells in their 3D cultures in two out of four cell lines over time *in vitro* lines showed a higher percent of B3 Tubulin positive cells in 3D as compared to 2D cultures.

3.7.3 Astroglial Differentiation - 2D vs 3D cultures

GFAP expression is seen at week-0 post differentiation and gradually decreases with time in both 2D and 3D cultures. The iPSC derived NSC seem to express a high proportion of astrocytic marker GFAP, at week 0 post differentiation. Although there seems to be no significant difference in the relative proportions between the different cell lines at week 0 post differentiation. The IF analysis of GFAP in the 2D cultures at 6 weeks post differentiation shows higher proportion of GFAP positive cells in the control groups when compared to the AD cell line 2D-hAD3. There seems to be a significantly lower proportion of astrocytes in the AD culture 2D-hAD3 as compared to the control 2D-hN8 cultures. The IF analysis of GFAP in the 3D cultures shows no significant difference across the cell lines except for 3D-hAD3 cultures which seem to have a higher proportion than the rest of the cell lines at 6 weeks post differentiation. At 12 weeks post differentiation there is a slightly higher proportion of GFAP positive cells in the cell line 3D-hAD3. When the timeline for differentiation is considered there is a steep decrease of GFAP positive cells from week 0 to week 6 but then slight increase

in the proportions at 12 weeks post differentiation. Unfortunately, as mentioned before, the 18 weeks information would have been insightful to see how this trend progresses over time *in vitro.* In recent years, the role of radial glial cells as stem cells has become more evident which primarily was thought to be as guiding and supporting cells to the migrating neurons during embryonic development. GFAP is not just an astrocytic marker but also a marker seen in the radial glial cells (Levitt and Rakic, 1980) (Hartfuss *et al.*, 2001) the higher proportion at week 0 post differentiation could reflect the population of undifferentiated stem cells as well as astrocytes in cultures. Perhaps, co-staining with a marker representing mature astrocytes like S100-β would shed more light on the actual phenotype of the cells. When the IF analysis for GFAP in the 2D cultures was compared to that in the 3D cultures at 6 weeks post differentiation, there seems to be a decrease in the proportions of GFAP positive cells in the 3D cultures of control-hN9 but a higher proportion in the 3D cultures of the AD cell line hAD3. However, more information from the other cell lines would have been more insightful. Due to the lack of time more samples could not be processed and analysed for GFAP. In the Marchini study, they see a rise in two out of four different hNSC cell lines in the proportions of GFAP positive cells between Day1 and week1 but with a slight decrease at week 6 when compared to week 1 *in vitro* across all cell lines. When they compare their 2D cultures against their 3D cultures they see lower proportions of GFAP positive cells in their 3D in three out of four hNSC lines at 1 week *in vitro.* There are studies which show astrocytes prefer stiffer matrices unlike neurons that prefer softer matrices(Georges *et al.*, 2006; Saha *et al.*, 2008; Leipzig and Shoichet, 2009). The results we see could be a reflection of these factors of matrix stiffness playing a role in *in vitro* differentiation. This could be a possible reason why there are comparably higher expression of GFAP expression in the 2D cultures on stiffer plastic.

3.7.4 Tau in 2D vs 3D cultures

We see a higher proportion of Tau expressing cells in three out of four cell lines in 3D cultures compared to the 2D cultures. Tau is a protein that belongs to the MAPT protein family like MAP2 both of which are neuron specific and hence would follow a similar pattern during development (Dehmelt and Halpain, 2004). For instance, in Ngamkham et al 2017 study, there is an increase in Tau and MAP2 positive cells in their 3D cultures with aligned electro-spun fibres (10% poly l-lactide) used to cultures hESCs, as opposed to their 2D cultures (Ngamkham, Rivolta and Battaglia, 2017).

In conclusion, we have achieved our primary aim for this Chapter which was to quantify our findings for both the 3D and 2D cultures so as to be able to compare between the two culture

methods. On comparison, we thus conclude that the 3D cultures are efficient for long term differentiation in vitro. We have successfully analysed the differentiation of the 3D cultures over a period of 12 weeks *in vitro* using markers such as MAP2, Nestin, GFAP and B3 Tubulin.

3.7.5 Summary and Future Work

Based on the results from this Chapter combined with the initial results seen with the pilot experiments (Chapter 2) where we see a difference in the Total Tau levels in 3D cultures between control and AD cell lines as early as 6 weeks post differentiation and the expression of the adult-specific- 4R tau isoform seen in the 3D cultures (Chapter 2 and 4) which has never been demonstrated in a physiologically represented 2D neural culture system as early as 6 weeks post differentiation before, we strongly believe that the 3D cultures are the best method available to study and model a neurodegenerative disease since it is the physiologically closest system we have to represent an brain tissue *in vitro*. Although 2D cultures portray an unrealistic picture of cells and their function *in vivo* they are important additional tools for cell-based studies such as assessing a differentiation protocol *in vitro*.

There are still some unanswered questions related to the 3D culture system developed here. For instance, an assessment of the change in matrix stiffness and the periodic change in the ECM seen in the 3D cultures. An assessment of the proliferation rate of each cell line before and during neural induction might help us better understand the rate of differentiation seen in the cultures. There is a need to better understand the neurite extension and branching pattern seen in these cultures. Ultimately, validating these finding against human resected tissues would give an overall impression of the age and maturity of these cells.

Chapter 4 – Early Pathological Changes

4.1 Introduction

The main aim of this Chapter is to investigate any early biochemical changes seen in the optimised and standardised 3D cultures. The main risk factor for AD is age. In AD patients, the clinical manifestations that appear later in life seems to start with changes at the molecular and biochemical levels early on and gradually progresses into the clinical symptoms. A suitable model is crucial to detect these early changes happening at the molecular and biochemical levels.

Aβ oligomers have been implicated in AD pathophysiology. To determine the presence of the Aβ oligomers, a pilot experiment was performed by Dr. Elodie Siney. hAD2 was cultured and differentiated by Dr. Elodie Siney (using 100ng/ml RA). Lysates from hAD2 and control neural precursor cells (hfNSCs)- 3D cultures at 6 weeks post differentiation were used for fractionation. Equal volumes of each fraction were loaded. The blot was run against a human purified Aβ ladder as positive control and stained with Aβ 6E10 antibody (Cambridge Biosciences, 803001), which detects the amino acid sequence 1-17 of the human Aβ peptide. As seen in the figure 4.1, there are no bands detected in the control cell lines, however, there are bands present in the S1 fraction of hAD2 cell line (barely visible in S2 fraction). The majority of the protein is expressed in S1 while there are very low levels detectable in the S2 and S3 fractions.

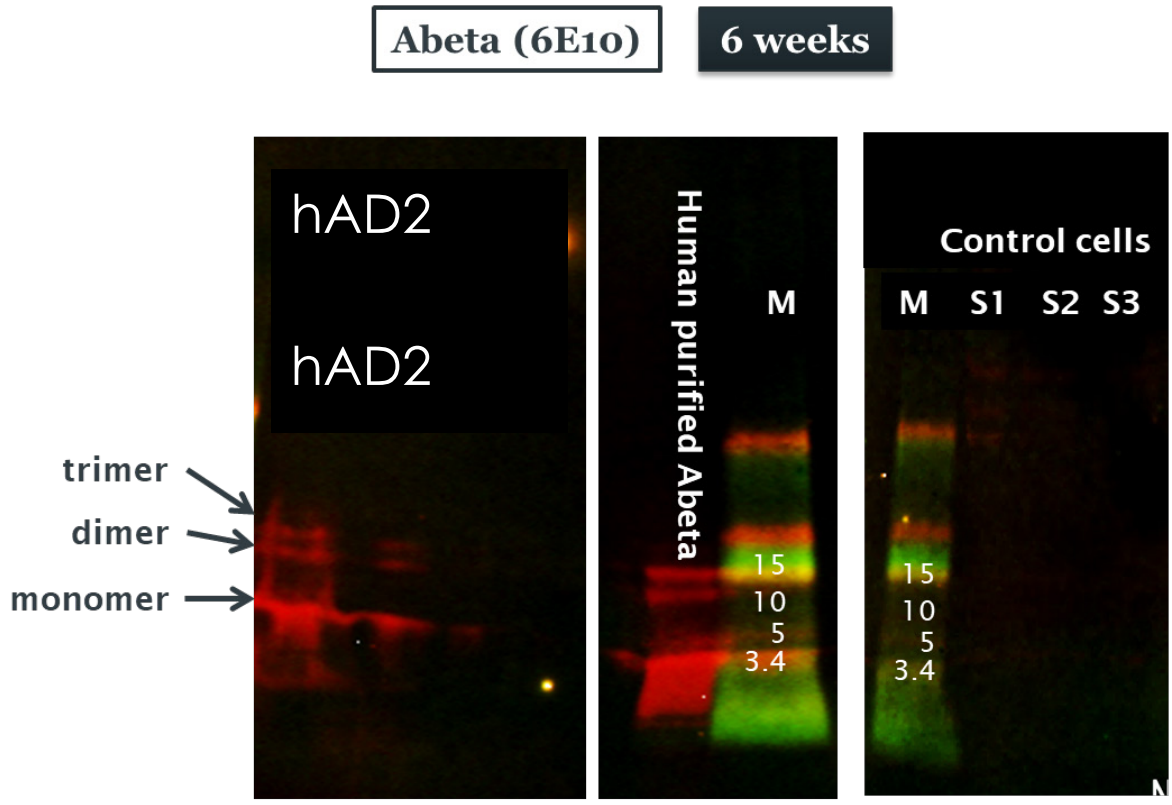

Figure 4.1: Western blot of Aβ in hAD2-AD and control 3D cultures at 6 weeks post differentiation, blot done by Dr. Elodie Siney, data from pilot experiment. The blots are stained with 6E10 (1:1000). A recombinant human purified Aβ marker was used as positive control.

To further detect the presence of Aβ isoforms in the media secreted by the 3D cultures, week 1 and week 11 post differentiation media samples of hAD2-L286V and control NPC were used for mesoscale analysis against Aβ40 and Aβ42 (Fig 4.2). The cultures were grown by Dr. Elodie Siney and the mesoscale was performed in collaboration with Prof Jessica Teeling. The data on analysis shows that Aβ40 and Aβ42 are secreted in the media. Due to different dilutions used for different samples, no comparison can be made from absolute concentrations of either Aβ40 or Aβ42. However, ratio of Aβ42/40 can be considered. There is a clear difference between the Aβ42/40 ratio levels in the media collected from AD and the control 3D cultures irrespective of the timepoint. The AD cultures express a higher ratio of Aβ42/40 right from the early week 1 timepoint and this ratio stays high at the later week 11 timepoint. However, this was a pilot study (n-1) and more needs to be done in terms of repeatability and comparison with the other cell lines.

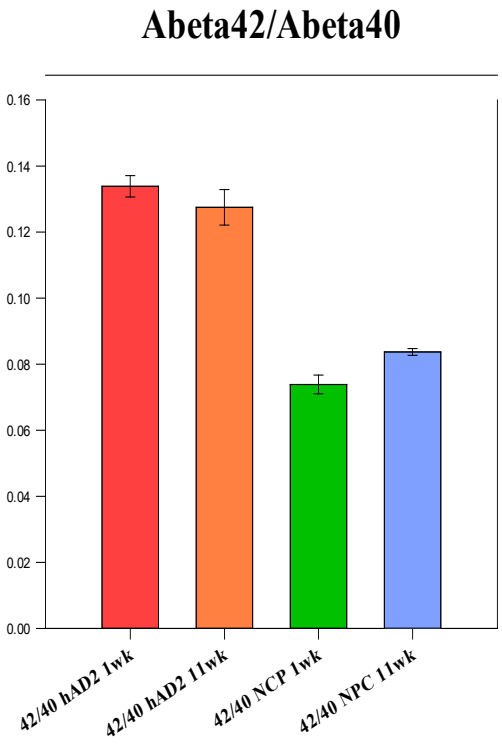

Figure 4.2: Mesoscale analysis of Aβ40 and Aβ42 levels in the media collected from hAD2-AD and control 3D cultures at week1 and 11 post differentiation (n=1 culture sample with 3 mesoscale measurement technical repeats) These cultures were grown by Dr. Elodie Siney, data from pilot studies.

Given that the 3D cultures derived from iPSCs from AD-patients with PSEN1 mutations showed signs of Aβ-associated pathological changes early during differentiation in our preliminary studies, the next question was to determine if any pathological changes were seen in Tau early during differentiation of the 3D cultures *in vitro.* This *in vitro* human 3D neural culture model described so far will provide a great platform to answer the following questions:

- Is there a change in the Total Tau or phospho Tau expression early on during differentiation and maturation?
- Are the AD cell lines prone to Tau aggregation during differentiation and maturation?
- Do the Tau isoforms have any changes in solubility during differentiation and maturation?
- Are the AD cell lines predisposed to changes in Aβ production?
- Are the cultures predisposed to changes in Aβ42/40 ratio during differentiation and maturation?

4.2 Aims

To analyse the early-stage pathogenesis of AD in the 3D cultures: NPCs derived from three iPSCs of AD patients with PSEN1 mutations L286V, A246E and M146L and from two healthy individuals, differentiated in 3D cultures, will be investigated at different time points for:

- difference in the expression of total tau AD vs control cell lines at early time points
- difference in aggregation of tau in AD vs control cell lines at early time points
- difference in expression of 3R Tau isoform in AD vs control cell lines
- difference in expression of 4R Tau isoform in AD vs control cell lines
- difference in phosphorylated tau in AD vs control cell lines

4.3 Methods

All the 3D cultures used for this Chapter were from the experimental set described in the previous Chapter (Chapter 3-Methods section). Please refer the methods section for details on the method followed for:

4.3.1 Western Blotting

Western Blot was performed on fractionated lysates from 3D cultures from the 6-week cultures.

4.3.1.1 Sample Preparation for Western Blot – Lysate Fractionation

The samples for lysate fractionation were prepared as described in Chapter 2- Part B with modifications (Fig 4.3). Three fractions (S1, S2, and S3) were recovered from each sample processed. 3D cultures (1 well) were lysed using the TBST/SDS/Urea extraction method. The samples were homogenised in the TBS/Lysis Buffer (Table 2.17). All volumes of homogenisation for all fractions were determined based on the BCA-total protein readout of the respective cell line.

The cells were homogenized at 4°C in TBS Lysis buffer in Beckman's eppendorf tubes with plastic pestle (Fig 2.17). The lysate was then ultra-centrifuged at 186,000g for 2 hours at 4°C. The supernatant (S1-TBS soluble fraction) was stored at -80°C. The pellet was resuspended in 5% SDS/TBS buffer (Table 2.17) and rehomogenised. The lysate was then ultra-centrifuged at

186,000g for 2 hours at 25°C. The supernatant (S2- SDS-soluble fraction) was stored in -80°C. The subsequent pellet was resuspended in 100 µl SDS/TBS buffer again and ultra-centrifuged at 186,000g for 1 hour at 25°C. Since this was a wash spin, the supernatant was discarded and the pellet rehomogenised in UREA buffer (Table 2.17) and agitated for 12-18 hours at room temperature to resuspend in buffer. Once the lysate (S3-SDS insoluble) dissolves completely the lysates are suspended in equal volumes of 2 x Loading Buffer (LB) and boiled for 5 min at 95°C. S3 fraction was then stored at -80°C. This is done for all the fractions before they are stored in -80°C.

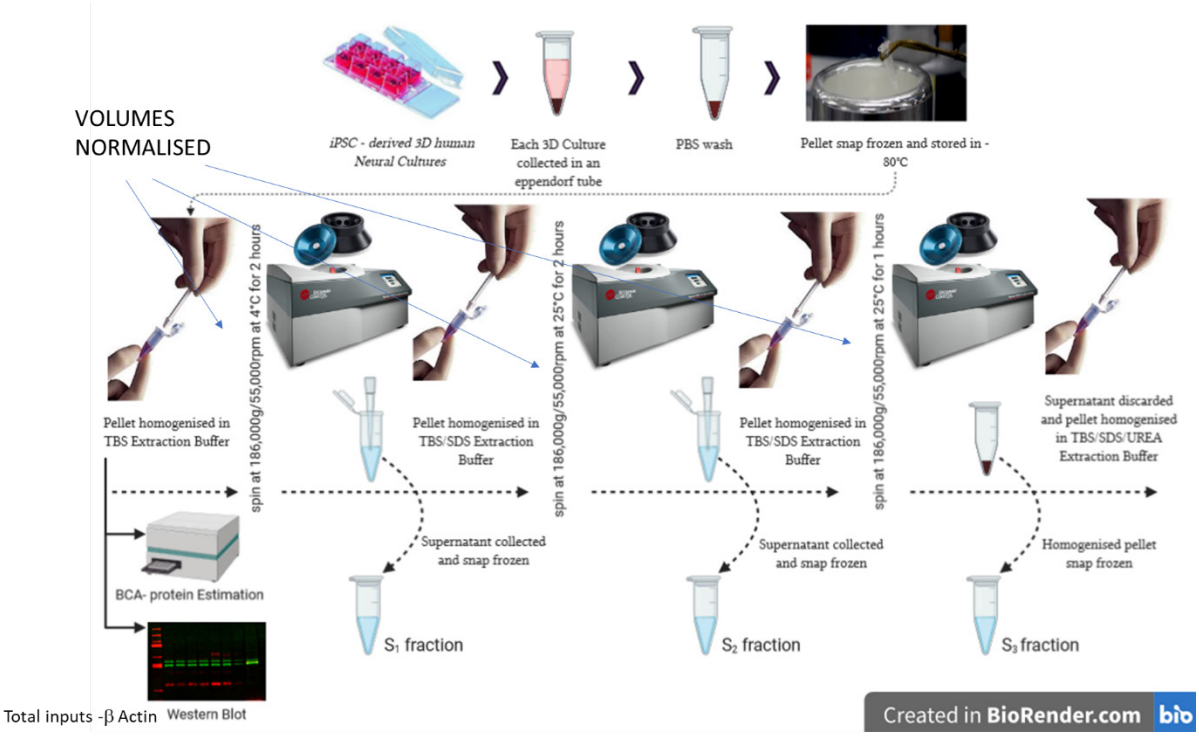

Figure 4.3: A schematic illustration of the serial extraction of fractions from 3D cultures . Created with BioRender.com

For total protein blots, 15 µg of sample with equal volume of loading dye (2xSDS dye) were resolved in a 10% polyacrylamide gel. For the fractions, protein fractions (10 µl protein fraction and 10 µl loading dye-2xSDS dye) S1, S2 and S3 were resolved in a 10% polyacrylamide gel. For the WB technique, refer Chapter 2-Part B-2.4.1.3 Details of the Abs used for WB are provided in Table 2.21.

4.3.1.2 Statistical analysis

All values are presented as the mean ± standard error of the mean. To compare differences between the groups, statistical analysis was performed using GraphPad Prism version 8.4 (GraphPad software, Inc). For normally distributed data, One-way Anova was used for statistical analysis with Bonferroni's multiple comparison for comparison across groups. For non-parametric data Kruskal Wallis test with Dunn's correction was performed. For comparison between two groups (control lines vs AD) a two-tailed unpaired t-test was performed.

4.4 Results

4.4.1.1 There is more Total Tau in the 3D- AD cultures at 6 weeks post differentiation

As seen previously in Chapter 1, we saw an increase in the total tau expression in AD cell lines, but since it was a pilot experiment to optimize the characterization techniques in 3D cultures, the total protein estimates were not performed and experiments were mostly an N=1. In this experiment, all 5 cell lines samples (min N=3 for each cell line) were run at the same time under the same conditions to analyse the expression levels of total tau protein across the groups. The 3D culture lysates were evenly loaded at 15µg per well across all cell lines. At 6 weeks post differentiation both the controls and AD cell lines express total tau (Fig 4.4).

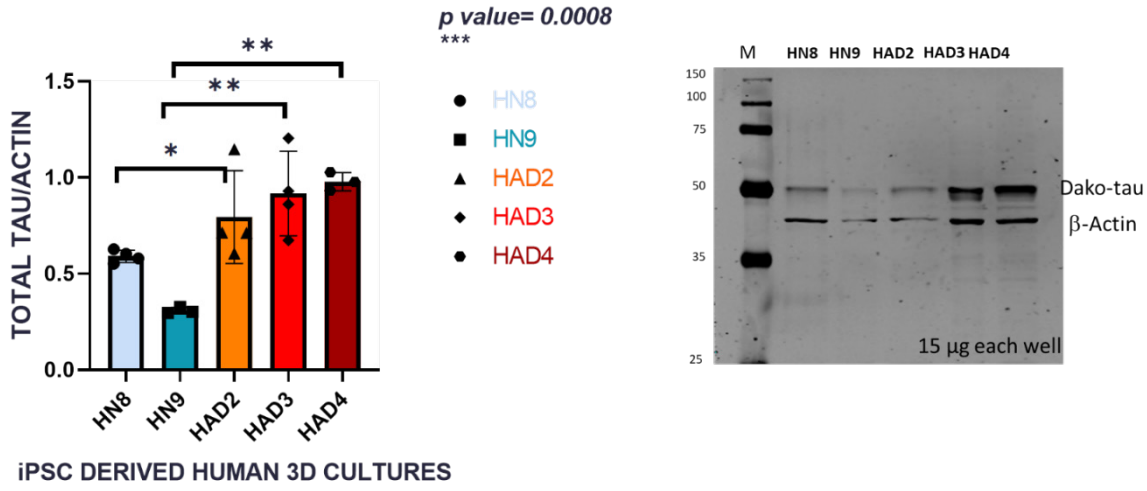

Figure 4.4: Western blot and analysis of Total Tau (Dako) in 3D cultures at 6 week post differentiation (n=3). The blots are stained with Dako Tau (55kDa) and β-Actin (42kDa). 15ug of protein from total lysates

of each group was loaded in each gel lane. Data was normally distributed. One-way Anova with Bonferroni's multiple comparison post-hoc test was used for analysis M = marker. *p<0.05, ** p<0.01, *** p<0.001.

As seen in the graph, there is more total tau expression in the AD cell lines compared to the control cell lines grown in 3D cultures at 6 weeks post differentiation. There is a significant difference between the control cell line hN9 and the AD lines hAD4 and hAD3, and there is a significant difference between hN8 and hAD2.

4.4.1.2 There is more aggregated Tau in 3D-AD cultures at 6weeks post differentiation

In AD brains, tau undergoes conformational changes to form monomers, oligomers and fibrils. When tau undergoes conformational changes it tends to form insoluble aggregates. Abnormally aggregated tau is a pathological feature in AD, which is thought to happen years before the clinical features manifest. In this experiment, biochemical characterisation of insoluble tau using buffers of increasing detergent strength combined with very high speed ultracentrifugation provides a platform to understand the progression of pathology in terms of aggregation. The TBS soluble-S1 fraction shows the presence of monomeric tau. The TBS insoluble/SDS soluble – S2 fraction shows the presence of oligomers. The Urea soluble S3 fraction shows the prescence of insoluble aggregated tau. In order to check the proportion of tau in each of the three fractions, all cell lines were fractionated (normalised based on their total proteinn concentration estimate with BCA assay) and equal volumes loaded across all cell lines. In fractionated lystes the β-actin (gel loading control) is seen to be variable from fraction to fraction, as expected, as well as sample to sample. Hence as a general practice, it is not commonly used as a reliable tool to normalize the fractions. Each fraction is calculated and measured as a ratio of the fraction over total tau, which is a sum of all the fractions - S1+S2+S3 (normalized against the actin from the total lysates).

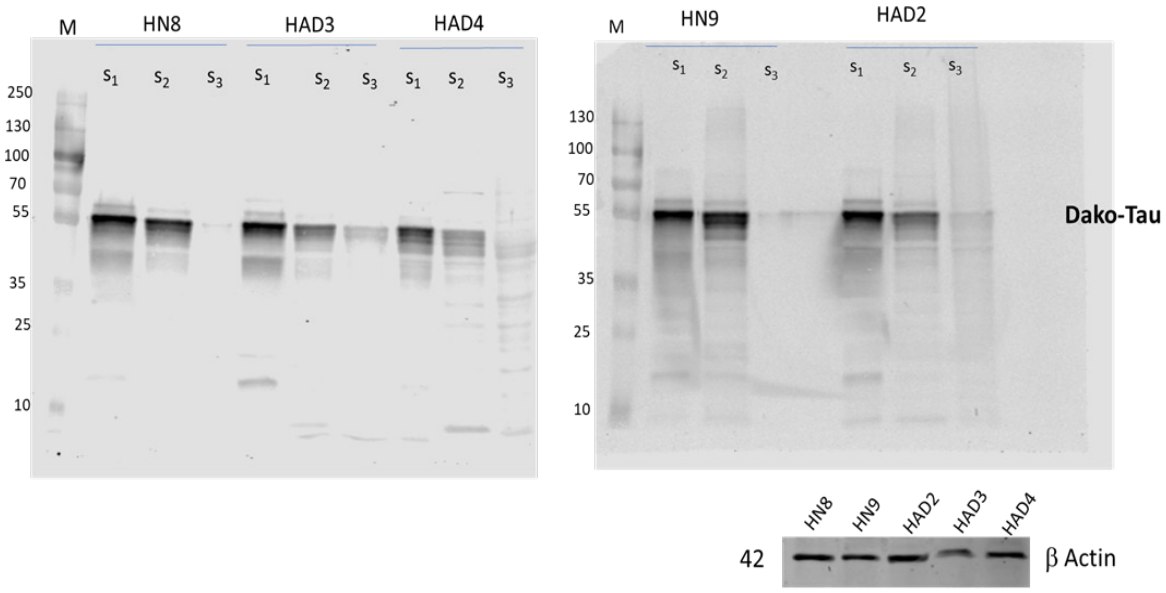

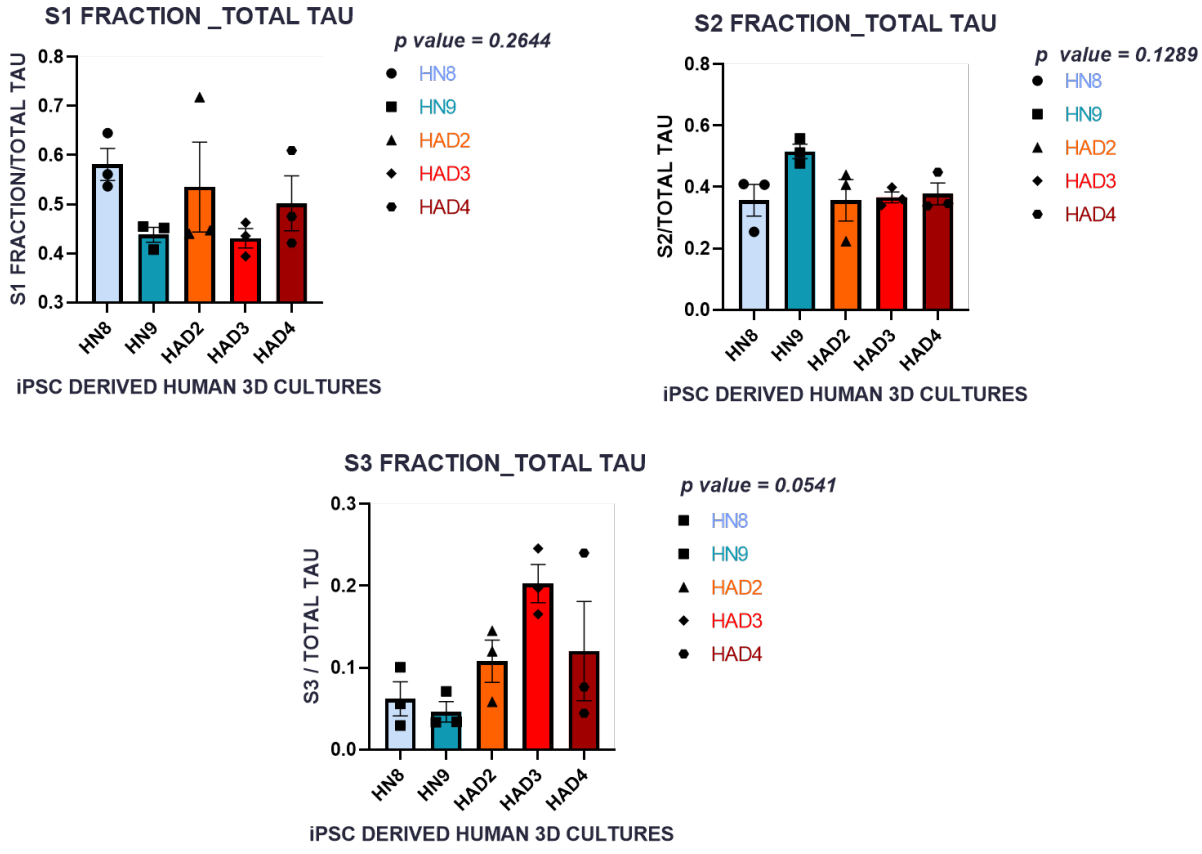

Figure 4.5: Western blot of fractionated lysates of 3D cultures at 6 weeks post differentiation (n=3 culture samples) to analyse the relative proportion of soluble and insoluble tau across cell lines. The blot is stained with Dako Tau (55kDa). Equal volumes (normalised against β-Actin- total lysate) loaded across fractions in each well. Each fraction is measured as a ratio over Total Tau where it is the sum of all fractions – S1+S2+S3.All data were not normally distributed. Kruskal Wallis test with Dunn's correction was performed to analyse all fractions.

When analysed, it is observed that the major proportion of soluble tau is found in the S1 and S2 fractions both in the control and AD lines grown in 3D cultures at 6 weeks post differentiation. Further, there is only a small proportion of insoluble tau detected in the S3 fraction when compared to the S1 fractions and the S2 fractions, as seen in the figure above. On analysis, there is no significant difference in the fractions across cell lines at this timepoint. However, the proportion of insoluble tau found in the S3 fraction is at least 2 to 3 fold more in the AD cell lines when compared to the control lines (Fig4.6) .

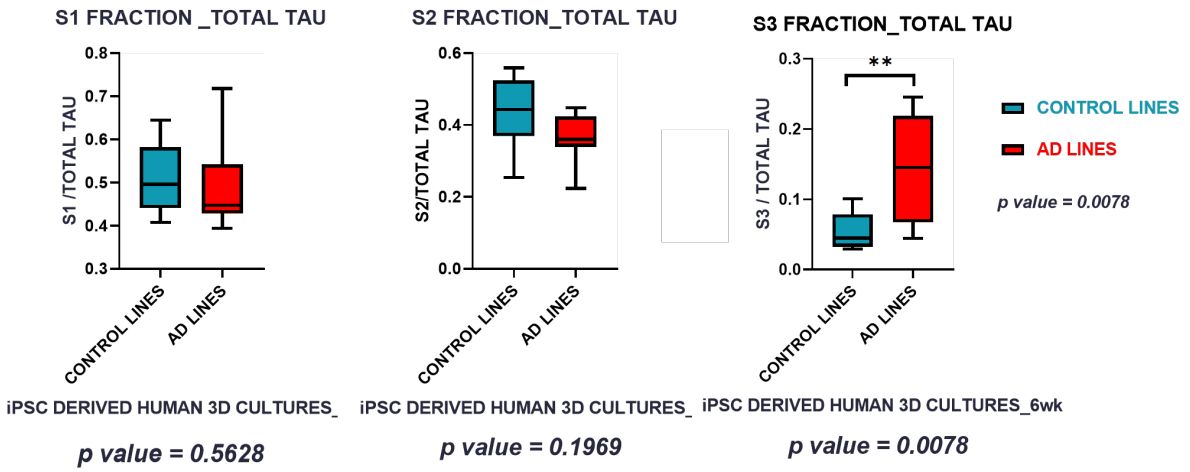

Figure 4.6: Comparative analysis of the fractions from control and AD lines grown in 3D cultures at 6 weesk post differentiation (n=3culture samples) to analyse the solubility of tau. Each fraction is measured as a ratio over Total Tau where it is the sum of all fractions – S1+S2+S3. All data except S1 fraction were normally distributed. Unpaired t-test with Mann-Whitney test for S1 fraction was performed whereas Welch's correction was used for other fractions. ** p<0.01.

When an unpaired two-tailed t-test (with Welch's correction) was performed between the combined control and AD cell lines there is a very significant increase in the proportion of insoluble aggregated tau in the S3 fraction in the AD lines as compared to the control lines at 6 weeks post differentiation in the 3D cultures.

4.4.1.3 3D cultures express 3R Tau isoforms at 6 weeks post differentiation

Tau exist as 6 isoforms in the human adult brain, three of which are 3R tau and three are 4R tau. The two isoforms are differentially regulated during development. Hence, this experiment was performed not just to check for the prescence of the isoform in the 3D cultures at the given timepoint but also to answer the question whether there is a difference in solubility of these isoforms between the control and the AD cell lines during differentiation.

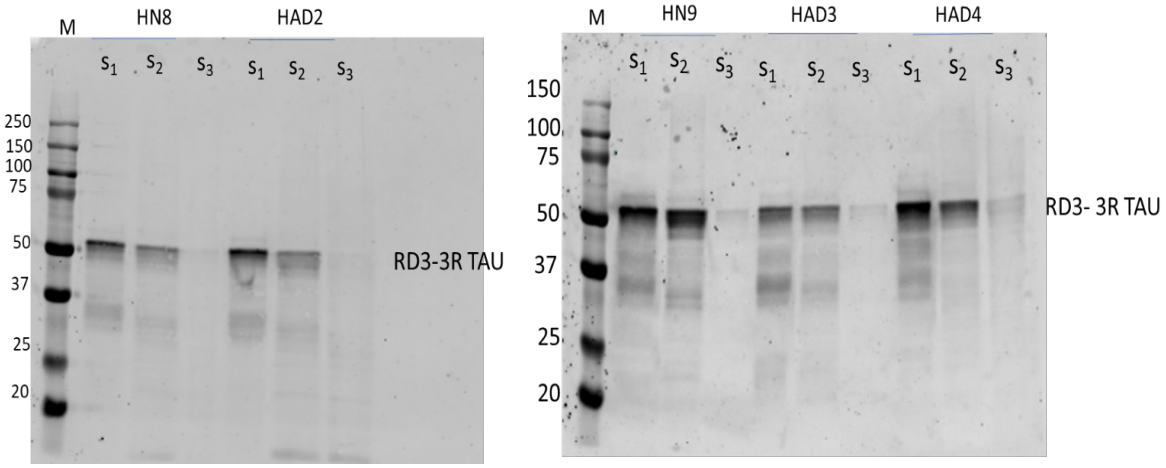

Figure 4.7: Western blot of fractionated lysates of 3D cultures at 6 weeks post differentiation to analyse the relative proportion of soluble and insoluble 3R tau across cell lines. The blot is stained with RD3 (45-65kDa, phosphorylated forms 68-72kDa). Equal volumes (normalised against β-Actin- total lysate) loaded across fractions in each lane M=marker.

To understand the solubility of tau isoform 3R tau in the different fractions across cell lines, the same procedure was followed as the previous experiment and the blots stained with 3R Tau antibody (Fig4.7). This antibody will detect both the phosphorylated and non-phosphorylated isoforms of tau. The immunogen corresponds to amino acids 209-224 (KHQPGGGKVQIVYKPV) of human tau. This sequence spans amino acids 267-316, omitting the second repeat domain where it bridges RD1 and RD3.

On analysis, we found that the 3R tau isoforms follow a similar trend to the Total Tau fractions in solubility (Fig4.8). Majority of the protein is found in the S1 and S2 fractions while comparatively only a small proportion is found in the unsoluble aggregated S3 fraction. Although there is no statistical difference in the S3 fractions there seems to be some trend between the control and the AD cell lines.

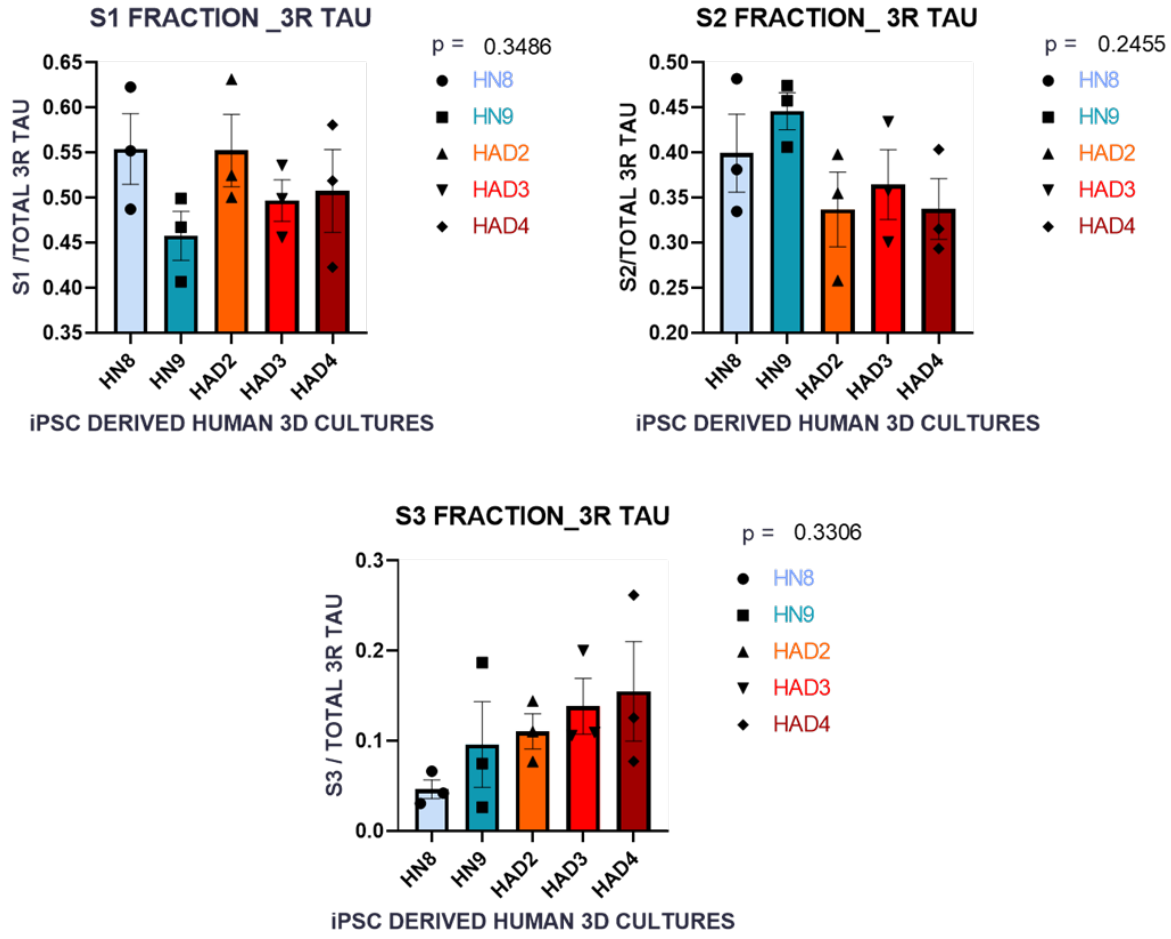

Figure 4.8: Western blot analysis of fractionated lysates of 3D cultures at 6 weeks post differentiation (n=3 culture samples) to analyse the relative proportion of soluble and insoluble 3R tau across cell lines. Each fraction is measured as a ratio over Total Tau where it is the sum of all fractions – S1+S2+S3.One-way Anova was used for analysis. All data were normally distributed. One-way Anova with Bonferroni's multiple comparison post-hoc test was used for analysis.

When an unpaired two-tailed t-test (with Welch's correction) (Fig4.9) was performed between the combined control and AD cell lines across all the fractions there seems to be a significant increase in the proportion of insoluble aggregated tau in the S3 fraction and a significant decrease in the S2 fraction in the AD lines as compared to the control lines at 6 weeks post differentiation in the 3D cultures.

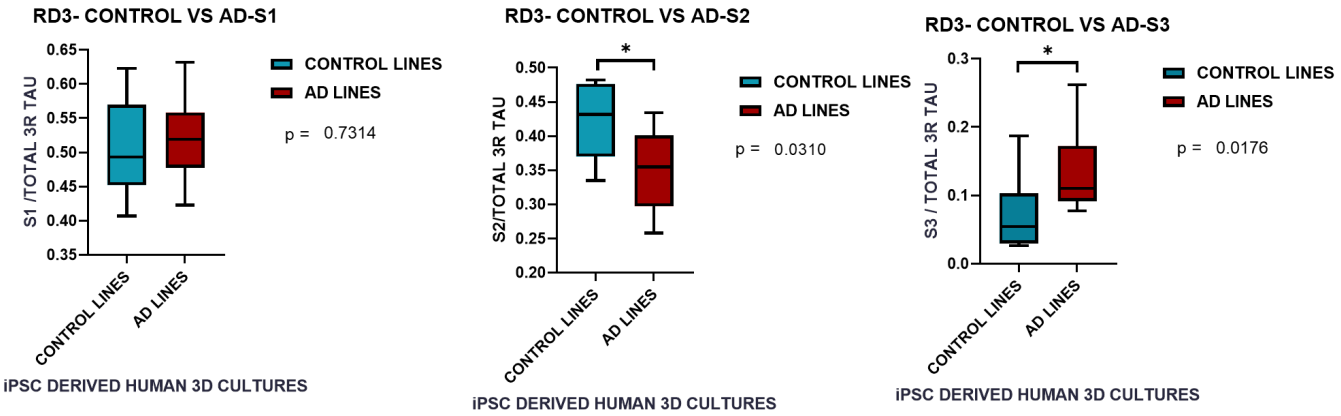

Figure 4.9: Comparative analysis of the fractions from control and AD lines grown in 3D cultures at 6 weeks post differentiation (n=3 culture samples). Each fraction is measured as a ratio over Total Tau where it is the sum of all fractions – S1+S2+S3.All data except for the S3 fraction were normal. Unpaired t-test with Welch's correction was used except for S3 fraction wherein Mann-Whitney test was performed to analyse all fractions. *p<0.05

4.4.1.4 3D cultures express 4R tau isoforms at 6 weeks post differentiation

4R tau are adult specific isoforms of tau. Unlike 3R tau which begin its expression early during the foetal stage, 4R tau is only found in the adults. The presence of the isoform itself gives a clear indication of the maturity of the 3D cultures. Further, 4R tau is implicated in AD. Hence, this experiment was performed not just to check for the prescence of the isoforms in the 3D cultures at the given timepoint but also to answer the question whether there is a difference in solubility of these isoforms between the control and the AD cell lines this early in differentiation. Also, this experiment becomes exceedingly crucial since no other 3D models have shown the presence of 4R tau this early in maturation *in vitro* in a physiologically relevant model.

To understand the solubility of 4R tau isoforms in the different fractions across cell lines, the same procedure was followed as the previous experiment and the blots stained with 4R Tau antibody (n=3 culture samples) (Fig 4.10). This antibody will detect both the phosphorylated and non-phosphorylated isoforms of tau. The immunogen corresponds to amino acids 275-291 (VQIINKKLDLSNVQSKC) of human tau. Region is flanking junction coded by adjacent exons 9 & 11 with the inclusion of exon 10.

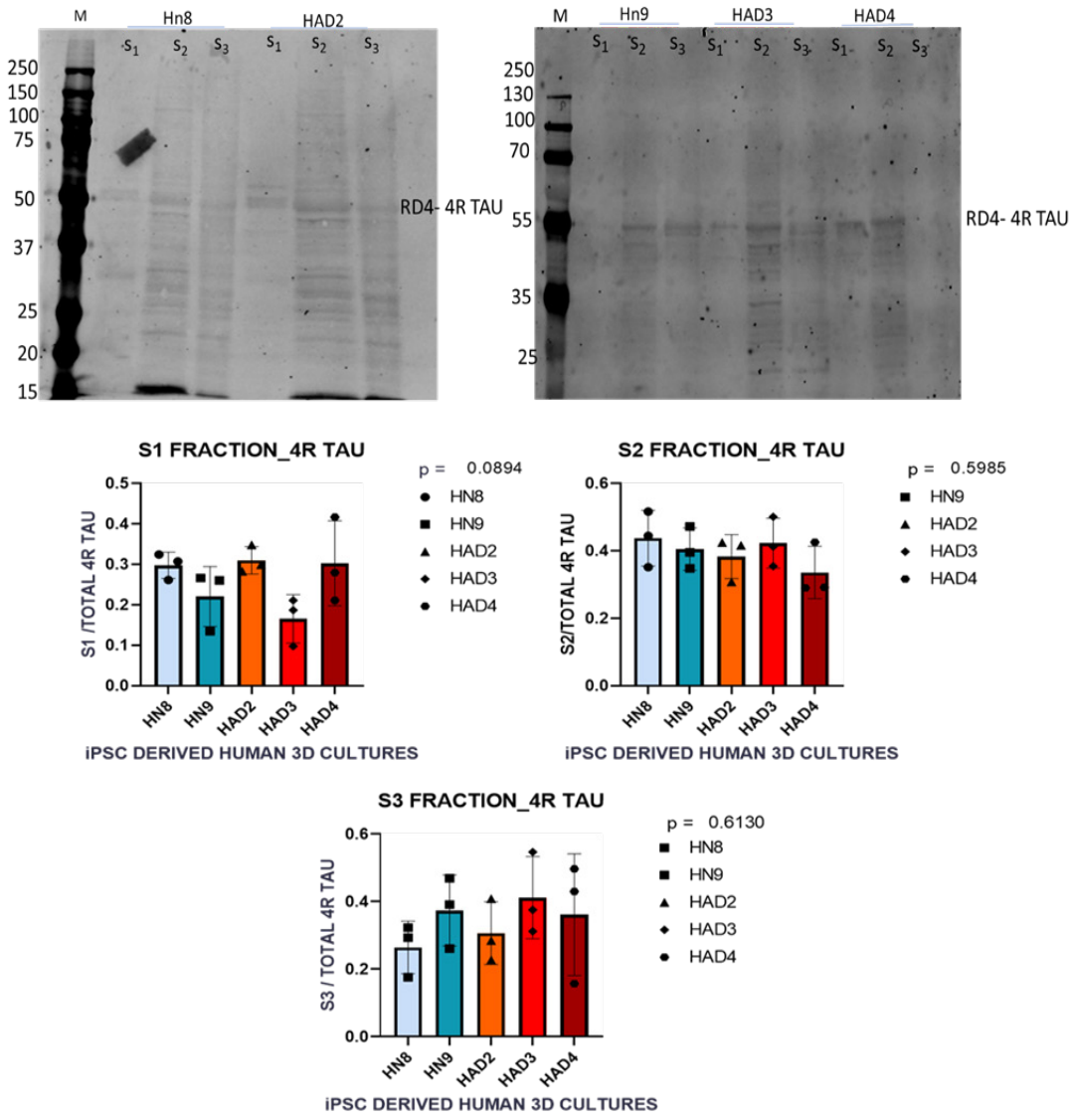

Figure 4.10: Western blot of fractionated lysates of 3D cultures at 6 weeks post differentiation (n=3 culture samples) to analyse the relative proportion of soluble and insoluble 4R tau across cell lines. The blot is stained with RD4 (45-65kDa, phosphorylated forms 68-72kDa). Equal volumes (normalised against β-Actin- total lysate) loaded across fractions in each well. Faint 4R tau bands are seen at 55kDa. Each fraction is measured as a ratio over Total Tau where it is the sum of all fractions – S1+S2+S3.All data except S2 fraction were normally distributed. One-way Anova with Bonferroni's post-hoc test was used for analysis except for S2 fraction wherein Kruskal Wallis test with Dunn's correction was performed

On analysis we found that the 4R tau isoforms are expressed in all fractions across all cell lines at around 55kDa at 6 weeks post differentiation in 3D cultures. However, it does not follow the same pattern of expression as seen before with Total Tau and 3R tau. The intensity of the bands is faint in comparison, however there is a laddering pattern seen in the S2 and S3 fractions across cell lines. On analysis, we found no statistical difference across the different cell lines for each fraction.

4.4.1.5 Phosphorylated tau in 3D CULTURES

Phosphorylation of tau is considered an important aspect of tau induced toxicity in the disease progression. Thus, it was crucial to check if there were any differences between the control and AD lines in the early and late timepoints. PHF1 is an AD associated phosphorylation epitope – Ser 396/Ser404.

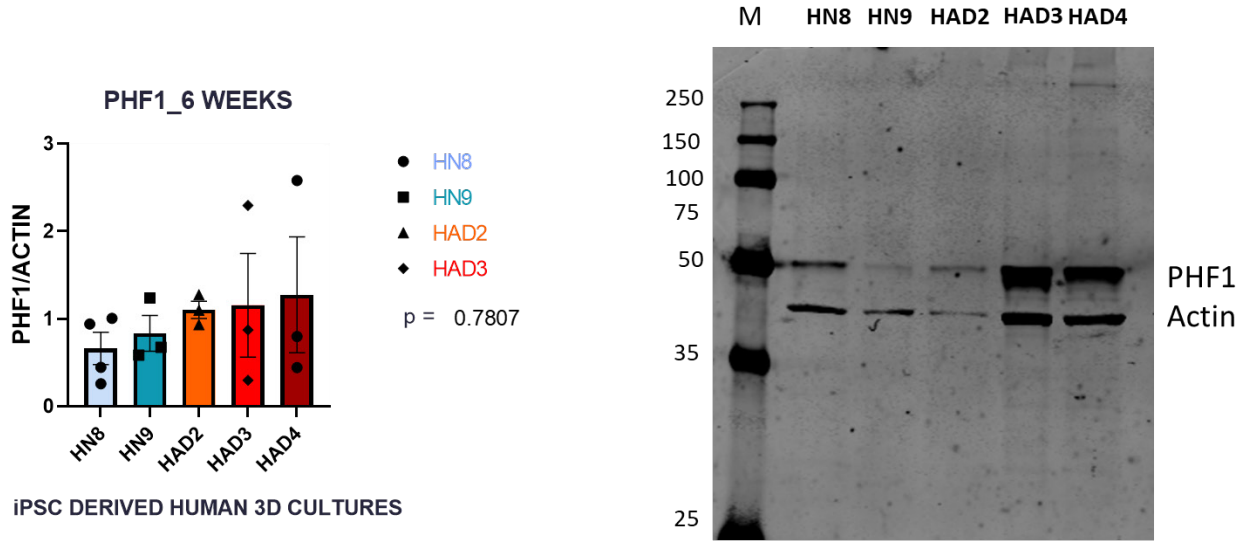

Figure 4.11: Western blot and analysis of PHF1 Tau in 3D cultures at 6 weeks post differentiation (n=3 culture samples). The blots are stained with PHF1 Tau (55kDa) and β-Actin (42kDa). 15ug of protein from total lysates of each group was loaded in each well. One-way Anova with Bonferroni's post-hoc test was used for analysis.

The total lysates from each cell line were used to analyse the expression of PHF1 across the cell lines in 3D cultures at 6 weeks (Fig 4.11) and 12 weeks post differentiation (Fig 4.12). PHF1 is seen in both the controls and the AD-3D cultures as early as 6 weeks post differentiation. Although there seems to be more expression in the AD lines in the blots there

is no statistical difference between the AD and the control lines at 6 weeks post differentiation due to high sample variability. This could possibly be because of the lower amounts of protein detected in controls. The PHF1 6-week blots are not ideal, this is mainly due to sample degradation on account of its poor quality due to batch variations seen in our latest purchase of cell lines from Axol Biosciences. Hence, not the best of the samples could be used for the PHF1 experiments. During culture and expansion phase few cell lines especially HN9 was particularly hard to revive and expand since there was not much viable cells in the vials. At 12 weeks post differentiation, there seems to be PHF1 expression in all cell lines. However, there seems to be no significant difference across the groups.

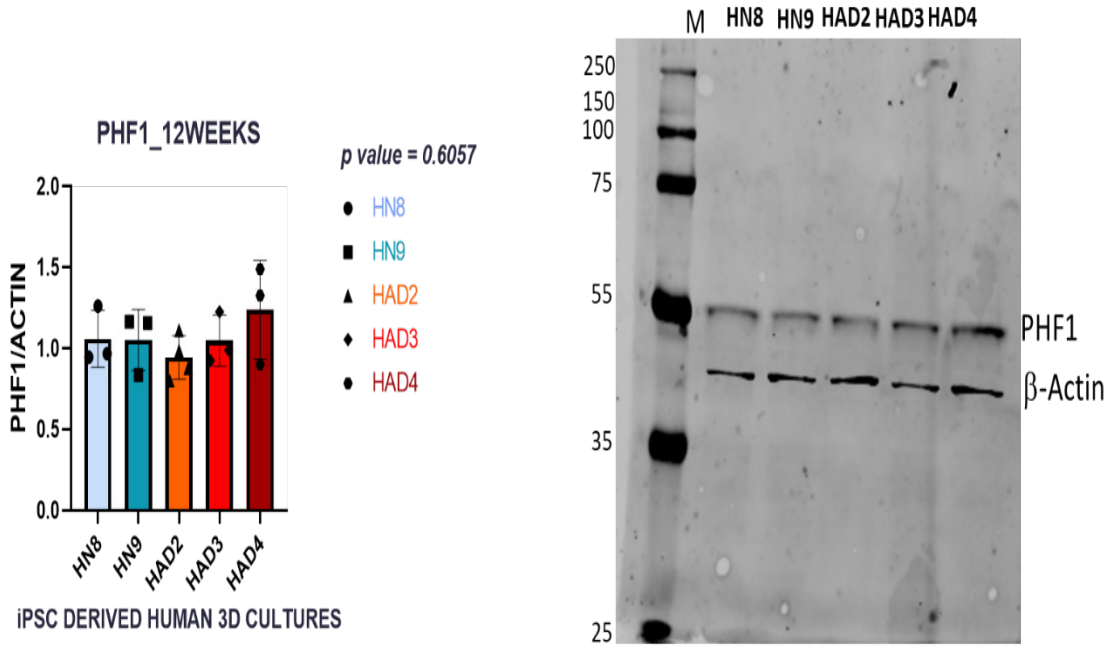

Figure 4.12: Western blot and analysis of PHF1 Tau in 3D cultures at 12 weeks post differentiation (n=3 culture samples). The blots are stained with PHF1 Tau (55kDa) and β-Actin (42kDa). 15ug of protein from total lysates of each group was loaded in each well. Since data was not normally distributed a Kruskal Wallis test with ~Dunn's correction was used for analysis.

4.5 Discussion

4.5.1 Tau and Phospho-Tau in FAD-AD cultures

Tau, a protein that is an integral part of the microtubule associated transport structure, is implicated in AD. Total Tau expression in the soluble lysates (total lysates) is seen at 6 weeks post differentiation in both the 2D and the 3D cultures. Moreover, there is more Tau expressed in the AD cell lines as compared to the control lines at both 6 weeks and 12 weeks post differentiation in 3D cultures. This is a pattern only seen in our 3D cultures as opposed to the 6 week -2D cultures where there is not much of a difference between the different cell lines. Similar to the MAP2 expression in the 2D vs 3D cultures, Tau – also a member of the MAPT family, follows the same trend of expression in our cultures.

Hyperphosphorylation of Tau is one of the features seen in AD brains. The phosphorylation of Tau at specific epitopes plays an important role deciding either normal function or disfunction of the protein. Tau phosphorylation at specific residues such as PHF1-Ser 396/Ser404 (Otvos *et al.*, 1994) and AT8- Ser202/Thr205 is considered an early event in the pathology of the disease (Braak, Braak and Mandelkow, 1994; Braak *et al.*, 2011). PHF1-phospho-Tau (Ser396/Ser404) was analysed in the total lysates of the 3D cultures. There seems to be no significant difference between the cell lines, as we do see high levels in our AD and control cell lines. This could possibly be because phosphorylation of tau is not always associated with the diseased state as seen in AD and tauopathies. Tau is a phosphoprotein and is developmentally regulated. There is transient hyperphosphorylation seen in the foetal brain during development. Foetal Tau is more hyperphosphorylated than adult Tau (Goedert, Crowther and Garner, 1991). However, the blot is not ideal due to poor quality of samples since we had issues with the quality of the cell lines brought from Axol Biosciences. We have shown that although there is a low expression of 4R Tau in our 3D cultures the Total Tau at 6 weeks post differentiation is predominantly 3R Tau which is the foetal Tau form. Hence it is not surprising to see hyperphosphorylation at this stage of differentiation in the control cells. Other iPSC studies also show similar pattern of hyperphosphorylation where in the initial 35-60 days there are no differences between the control and AD Tau phosphorylation states but as the cultures differentiate a difference appears in the control and AD lines around 100 days *in vitro* (Muratore *et al.*, 2014; Raja *et al.*, 2016). This developmental phosphorylation state is transient and reversible whereas the irreversible phosphorylation of Tau in the AD brain is

what characterize the pathological phenotype. A detailed study of the levels of tau in soluble and insoluble fractions would be more insightful.

Increasing amount of Tau protein in the CSF and blood plasma is something seen in AD patients and there is an ongoing research to translate this into early biomarkers for the disease (Blennow *et al.*, 1995; Sunderland *et al.*, 2003). The Total tau protein levels in CSF show strong correlation with the severity of the disease, and even more so with the neuronal damage level. However, phospho-Tau is implicated in the formation of neurofibrillary tangles (Hesse *et al.*, 2001). Both tau and phospho-tau increase in the CSF in AD (Sjögren *et al.*, 2001). Testing if Tau and phospho-Tau are released into the media over time in the 3D cultures would be a great tool to study the underlying pathophysiological state of the diseased cells *in vitro.*

4.5.2 Aggregation of Tau and its isoforms at an early stage of differentiation in vitro

NFTs are a primary hallmark of the neurodegenerative disease AD. Tangles are aggregated and hyperphosphorylated forms of tau. When the 3D cultures were analysed and quantified for the insoluble aggregated tau fraction in the cultures, it was observed that there was a higher proportion of detergent insoluble/urea soluble fractions (S3) in the AD lines as compared to the control lines at 6 weeks post differentiation *in vitro*. A similar pattern of aggregation is seen in the S3 fraction of the 3R tau isoforms at 6 weeks post differentiation. The 4R Tau isoforms have a different pattern of expression. Although present, the 4R Tau expression level is low compared to the 3R Tau levels. There is almost equal proportion of the 4R soluble proteins in each of the S1, S2 and the S3 fractions unlike what is seen for Total Tau and 3R Tau (approximately 50% in the S1 fraction, 40% in the S2 fraction and 10-15% in the S3 fraction). Hence, it could be summarised that the majority of the Total Tau seen in the 3D cultures must be predominantly 3R Tau isoforms. Comparing the known molecular weight of 4R Tau isoforms with that stained by the isoform specific antibody RD4 in our 3D cultures, it is suggestive that the cultures must be transitioning to the expression of 4R tau and therefore do not be express all the 4R isoforms, rather just faintly expresses the 0N4R and possibly the 1N4R isoforms. This could have been clarified if the samples were treated with phosphatase to show individual bands representing individual isoforms compared against a recombinant Tau ladder. Unfortunately, due to lack of time this could not be performed. The poor quality of the 4R Tau antibody could be the reason for seeing a lot of the non-specific bands across the gels,

which is not what we see with the other antibodies. The fact that the amount of the target protein is quite low in our samples does make the situation further difficult to assess. However, there is a study that validated the quality and specificity of tau antibodies (including 4RTAU-05-804) and state that the antibody in question is weak but rather specific to tau (Ercan *et al.*, 2017). The consideration that should also be kept in mind while analysing this data is that the quality of the cell-lines were not ideal to begin with, there were batch quality issues with the cell-lines later brought form Axol biosciences. These could be some the reasons why the quality of this data is not ideal. Furthermore, analysis of the gene expression of the 3R and 4R isoforms at 0 weeks and 6 weeks could be more informative if there was a transition from an early predominant 3R tau phase to an equimolar 3R: 4R phase in the cultures as is seen developmentally in humans. However, this is yet another proof that although the 6 weeks is a very early timepoint in the differentiation timeline, the cultures have a more physiological environment in the 3D culture system and the differences can be seen very early in the 3D cultures as compared to the traditional 2D cultures and other cultures, requiring a minimum of 200 or even more days *in vitro* to show the prescence of the 4R isoforms (Miguel *et al.*, 2019)(Lovejoy *et al.*, 2020). Unfortunately, due to shortage of time the 12- and 18-week samples could not be analysed further.

4.5.3 Presence of Aβ in early 3D- hAD2 cultures.

Aβ is a protein peptide produced by the sequential cleavage of APP by β-secretases and γ-secretases generating Aβ species of different lengths. Aβ peptide accumulation in the amyloid plaques is one of the hallmarks of AD brains. Aβ can aggregate to form soluble oligomeric species and insoluble/fibrillar aggregated species. These aggregated forms of Aβ are toxic to the neurons.

In the pilot study of this 3D model, the 3D cultures were fractionated using increasing strength of different detergents for biochemical analysis. Western blot analysis with anti Aβ antiboy-6E10 showed Aβ in the S1-TBS soluble fraction and S2-SDS insoluble/TBS soluble fraction and barely visible levels in the S3-detergent insoluble/Urea soluble fraction of the hAD2 samples. In addition to the Aβ-monomeric peptide, which is approximately 4kDa, a higher molecular weight dimer and trimer in the soluble fractions. The control cells don't seem to express any Aβ. The absence of Aβ in the control cells could possibly be because the controls

used in this experiment were a foetal hNSC rather than age-matched iPSC-derived NSC. A better understanding could be gathered if this experiment is repeated with the current set of AD cell lines and age-matched iPSC-derived lines with enough repeats for statistical analysis.

A similar study was performed by Choi et al 2014 showing a similar pattern of expression in their 3D cultures. The control lines -ReN-G (GFP) and ReN-m-(mCherry) show barely visible Aβ bands whereas the AD-lines ReN-GA (APPSL/GFP), ReN-mGAP (APPSL/GFP+PS1△E9/mCherry) and HReN-mGAP (GFP+APPSL/ PS1△E9/mCherry) show slightly darker bands, the darkest being the HReN-mGAP. They have a slightly different extraction protocol with their SDS- soluble fraction correlating to our S2 fraction and the FA-soluble corresponding to our S3 fraction. They see a 4th-band for the tetramer as well at 6-week differentiation. Nonetheless, it is important to remember that their cell lines, including the controls, overexpress AD genes. Their AD lines have been transfected with one or two FAD-mutations to force the pathology *in vitro* and the results we see could be an outcome of the overexpression of multiple mutations in the same cell, which is not generally seen in AD patients (Choi *et al.*, 2014a).

4.5.4 Altered 42/40 ratio in early 3D- hAD2-L286V cultures.

An altered Aβ42/40 ratio is commonly seen in FAD patients. An increase in Aβ42/40 is a phenomenon seen both *in vitro* and *in vivo* for AD models with-L286V mutation (Citron *et al.*, 1997; Murayama *et al.*, 1999). In the pilot experiments we see an increase in the ratio of Aβ42/40 in the 3D-L286V cell line as compared to the control cell line. This increase in the ratio was seen as early as week1 as well as at later timepoint week 11. However, this is a n=1 experiment (performed by Dr. Elodie Siney) which needs to be validated in the other AD- cell lines with appropriate controls and enough repeats for statistical analysis.

In conclusion, we successfully achieved the aim of finding differences in total tau expression and differences in aggregation of tau between control and AD cell lines grown in 3D early during differentiation. The prescence of 4R tau is questionable and the cultures predominantly express 3R Tau. We did see similar differences in aggregation as seen in total Tau in AD and control cell lines.

4.5.4.1 Summary and Future Work

The pilot studies on the 3D-neural culture model give us confidence that there are early changes in pathology in the 3D cultures which should be validated with further probing and include more timepoints to have a better understanding of the key players in the pathology of the disease. The fact that we see early changes in tau and its isoforms in cell lines predominantly with PSEN1 mutations is promising and requires an in-depth investigation of the biochemistry of Aβand its changes seen in these 3D-cultures. These findings could be key to unanswered questions, especially regarding the interactions of Aβ and Tau during early development of the disease.

Chapter 5 - Discussion

5.1 iPSC-based *in vitro* human AD model

Development of a human *in vitro* model which replicates the principal pathophysiological hallmarks of the disease if not all is rather challenging. However, it is vital to understand the underlying mechanisms driving AD pathology. The iPSC technology provides several advantages over other cell or tissue based *in vitro* models. iPSCs like ESCs are pluripotent and can be used to generate functionally defined and region-specified cell types. Modelling diseases with iPSCs provides deep insight into the onset or early stages of development of the pathology even before the symptoms would manifest. iPSCs are the best source of isogenic models and can be used to analyse patient-specific and physiologically relevant pathology underlying the disease. Moreover, they are not associated with the same ethical concerns as the ESCs for their use in research and clinic. Apart from these key features, what really makes iPSCs unique is their ability to generate patient-specific or disease-specific models which can replicate or mimic some aspects of the phenotype *in vitro.* This becomes a game changer when considering creating models to study Sporadic-AD. More than 95% of AD cases are sporadic with age, lifestyle and the APOE-E4 allele as risk factors. APOE-E4 allele is present in only 45-65% of SAD cases (Hall and Roberson, 2012b; Rincon and Wright, 2013) and has a limited 70% homology with its murine counterpart (Tai *et al.*, 2011). Unfortunately, this makes modelling SAD quite challenging. With iPSCs it becomes quite easy to replicate the SAD genetic background simply by using patient-specific cells for reprogramming.

Here, we have developed a human 3D neural culture model using iPSC-derived NSC from healthy individuals and AD patients with Presenilin-1 mutations-L286V, A246E and M146L, maintained for 18 weeks post 3D plating *in vitro.* PSEN1 mutations are the most common causes of the FAD which accounts for EOAD. Pedigree analysis reveals that more than 70% of FAD pedigrees show linkage to the PSEN1 locus rather than APP locus (Adkinson, 2012).

Is 3D better than 2D culture system for neuronal differentiation *in vitro*?

Most of the *in vitro* research in this field of study has been carried out in 2D cultures. Although 2D cultures have played a major role in the current understanding of the disease, they seem to lack certain key pathology phenotypes *in vitro*. We believe that, in order to generate mature and electrophysiologically functional neurons, a 3D culture system would provide a better

platform for the cells to grow and differentiate in their own 3D defining space. 3D cultures could be developed with specific conditions including material for scaffold, the extra-cellular matrix components and growth factors depending on the cell/tissue type of interest. These conditions could be modified as per the need of the study. 3D cultures could integrate a heterogeneous population of cell types dispersed in three dimension enhancing cell-cell communication in the intracellular niche. This provides for the better maturation and functionality of cells which would closely mimic the *in vivo* microenvironment. 3D cultures could be more advantageous in modelling pathologies like AD as they provide a conducive niche for the neurons to accumulate the pathological hallmarks over time, a factor which is lacking in a typical 2D culture system. For instance, the Choi *et al.* study was the first to show *in vitro* the evidence of both extracellular accumulation of Aβ deposition and aggregation of hyperphosphorylated tau filaments (Choi *et al.*, 2014a). To investigate the best possible method of culture a pilot experiment with iPSC-derived NSC from healthy individuals and AD patients with Presenilin-1 mutations-L286V, A246E and M146L which were maintained for 6 weeks in both 2D and 3D culture formats keeping the same cultures conditions were analysed. We see a robust differentiation in 3D cultures compared to the 2D cultures, with higher proportions of neurons seen in the 3D cultures.

5.2 An *in vitro* 3D human neural culture system.

In this study, human iPSCs-derived NPCs were expanded in 2D for 6 days in culture. Cells were then differentiated in thick layer of Matrigel providing a 3D scaffold. Matrigel was used as a scaffold because of its heterogeneous composition of proteins that provides a favourable microenvironment to the cells. Matrigel has proteins common to the extracellular matrix found in the brain like laminin, entactin, heparin-sulphate proteoglycans and collagen. These provide a surface for attachment, growth, differentiation and migration. Time points week 1, week 6, week 12 and week 18 were used for biochemical and immunohistochemistry analysis.

The human 3D neural culture model was characterised using immunofluorescence technique for an array of biomarkers at different time points to follow the differentiation of cells *in vitro.* B3 tubulin, a Class III isoform of the tubulin protein family, is one of the components of the microtubule assembly. B3 tubulin is primarily expressed in neurons (Lee *et al.*, 1990). It's role in neuronal development allows for it to be utilized as an early biomarker in identification of early neuronal lineage. 3D cultures express β3 tubulin at 6 weeks and 12 weeks post 3D plating. Microtubule-associated protein 2 (MAP2), a protein implicated in stabilization of microtubules (Takemura *et al.*, 1995) has been used as a biomarker for mature neuronal phenotype (Izant

and McIntosh, 1980). MAP2 plays a major role in the neuronal growth, differentiation and plasticity of neurons (Johnson and Jope, 1992). It is a cytoskeletal protein whose expression seen in the progenitor or immature cells but develops as the cells are more differentiated and found in the cell bodies and dendritic compartment of neurons (Dehmelt and Halpain, 2005). 3D cultures express MAP2 as early as week 6 post 3D plating, highlighting the presence of differentiated neurons. Synapsin 1, is a protein that belongs to the Synapsin family of proteins. Synapsin is a family of neuro-phosphoproteins associated with the cytoplasmic surface of the synaptic membrane (Huttner *et al.*, 1983). This family of proteins is implicated in the formation of synapses and regulation of neurotransmitter release at the pre-synaptic nerve terminals. The 3D cultures express VGLUT1 at 6 weeks post 3D plating. VGLUT 1 plays an important role in glutamate transport. Glutamate is the major excitatory transmitter in the vertebrate nervous system. Glutamate is recycled by vesicular glutamate transporters (VGLUTs) to maintain synaptic efficacy (Bellocchio *et al.*, 2000; Takamori *et al.*, 2000). VGLUT 1 is a vesicle bound sodium dependent phosphate transporter that is expressed specifically in excitatory neurons (Ni *et al.*, 1994). The 3D cultures express this presynaptic marker Synapsin 1 as early as 6 weeks post 3D plating, indicating some synapse formation. The 3D cultures also show expression of GFAP at 6 weeks post 3D plating. GFAP is an unique intermediate filament protein used to distinguish between astrocytes and other glial cells (Eng *et al.*, 1971). Presence of astrocytes in cultures is advantageous as they are prime in the modulation of synaptic efficacy and GFAP plays an important role in astrocyte-neuronal interaction as seen in the CNS (McCall *et al.*, 1996; Pfrieger and Barres, 1997). Astrocytes increase the number and maturity of functional synapses *in vivo* and *in vitro* thus making them active participants in synaptic plasticity (Ullian *et al.*, 2001). Expression of Nestin in cultures is the indication of presence of Neural Progenitor or Stem Cells (Lendahl, Zimmerman and McKay, 1990). Nestin-expressing cells are vital in their capacity to differentiate into neural and glial cells. A high percentage of cells in the 3D cultures show Nestin expression at 6 weeks and 12 weeks post 3D differentiation. The persistence of this subpopulation of undifferentiated cells in the 3D cultures was concerning and one of the major reasons to optimize the differentiation protocol to ensure that most of the undifferentiated cells become committed to differentiate. The protocol was optimized and a RA concentration of 0.5μM was confirmed as the best dose to generate maximum percent of neurons with a higher percent of supporting astrocytes accompanied by the decline of undifferentiated cells.

Any model can only be completely reliable when it has been reproducible. Once the 3D culture system was standardised and the differentiation protocol was optimized, the model was validated using the same iPSC derived cell lines for differentiation with the optimized protocol at timepoints 0week, 6week, 12week and 18week post differentiation. Unfortunately, due to shortage of time 18week samples could not be processed. The cultures revealed a robust differentiation with the expression of neuronal markers B3 Tubulin and Map2 increasing up from week 0 through week 6 to week 12 post differentiation. Whereas the expression of astrocytic marker decreased from week 0 to 6 and then steadily increased to week 12. There was a steady decline of the NSC marker Nestin from week 0 to week 6 and 12 post differentiation. Thus, we have a heterogeneous human neural culture model which shows evidence of progression towards maturity and synapse formation as early as 6 weeks post 3D plating.

5.3 Modelling AD in an in *vitro* 3D human neural culture system.

Western blot analysis showed that the 3D cultures of all five cell lines express total tau protein at 6 weeks post 3D plating. The total tau is highly expressed in the AD cell lines as compared to the control cell lines at 6 weeks post differentiation (normalised to β-actin or GAPDH which were used as housekeeping protein). To have a better understanding of the solubility of Total Tau and its isoforms cell lysates were serially extracted into three fractions. The lysates were fractionated into S1, S2 and S3, S1 being the TBS soluble fraction, S2 – SDS soluble fraction and S3- the Urea soluble/ SDS insoluble fraction. The S1 fraction contains the monomers while the S2 fraction contains monomers and the stable forms of oligomers and higher molecular weight proteins whereas the S3 contains the insoluble proteins and aggregates. SDS is an anionic detergent which solubilises oligomeric forms of protein which could also include membrane bound forms of protein. Urea is a chaotropic reagent which denatures the insoluble aggregated, fibrillary forms and amyloidogenic forms of proteins (Bandopadhyay, 2016). 3R tau, the foetal isoforms of the protein are seen in the fractions and total lysate of all the cell lines at 6 weeks and 12 weeks post 3D plating. The 4R tau-the adult isoforms of the protein tau were seen at 6 weeks across all fractions. 4R Tau were also seen in AD cell line hAD2 at 18 weeks post differentiation (Chapter 2). There is more aggregated Total tau in the AD cell lines compared to the control lines at 6 weeks post differentiation. Similarly, more aggregated 3RTau

was seen in the AD cell lines as compared to the control lines. However, since the expression of 4R tau was faint compared to the 3R tau the quantification cannot be conclusive.

PHF-1 recognises hyperphosphorylated sites Ser396 and/or Ser404 on tau protein (Otvos *et al.*, 1994). Tau is abnormally hyperphosphorylated and aggregated in the form of paired helical filaments (PHFs) which progresses to form tangles in AD (Grundke-Iqbal *et al.*, 1987). PHF-1 is expressed in the AD cell line hAD2 at 6 weeks post 3D plating. There is a slight but not significant increase in the PHF1 in AD lines when compared to controls at 6 weeks and 12 weeks post differentiation. Pilot experiment on hAD2-L286V (performed by Dr. Elodie Siney) showed the presence of Aβ oligomers as early as 6 weeks post differentiation and an increase in Aβ42/40 ratio as early as week 1 and maintained at week 11 post differentiation. However, these experiments need to be validated across all the cell lines with statistical repeats.

Thus, we have a model that expresses total tau as well as its 3R and 4R isoforms and shows evidence of tau phosphorylation and aggregation as early as 6 weeks in the 3D culture, Aβ oligomers at 6 weeks post differentiation in hAD2 and an increase in Aβ42/40 ratio. However, further studies and investigation of other pathological markers like AT8 and AT100 in 3D cultures will be required.

5.4 Unique features of the AD-3D – in vitro human neural culture system.

Unlike some of the studies carried out in this particular field of research, this model does not rely on overexpression of FAD mutations which accelerates the progress of the pathology in a non-physiological way (Choi *et al.*, 2014c; Verheyen *et al.*, 2015). Our model is driven by the presence of the mutation in the patient from whom the iPSC was developed. Patient-derived iPSCs in the 3D cultures allows for developing certain key aspects of the disease *in vitro* in a more physiologically relevant manner without the need to genetically manipulate and force the disease phenotype. One of the challenges in modelling an age-related neurodegenerative disease like AD is to generate aged and mature neurons. Although the research groups trying to develop 3D-AD culture models have shown maturity in their cultures with different mature neuronal differentiation markers, none of them have shown protein level expression that recapitulate the physiological levels of the adult 4R tau isoform seen in the human brain (Choi *et al.*, 2014a; Lee *et al.*, 2016; Raja *et al.*, 2016). However, there are few studies that see the

protein level expression of 4R Tau in their 3D/organoid models, but not all the isoforms seem in the adult but either due to long term cultures of 365 days *(Sposito 2015),* or long term use of Brain-Phys to see expression at 25 weeks (Miguel *et al.*, 2019) or after 300 days (Lovejoy *et al.*, 2020). Although, we possibly do not see all the isoforms we do see a transition into 4R tau as early as 6-week post differentiation. This clearly shows that the 3D environment provides better differentiation and more efficient maturation and aging of the neurons. However, certain studies have shown that premature neuronal differentiation might occur early during development in AD patients with PSEN1 mutations both *in vitro* and *in vivo* (Veeraraghavalu *et al.*, 2010; Yang *et al.*, 2016). This could possibly be one of the reasons for seeing early pathogenic differences between the control and the AD cell lines in 3D cultures.

Cerebral organoids are widely used to study brain development (Chambers, Tchieu and Studer, 2013; Paşca *et al.*, 2015). The foundation of organoids was built on the need of human culture models which could recapitulate physiological as well as pathological conditions *in vitro.* It also develops from the initial work of 2D neural cultures mimicking tissue like structures namely rosettes during in vitro differentiation which later led to embryoid body (EB) induced differentiation of cells (Zhang *et al.*, 2001; Eiraku *et al.*, 2008). These were the ground studies that influenced the onset of cerebral organoids, spheroids and 3D cultures either embedded in matrix or agitated in suspension cultures. There is a constant effort to make improvements in this area of research since then, especially when it comes to directed differentiation of a specific brain region. Forebrain, midbrain and hippocampal organoids are among some of the organoids been reported in the past few years (Di Lullo and Kriegstein, 2017). Most of the protocols follow spontaneous or undirected differentiation, which effectively develops into different structural areas of the brain but in a very uncontrolled and random pattern making it difficult to predict the proportion of cells types in each culture. This variation is one of the biggest limitations of using organoids. However, this makes them very interesting for developmental studies and less predictable towards neurodegenerative studies. A certain proportion of cells in the organoids tend to differentiate into non-ectodermal cell types (Camp *et al.*, 2015). However, efforts are being made to narrow down the specificity of cell type differentiation using exogenous factors (Sloan *et al.*, 2017). Recently, efforts are being made to differentiate organoids into brain specific region and then in a later step fuse these different region-organoids (Bagley *et al.*, 2017). A sophisticated model of organoids demonstrated accelerated accumulation of amyloidogenic Aβ peptides in AD or Down's Syndrome -iPSC derived organoids when compared to controls such as healthy iPSC or mouse ESCs and iPSCs. AD-

organoids also showed prominent structures similar to plaques and NFTs in AD rather than controls. These features were also absent in iPSCs derived from patients suffering from Creutzfeldt-Jakob disease (Gonzalez *et al.*, 2018). In another study, Park et al developed a new way to integrate 3 cell types together using microfluidics system. A 3D- human triculture model involving neurons, astrocytes and the other critical player of AD -microglia was developed. The system shows migration of microglia along with the AD phenotypes such as Aβ aggregation, tau hyperphosphorylation, neuroinflammation, axonal cleavage and release of NO all-together causing a toxic environment for AD cultures (Park *et al.*, 2018). Organoids directed towards Choroid Plexus epithelium could be a new approach to understand the CSF and blood-brain barrier aspect of the disease. Another limitation of organoids are its necrotic cores. This could be due to the lack of perfusion in cultures, something that physiologically resembles vasculature. Efforts are now being made to overcome this challenge by engineering organoids with vasculture (Jacob *et al.*, 2020; Pellegrini *et al.*, 2020).

Thus, our human 3D iPSC-derived neural culture model is a promising, robust and physiologically relevant system with is a heterogeneous mix mature neurons and astrocytes including both excitatory and inhibitory neurons, expressing some features of the Tau and Aβ pathology as early as 6 weeks *in vitro* without forcing pathology using genetic manipulation. The expression of 4R tau is indicative of the maturation of these neurons. However, further investigation at later timepoints with phosphatase treatment to determine the expression of all 6 isoforms needs to be done.

5.5 Limitations

The general concerns around iPSCs are their line variability and reduced efficiency in producing neurons as compared to ESCs, along with their latency in producing mature neurons (Hu *et al.*, 2010). One of the major reasons for line variability is the differences due to the genetic background of the donors (Burrows *et al.*, 2016; Kilpinen *et al.*, 2017). It is reported that the variation in phenotype due to (healthy) inter-individual variation makes up for a significant 23%. Non-genetic factors like the protocols and conditions used for induction and differentiation itself could result in variations(Schwartzentruber *et al.*, 2018) although there is less variation in lines generated from the same individual (Rouhani *et al.*, 2014). With new advances in the iPSC technology there is a reduction in these variabilities to some extent by including non-viral and non-integrating systems to reprogram these cells *in vitro* (Hu, 2014) Using isogenic lines where possible is another way to reduce variability. With the advent of CRISPR/Cas9 gene editing becomes a critical tool to develop mutant lines either by editing in/ out mutations from lines to better understand the disease aetiology (Cong *et al.*, 2013)(Paquet *et al.*, 2016). These edited lines along with isogenic controls are a great tool to study individual mutations and investigate their impact on cortical development and function. In the 3D cultures we do see some slight variations which could possibly be reduced to a certain extent by using isogenic controls to our AD lines.

There is no doubt that the 3D cultures have the potential to be developed into models for various diseases, but the limitations include the technical difficulties that come with it. Due to the thickness of the cultures the cultures have low optical transparency especially while taking high resolution images. Some studies have a way around this limitation by having both a thick 3D culture system for biochemical analysis and thin layer 3D cultures for staining and electrophysiological experiments (Choi *et al.*, 2014a). The cell density plays a very important role in rate of proliferation and differentiation and this might differ between thin and tick cultures. Such studies don't have a method to neutralise the differences seen due to changes in thickness. There are advances in this area of research and possibly could help improve the clearance techniques for improved imaging of thick 3D cultures (Du *et al.*, 2018).

Another limitation of the iPSC-disease modelling system is the *in vivo* age and maturity of the neurons for modelling age-related diseases like AD, Parkinson's disease and ALS. Even

though the differentiation in 3D/spheroid/organoid systems shows improvement in maturation and function these cultures are not equivalent to the state of maturation seen at age 65 years and above in humans, the age around which the symptoms of the SAD become evident. As stated, before expression of 4R tau isoforms is an indication of maturity in the neurons. There are studies with cell cultures with extended period of time– such as 365 days (Sposito *et al.*, 2015) and 300 days (Lovejoy *et al.*, 2020) to finally see the 4R tau isoforms being expressed. Studies have explored ways to achieve neuronal maturity faster in culture by forcing expression of the protein progerin implicated in pe-mature ageing syndrome Progeria (Miller *et al.*, 2013) or by exposing cells to toxins like reactive oxygen species (Campos, Paulsen and Rehen, 2014) to recapitulate changes induced due to stress. Another approach is to generate induced Neurons (iNs), inspired by the principles of iPSC technology. Exploring the concept of cellular plasticity, iNs are generated by directly forcing fibroblasts to transdifferentiate into neurons by overexpressing genes such as Brn2, Ascl1, and Myt1l (BAM) thereby skipping the middle primitive phase seen in iPSC generation (Vierbuchen *et al.*, 2010). However, there are limitations involving the use of iNs, iNs are generated as post-mitotic cells and hence cannot be expanded. The fibroblasts are also limited in their capacity to proliferate and enter senescence after a few cycles. Hence one of the major issues of iNs is a limited number of starting cells. The iNs also need to be co-cultured with astrocytes for at least 5-6 weeks to induce matured physiological functions (Mertens *et al.*, 2018). This said there is a possibility that the 3D cultures won't fully express late-stage plaques and tangles as seen in post-mortem brain slices of AD patients. The time in culture may not be sufficient enough as compared to the years it takes for these hallmarks to appear in the human pathology state. Nonetheless, 3D cultures could be a great platform to study the early or preclinical changes that the system undergoes even before the pathology becomes evident.

Another possible limitation of the model is the absence of microglia in the cultures. Microglia are resident macrophages in the brain which are activated in response to disease or damage. In recent years, it has become evident that microglia play a major role in the AD pathogenesis, especially its association to amyloid plaques. Activated microglia is a common pathological feature of several neurodegenerative diseases including AD. However, it is still unknown if they are a boon or bane or simply neutral in their role in neuropathology development (Tremblay and Sierra, 2014). Thus, modelling a pathology independent of a key player may hinder the complete replication of pathogenic phenotypes desired for the model. It is rather challenging to include microglia in a neural differentiation model. During development,

microglia originate from embryonic mesoderm unlike the neurons and astrocytes that develop from the neuroectoderm. They populates the human brain during the 4th and the 24th week of gestation (Menassa and Gomez-Nicola, 2018). NSCs are limited in their potency to differentiate into neural cell types hence iPSC derived NSCs cannot be differentiated into microglia in the same culture conditions. The possible approach would be to co-culture mature microglia along with mature neurons and astrocytes differentiated from the same iPSCs but in separate culture systems which limits the interaction of these cell types early during differentiation. Park et al 2018 have developed a triculture system where they coculture neuronal progenitor cells with adult microglia in a microfluidic system to show microglial migration (Park *et al.*, 2018)

Lack of vascularisation is another limitation of the 3D cultures. The circulatory system plays a major role in providing nutrition, gaseous exchange and extraction of waste. This could possibly be one of the reasons why spheroid cultures which are generally large (approximately 400µm in diameter) have a necrotic centre (Sutherland *et al.*, 1981). Worsdorfer et al has showed endothelial cell-cell junctions, a basement membrane, luminal caveolae and macrovesicles as well as a typical blood Bessel ultrastructure in human tumor as well as neural organoids (Wörsdörfer *et al.*, 2019). The other possible approach would be the use of microfluidic systems. There are several studies that integrate microfluidic systems with 3D cultures which could be customisable as per the research questions. This could also solve the commonly seen issues of contamination in stem cell cultures by reducing the day to day handling of cultures for media changes. Another limitation of 3D culture is the technical difficulties to performing electrophysiological studies. The dense nature of the 3D cultures not only makes it optically difficult to probe but also hard to clamp on in 3D cultures as opposed to the 2D cultures where cells are firmly attached to the coverslips.

One of the major limitations of this project is the small sample size. Since the cell lines are expensive and cannot be expanded beyond a limit in culture, we are restricted by cell numbers to carry out different analysis on the cultures. The 3D cultures have a heterogeneous population of cells. However, we are not sure what different type of cells are present in the culture also which cortical layer phenotype they differentiate into. Lastly, our model does not completely replicate the *in vivo* human neural tissue. In order to validate the extent of similarity or difference, studies to compare and contrast these 3D cultures with human resected brain tissue will have to be undertaken.

5.6 Future Work

Further work needs to be done not just in characterising the cell types to have a complete profile of the nature of the cultures but also to complete Western Blot analysis to study the solubility of Tau and is isoform at 12- and 18-weeks post differentiation. Work also needs to further investigate the Aβ pathology across cell lines to analyse Aβ oligomers using Western Blot technique and ratio of Aβ42 over Aβ40 by Meso-scale analysis. To analyse tau pathology, analysis with specific antibodies such as AT8 and AT100 is required. For functional analysis of the neurons, Whole-Cell Patch-Clamp technique is required. Further characterisation of pre-synaptic and post-synaptic proteins to better understand the synaptic functions of the cells also needs to be done.

Bibliography

Abe, Y. *et al.* (2003) 'Analysis of neurons created from wild-type and Alzheimer's mutation knock-in embryonic stem cells by a highly efficient differentiation protocol', *Journal of Neuroscience*, 23(24), pp. 8513–8525. doi: 10.1523/jneurosci.23-24-08513.2003.

Adams, S. J. *et al.* (2010) 'Three Repeat Isoforms of Tau Inhibit Assembly of Four Repeat Tau Filaments', *PloS one*, 5(5), pp. 1–9. doi: 10.1371/journal.pone.0010810.

Adkinson, L. (2012) 'Neurologic Diseasee', *Journal of Chemical Information and Modeling*, (2012), pp. 133–158.

Agholme L FAU - Lindstrom, T. *et al.* (2010) 'An in vitro model for neuroscience: differentiation of SH-SY5Y cells into cells with morphological and biochemical characteristics of mature neurons. PG - 1069-82 LID - 10.3233/JAD-2010-091363 [doi]', (20), pp. 1069–1082. doi: 10.3233/JAD-2010-091363.

Agüero-Torres, H. *et al.* (1998) 'Prognostic factors in very old demented adults: a seven-year follow-up from a population-based survey in Stockholm.', *Journal of the American Geriatrics Society*, 46(4), pp. 444–52.

Ahlijanian, M. K. *et al.* (2000) 'Hyperphosphorylated tau and neurofilament and cytoskeletal disruptions in mice overexpressing human p25, an activator of cdk5', *Proceedings of the National Academy of Sciences of the United States of America*, 97(6), pp. 2910–5. doi: 10.1073/pnas.040577797.

Alagappan, D. *et al.* (2014) 'Insulin-like growth factor receptor signaling is necessary for epidermal growth factor mediated proliferation of SVZ neural precursors in vitro following neonatal hypoxia-ischemia', *Frontiers in Neurology*, 5 MAY. doi: 10.3389/fneur.2014.00079.

Alliquant, B. *et al.* (1995) 'Downregulation of Amyloid Precursor Protein Inhibits Neurite Outgrowth

In Vitro', *Journal of Cell Biology*, 128(5), pp. 919–927.

Alonso, A. D. C. *et al.* (1994) 'Role of abnormally phosphorylated tau in the breakdown of microtubules in Alzheimer disease', *Proceedings of the National Academy of Sciences of the United States of America*, 91(12), pp. 5562–5566. doi: 10.1073/pnas.91.12.5562.

Alonso, A. D. C. *et al.* (1997) 'Abnormal phosphorylation of tau and the mechanism of Alzheimer neurofibrillary degeneration: Sequestration of microtubule-associated proteins 1 and 2 and the disassembly of microtubules by the abnormal tau', *Proceedings of the National Academy of Sciences of the United States of America*, 94(1), pp. 298–303. doi: 10.1073/pnas.94.1.298.

Alvarez, A. *et al.* (1999) 'Inhibition of tau phosphorylating protein kinase cdk5 prevents β-amyloid-induced neuronal death', *FEBS Letters*, 459(3), pp. 421–6. doi: 10.1016/S0014-5793(99)01279-X.

Alvarez, G. *et al.* (1999) 'Lithium protects cultured neurons against β-amyloid-induced neurodegeneration', *FEBS Letters*, 453(3), pp. 260–264. doi: 10.1016/S0014-5793(99)00685-7.

ALZFORM (2019) *Mutations | ALZFORUM*, *ALZFORUM*. Available at: https://www.alzforum.org/mutations (Accessed: 2 June 2020).

Alzheimer, A. *et al.* (1995) 'An english translation of alzheimer's 1907 paper, "Uber eine eigenartige Erkankung der Hirnrinde"', *Clinical Anatomy*, 8(6), pp. 429–431. doi: 10.1002/ca.980080612.

An, W. L. *et al.* (2003) 'Up-regulation of phosphorylated/activated p70 S6 kinase and its relationship to neurofibrillary pathology in Alzheimer's disease', *American Journal of Pathology*, 163(2), pp. 591–607. doi: 10.1016/S0002-9440(10)63687-5.

Anderson, J. P. *et al.* (1991) 'Exact cleavage site of Alzheimer amyloid precursor in neuronal PC-12 cells', *Neuroscience Letters*, 128(1), pp. 126–128. doi: 10.1016/0304-3940(91)90775-O.

Andreadis, A., Broderick, J. A. and Kosik, K. S. (1995) 'Relative exon affinities and suboptimal splice site signals lead to non-equivalence of two cassette exons', *Nucleic Acids Research*, 23(17), pp. 3585–

3593. doi: 10.1093/nar/23.17.3585.

Andreadis, A., Brown, W. M. and Kosik, K. S. (1992) 'Structure and Novel Exons of the Human-tau Gene', *Biochemistry*, 31(43), pp. 10626–10633.

Aoi, M. *et al.* (2000) 'The effect of intrastriatal single injection of GDNF on the nigrostriatal dopaminergic system in hemiparkinsonian rats: Behavioral and histological studies using two different dosages', *Neuroscience Research*, 36(4), pp. 319–325. doi: 10.1016/S0168-0102(00)00097-3.

ARUK Dementia Statistics Hub (no date) *Prevalence by gender in the UK | Dementia Statistics Hub*, *Alzheimer's Research UK* . Available at: https://www.dementiastatistics.org/statistics/prevalence-by-gender-in-the-uk/ (Accessed: 12 June 2018).

Asano, H. *et al.* (2009) 'Astrocyte differentiation of neural precursor cells is enhanced by retinoic acid through a change in epigenetic modification', *Stem Cells*, 27(11), pp. 2744–2752. doi: 10.1002/stem.176.

Axolbio (no date) *Human iPSC-Derived Neural Stem Cells*. Available at: https://www.axolbio.com/page/neural-stem-cells-cerebral-cortex (Accessed: 12 June 2018).

Bagley, J. A. *et al.* (2017) 'Fused cerebral organoids model interactions between brain regions', *Nature Methods*, 14(7), pp. 743–751. doi: 10.1038/nmeth.4304.

Bain, G. *et al.* (1995) 'Embryonic stem cells express neuronal properties in vitro', *Developmental Biology*, pp. 342–357. doi: 10.1006/dbio.1995.1085.

Bandopadhyay, R. (2016) 'Sequential Extraction of Soluble and Insoluble Alpha-Synuclein from Parkinsonian Brains', *Journal of Visualized Experiments*, (107), p. e53415. doi: 10.3791/53415.

Baratchi, S. *et al.* (2012) 'Secreted amyloid precursor proteins promote proliferation and glial differentiation of adult hippocampal neural progenitor cells', *Hippocampus*, 22(7), pp. 1517–1527.

doi: 10.1002/hipo.20988.

Baumann, K. *et al.* (1993) 'Abnormal Alzheimer-like phosphorylation of tau-protein by cyclin-dependent kinases cdk2 and cdk5', *FEBS Letters*, 336(3), pp. 417–424. doi: 10.1016/0014-5793(93)80849-P.

Beck, K. D. *et al.* (1995) 'Igf1 gene disruption results in reduced brain size, CNS hypomyelination, and loss of hippocampal granule and striatal parvalbumin-containing neurons', *Neuron*, 14(4), pp. 717–730. doi: 10.1016/0896-6273(95)90216-3.

Bekris, L. M. *et al.* (2010) 'Genetics of Alzheimer disease', *Journal of Geriatric Psychiatry and Neurology*, 23(4), pp. 213–227. doi: 10.1177/0891988710383571.

Bellocchio, E. E. *et al.* (2000) 'Uptake of glutamate into synaptic vesicles by an inorganic phosphate transporter', *Science*, 289(5481), pp. 957–960. doi: 10.1126/science.289.5481.957.

Benilova, I. and De Strooper, B. (2013) 'Promiscuous Alzheimer's amyloid: Yet another partner', *Science*, 341(6152), pp. 1354–5. doi: 10.1126/science.1244166.

Beyer, C. and Karolczak, M. (2000) 'Estrogenic stimulation of neurite growth in midbrain dopaminergic neurons depends on cAMP/protein kinase A signalling', *Journal of Neuroscience Research*, 59(1), pp. 107–116. doi: 10.1002/(SICI)1097-4547(20000101)59:1<107::AID-JNR13>3.0.CO;2-W.

Biernat, J. *et al.* (1993) 'Phosphorylation of Ser262strongly reduces binding of tau to microtubules: Distinction between PHF-like immunoreactivity and microtubule binding', *Neuron*, 11(1), pp. 153–163. doi: 10.1016/0896-6273(93)90279-Z.

Blennow, K. *et al.* (1995) 'Tau protein in cerebrospinal fluid - A biochemical marker for axonal degeneration in Alzheimer disease?', *Molecular and Chemical Neuropathology*, 26(3), pp. 231–245. doi: 10.1007/BF02815140.

Blennow, K. and Hampel, H. (2003) 'CSF markers for incipient Alzheimer's disease', *Lancet Neurology*, 2(10), pp. 605–613. doi: 10.1016/S1474-4422(03)00530-1.

Blumberg, B. (1997) 'An essential role for retinoid signaling in anteroposterior neural specification and neuronal differentiation', *Seminars in Cell and Developmental Biology*, 8(4), pp. 417–428. doi: 10.1006/scdb.1997.0165.

Bobinski, Maciej *et al.* (1996) 'Neurofibrillary pathology - Correlation with hippocampal formation atrophy in Alzheimer disease', *Neurobiology of Aging*, 17(6), pp. 909–919. doi: 10.1016/S0197-4580(96)00160-1.

Bons, N. *et al.* (2006) 'Microcebus murinus: A useful primate model for human cerebral aging and Alzheimer's disease?', *Genes, Brain and Behavior*, 5(2), pp. 120–30. doi: 10.1111/j.1601-183X.2005.00149.x.

Borchelt, D. R. *et al.* (1996) 'Familial Alzheimer's Disease–Linked Presenilin 1 Variants Elevate Aβ1–42/1–40 Ratio In Vitro and In Vivo', *Neuron*, 17(43), pp. 1005–1013.

Borchelt, D. R. *et al.* (1997) 'Accelerated amyloid deposition in the brains of transgenic mice coexpressing mutant presenilin 1 and amyloid precursor proteins', *Neuron*, 19(4), pp. 939–45. doi: 10.1016/S0896-6273(00)80974-5.

Braak, E., Braak, H. and Mandelkow, E.-M. (1994) 'A sequence of cytoskeleton changes related to the formation of neurofibrillary tangles and neuropil threads', *Acta Neuropathologica*, 87(6), pp. 554–567. doi: 10.1007/s004010050124.

Braak, H. *et al.* (2011) 'Stages of the pathologic process in alzheimer disease: Age categories from 1 to 100 years', *Journal of Neuropathology and Experimental Neurology*, 70(11), pp. 960–969. doi: 10.1097/NEN.0b013e318232a379.

Braak, H. and Braak, E. (1991) 'Demonstration of Amyloid Deposits and Neurofibrillary Changes in Whole Brain Sections', *Brain Pathology*, 1(3), pp. 213–216. doi: 10.1111/j.1750-

3639.1991.tb00661.x.

Braggin, J. E. *et al.* (2019) 'Alternative splicing in a presenilin 2 variant associated with Alzheimer disease', *Annals of Clinical and Translational Neurology*, 6(4), pp. 762–777. doi: 10.1002/acn3.755.

Braidy, N. *et al.* (2015) 'Accelerating Alzheimer's research through "natural" animal models', *Current Opinion in Psychiatry*, 28(2), pp. 155–164. doi: 10.1097/YCO.0000000000000137.

Brandt, R. *et al.* (1994) 'Differential effect of phosphorylation and substrate modulation on tau's ability to promote microtubule growth and nucleation', *Journal of Biological Chemistry*, 269(16), pp. 11776–11782.

Brandt, R. and Lee, G. (1993) 'The Balance Between τ Protein's Microtubule Growth and Nucleation Activities: Implications for the Formation of Axonal Microtubules', *Journal of Neurochemistry*, 61(3), pp. 997–1005. doi: 10.1111/j.1471-4159.1993.tb03613.x.

Brännvall, K. *et al.* (2007) 'Enhanced neuronal differentiation in a three-dimensional collagen-hyaluronan matrix', *Journal of Neuroscience Research*, 85(2007), pp. 2138–2146. doi: 10.1002/jnr.21358.

Brooker, G. J. *et al.* (2000) 'Endogenous IGF-1 regulates the neuronal differentiation of adult stem cells.', *Journal of neuroscience research*, 59(3), pp. 332–341. doi: 10.1002/(SICI)1097-4547(20000201)59:3<332::AID-JNR6>3.0.CO;2-2.

Brunkan, A. L. *et al.* (2005) 'Presenilin endoproteolysis is an intramolecular cleavage', *Molecular and Cellular Neuroscience*, 29(1), pp. 65–73. doi: 10.1016/j.mcn.2004.12.012.

Buée, L. *et al.* (2000) 'Tau protein isoforms, phosphorylation and role in neurodegenerative disorders', *Brain Research Reviews*, 33(1), pp. 95–130. doi: 10.1016/S0165-0173(00)00019-9.

Burrows, C. K. *et al.* (2016) 'Genetic Variation, Not Cell Type of Origin, Underlies the Majority of Identifiable Regulatory Differences in iPSCs', *PLoS Genetics*, 12(1), pp. 1–18. doi:

10.1371/journal.pgen.1005793.

Butner, K. A. and Kirschner, M. W. (1991) 'Tau protein binds to microtubules through a flexible array of distributed weak sites', *Journal of Cell Biology*, 115(3 I), pp. 717–730. doi: 10.1083/jcb.115.3.717.

Caceres, A., Kosik, K. and S. (1990) 'Inhibition of neurite polarity by tau antisense oligonucleotides in primary cerebellar neurons', *Nature*, 343(6257), pp. 461–463. doi: 10.1038/343461a0.

Caceres, A., Potrebic, S. and Kosik, K. S. (1991) 'The effect of tau antisense oligonucleotides on neurite formation of cultured cerebellar macroneurons.', *The Journal of neuroscience*, 11(6), pp. 1515–1523. doi: 10.1523/jneurosci.5392-05.2006.

Camp, J. G. *et al.* (2015) 'Human cerebral organoids recapitulate gene expression programs of fetal neocortex development', *Proceedings of the National Academy of Sciences of the United States of America*, 112(51), pp. 15672–15677. doi: 10.1073/pnas.1520760112.

Campion, D. *et al.* (1999) 'Early-onset autosomal dominant Alzheimer disease: Prevalence, genetic heterogeneity, and mutation spectrum', *American Journal of Human Genetics*, 65(3), pp. 664–670. doi: 10.1086/302553.

Campos, P. B., Paulsen, B. S. and Rehen, S. K. (2014) 'Accelerating neuronal aging in in vitro model brain disorders: A focus on reactive oxygen species', *Frontiers in Aging Neuroscience*, 6(OCT), pp. 1–10. doi: 10.3389/fnagi.2014.00292.

Cao, Y. *et al.* (2003) 'Insulin-Like Growth Factor (IGF)-1 Suppresses Oligodendrocyte Caspase-3 Activation and Increases Glial Proliferation after Ischemia in Near-Term Fetal Sheep', *Journal of Cerebral Blood Flow & Metabolism*, 23(6), pp. 739–747. doi: 10.1097/01.WCB.0000067720.12805.6F.

Carolindah, M. N. *et al.* (2013) 'An Overview of in Vitro Research Models for Alzheimer'S Disease (Ad)', *Regenerative Research*, 2(2), pp. 8–13.

Carrillo, M. C., Sanders, C. A. and Katz, R. G. (2009) 'Maximizing the Alzheimer's Disease

Neuroimaging Initiative II', *Alzheimer's and Dementia*, 5(3), pp. 271–275. doi: 10.1016/j.jalz.2009.02.005.

Carson, M. J. *et al.* (1993) 'Insulin-like growth factor I increases brain growth and central nervous system myelination in transgenic mice.', *Neuron*, 10(4), pp. 729–40. doi: 10.1016/0896-6273(93)90173-O.

Carter, D. B. *et al.* (2008) 'Changes in γ-secretase activity and specificity caused by the introduction of consensus aspartyl protease active motif in Presenilin 1', *Molecular Neurodegeneration*, 3(6). doi: 10.1186/1750-1326-3-6.

Castellani, R. J. *et al.* (2008) 'Phosphorylated tau: Toxic, protective, or none of the above', *Journal of Alzheimer's Disease*, 14(4), pp. 377–383. doi: 10.3233/JAD-2008-14404.

Chae, T. *et al.* (1997) 'Mice lacking p35, a neuronal specific activator of Cdk5, display cortical lamination defects, seizures, and adult lethality', *Neuron*, 18(1), pp. 29–42. doi: 10.1016/S0896-6273(01)80044-1.

Chambers, J. K. *et al.* (2015) 'The domestic cat as a natural animal model of Alzheimer's disease', *Acta neuropathologica communications*, 3(78), pp. 1–14. doi: 10.1186/s40478-015-0258-3.

Chambers, S. M. *et al.* (2009) 'Highly efficient neural conversion of human ES and iPS cells by dual inhibition of SMAD signaling', *Nature Biotechnology*, 27(3), pp. 275–280. doi: 10.1038/nbt.1529.

Chambers, S. M., Tchieu, J. and Studer, L. (2013) 'Build-a-brain', *Cell Stem Cell*. doi: 10.1016/j.stem.2013.09.010.

Chambon, P. (1996) 'A decade of molecular biology of retinoic acid receptors', *FASEB Journal*, 10, pp. 940–54. doi: 10, 940–954.

Chartier-Harlin, M. C. *et al.* (1994) 'Apolipoprotein E, epsilon 4 allele as a major risk factor for sporadic early and late-onset forms of Alzheimer's disease: analysis of the 19q13.2 chromosomal

region.', *Human molecular genetics*, 3(4), pp. 569–574. doi: 10.1093/hmg/3.4.569.

Chen, Y. *et al.* (2006) 'Agonist and antagonist of retinoic acid receptors cause similar changes in gene expression and induce senescence-like growth arrest in MCF-7 breast carcinoma cells', *Cancer Research*, 66(17), pp. 8749–8761. doi: 10.1158/0008-5472.CAN-06-0581.

Cheng, C. M. *et al.* (2001) 'Endogenous IGF1 enhances cell survival in the postnatal dentate gyrus', *Journal of Neuroscience Research*, 64(4), pp. 341–347. doi: 10.1002/jnr.1084.

Cheng, T. Y. *et al.* (2013) 'Neural stem cells encapsulated in a functionalized self-assembling peptide hydrogel for brain tissue engineering', *Biomaterials*, 34(8), pp. 2005–2016. doi: 10.1016/j.biomaterials.2012.11.043.

Choi, S. H. *et al.* (2014a) 'A three-dimensional human neural cell culture model of Alzheimer's disease', *Nature*, 515(7526), pp. 274–278. doi: 10.1038/nature13800.

Choi, S. H. *et al.* (2014b) 'A three-dimensional human neural cell culture model of Alzheimer's disease', *Nature*, 515(7526), pp. 274–278. doi: 10.1038/nature13800.

Choi, S. H. *et al.* (2014c) 'A three-dimensional human neural cell culture model of Alzheimer's disease', *Nature*. Nature Publishing Group, 515(7526), pp. 274–278. doi: 10.1038/nature13800.

Chowdhury, F. *et al.* (2010) 'Soft substrates promote homogeneous self-renewal of embryonic stem cells via downregulating cell-matrix tractions', *PLoS ONE*, 5(12), p. e15655. doi: 10.1371/journal.pone.0015655.

Chung, K. *et al.* (2013) 'Structural and molecular interrogation of intact biological systems', *Nature*, 497(7449), pp. 332–337. doi: 10.1038/nature12107.

Citron, M. *et al.* (1997) 'Mutant presenilins of Alzheimer's disease increase production of 42-residue amyloid beta-protein in both transfected cells and transgenic mice', *Nature Medicine*, 3(1), pp. 67–72. doi: 10.1038/nm0798-822.

Clark, R. F. *et al.* (1995) 'The structure of the presenilin 1 (S182) gene and identification of six novel mutations in early onset AD families', *Nature Genetics*, 11(2), pp. 219–22. doi: 10.1038/ng1095-219.

Clarris, H. J. *et al.* (1995) 'Expression of the amyloid protein precursor of Alzheimer's disease in the developing rat olfactory system.', *Brain research. Developmental brain research*, 88(1), pp. 87–95.

Clavaguera, F. *et al.* (2009) 'Transmission and spreading of tauopathy in transgenic mouse brain', *Nature Cell Biology*, 11(7), pp. 909–913. doi: 10.1038/ncb1901.

Cleveland, D. W., Hwo, S. Y. and Kirschner, M. W. (1977) 'Physical and chemical properties of purified tau factor and the role of tau in microtubule assembly', *Journal of Molecular Biology*, 116(2), pp. 227–247. doi: 10.1016/0022-2836(77)90214-5.

Condic, M. L. (2013) 'Totipotency: What it is and what it is not', *Stem Cells and Development*, 23(8), pp. 796–812. doi: 10.1089/scd.2013.0364.

Cong, L. *et al.* (2013) 'Cong, L., Ran, F. A., Cox, D., Lin, S., Barretto, R., Habib, N., … Zhang, F. (2013). Multiplex Genome Engineering Using CRISPR/Cas Systems. Science (New York, N.Y.)', *Science (New York, N.Y.)*, 339(6121), pp. 819–823. doi: 10.1126/science.1231143.Multiplex.

Corder, E. H. *et al.* (1993) 'Gene dose of apolipoprotein E type 4 allele and the risk of Alzheimer's disease in late onset families', *Science*, 261(5123), pp. 921–3. doi: 10.1126/science.8346443.

Cowan, C. M. *et al.* (2015) 'Rescue from tau-induced neuronal dysfunction produces insoluble tau oligomers', *Scientific Reports*. doi: 10.1038/srep17191.

Crowe, D. L., Kim, R. and Chandraratna, R. A. S. (2003) 'Retinoic acid differentially regulates cancer cell proliferation via dose-dependent modulation of the mitogen-activated protein kinase pathway', *Molecular Cancer Research*, 1(7), pp. 532–540.

Cruts, M., Theuns, J. and Van Broeckhoven, C. (2012) 'Locus-specific mutation databases for neurodegenerative brain diseases', *Human Mutation*, 33(9), pp. 1340–1344. doi:

10.1002/humu.22117.

Damianich, A. *et al.* (2018) 'Modulation of Tau Isoforms Imbalance Precludes Tau Pathology and Cognitive Decline in a Mouse Model of Tauopathy Report Modulation of Tau Isoforms Imbalance Precludes Tau Pathology and Cognitive Decline in a Mouse Model of Tauopathy', *Cell Reports*, 23(3), pp. 709–715. doi: 10.1016/j.celrep.2018.03.079.

Das, A. K. and Pal, R. (2010) 'Induced pluripotent stem cells (iPSCs): The emergence of a new champion in stem cell technology-driven biomedical applications', *Journal of Tissue Engineering and Regenerative Medicine*, pp. 413–421. doi: 10.1002/term.258.

Davies, P. *et al.* (1988) 'Neurofibrillary tangles and senile plaques in aged bears', *Journal of Neuropathology and Experimental Neurology*, 47(6), pp. 629–41. doi: 10.1097/00005072-198811000-00006.

Dayanandan, R. *et al.* (1999) 'Mutations in tau reduce its microtubule binding properties in intact cells and affect its phosphorylation', *FEBS Letters*, 446(2–3), pp. 228–232. doi: 10.1016/S0014-5793(99)00222-7.

Deacon, R. *et al.* (2015) 'Natural AD-Like Neuropathology in Octodon degus: Impaired Burrowing and Neuroinflammation', *Current Alzheimer Research*, 12(4), pp. 314–22. doi: 10.2174/1567205012666150324181652.

Dehmelt, L. and Halpain, S. (2004) 'Protein family review The MAP2 / Tau family of microtubule-associated proteins', *Genome Biology*, 6(1), pp. 1–10.

Dehmelt, L. and Halpain, S. (2005) 'The MAP2/Tau family of microtubule-associated proteins', *Genome Biology*. doi: 10.1186/gb-2004-6-1-204.

Dekkers, J. F. *et al.* (2019) 'High-resolution 3D imaging of fixed and cleared organoids', *Nature Protocols*, 14(6), pp. 1756–1771. doi: 10.1038/s41596-019-0160-8.

Delva, L. *et al.* (1999) 'Physical and Functional Interactions between Cellular Retinoic Acid Binding Protein II and the Retinoic Acid-Dependent Nuclear Complex', *Molecular and Cellular Biology*, 19(10), pp. 7158–7167. doi: 10.1128/mcb.19.10.7158.

DeMattos, R. B. *et al.* (2004) 'ApoE and Clusterin Cooperatively Suppress Aβ Levels and Deposition: Evidence that ApoE Regulates Extracellular Aβ Metabolism In Vivo', *Neuron*, 41(2), pp. 193–202. doi: 10.1016/S0896-6273(03)00850-X.

Deshpande, A. *et al.* (2006) 'Different Conformations of Amyloid β Induce Neurotoxicity by Distinct Mechanisms in Human Cortical Neurons', *The Journal of Neuroscience*, 26(22), pp. 6011–6018. doi: 10.1523/JNEUROSCI.1189-06.2006.

Dewachter, I. *et al.* (2000) 'Aging increased amyloid peptide and caused amyloid plaques in brain of old APP/V717I transgenic mice by a different mechanism than mutant presenilin1.', *The Journal of neuroscience : the official journal of the Society for Neuroscience*, 20(17), pp. 6452–6458. doi: 20/17/6452 [pii].

Dhara, S. and Stice, S. (2008) 'Neural differentiation of human embryonic stem cells', *Journal of cellular biochemistry*, 105(3), pp. 633–640. doi: 10.1002/jcb.21891.Neural.

Dingle, Y. T. L. *et al.* (2015) 'Three-Dimensional Neural Spheroid Culture: An In Vitro Model for Cortical Studies', *Tissue Engineering - Part C: Methods*, 21(12), pp. 1274–1283. doi: 10.1089/ten.tec.2015.0135.

DiTella, M. C. *et al.* (1996) 'MAP-1B/TAU functional redundancy during laminin-enhanced axonal growth', *Journal of Cell Science*, 109(2), pp. 467–477.

Dityatev, A. and Schachner, M. (2003) 'Extracellular matrix molecules and synaptic plasticity', *Nature Reviews Neuroscience*, 4(6), pp. 456–468. doi: 10.1038/nrn1115.

Doody, R. S. *et al.* (2013) 'A phase 3 trial of semagacestat for treatment of Alzheimer's disease.', *The New England journal of medicine*, 369(4), pp. 341–50. doi: 10.1056/NEJMoa1210951.

Doody, R. S. *et al.* (2014) 'Phase 3 trials of solanezumab for mild-to-moderate Alzheimer's disease.', *The New England journal of medicine*, 370(4), pp. 311–21. doi: 10.1056/NEJMoa1312889.

Dottori, M. and Pera, M. F. (2008) 'Neural differentiation of human embryonic stem cells.', *Methods in molecular biology*, 438, pp. 19–30. doi: 10.1007/978-1-59745-133-8_3.

Down, J. (1866) 'Observations on an ethnic classification of idiots', *Heredity*, 21(4), pp. 695–697. doi: 10.1038/hdy.1966.69.

Dragunow, M. (2008) 'The adult human brain in preclinical drug development', *Nat Rev Drug Discov*, 7(8), pp. 659–666. doi: nrd2617 [pii]\r10.1038/nrd2617.

Drechsel, D. N. *et al.* (1992) 'Modulation of the dynamic instability of tubulin assembly by the microtubule-associated protein tau.', *Molecular Biology of the Cell*, 3(10), pp. 1141–1154. doi: 10.1091/mbc.3.10.1141.

Drewes, G. *et al.* (1995) 'Microtubule-associated protein/microtubule affinity-regulating kinase (p110(mark)). A novel protein kinase that regulates tau-microtubule interactions and dynamic instability by phosphorylation at the Alzheimer- specific site serine 262', *Journal of Biological Chemistry*, pp. 7679–7688. doi: 10.1074/jbc.270.13.7679.

Drubin, D. G. and Kirschner, M. W. (1986) 'Tau protein function in living cells.', *Journal of Cell Biology*, 103(6 Pt 2), pp. 2739–2746.

Drukker, M. *et al.* (2006) 'Human Embryonic Stem Cells and Their Differentiated Derivatives Are Less Susceptible to Immune Rejection Than Adult Cells', *Stem Cells*, 24(2), pp. 221–229. doi: 10.1634/stemcells.2005-0188.

Du, H. *et al.* (2018) 'Advances in CLARITY-based tissue clearing and imaging', *Experimental and Therapeutic Medicine*, 16(3), pp. 1567–1576. doi: 10.3892/etm.2018.6374.

Duara, R. *et al.* (1993) 'A comparison of familial and sporadic alzheimer's disease', *Neurology*, 43(7),

pp. 1377–1384. doi: 10.1212/wnl.43.7.1377.

Duff, K. *et al.* (1996) 'Increased amyloid-beta42(43) in brains of mice expressing mutant presenilin 1.', *Nature*, 383(6602), pp. 710–3. doi: 10.1038/383710a0.

van Duijn, C. M. *et al.* (1991) 'Familial aggregation of Alzheimer's disease and related disorders: a collaborative re-analysis of case-control studies', *Int J Epidemiol*, 20 Suppl 2(2), pp. S13-20.

Dyrks, T. *et al.* (1993) 'Amyloidogenicity of rodent and human beta A4 sequences.', *FEBS letters*, 324(2), pp. 231–236. doi: 10.1016/0014-5793(93)81399-K.

E.Head *et al.* (2012) 'Alzheimer's disease in Down's syndrome.', *European journal of neurodegenerative disease*, 1(3), pp. 353–364.

Eiraku, M. *et al.* (2008) 'Self-Organized Formation of Polarized Cortical Tissues from ESCs and Its Active Manipulation by Extrinsic Signals', *Cell Stem Cell*, 3(5), pp. 519–532. doi: 10.1016/j.stem.2008.09.002.

El-Agnaf, O. M. *et al.* (2000) 'Oligomerization and toxicity of beta-amyloid-42 implicated in Alzheimer's disease.', *Biochemical and biophysical research communications*, 273(3), pp. 1003–7. doi: 10.1006/bbrc.2000.3051.

Eldar-Finkelman, H. and Martinez, A. (2011) 'GSK-3 Inhibitors: Preclinical and Clinical Focus on CNS', *Frontiers in Molecular Neuroscience*, 4(32). doi: 10.3389/fnmol.2011.00032.

Ellis, W. G., McCulloch, J. R. and Corley, C. L. (1974) 'Presenile dementia in Down's syndrome. Ultrastructural identity with Alzheimer's disease', *Neurology*, 24(2), pp. 101–106.

Eng, L. F. *et al.* (1971) 'An acidic protein isolated from fibrous astrocytes', *Brain Research*, 28(2), pp. 351–354. doi: 10.1016/0006-8993(71)90668-8.

Eng, L. F., Ghirnikar, R. S. and Lee, Y. L. (2000) 'Glial Fibrillary Acidic Protein : GFAP-Thirty-One Years (1969-2000)', *Neurochemical Research*, 25(9–10), pp. 1439–1451. doi: 10.1023/A:1007677003387.

Ercan, E. *et al.* (2017) 'A validated antibody panel for the characterization of tau post-translational modifications', *Molecular Neurodegeneration*, 12(1). doi: 10.1186/s13024-017-0229-1.

Espuny-Camacho, I. *et al.* (2017) 'Hallmarks of Alzheimer's Disease in Stem-Cell-Derived Human Neurons Transplanted into Mouse Brain', *Neuron*. Elsevier Inc., 0(0), pp. 1066-1081.e8. doi: 10.1016/j.neuron.2017.02.001.

Evans, M. J. and Kaufman, M. H. (1981) 'Establishment in culture of pluripotential cells from mouse embryos', *Nature*, 292(5819), pp. 154–156. doi: 10.1038/292154a0.

Eves, E. M. *et al.* (1992) 'Immortal rat hippocampal cell lines exhibit neuronal and glial lineages and neurotrophin gene expression.', *Proceedings of the National Academy of Sciences*, 89(10), pp. 4373–4377. doi: 10.1073/pnas.89.10.4373.

Farrer, L. A. *et al.* (1995) 'Apolipoprotein E genotype in patients with alzheimer's disease: Implications for the risk of dementia among relatives', *Annals of Neurology*, 38(5), pp. 797–808. doi: 10.1002/ana.410380515.

Farrer, L. A. *et al.* (1997) 'Effects of age, sex, and ethnicity on the association between apolipoprotein E genotype and Alzheimer disease: A meta-analysis', *Journal of the American Medical Association*, 278(16), pp. 1349–56. doi: 10.1001/jama.1997.03550160069041.

Fernandez, A. M. and Torres-Alemán, I. (2012) 'The many faces of insulin-like peptide signalling in the brain', *Nature Reviews Neuroscience*, pp. 225–239. doi: 10.1038/nrn3209.

Fraichard, A. *et al.* (1995) 'In vitro differentiation of embryonic stem cells into glial cells and functional neurons', *Journal of Cell Science*, 108(10), pp. 3181–3188.

Francis, R. *et al.* (2002) 'aph-1 and pen-2 are required for Notch pathway signaling, γ-secretase cleavage of βAPP, and presenilin protein accumulation', *Developmental Cell*, 3(1), pp. 85–97. doi: 10.1016/S1534-5807(02)00189-2.

Frost, B., Jacks, R. L. and Diamond, M. I. (2009) 'Propagation of Tau misfolding from the outside to the inside of a cell', *Journal of Biological Chemistry*, 284(19), pp. 12845–12852. doi: 10.1074/jbc.M808759200.

G.Allen (1974) 'Aetiology of Down's Syndrome inferred by Waardenburg in 1932', *Nature*, 250(2), pp. 436–437.

Gajović, S. *et al.* (1998) 'Retinoic acid mediates Pax6 expression during in vitro differentiation of embryonic stem cells', *Differentiation*, 62(4), pp. 187–192. doi: 10.1007/s002580050217.

Games, D. *et al.* (1995) 'Alzheimer-type neuropathology in transgenic mice overexpressing V717F beta-amyloid precursor protein.', *Nature*, 373(6514), pp. 523–7. doi: 10.1038/373523a0.

Gao, S. *et al.* (1998) 'The Relationships Between Age, Sex, and the Incidence of Dementia and Alzheimer Disease: A Meta-Analysis', *Archives of general psychiatry*, 55(9), pp. 809–815. doi: http://dx.doi.org/10.1001/archpsyc.55.9.809.

Gearing, M. *et al.* (1997) 'β-Amyloid (Aβ) deposition in the brains of aged orangutans', *Neurobiology of Aging*, 18(2), pp. 139–146. doi: 10.1016/S0197-4580(97)00012-2.

Georges, P. C. *et al.* (2006) 'Matrices with compliance comparable to that of brain tissue select neuronal over glial growth in mixed cortical cultures', *Biophysical Journal*. Elsevier, 90(8), pp. 3012–3018. doi: 10.1529/biophysj.105.073114.

Gerardo, H. *et al.* (2019) 'Soft culture substrates favor stem-like cellular phenotype and facilitate reprogramming of human mesenchymal stem/stromal cells (hMSCs) through mechanotransduction', *Scientific Reports*, 9(1), pp. 1–18. doi: 10.1038/s41598-019-45352-3.

Gerrard, L., Rodgers, L. and Cui, W. (2005) 'Differentiation of Human Embryonic Stem Cells to Neural Lineages in Adherent Culture by Blocking Bone Morphogenetic Protein Signaling', *Stem Cells*, 23(9), pp. 1234–1241. doi: 10.1634/stemcells.2005-0110.

Gilmore, E. C. *et al.* (1998) 'Cyclin-dependent kinase 5-deficient mice demonstrate novel developmental arrest in cerebral cortex', *Journal of Neuroscience*, 18(16), pp. 6370–7. doi: 10.1523/jneurosci.18-16-06370.1998.

Ginty, D. D., Bonni, A. and Greenberg, M. E. (1994) 'Nerve growth factor activates a Ras-dependent protein kinase that stimulates c-fos transcription via phosphorylation of CREB', *Cell*, 77(5), pp. 713–725. doi: 10.1016/0092-8674(94)90055-8.

Glasson, E. J. *et al.* (2002) 'The changing survival profile of people with Down's syndrome: Implications for genetic counselling', *Clinical Genetics*, 62(5), pp. 390–3. doi: 10.1034/j.1399-0004.2002.620506.x.

Glenner, G. G. (1983) 'Alzheimer's disease. The commonest form of amyloidosis', *Archives of Pathology and Laboratory Medicine*, 107(6), pp. 281–282.

Glenner, G G and Wong, C. W. (1984) 'Alzheimer's disease: Initial report of the purification and characterization of a novel cerebrovascular amyloid protein', *Biochem Biophys Res Communications*, 120(3), pp. 885–890. doi: S0006-291X(84)80190-4 [pii].

Glenner, George G. and Wong, C. W. (1984) 'Alzheimer's disease and Down's syndrome: Sharing of a unique cerebrovascular amyloid fibril protein', *Biochemical and Biophysical Research Communications*, 122(3), pp. 1131–1135. doi: 10.1016/0006-291X(84)91209-9.

Goate, A. *et al.* (1991) 'Segregation of a missense mutation in the amyloid precursor protein gene with familial Alzheimer's disease', *Nature*, 349(6311), pp. 704–706. doi: 10.1038/349704a0.

Goedert, M. *et al.* (1989a) 'Multiple isoforms of human microtubule-associated protein tau: sequences and localization in neurofibrillary tangles of Alzheimer's disease', *Neuron*, 3(4), pp. 519–526. doi: 10.1016/0896-6273(89)90210-9.

Goedert, M. *et al.* (1989b) 'Multiple isoforms of human microtubule-associated protein tau: sequences and localization in neurofibrillary tangles of Alzheimer's disease', *Neuron*, 3(4), pp. 519–

526. doi: 10.1016/0896-6273(89)90210-9.

Goedert, M., Crowther, R. A. and Garner, C. C. (1991) 'Molecular characterization of microtubule-associated proteins tau and map2', *Trends in Neurosciences*, 14(5), pp. 193–199. doi: 10.1016/0166-2236(91)90105-4.

Goedert, Michel and Jakes, R. (1990) 'Expression of separate isoforms of human tau protein: correlation with the tau pattern in brain and effects on tubulin polymerization.', *The EMBO journal*, 9(13), pp. 4225–4230.

Goedert, M. and Jakes, R. (1990) 'Expression of separate isoforms of human tau protein: Correlation with the tau pattern in brain and effects on tubulin polymerization', *EMBO Journal*, 9(13), pp. 4225–4230. doi: 10.1002/j.1460-2075.1990.tb07870.x.

Goedert, M. and Spillantini, M. G. (2017) 'Propagation of Tau aggregates Tim Bliss', *Molecular Brain*. Molecular Brain, 10(1), pp. 1–9. doi: 10.1186/s13041-017-0298-7.

Gomez-Nicola, D. and Boche, D. (2015) 'Post-mortem analysis of neuroinflammatory changes in human Alzheimer's disease', *Alzheimer's Research and Therapy*, 7(42). doi: 10.1186/s13195-015-0126-1.

Gonzalez, C. *et al.* (2018) 'Modeling amyloid beta and tau pathology in human cerebral organoids', *Molecular Psychiatry*, 23(12), pp. 2363–2374. doi: 10.1038/s41380-018-0229-8.

Gottlieb, D. I. and Huettner, J. E. (1999) 'An in vitro pathway from embryonic stem cells to neurons and glia', *Cells Tissues Organs*, 165(3–4), pp. 165–172. doi: 10.1159/000016696.

Goutte, C. *et al.* (2002) 'APH-1 is a multipass membrane protein essential for the Notch signaling pathway in Caenorhabditis elegans embryos', *Proceedings of the National Academy of Sciences of the United States of America*, 99(2), pp. 775–9. doi: 10.1073/pnas.022523499.

Granholm, a C. *et al.* (2000) 'Glial cell line-derived neurotrophic factor is essential for postnatal

survival of midbrain dopamine neurons.', *The Journal of neuroscience : the official journal of the Society for Neuroscience*, 20(9), pp. 3182–90.

Green, R. C. *et al.* (2009) 'Effect of tarenflurbil on cognitive decline and activities of daily living in patients with mild Alzheimer disease: a randomized controlled trial.', *JAMA*, 302(23), pp. 2557–64. doi: 10.1001/jama.2009.1866.

Grundke-Iqbal, I. *et al.* (1986) 'Microtubule-associated protein tau. A component of Alzheimer paired helical filaments.', *The Journal of biological chemistry*, 261(13), pp. 6084–9. doi: 10.1074/jbc.M111.271320.

Grundke-Iqbal, I. *et al.* (1987) 'Abnormal phosphorylation of the microtubule-associated protein? (tau) in Alzheimer cytoskeletal pathology', *Alzheimer Disease & Associated Disorders*, 1(3), p. 202. doi: 10.1097/00002093-198701030-00020.

Grupe, A. *et al.* (2007) 'Evidence for novel susceptibility genes for late-onset Alzheimer's disease from a genome-wide association study of putative functional variants', *Human Molecular Genetics*, 16(8), pp. 865–73. doi: 10.1093/hmg/ddm031.

Gunn-Moore, D. *et al.* (2018) 'Alzheimer's disease in humans and other animals: A consequence of postreproductive life span and longevity rather than aging', *Alzheimer's and Dementia*, 14(2), pp. 195–204. doi: 10.1016/j.jalz.2017.08.014.

Guo, Q. *et al.* (1996) 'Alzheimer's PS-1 mutation perturbs calcium homeostasis and sensitizes PC12 cells to death induced by amyloid beta-peptide.', *Neuroreport*, 8(1), pp. 379–83. doi: 10.1097/00001756-199612200-00074.

Haass, C. and Selkoe, D. J. (2007) 'Soluble protein oligomers in neurodegeneration: Lessons from the Alzheimer's amyloid β-peptide', *Nature Reviews Molecular Cell Biology*, 8(2), pp. 101–112. doi: 10.1038/nrm2101.

Hagestedt, T. *et al.* (1989) 'Tau protein becomes long and stiff upon phosphorylation: Correlation

between paracrystalline structure and degree of dephosphorylation', *Journal of Cell Biology*, 109(4 I), pp. 1643–1651. doi: 10.1083/jcb.109.4.1643.

Hall, A. M. and Roberson, E. D. (2012a) 'Mouse models of Alzheimer's disease', *Brain Research Bulletin*. Elsevier Inc., 88(1), pp. 3–12. doi: 10.1016/j.brainresbull.2011.11.017.

Hall, A. M. and Roberson, E. D. (2012b) 'Mouse models of Alzheimer's disease', *Brain Research Bulletin*, 88(1), pp. 3–12. doi: 10.1016/j.brainresbull.2011.11.017.

Hanes, J. *et al.* (2009) 'Rat tau proteome consists of six tau isoforms: Implication for animal models of human tauopathies', *Journal of Neurochemistry*, 108(2009), pp. 1167–1176. doi: 10.1111/j.1471-4159.2009.05869.x.

Hanger, D. P. *et al.* (1992) 'Glycogen synthase kinase-3 induces Alzheimer's disease-like phosphorylation of tau: Generation of paired helical filament epitopes and neuronal localisation of the kinase', *Neuroscience Letters*, 147(1), pp. 48–62. doi: 10.1016/0304-3940(92)90774-2.

Hanger, D. P., Anderton, B. H. and Noble, W. (2009) 'Tau phosphorylation: the therapeutic challenge for neurodegenerative disease', *Trends in Molecular Medicine*, 15(3), pp. 112–119. doi: 10.1016/j.molmed.2009.01.003.

Harada, A. *et al.* (1994) 'Altered microtubule organization in small-calibre axons of mice lacking tau protein', *Nature*, 369(6480), pp. 488–491. doi: 10.1038/369488a0.

Hardy, J. (2009) 'The amyloid hypothesis for Alzheimer's disease: A critical reappraisal', *Journal of Neurochemistry*, pp. 1129–1134. doi: 10.1111/j.1471-4159.2009.06181.x.

Hardy, J. A. and Higgins, G. A. (1992) 'Alzheimer's disease: The amyloid cascade hypothesis', *Science*, 256(5054), pp. 184–185. doi: 10.1126/science.1566067.

Hardy, J. and Allsop, D. (1991) 'Amyloid Deposition As the Central Event in the Etiology of Alzheimers-Disease', *Trends in Pharmacological Sciences*, 12(10), pp. 383–388. doi: 10.1016/0165-

6147(91)90609-v.

Hardy, J. and Selkoe, D. J. (2002) 'The amyloid hypothesis of Alzheimer's disease: Progress and problems on the road to therapeutics', *Science*, 297(5580), pp. 353–356. doi: 10.1126/science.1072994.

Harold, D. *et al.* (2009) 'Genome-wide association study identifies variants at CLU and PICALM associated with Alzheimer's disease', *Nature Genetics*, 41(10), pp. 1088–93. doi: 10.1038/ng.440.

Hartfuss, E. *et al.* (2001) 'Characterization of CNS precursor subtypes and radial glia', *Developmental Biology*, 229(1), pp. 15–30. doi: 10.1006/dbio.2000.9962.

Härtig, W. *et al.* (2000) 'Abnormally phosphorylated protein tau in the cortex of aged individuals of various mammalian orders', *Acta Neuropathologica*, 100(3), pp. 305–12. doi: 10.1007/s004010000183.

Hasegawa, M. (2016) 'Molecular mechanisms in the pathogenesis of alzheimer's disease and Tauopathies-Prion-Like seeded aggregation and phosphorylation', *Biomolecules*, 6(2), p. 24. doi: 10.3390/biom6020024.

Heilig, E. A. *et al.* (2010) 'A presenilin-1 mutation identified in familial Alzheimer disease with cotton wool plaques causes a nearly complete loss of γ-secretase activity', *Journal of Biological Chemistry*, 285(29), pp. 22350–9. doi: 10.1074/jbc.M110.116962.

Henderson, C. *et al.* (1994) 'GDNF: a potent survival factor for motoneurons present in peripheral nerve and muscle', *Science*, 266(5187), pp. 1062–1064. doi: 10.1126/science.7973664.

Hernández, F. *et al.* (2020) 'Differences Between Human and Murine Tau at the N-terminal End', *Frontiers in Aging Neuroscience*, 20(11), pp. 1–11. doi: 10.3389/fnagi.2020.00011.

Herreman, A. *et al.* (1999) 'Presenilin 2 deficiency causes a mild pulmonary phenotype and no changes in amyloid precursor protein processing but enhances the embryonic lethal phenotype of

presenilin 1 deficiency', *Proceedings of the National Academy of Sciences*, 96(21), pp. 11872–11877. doi: 10.1073/pnas.96.21.11872.

Herrera, F. *et al.* (2009) 'Synaptojanin-1 plays a key role in astrogliogenesis: Possible relevance for Down's syndrome', *Cell Death and Differentiation*, 16(6), pp. 910–920. doi: 10.1038/cdd.2009.24.

Herrera, F., Chen, Q. and Schubert, D. (2010) 'Synergistic effect of retinoic acid and cytokines on the regulation of glial fibrillary acidic protein expression', *Journal of Biological Chemistry*, 285(50), pp. 38915–38922. doi: 10.1074/jbc.M110.170274.

Herzog, E. *et al.* (2004) 'Expression of vesicular glutamate transporters, VGLUT1 and VGLUT2, in cholinergic spinal motoneurons', *European Journal of Neuroscience*, 20(7), pp. 1752–1760. doi: 10.1111/j.1460-9568.2004.03628.x.

Hesse, C. *et al.* (2001) 'Transient increase in total tau but not phospho-tau in human cerebrospinal fluid after acute stroke', *Neuroscience Letters*, 297(3), pp. 187–190. doi: 10.1016/S0304-3940(00)01697-9.

Hodge, R. D., D'Ercole, A. J. and O'Kusky, J. R. (2007) 'Insulin-like growth factor-I (IGF-I) inhibits neuronal apoptosis in the developing cerebral cortex in vivo.', *International journal of developmental neuroscience : the official journal of the International Society for Developmental Neuroscience*, 25(4), pp. 233–41. doi: 10.1016/j.ijdevneu.2007.03.004.

Holcomb, L. *et al.* (1998) 'Accelerated Alzheimer-type phenotype in transgenic mice carrying both mutant amyloid precursor protein and presenilin 1 transgenes', *Nature Medicine*, 4(1), pp. 97–100. doi: 10.1038/nm0198-097.

Honda, M. *et al.* (2016) 'The modeling of Alzheimer's disease by the overexpression of mutant Presenilin 1 in human embryonic stem cells', *Biochemical and Biophysical Research Communications*. Elsevier Ltd, 469(3), pp. 587–592. doi: 10.1016/j.bbrc.2015.12.025.

Horvitz, H. R. and Herskowitz, I. (1992) 'Mechanisms of asymmetric cell division: Two Bs or not two

Bs, that is the question', *Cell*, 68(2), pp. 237–55. doi: 10.1016/0092-8674(92)90468-R.

Hossini, A. M. *et al.* (2015) 'Induced pluripotent stem cell-derived neuronal cells from a sporadic Alzheimer's disease donor as a model for investigating AD-associated gene regulatory networks', *BMC Genomics*, 16(84). doi: 10.1186/s12864-015-1262-5.

Hsiao, K. *et al.* (1996) 'Amyloid Plaques in Transgenic Mice', *Science*, 274(October), pp. 7–10.

Hsieh, J. *et al.* (2004) 'IGF-I instructs multipotent adult neural progenitor cells to become oligodendrocytes', *Journal of Cell Biology*, 164(1), pp. 111–122. doi: 10.1083/jcb.200308101.

Hsiung, G.-Y. R., Sadovnick, A. D. and Feldman, H. (2004) 'Apolipoprotein E epsilon4 genotype as a risk factor for cognitive decline and dementia: data from the Canadian Study of Health and Aging.', *Canadian Medical Association journal*, 171(8), pp. 863–7. doi: 10.1503/cmaj.1031789.

Hu, B.-Y. *et al.* (2010) 'Neural differentiation of human induced pluripotent stem cells follows developmental principles but with variable potency', *Proceedings of the National Academy of Sciences*, 107(9), pp. 4335–4340. doi: 10.1073/pnas.0910012107.

Hu, K. (2014) 'Vectorology and factor delivery in induced pluripotent stem cell reprogramming', *Stem Cells and Development*, 23(12), pp. 1301–1315. doi: 10.1089/scd.2013.0621.

Hu, S. *et al.* (2009) 'GSK3 inhibitors show benefits in an Alzheimer's disease (AD) model of neurodegeneration but adverse effects in control animals', *Neurobiology of Disease*, 33(2), pp. 193–206. doi: 10.1016/j.nbd.2008.10.007.

Hüll, M. *et al.* (1998) 'Early-onset Alzheimer's disease due to mutations of the presenilin-1 gene on chromosome 14: A 7-year follow-up of a patient with a mutation at codon 139', *European Archives of Psychiatry and Clinical Neuroscience*, 248(3), pp. 123–129. doi: 10.1007/s004060050028.

Humbert, S., Dhavan, R. and Tsai, L. H. (2000) 'p39 activates cdk5 in neurons, and is associated with the actin cytoskeleton', *Journal of Cell Science*, 113(6), pp. 975–83.

Huttner, W. B. *et al.* (1983) 'Synapsin I (protein I), a nerve terminal-specific phosphoprotein. III. Its association with synaptic vesicles studied in a highly purified synaptic vesicle preparation', *Journal of Cell Biology*, 96(5), pp. 1374–1388. doi: 10.1083/jcb.96.5.1374.

Hutton, M. *et al.* (1996) 'Complete analysis of the presenilin 1 gene in early onset Alzheimer's disease', *NeuroReport*, 7(3), pp. 801–5. doi: 10.1097/00001756-199602290-00029.

Hutton, M. and Hardy, J. (1997) 'The presenilins and Alzheimer's disease', *Human Molecular Genetics*, 6(10), pp. 1639–1646. doi: 10.1093/hmg/6.10.1639.

Hyman, B. T. (2011) 'Amyloid-dependent and amyloid-independent stages of alzheimer disease', *Archives of Neurology*, 68(8), pp. 1062–1064. doi: 10.1001/archneurol.2011.70.

Iacono, D. *et al.* (2009) 'The Nun Study: Clinically silent AD, neuronal hypertrophy, and linguistic skills in early life', *Neurology*, 73(9), pp. 665–673. doi: 10.1212/WNL.0b013e3181b01077.

Inda, C. *et al.* (2017) 'CAMP-dependent cell differentiation triggered by activated CRHR1 in hippocampal neuronal cells', *Scientific Reports*, 7(1), pp. 1–17. doi: 10.1038/s41598-017-02021-7.

Ino, H. *et al.* (1994) 'Expression of CDK5 (PSSALRE kinase), a neural cdc2-related protein kinase, in the mature and developing mouse central and peripheral nervous systems', *Brain Research*, 661(1–2), pp. 196–206. doi: 10.1016/0006-8993(94)91197-5.

Ishiguro, K. *et al.* (1992) 'Tau protein kinase I converts normal tau protein into A68-like component of paired helical filaments', *Journal of Biological Chemistry*, 267(15), pp. 10897–10901.

Ishiguro, K. *et al.* (1993) 'Glycogen synthase kinase 3β is identical to tau protein kinase I generating several epitopes of paired helical filaments', *FEBS Letters*, 325(3), pp. 167–172. doi: 10.1016/0014-5793(93)81066-9.

Israel, M. A. *et al.* (2012) 'Probing sporadic and familial Alzheimer's disease using induced pluripotent stem cells', *Nature*, 482(7384), pp. 216–220. doi: 10.1038/nature10821.

Izant, J. G. and McIntosh, J. R. (1980) 'Microtubule-associated proteins: a monoclonal antibody to MAP2 binds to differentiated neurons.', *Proceedings of the National Academy of Sciences of the United States of America*, 77(8), pp. 4741–5. doi: 10.1073/pnas.77.8.4741.

Jacob, F. *et al.* (2020) 'Human Pluripotent Stem Cell-Derived Neural Cells and Brain Organoids Reveal SARS-CoV-2 Neurotropism Predominates in Choroid Plexus Epithelium', *Cell Stem Cell*, 27(6), pp. 937–950. doi: 10.1016/j.stem.2020.09.016.

Jakobsson, A. *et al.* (2017) 'Three-dimensional functional human neuronal networks in uncompressed low-density electrospun fiber scaffolds', *Nanomedicine: Nanotechnology, Biology, and Medicine*. The Authors, 13(4), pp. 1563–1573. doi: 10.1016/j.nano.2016.12.023.

Jämsä, A. *et al.* (2004) 'The retinoic acid and brain-derived neurotrophic factor differentiated SH-SY5Y cell line as a model for Alzheimer's disease-like tau phosphorylation', *Biochemical and Biophysical Research Communications*, 319(3), pp. 993–1000. doi: 10.1016/j.bbrc.2004.05.075.

Jang, Y. K. *et al.* (2004) 'Retinoic Acid-Mediated Induction of Neurons and Glial Cells from Human Umbilical Cord-Derived Hematopoietic Stem Cells', *Journal of Neuroscience Research*, 75(4), pp. 573–584. doi: 10.1002/jnr.10789.

Janke, C. *et al.* (1999) 'Phylogenetic diversity of the expression of the microtubule-associated protein tau: Implications for neurodegenerative disorders', *Molecular Brain Research*, 68(1–2), pp. 119–128. doi: 10.1016/S0169-328X(99)00079-0.

Jin, X. and Yamashita, T. (2016) 'Microglia in central nervous system repair after injury', *Journal of Biochemistry*, 159(5), pp. 491–6. doi: 10.1093/jb/mvw009.

Johnson, G. V. W. and Jope, R. S. (1992) 'The role of microtubule-associated protein 2 (MAP-2) in neuronal growth, plasticity, and degeneration', *Journal of Neuroscience Research*, pp. 505–512. doi: 10.1002/jnr.490330402.

Johnson, V. E., Stewart, W. and Smith, D. H. (2012) 'Widespread tau and amyloid-beta pathology

many years after a single traumatic brain injury in humans', *Brain Pathology*, 22(2), pp. 142–149. doi: 10.1111/j.1750-3639.2011.00513.x.

Joie, R. La *et al.* (2020) 'Prospective longitudinal atrophy in Alzheimer's disease correlates with the intensity and topography of baseline tau-PET', *Science Translational Medicine*, 12(524), pp. 1–13. doi: 10.1126/scitranslmed.aau5732.

Jorm, A. F. and Jolley, D. (1998) 'The incidence of dementia: A meta-analysis', *Neurology*, 51(3), pp. 728–733. doi: 10.1212/WNL.51.3.728.

Junying, Y. *et al.* (2009) 'Human induced pluripotent stem cells free of vector and transgene sequences', *Science*, 324(5928), pp. 797–801. doi: 10.1126/science.1172482.

Kadoshima, T. *et al.* (2013) 'Self-organization of axial polarity, inside-out layer pattern, and species-specific progenitor dynamics in human ES cell-derived neocortex', *Proceedings of the National Academy of Sciences*, 110(50), pp. 20284–20289. doi: 10.1073/pnas.1315710110.

Kanemaru, K. *et al.* (1992) 'Fetal-Type Phosphorylation of the τ in Paired Helical Filaments', *Journal of Neurochemistry*, 58(5), pp. 1667–1675. doi: 10.1111/j.1471-4159.1992.tb10039.x.

Kang, J. *et al.* (1987) 'The precursor of Alzheimer's disease amyloid A4 protein resembles a cell-surface receptor', *Nature*, 325(6106), pp. 733–736. doi: 10.1038/325733a0.

Kaufman, M. H. and Evans, M. J. (1981) 'Establishment in culture of pluripotential cells from mouse embryos', *Nature*, 292(July), pp. 154–156.

Kaufman, S. K. *et al.* (2016) 'Tau Prion Strains Dictate Patterns of Cell Pathology, Progression Rate, and Regional Vulnerability In Vivo', *Neuron*, 92(4), pp. 796–812. doi: 10.1016/j.neuron.2016.09.055.

Kempf, M. *et al.* (1996) 'Tau binds to the distal axon early in development of polarity in a microtubule- and microfilament-dependent manner.', *The Journal of neuroscience*, 16(18), pp. 5583–92. doi: 10.1097/00001756-199708180-00029.

Khatoon, S., Grundke-Iqbal, I. and Iqbal, K. (1992) 'Brain Levels of Microtubule-Associated Protein τ Are Elevated in Alzheimer's Disease: A Radioimmuno-Slot-Blot Assay for Nanograms of the Protein', *Journal of Neurochemistry*, 59(2), pp. 750–753. doi: 10.1111/j.1471-4159.1992.tb09432.x.

Kiatipattanasakul, W. *et al.* (2000) 'Abnormal neuronal and glial argyrophilic fibrillary structures in the brain of an aged albino cynomolgus monkey (Macaca fascicularis)', *Acta Neuropathologica*, 10(5), pp. 580–6. doi: 10.1007/s004010000215.

Kilpinen, H. *et al.* (2017) *Common genetic variation drives molecular heterogeneity in human iPSCs*, *Nature*. doi: 10.1038/nature22403.

Kimberly, W. T. *et al.* (2001) 'The Intracellular Domain of the β-Amyloid Precursor Protein Is Stabilized by Fe65 and Translocates to the Nucleus in a Notch-like Manner', *Journal of Biological Chemistry*, 276(43), pp. 40288–40292. doi: 10.1074/jbc.C100447200.

Kivipelto, M. *et al.* (2001) 'Midlife vascular risk factors and Alzheimer's Disease in later life: Longitudinal, population based study', *Bmj*, 322(June), pp. 1447–1451. doi: 10.1136/bmj.322.7300.1447.

Konigsberg, U. R., Lipton, B. H. and Konigsberg, I. R. (1975) 'The regenerative response of single mature muscle fibers isolated in vitro', *Developmental Biology*, 45(2), pp. 260–75. doi: 10.1016/0012-1606(75)90065-2.

Koo, E. H. *et al.* (1990) 'Precursor of amyloid protein in Alzheimer disease undergoes fast anterograde axonal transport', *Proceedings of the National Academy of Sciences of the United States of America*, 87(4), pp. 1561–1565. doi: 10.1073/pnas.87.4.1561.

Koo, E. H. and Squazzo, S. L. (1994) 'Evidence that production and release of amyloid β-protein involves the endocytic pathway', *Journal of Biological Chemistry*, 269(26), pp. 17386–9.

Kopke, E. *et al.* (1993) 'Microtubule-associated protein tau. Abnormal phosphorylation of a non-paired helical filament pool in Alzheimer disease', *Journal of Biological Chemistry*, 268(32), pp.

24374–24384. doi: 10.1016/j.bbrc.2011.11.056.

Korsching, S. (1993) 'The neurotrophic factor concept: a reexamination.', *The Journal of neuroscience : the official journal of the Society for Neuroscience*, 13(7), pp. 2739–2748.

Kosik, K S *et al.* (1989) 'Developmentally regulated expression of specific tau sequences.', *Neuron*, 2(4), pp. 1389–1397. doi: 0896-6273(89)90077-9 [pii].

Kosik, Kenneth S. *et al.* (1989) 'Developmentally regulated expression of specific tau sequences', *Neuron*, 2(4), pp. 1389–97. doi: 10.1016/0896-6273(89)90077-9.

Kosik, K. S. and Finch, E. a (1987) 'MAP2 and tau segregate into dendritic and axonal domains after the elaboration of morphologically distinct neurites: an immunocytochemical study of cultured rat cerebrum.', *The Journal of neuroscience : the official journal of the Society for Neuroscience*, 7(10), pp. 3142–3153. doi: 1987/10/01 00:01.

Kosik, K. S., Joachim, C. L. and Selkoe, D. J. (1986) 'Microtubule-associated protein tau (tau) is a major antigenic component of paired helical filaments in Alzheimer disease.', *Proceedings of the National Academy of Sciences of the United States of America*, 83(11), pp. 4044–8. doi: 10.1097/00002093-198701030-00022.

Kothapalli, C. R. and Kamm, R. D. (2013) '3D matrix microenvironment for targeted differentiation of embryonic stem cells into neural and glial lineages', *Biomaterials*. Elsevier Ltd, 34(25), pp. 5995–6007. doi: 10.1016/j.biomaterials.2013.04.042.

Kumar, A. *et al.* (2014) 'Dual-view plane illumination microscopy for rapid and spatially isotropic imaging', *Nature Protocols*, 9(11), pp. 2555–2573. doi: 10.1038/nprot.2014.172.

Kusakawa, G. I. *et al.* (2000) 'Calpain-dependent proteolytic cleavage of the p35 cyclin-dependent kinase 5 activator to p25', *Journal of Biological Chemistry*, 275(22), pp. 17166–72. doi: 10.1074/jbc.M907757199.

Lamb, B. T. *et al.* (1999) 'Amyloid production and deposition in mutant amyloid precursor protein and presenilin-1 yeast artificial chromosome transgenic mice', *Nature Neuroscience*, 2(8), pp. 695–7. doi: 10.1038/11154.

Lambert, J. C. *et al.* (2009) 'Genome-wide association study identifies variants at CLU and CR1 associated with Alzheimer's disease', *Nature Genetics*, 41(10), pp. 1094–9. doi: 10.1038/ng.439.

Lasagna-Reeves, C. A. *et al.* (2012) 'Alzheimer brain-derived tau oligomers propagate pathology from endogenous tau', *Scientific Reports*, 2(700). doi: 10.1038/srep00700.

Launer, L. J. *et al.* (2000) 'Midlife blood pressure and dementia: The Honolulu-Asia aging study', *Neurobiology of Aging*, 21(1), pp. 49–55. doi: 10.1016/S0197-4580(00)00096-8.

Launer, L. J. (2002) 'Demonstrating the case that AD is a vascular disease: Epidemiologic evidence', *Ageing Research Reviews*, pp. 61–77. doi: 10.1016/S0047-6374(01)00364-5.

Lee, G., Neve, R. L. and Kosik, K. S. (1989) 'The microtubule binding domain of tau protein.', *Neuron*, 2(6), pp. 1615–1624. doi: 10.1016/0896-6273(89)90050-0.

Lee, H.-K. *et al.* (2016) 'Three Dimensional Human Neuro-Spheroid Model of Alzheimer's Disease Based on Differentiated Induced Pluripotent Stem Cells', *PLOS ONE*, 11(9), p. e0163072. doi: 10.1371/journal.pone.0163072.

Lee, H. G. *et al.* (2005) 'Tau phosphorylation in Alzheimer's disease: Pathogen or protector?', *Trends in Molecular Medicine*, 11(4), pp. 164–169. doi: 10.1016/j.molmed.2005.02.008.

Lee, M. K. *et al.* (1990) 'The expression and posttranslational modification of a neuron-specific β-tubulin isotype during chick embryogenesis', *Cell Motility and the Cytoskeleton*, 17(2), pp. 118–132. doi: 10.1002/cm.970170207.

Lee, M. S. *et al.* (2000) 'Neurotoxicity induces cleavage of p35 to p25 by calpain', *Nature*, 405(6784), pp. 360–4. doi: 10.1038/35012636.

Lei, P. *et al.* (2014) 'Motor and cognitive deficits in aged tau knockout mice in two background strains', *Molecular Neurodegeneration*, 9(1). doi: 10.1186/1750-1326-9-29.

Leibrock, J. *et al.* (1989) 'Molecular cloning and expression of brain-derived neurotrophic factor.', *Nature*, 341(6238), pp. 149–152. doi: 10.1038/341149a0.

Leipzig, N. D. and Shoichet, M. S. (2009) 'The effect of substrate stiffness on adult neural stem cell behavior', *Biomaterials*. Elsevier Ltd, 30(36), pp. 6867–6878. doi: 10.1016/j.biomaterials.2009.09.002.

Lejeune, J., Gautier, M. and Turpin, R. (1959a) '[Study of somatic chromosomes from 9 mongoloid children.]', *Comptes rendus hebdomadaires des seances de l'Academie des sciences*, 248(11), pp. 1721–2.

Lejeune, J., Gautier, M. and Turpin, R. (1959b) 'A study of somatic chromosomes in nine infants with mongolism', *C.R. Acad. Sci. (Paris)*, 248, pp. 1721–1722.

Lendahl, U., Zimmerman, L. B. and McKay, R. D. (1990) 'CNS stem cells express a new class of intermediate filament protein.', *Cell*, 60(4), pp. 585–595. doi: 10.1016/0092-8674(90)90662-X.

Lennon, M. J. *et al.* (2019) 'Midlife Hypertension and Alzheimer's Disease: A Systematic Review and Meta-Analysis', *Journal of Alzheimer's Disease*, 71(1), pp. 307–316. doi: 10.3233/JAD-190474.

Leroy, K. *et al.* (2012) 'Lack of tau proteins rescues neuronal cell death and decreases amyloidogenic processing of APP in APP/PS1 mice', *American Journal of Pathology*, 181(6), pp. 1928–1940. doi: 10.1016/j.ajpath.2012.08.012.

Levitt, P. and Rakic, P. (1980) 'Immunoperoxidase localization of glial fibrillary acidic protein in radial glial cells and astrocytes of the developing rhesus monkey brain', *Journal of Comparative Neurology*, 193(3), pp. 815–840. doi: 10.1002/cne.901930316.

Levy-Lahad, E. *et al.* (1995) 'Candidate gene for the chromosome 1 familial Alzheimer's disease

locus.', *Science (New York, N.Y.)*, 269(5226), pp. 973–7. doi: 10.1126/science.7638622.

Li, G. N. *et al.* (2007) 'Genomic and morphological changes of neuroblastoma cells in response to three-dimensional matrices', *Tissue Engineering*, 13(5), pp. 1035–1047. doi: 10.1089/ten.2006.0251.

Li, Y. *et al.* (2014) 'Structural interactions between inhibitor and substrate docking sites give insight into mechanisms of human PS1 complexes', *Structure*, 22(1), pp. 125–135. doi: 10.1016/j.str.2013.09.018.

Li, Y. P. *et al.* (1996) 'β - Amyloid induces apoptosis in human-derived neurotypic SH-SY5Y cells', *Brain Research*, 738(2), pp. 196–204. doi: 10.1016/S0006-8993(96)00733-0.

Liedmann, A., Rolfs, A. and Frech, M. J. (2012) 'Cultivation of Human Neural Progenitor Cells in a 3-dimensional Self-assembling Peptide Hydrogel', *Journal of Visualized Experiments*, (59). doi: 10.3791/3830.

Lin, L. F. *et al.* (1993) 'GDNF: a glial cell line-derived neurotrophic factor for midbrain dopaminergic neurons.', *Science (New York, N.Y.)*, 260(5111), pp. 1130–2. doi: 10.1126/science.8493557.

Lin, Y. T. *et al.* (2018) 'APOE4 Causes Widespread Molecular and Cellular Alterations Associated with Alzheimer's Disease Phenotypes in Human iPSC-Derived Brain Cell Types', *Neuron*. Elsevier Inc., 98(6), pp. 1141-1154.e7. doi: 10.1016/j.neuron.2018.05.008.

Lindwall, G. and Cole, R. D. (1984) 'Phosphorylation affects the ability of tau protein to promote microtubule assembly', *Journal of Biological Chemistry*, 259(8), pp. 5301–5305.

Lippa, C. F. *et al.* (1996) 'Familial and sporadic Alzheimer's disease: Neuropathology cannot exclude a final common pathway', *Neurology*, 46(2), pp. 406–12. doi: 10.1212/WNL.46.2.406.

Lippa, C. F. *et al.* (1998) 'Aβ-42deposition precedes other changes in PS-1 Alzheimer's disease', *Lancet*, 352(9134), pp. 1117–1118. doi: 10.1016/S0140-6736(05)79757-9.

Liu, C. and Götz, J. (2013) 'Profiling Murine Tau with 0N , 1N and 2N Isoform-Specific Antibodies in

Brain and Peripheral Organs Reveals Distinct Subcellular Localization , with the 1N Isoform Being Enriched in the Nucleus', *PloS one*, 8(12), pp. 1–18. doi: 10.1371/journal.pone.0084849.

Lo, B. and Parham, L. (2009) 'Ethical issues in stem cell research', *Endocrine Reviews*, 30(3), pp. 204–213. doi: 10.1210/er.2008-0031.

LoPresti, P. *et al.* (1995) 'Functional implications for the microtubule-associated protein tau: localization in oligodendrocytes.', *Proceedings of the National Academy of Sciences*, 92(22), pp. 10369–10373. doi: 10.1073/pnas.92.22.10369.

Lovejoy, C. *et al.* (2020) 'Engineered Cerebral Organoids Recapitulate Adult Tau Expression and Disease-relevant Changes in Tau Splicing', *Research Square*, pp. 1–31. doi: 10.21203/rs.3.rs-37620/v1.

Di Lullo, E. and Kriegstein, A. R. (2017) 'The use of brain organoids to investigate neural development and disease', *Nature Reviews Neuroscience*, pp. 573–584. doi: 10.1038/nrn.2017.107.

Ma, X. *et al.* (2018) 'The nuclear receptor RXRA controls cellular senescence by regulating calcium signaling', *Aging Cell*, 17(6), pp. 1–14. doi: 10.1111/acel.12831.

Maden, M. (2007) 'Retinoic acid in the development, regeneration and maintenance of the nervous system', *Nature Reviews Neuroscience*, pp. 755–765. doi: 10.1038/nrn2212.

Mandelkow, E. *et al.* (2011) 'Overexpression of Tau Protein Inhibits Kinesin-dependent Trafficking of Vesicles, Mitochondria, and Endoplasmic Reticulum: Implications for Alzheimer's Disease', *Cell*, 143(3), pp. 777–794.

Mandelkow, E. M. *et al.* (1992) 'Glycogen synthase kinase-3 and the Alzheimer-like state of microtubule-associated protein tau', *FEBS Letters*, 314(3), pp. 315–21. doi: 10.1016/0014-5793(92)81496-9.

Marchini, A., Favoino, C. and Gelain, F. (2020) 'Multi-Functionalized Self-Assembling Peptides as

Reproducible 3D Cell Culture Systems Enabling Differentiation and Survival of Various Human Neural Stem Cell Lines', *Frontiers in Neuroscience*, 14(May), pp. 1–11. doi: 10.3389/fnins.2020.00413.

Marí-Buyé, N. and Semino, C. E. (2011) 'Differentiation of mouse embryonic stem cells in self-assembling peptide scaffolds', *Methods in Molecular Biology*, 690, pp. 217–237. doi: 10.1007/978-1-60761-962-8_15.

Martin, G. R. (1981) 'Isolation of a pluripotent cell line from early mouse embryos cultured in medium conditioned by teratocarcinoma stem cells.', *Proceedings of the National Academy of Sciences*, 78(12), pp. 7634–7638. doi: 10.1073/pnas.78.12.7634.

Matsubara, M. *et al.* (1996) 'Site-specific phosphorylation of synapsin I by mitogen-activated protein kinase and Cdk5 and its effects on physiological functions', *Journal of Biological Chemistry*, 271(35), pp. 21108–13. doi: 10.1074/jbc.271.35.21108.

Mawal-Dewan, M. *et al.* (1994) 'The phosphorylation state of tau in the developing rat brain is regulated by phosphoprotein phosphatases', *Journal of Biological Chemistry*, 269(49), pp. 30981–30987.

Mazumder, A. *et al.* (2010) *Prestressed Nuclear Organization in Living Cells*, *Methods in Cell Biology*. Elsevier Masson SAS. doi: 10.1016/S0091-679X(10)98010-2.

McCall, M. a *et al.* (1996) 'Targeted deletion in astrocyte intermediate filament (Gfap) alters neuronal physiology.', *Proceedings of the National Academy of Sciences of the United States of America*, 93(June 1996), pp. 6361–6366. doi: 10.1073/pnas.93.13.6361.

McGowan, E. *et al.* (1999) 'Amyloid phenotype characterization of transgenic mice overexpressing both mutant amyloid precursor protein and mutant presenilin 1 transgenes', *Neurobiology of Disease*, 6(4), pp. 231–44. doi: 10.1006/nbdi.1999.0243.

McMillan, P. *et al.* (2008) 'Tau isoform regulation is region- and cell-specific in mouse brain', *Journal of Comparative Neurology*, 511(6), pp. 788–803. doi: 10.1002/cne.21867.

Means, A. L. and Gudas, L. J. (1995) 'The roles of retinoids in vertebrate development', *Annual Review of Biochemistry*, 64, pp. 201–233. doi: 10.1146/annurev.bi.64.070195.001221.

Mecocci, P. *et al.* (1998) 'Tau protein in cerebrospinal fluid: A new diagnostic and prognostic marker in Alzheimer disease?', *Alzheimer Disease and Associated Disorders*, 12(3), pp. 211–214. doi: 10.1097/00002093-199809000-00015.

Menassa, D. A. and Gomez-Nicola, D. (2018) 'Microglial dynamics during human brain development', *Frontiers in Immunology*, 9(MAY). doi: 10.3389/fimmu.2018.01014.

Mertens, J. *et al.* (2013) 'Embryonic stem cell-based modeling of tau pathology in human neurons', *American Journal of Pathology*. American Society for Investigative Pathology, 182(5), pp. 1769–1779. doi: 10.1016/j.ajpath.2013.01.043.

Mertens, J. *et al.* (2018) 'Aging in a dish: IPSC-derived and directly induced neurons for studying brain aging and age-related neurodegenerative diseases', *Annual Review of Genetics*, 52(August), pp. 271–293. doi: 10.1146/annurev-genet-120417-031534.

Miguel, L. *et al.* (2019) 'Detection of all adult Tau isoforms in a 3D culture model of iPSC-derived neurons', *Stem Cell Research*. Elsevier, 40(January), p. 101541. doi: 10.1016/j.scr.2019.101541.

Miller, J. D. *et al.* (2013) 'Human iPSC-based modeling of late-onset disease via progerin-induced aging', *Cell Stem Cell*, 5(13), pp. 691–705. doi: 10.1016/j.stem.2013.11.006.

Minichiello, L. *et al.* (1999) 'Essential role for TrkB receptors in hippocampus-mediated learning', *Neuron*, 24(2), pp. 401–414. doi: 10.1016/S0896-6273(00)80853-3.

Möller, H. J. and Graeber, M. B. (1998) 'The case describe by Alois Alzheimer in 1911', *Psychiatry Clinical Neuroscience*, 248, pp. 111–122. doi: 10.1007/s004060050027.

Morrison, S. J. and Kimble, J. (2006) 'Asymmetric and symmetric stem-cell divisions in development and cancer', *Nature*, 441, pp. 1068–1074. doi: 10.1038/nature04956.

Muaro, A. (1961) 'Satellite cell of skeletal muscle fibers.', *The Journal of biophysical and biochemical cytology*, 9(2), pp. 493–495. doi: 10.1083/jcb.9.2.493.

Mullan, M. *et al.* (1992) 'A pathogenic mutation for probable Alzheimer's disease in the APP gene at the N–terminus of β–amyloid', *Nature Genetics*, 1(5), pp. 345–7. doi: 10.1038/ng0892-345.

Müller, R. *et al.* (1997) 'Expression of microtubule-asssciated proteins MAP2 and tau in cultured rat brain oligodendrocytes', *Cell and Tissue Research*, 288(2), pp. 239–249. doi: 10.1007/s004410050809.

Muratore, C. R. *et al.* (2014) 'The familial alzheimer's disease APPV717I mutation alters APP processing and Tau expression in iPSC-derived neurons', *Human Molecular Genetics*, 23(13), pp. 3523–3536. doi: 10.1093/hmg/ddu064.

Murayama, O. *et al.* (1999) 'Enhancement of amyloid β 42 secretion by 28 different presenilin 1 mutations of familial Alzheimer's disease', *Neuroscience Letters*, 265(1), pp. 61–63. doi: 10.1016/S0304-3940(99)00187-1.

Namba, Y. *et al.* (1991) 'Apolipoprotein E immunoreactivity in cerebral amyloid deposits and neurofibrillary tangles in Alzheimer's disease and kuru plaque amyloid in Creutzfeldt-Jakob disease', *Brain Research*, 541(1), pp. 163–166. doi: 10.1016/0006-8993(91)91092-F.

Ngamkham, K., Rivolta, M. N. and Battaglia, G. (2017) 'Optimising 3D scaffold for otic neural progenitor differentiation', *bioRxiv*, 44(0), pp. 1–33. doi: 10.1101/120279.

Ni, B. *et al.* (1994) 'Cloning and expression of a cDNA encoding a brain-specific Na(+)-dependent inorganic phosphate cotransporter.', *Proceedings of the National Academy of Sciences of the United States of America*, 91(12), pp. 5607–11. doi: 10.1073/pnas.91.12.5607.

Niederreither, K. and Dollé, P. (2008) 'Retinoic acid in development: Towards an integrated view', *Nature Reviews Genetics*, 9(7), pp. 541–553. doi: 10.1038/nrg2340.

Nikolic, M. *et al.* (1996) 'The cdk5/p35 kinase is essential for neurite outgrowth during neuronal differentiation', *Genes and Development*, 10(7), pp. 816–825. doi: 10.1101/gad.10.7.816.

Nonaka, T. *et al.* (2010) 'Seeded aggregation and toxicity of α-synuclein and tau: Cellular models of neurodegenerative diseases', *Journal of Biological Chemistry*, 285(45), pp. 34885–34898. doi: 10.1074/jbc.M110.148460.

Nussbaum, J. *et al.* (2007) 'Transplantation of undifferentiated murine embryonic stem cells in the heart: teratoma formation and immune response', *The FASEB Journal*, 21(7), pp. 1345–1357. doi: 10.1096/fj.06-6769com.

Nuutinen, T. *et al.* (2009) 'Clusterin: A forgotten player in Alzheimer's disease', *Brain Research Reviews*, 61(2), pp. 89–104. doi: 10.1016/j.brainresrev.2009.05.007.

O'Brien, R. J. and Wong, P. C. (2011) 'Amyloid Precursor Protein Processing and Alzheimer's Disease', *Annual Review of Neuroscience*, 34(1), pp. 185–204. doi: 10.1146/annurev-neuro-061010-113613.

O'Kusky, J. and Ye, P. (2012) 'Neurodevelopmental effects of insulin-like growth factor signaling', *Frontiers in Neuroendocrinology*, pp. 230–251. doi: 10.1016/j.yfrne.2012.06.002.

Oakley, H. *et al.* (2006) 'Intraneuronal beta-Amyloid Aggregates, Neurodegeneration, and Neuron Loss in Transgenic Mice with Five Familial Alzheimer's Disease Mutations: Potential Factors in Amyloid Plaque Formation', *Journal of Neuroscience*, 26(40), pp. 10129–40. doi: 10.1523/JNEUROSCI.1202-06.2006.

Ochalek, A. *et al.* (2017) 'Neurons derived from sporadic Alzheimer's disease iPSCs reveal elevated TAU hyperphosphorylation, increased amyloid levels, and GSK3B activation', *Alzheimer's Research and Therapy*. Alzheimer's Research & Therapy, 9(1), pp. 1–19. doi: 10.1186/s13195-017-0317-z.

Okabe, S. *et al.* (1996) 'Development of neuronal precursor cells and functional postmitotic neurons from embryonic stem cells in vitro', *Mechanisms of Development*, 59(1), pp. 89–102. doi: 10.1016/0925-4773(96)00572-2.

Okita, K. *et al.* (2008) 'Generation of mouse induced pluripotent stem cells without viral vectors.', *Science (New York, N.Y.)*, 322(5903), pp. 949–53. doi: 10.1126/science.1164270.

Okita, K. *et al.* (2011) 'A more efficient method to generate integration-free human iPS cells', *Nature Methods*, 8(5), pp. 409–412. doi: 10.1038/nmeth.1591.

Ortinau, S. *et al.* (2010) 'Effect of 3D-scaffold formation on differentiation and survival in human neural progenitor cells', *BioMedical Engineering Online*, 9. doi: 10.1186/1475-925X-9-70.

Otaegi, G. *et al.* (2006) 'Modulation of the PI 3-kinase-Akt signalling pathway by IGF-I and PTEN regulates the differentiation of neural stem/precursor cells', *Journal of Cell Science*, 119(13), pp. 2739–2748. doi: 10.1242/jcs.03012.

Otvos, L. *et al.* (1994) 'Monoclonal antibody PHF-1 recognizes tau protein phosphorylated at serine residues 396 and 404', *Journal of Neuroscience Research*, 39(6), pp. 669–673. doi: 10.1002/jnr.490390607.

Pajerowski, J. D. *et al.* (2007) 'Physical plasticity of the nucleus in stem cell differentiation', *Proceedings of the National Academy of Sciences of the United States of America*, 104(40), pp. 15619–15624. doi: 10.1073/pnas.0702576104.

Palombo, F. *et al.* (2018) 'Detection of Aβ plaque-associated astrogliosis in Alzheimer's disease brain by spectroscopic imaging and immunohistochemistry', *Analyst*, 143(4), pp. 850–857. doi: 10.1039/c7an01747b.

Panda, D. *et al.* (1995) 'Kinetic Stabilization of Microtubule Dynamics at Steady State by Tau and Microtubule-Binding Domains of Tau', *Biochemistry*, 34(35), pp. 11117–11127. doi: 10.1021/bi00035a017.

Papasozomenos, S. C. and Binder, L. I. (1987) 'Phosphorylation determines two distinct species of Tau in the central nervous system.', *Cell motility and the cytoskeleton*, 8(3), pp. 210–226. doi: 10.1002/cm.970080303.

Paquet, D. *et al.* (2016) 'Efficient introduction of specific homozygous and heterozygous mutations using CRISPR/Cas9', *Nature*. Nature Publishing Group, 533(7601), pp. 125–129. doi: 10.1038/nature17664.

Park, J. *et al.* (2018) 'A 3D human triculture system modeling neurodegeneration and neuroinflammation in Alzheimer's disease', *Nature Neuroscience*, 21(2018), pp. 941–951. doi: 10.1038/s41593-018-0175-4.

Park, S. H., Lim, J. S. and Jang, K. L. (2011) 'All-trans retinoic acid induces cellular senescence via upregulation of p16, p21, and p27', *Cancer Letters*. Elsevier Ireland Ltd, 310(2), pp. 232–239. doi: 10.1016/j.canlet.2011.07.009.

Paşca, A. M. *et al.* (2015) 'Functional cortical neurons and astrocytes from human pluripotent stem cells in 3D culture', *Nat Methods.*, 12(7), pp. 671–678. doi: 10.1038/nmeth.3415.

Patrick, G. N. *et al.* (1999) 'Conversion of p35 to p25 deregulates Cdk5 activity and promotes neurodegeneration', *Nature*, 402(6762), pp. 615–622. doi: 10.1038/45159.

Pei, J. J. *et al.* (2003) 'Okadaic-acid-induced inhibition of protein phosphatase 2A produces activation of mitogen-activated protein kinases ERK1/2, MEK1/2, and p70 S6, similar to that in Alzheimer's disease', *American Journal of Pathology*, 163(3), pp. 845–858. doi: 10.1016/S0002-9440(10)63445-1.

Pellegrini, L. *et al.* (2020) 'Human CNS barrier-forming organoids with cerebrospinal fluid production', *Science*, 369(6500). doi: 10.1126/science.aaz5626.

Pfrieger, F. W. and Barres, B. A. (1997) 'Synaptic efficacy enhanced by glial cells in vitro', *Science (New York, N.Y.)*, 277(5332), pp. 1684–1687. doi: 10.1126/science.277.5332.1684.

Poorkaj, P. *et al.* (1998) 'Tau is a candidate gene for chromosome 17 frontotemporal dementia.', *Annals of neurology*, 43(6), pp. 815–825. doi: 10.1002/ana.410430617.

Poppek, D. *et al.* (2006) 'Phosphorylation inhibits turnover of the tau protein by the proteasome:

Influence of RCAN1 and oxidative stress', *Biochemical Journal*, 400(3), pp. 511–520. doi: 10.1042/BJ20060463.

Power, R. M. and Huisken, J. (2017) 'A guide to light-sheet fluorescence microscopy for multiscale imaging', *Nature Methods*, 14(4), pp. 360–373. doi: 10.1038/nmeth.4224.

Price, D. L. *et al.* (1991) 'Aged Non-Human Primates: An Animal Model of Age-Associated Neurodegenerative Disease', *Brain Pathology*, 1(4), pp. 287–296. doi: 10.1111/j.1750-3639.1991.tb00672.x.

Prince, M. *et al.* (2015) 'World Alzheimer Report 2015. London, UK', *Alzheimer's Disease International*.

Raja, W. K. *et al.* (2016) 'Self-Organizing 3D Human Neural Tissue Derived from Induced Pluripotent Stem Cells Recapitulate Alzheimer's Disease Phenotypes', *PLOS ONE*, 11(9), p. e0161969. doi: 10.1371/journal.pone.0161969.

Ratovitski, T. *et al.* (1997) 'Endoproteolytic processing and stabilization of wild-type and mutant presenilin', *Journal of Biological Chemistry*, 272(39), pp. 24536–41. doi: 10.1074/jbc.272.39.24536.

Rawlings, A. M. *et al.* (2019) 'Cognitive Reserve in Midlife is not Associated with Amyloid-β Deposition in Late-Life', *Journal of Alzheimer's Disease*, 68(2), pp. 517–521. doi: 10.3233/JAD-180785.

Reiman, E. *et al.* (2007) 'GAB2 alleles modify Alzheimer's risk in APOE epsilon4 carriers.', *Neuron*, 54(5), pp. 13–20.

Reynolds, C. A. *et al.* (2019) 'APOE effects on cognition from childhood to adolescence', *Neurobiology of Aging*, 84(2019), pp. 239.e1-239.e8. doi: 10.1016/j.neurobiolaging.2019.04.011.

Rhinn, M. and Dollé, P. (2012) 'Retinoic acid signalling during development', *Development*, 139(5), pp. 843–858. doi: 10.1242/dev.065938.

Rincon, F. and Wright, C. B. (2013) 'Vascular cognitive impairment', *Current Opinion in Neurology*, 26(1), pp. 29–36. doi: 10.1097/WCO.0b013e32835c4f04.

Roberson, E. D. *et al.* (2007) 'Reducing endogenous tau ameliorates amyloid beta-induced deficits in an Alzheimer's disease mouse model.', *Science*, 316(5825), pp. 750–754.

Roberts, R. O. *et al.* (2014) 'Higher risk of progression to dementia in mild cognitive impairment cases who revert to normal', *Neurology*, 82(4), pp. 317–325. doi: 10.1212/WNL.0000000000000055.

Rogaev, E. I. (1995) 'Familial Alzheimer's disease in kindreds with missense mutations in a gene on chromosome 1 related to the Alzheimer's disease type 3 gene.', *Nature*, 376, pp. 775–778. doi: 10.1038/376775a0.

Rompolas, P., Mesa, K. R. and Greco, V. (2013) 'Spatial organization within a niche as a determinant of stem-cell fate', *Nature*, 502(7472), pp. 513–518. doi: 10.1038/nature12602.

Rosen, R. F. *et al.* (2008) 'Tauopathy with paired helical filaments in an aged chimpanzee', *Journal of Comparative Neurology*, 509(3), pp. 259–70. doi: 10.1002/cne.21744.

Ross, S. A. *et al.* (2000) 'Retinoids in embryonal development', *Physiological Reviews*, 80(3), pp. 1021–1054. doi: 10.1152/physrev.2000.80.3.1021.

Rouhani, F. *et al.* (2014) 'Genetic Background Drives Transcriptional Variation in Human Induced Pluripotent Stem Cells', *PLoS Genetics*, 10(6). doi: 10.1371/journal.pgen.1004432.

Russo, V. C. *et al.* (2005) 'The insulin-like growth factor system and its pleiotropic functions in brain', *Endocrine Reviews*, pp. 916–943. doi: 10.1210/er.2004-0024.

Saha, K. *et al.* (2008) 'Substrate modulus directs neural stem cell behavior', *Biophysical Journal*. Elsevier, 95(9), pp. 4426–4438. doi: 10.1529/biophysj.108.132217.

Sahab Negah, S. *et al.* (2017) 'Enhancement of Neural Stem Cell Survival, Proliferation, Migration, and Differentiation in a Novel Self-Assembly Peptide Nanofibber Scaffold', *Molecular Neurobiology*.

Molecular Neurobiology, 54(10), pp. 8050–8062. doi: 10.1007/s12035-016-0295-3.

Saito, T. *et al.* (2019) 'Humanization of the entire murine Mapt gene provides a murine model of pathological human tau propagation', *Journal of Biological Chemistry*, 294(34), pp. 12754–12765. doi: 10.1074/jbc.RA119.009487.

Salloway, S. *et al.* (2014) 'Two phase 3 trials of bapineuzumab in mild-to-moderate Alzheimer's disease.', *The New England journal of medicine*, 370(4), pp. 322–33. doi: 10.1056/NEJMoa1304839.

Sato, T. *et al.* (2007) 'Active γ-secretase complexes contain only one of each component', *Journal of Biological Chemistry*, 282(47), pp. 33985–93. doi: 10.1074/jbc.M705248200.

Saura, C. A. *et al.* (2004a) 'Loss of presenilin function causes impairments of memory and synaptic plasticity followed by age-dependent neurodegeneration', *Neuron*, 42(1), pp. 23–36. doi: 10.1016/S0896-6273(04)00182-5.

Saura, C. A. *et al.* (2004b) 'Loss of presenilin function causes impairments of memory and synaptic plasticity followed by age-dependent neurodegeneration', *Neuron*, 8(42(1)), pp. 23–36. doi: 10.1016/S0896-6273(04)00182-5.

Schellenberg, G. D. *et al.* (1992) 'Genetic linkage evidence for a familial Alzheimer's disease locus on chromosome 14', *Science*, 258(5082), pp. 668–71. doi: 10.1126/science.1411576.

Scheuner, D. *et al.* (1996) 'Secreted amyloid β-protein similar to that in the senile plaques of Alzheimer's disease is increased in vivo by the presenilin 1 and 2 and APP mutations linked to familial Alzheimer's disease', *Nature Medicine*, 2(8), pp. 864–870. doi: 10.1038/nm0896-864.

Schmitt, J. M. and Stork, P. J. S. (2002) 'PKA phosphorylation of Src mediates cAMP's inhibition of cell growth via Rap1', *Molecular Cell*, 9(1), pp. 85–94. doi: 10.1016/S1097-2765(01)00432-4.

Schultz, C. *et al.* (2000) 'Filamentous tau pathology in nerve cells, astrocytes, and oligodendrocytes of aged baboons', *Journal of Neuropathology and Experimental Neurology*, 59(1), pp. 39–52. doi:

10.1093/jnen/59.1.39.

Schupf, N. *et al.* (1998) 'Earlier onset of Alzheimer's disease in men with Down syndrome', *Neurology*, 50(4), pp. 991–995. doi: 10.1212/WNL.50.4.991.

Schwartzentruber, J. *et al.* (2018) 'Molecular and functional variation in iPSC-derived sensory neurons', *Nature Genetics*, 50(1), pp. 54–61. doi: 10.1038/s41588-017-0005-8.

Selkoe, D. J. *et al.* (1987) 'Conservation of brain amyloid proteins in aged mammals and humans with Alzheimer's disease', *Science*, 235(4791), pp. 873–877. doi: 10.1126/science.3544219.

Selkoe, D. J. and Hardy, J. (2016) 'The amyloid hypothesis of Alzheimer's disease at 25 years', *EMBO Molecular Medicine*, 8(6), pp. 595–608. doi: 10.15252/emmm.201606210.

Sengupta, U., Nilson, A. N. and Kayed, R. (2016) 'The Role of Amyloid-β Oligomers in Toxicity, Propagation, and Immunotherapy', *EBioMedicine*, 6(April), pp. 42–49. doi: 10.1016/j.ebiom.2016.03.035.

Shahriyari, L. and Komarova, N. L. (2013) 'Symmetric vs. asymmetric stem cell divisions: an adaptation against cancer?', *PloS one*, 8(10), p. e76195. doi: 10.1371/journal.pone.0076195.

Shen, J. *et al.* (1997) 'Skeletal and CNS defects in Presenilin-1-deficient mice', *Cell*, 89(4), pp. 629–39. doi: 10.1016/S0092-8674(00)80244-5.

Shen, J. and Kelleher, R. J. (2007) 'The presenilin hypothesis of Alzheimer's disease: Evidence for a loss-of-function pathogenic mechanism', *Proceedings of the National Academy of Sciences*, 9(104 (2)), pp. 403–409. doi: 10.1073/pnas.0608332104.

Sheng, N. *et al.* (2010) 'Retinoic acid regulates bone morphogenic protein signal duration by promoting the degradation of phosphorylated Smad1', *Proceedings of the National Academy of Sciences of the United States of America*, 107(44), pp. 18886–18891. doi: 10.1073/pnas.1009244107.

Sherrington, R. *et al.* (1995) 'Cloning of a gene bearing missense mutations in early-onset familial

Alzheimer's disease', *Nature*, 375(6534), pp. 754–760. doi: 10.1038/375754a0.

Sherrington, R. *et al.* (1996) 'Alzheimer's disease associated with mutations in presenilin 2 is rare and variably penetrant', *Human Molecular Genetics*, 5(7), pp. 985–988. doi: 10.1093/hmg/5.7.985.

Shi, Y. *et al.* (2012a) 'Human cerebral cortex development from pluripotent stem cells to functional excitatory synapses', *Nature Neuroscience*, 15(3), pp. 477–486. doi: 10.1038/nn.3041.

Shi, Y. *et al.* (2012b) 'Human cerebral cortex development from pluripotent stem cells to functional excitatory synapses', *Nature Neuroscience*. Nature Publishing Group, 15(3), pp. 477–486. doi: 10.1038/nn.3041.

Shi, Y., Kirwan, P. and Livesey, F. J. (2012) 'Directed differentiation of human pluripotent stem cells to cerebral cortex neurons and neural networks', *Nature Protocols*, 7(10), pp. 1836–1846. doi: 10.1038/nprot.2012.116.

Shilkaitis, A., Green, A. and Christov, K. (2015) 'Retinoids induce cellular senescence in breast cancer cells by RAR-β dependent and independent pathways: Potential clinical implications (Review)', *International Journal of Oncology*, 47(1), pp. 35–42. doi: 10.3892/ijo.2015.3013.

Siney, E. *et al.* (2018) 'Modelling neurodegenerative diseases in vitro: Recent advances in 3D iPSC technologies', *AIMS Cell and Tissue Engineering*, 2(1), pp. 1–23. doi: 10.3934/celltissue.2018.1.1.

Sjögren, M. *et al.* (2000) 'CSF levels of tau, β-amyloid1-42 and GAP-43 in frontotemporal dementia, other types of dementia and normal aging', *Journal of Neural Transmission*, 105(5), pp. 563–579. doi: 10.1007/s007020070079.

Sjögren, M. *et al.* (2001) 'Both total and phosphorylated tau are increased in Alzheimer's disease', *Journal of Neurology Neurosurgery and Psychiatry*, 70(5), pp. 624–630. doi: 10.1136/jnnp.70.5.624.

Sloan, S. A. *et al.* (2017) 'Human Astrocyte Maturation Captured in 3D Cerebral Cortical Spheroids Derived from Pluripotent Stem Cells', *Neuron*, 95(4), pp. 779–790. doi:

10.1016/j.neuron.2017.07.035.

Small, D. H. *et al.* (1994) 'A heparin-binding domain in the amyloid protein precursor of Alzheimer's disease is involved in the regulation of neurite outgrowth.', *The Journal of Neuroscience: The Official Journal of the Society for Neuroscience*, 14(4), pp. 2117–27.

Snowdon, D. A. (1997) 'Aging and Alzheimer's disease: Lessons from the Nun Study', *Gerontologist*, 37(2), pp. 150–156. doi: 10.1093/geront/37.2.150.

Snowdon, D. A. (2003) 'Healthy Aging and Dementia: Findings from the Nun Study', *Annals of Internal Medicine*, 139(5 part 2), pp. 450–454. doi: 10.7326/0003-4819-139-5_part_2-200309021-00014.

Spangrude, G. J., Heimfeld, S. and Weissman, I. L. (1988) 'Purification and characterization of mouse hematopoietic stem cells', *Science*, 241(4861), pp. 58–62. doi: 10.1126/science.2898810.

Spasic, D. *et al.* (2006) 'Presenilin-1 maintains a nine-transmembrane topology throughout the secretory pathway', *Journal of Biological Chemistry*, 281(36), pp. 26569–26577. doi: 10.1074/jbc.M600592200.

Spillantini, M. G. *et al.* (1998) 'Mutation in the tau gene in familial multiple system tauopathy with presenile dementia', *Proceedings of the National Academy of Sciences*, 95(13), pp. 7737–7741. doi: 10.1073/pnas.95.13.7737.

Sposato, L. A. *et al.* (2015) 'Declining incidence of stroke and dementia: Coincidence or prevention opportunity?', *JAMA Neurology*, pp. 1529–1531. doi: 10.1001/jamaneurol.2015.2816.

Sposito, T. *et al.* (2015) 'Developmental regulation of tau splicing is disrupted in stem cell-derived neurons from frontotemporal dementia patients with the 10 + 16 splice-site mutation in MAPT', *Human Molecular Genetics*, 24(18), pp. 5260–5269. doi: 10.1093/hmg/ddv246.

St George-Hyslop, P. *et al.* (1987) 'The genetic defect causing familial Alzheimer's disease maps on

chromosome 21', *Science*, 235(4791), pp. 885–890. doi: 10.1126/science.2880399.

St George-Hyslop, P. H. *et al.* (1987) 'The genetic defect causing familial Alzheimer's disease maps on chromosome 21.', *Science (New York, N.Y.)*, 235(4791), pp. 885–90. doi: 10.1126/science.2880399.

Stachowiak, E. K. *et al.* (2003) 'cAMP-induced differentiation of human neuronal progenitor cells is mediated by nuclear fibroblast growth factor receptor-1 (FGFR1)', *Journal of Neurochemistry*, 84(6), pp. 1296–1312. doi: 10.1046/j.1471-4159.2003.01624.x.

Stadtfeld, M. *et al.* (2008) 'Induced pluripotent stem cells generated without viral integration.', *Science (New York, N.Y.)*, 322(5903), pp. 945–9. doi: 10.1126/science.1162494.

Steffen, J. *et al.* (2016) 'Revisiting rodent models: Octodon degus as Alzheimer's disease model?', *Acta neuropathologica communications*, 4(91). doi: 10.1186/s40478-016-0363-y.

Stevens, L. C. (1970) 'The development of transplantable teratocarcinomas from intratesticular grafts of pre- and postimplantation mouse embryos', *Developmental Biology*, 21(3), pp. 364–382. doi: 10.1016/0012-1606(70)90130-2.

Stoothoff, W. H. and Johnson, G. V. W. (2005) 'Tau phosphorylation: Physiological and pathological consequences', *Biochimica et Biophysica Acta - Molecular Basis of Disease*, 1739(2–3), pp. 280–97. doi: 10.1016/j.bbadis.2004.06.017.

De Strooper, B. *et al.* (1998) 'Deficiency of presenilin-1 inhibits the normal cleavage of amyloid precursor protein', *Nature*, 391(6665), pp. 387–390. doi: 10.1038/34910.

De Strooper, B. (2007) 'Loss-of-function presenilin mutations in Alzheimer disease. Talking Point on the role of presenilin mutations in Alzheimer disease', *EMBO Reports*, 8(2), pp. 141–146. doi: 10.1038/sj.embor.7400897.

Struhl, G. and Greenwald, I. (1999) 'Presenilin is required for activity and nuclear access of notch in drosophila', *Nature*, 398(6727), pp. 522–5. doi: 10.1038/19091.

Sunderland, T. *et al.* (2003) 'Decreased β-Amyloid1-42 and Increased Tau Levels in Cerebrospinal Fluid of Patients with Alzheimer Disease', *Journal of the American Medical Association*, 289(16), pp. 2094–2103. doi: 10.1001/jama.289.16.2094.

Sutherland, E. W. and Rall, T. W. (1958) 'Fractionation and characterization of a cyclic adenine ribonucleotide formed by tissue particles.', *The Journal of biological chemistry*, 232(2), pp. 1077–1091. doi: 10.1017/CBO9781107415324.004.

Sutherland, R. *et al.* (1981) 'Spheroids in Cancer Research', *Cancer Research*, 41(7), pp. 2980–2984. doi: 10.1007/978-3-642-82340-4.

Tai, L. M. *et al.* (2011) 'Introducing human APOE into Aβ transgenic mouse models', *International Journal of Alzheimer's Disease*, 2011(2). doi: 10.4061/2011/810981.

Takahashi, K. and Yamanaka, S. (2006) 'Induction of Pluripotent Stem Cells from Mouse Embryonic and Adult Fibroblast Cultures by Defined Factors', *Cell*, 126(4), pp. 663–676. doi: 10.1016/j.cell.2006.07.024.

Takamori, S. *et al.* (2000) 'Identification of a vesicular glutamate transporter that defines a glutamatergic phenotype in neurons', *Nature*, 407(6801), pp. 189–194. doi: 10.1038/35025070.

Takemura, R. *et al.* (1995) 'Polarity orientation and assembly process of microtubule bundles in nocodazole-treated, MAP2c-transfected COS cells', *Mol Biol Cell*, 6(8), pp. 981–96. doi: 10.1091/mbc.6.8.981.

Takuma, H., Arawaka, S. and Mori, H. (2003) 'Isoforms changes of tau protein during development in various species', *Developmental Brain Research*, 142(2), pp. 121–127. doi: 10.1016/S0165-3806(03)00056-7.

Tan, B. T. *et al.* (2015) 'Retinoic acid induced the differentiation of neural stem cells from embryonic spinal cord into functional neurons in vitro', *International Journal of Clinical and Experimental Pathology*, 8(7), pp. 8129–8135.

Tanimukai, H., Grundke-Iqbal, I. and Iqbal, K. (2005) 'Up-regulation of inhibitors of protein phosphatase-2A in Alzheimer's disease', *American Journal of Pathology*, 166(6), pp. 1761–71. doi: 10.1016/S0002-9440(10)62486-8.

Thinakaran, G. *et al.* (1996) 'Endoproteolysis of presenilin 1 and accumulation of processed derivatives in vivo', *Neuron*, 17(1), pp. 181–90. doi: 10.1016/S0896-6273(00)80291-3.

Tint, I. *et al.* (1998) 'Acute inactivation of tau has no effect on dynamics of microtubules in growing axons of cultured sympathetic neurons', *Journal of Neuroscience*, 18(21), pp. 8660–8673. doi: 10.1523/JNEUROSCI.18-21-08660.1998.

Tremblay, M. È. and Sierra, A. (2014) *Microglia in health and disease*, *Microglia in Health and Disease*. doi: 10.1007/978-1-4939-1429-6.

Trinczek, B. *et al.* (1995) 'Domains of tau protein, differential phosphorylation, and dynamic instability of microtubules.', *Molecular Biology of the Cell*, 6(12), pp. 1887–1902. doi: 10.1091/mbc.6.12.1887.

Tsai, L. H. *et al.* (1993) 'Activity and expression pattern of cyclin-dependent kinase 5 in the embryonic mouse nervous system', *Development*, 119(4), pp. 1029–40.

Tsai, L. H. *et al.* (1994) 'p35 is a neural-specific regulatory subunit of cyclin-dependent kinase 5', *Nature*, 371(6496), pp. 419–23. doi: 10.1038/371419a0.

Tsai, M. S. *et al.* (1994) 'Apolipoprotein E: Risk factor for Alzheimer disease.', *American journal of human genetics*, 54(4), pp. 643–9.

Ullian, E. M. *et al.* (2001) 'Control of synapse number by glia', *Science*, 291(5504), pp. 657–661. doi: 10.1126/science.291.5504.657.

Veeraraghavalu, K. *et al.* (2010) 'Presenilin 1 Mutants Impair the Self-Renewal and Differentiation of Adult Murine Subventricular Zone-Neuronal Progenitors via Cell-Autonomous Mechanisms Involving

Notch Signaling', *Journal of Neuroscience*, 30(20), pp. 6903–6915. doi: 10.1523/JNEUROSCI.0527-10.2010.

Vemuri, P. and Mormino, E. C. (2013) 'Cognitively stimulating activities to keep dementia at bay', *Neurology*, 81(4), pp. 308–309. doi: 10.1212/WNL.0b013e31829c5f05.

Verghese, P. B., Castellano, J. M. and Holtzman, D. M. (2011) 'Apolipoprotein E in Alzheimer's disease and other neurological disorders', *The Lancet Neurology*, 10(3), pp. 241–52. doi: 10.1016/S1474-4422(10)70325-2.

Verheyen, A. *et al.* (2015) 'Using Human iPSC-Derived Neurons to Model TAU Aggregation', *plos One*, pp. 1–15. doi: 10.1371/journal.pone.0146127.

Vierbuchen, T. *et al.* (2010) 'Nihms169004', 463(7284), pp. 1035–1041.

Wagner, U. *et al.* (1996) 'Cellular phosphorylation of tau by GSK-3β influences tau binding to microtubules and microtubule organisation', *Journal of Cell Science*, pp. 1537–1543.

Walker, E. S. *et al.* (2005) 'Presenilin 2 familial Alzheimer's disease mutations result in partial loss of function and dramatic changes in Aβ 42/40 ratios', *Journal of Neurochemistry*, 92(2), pp. 294–301. doi: 10.1111/j.1471-4159.2004.02858.x.

Wang, F. *et al.* (2011) 'GDNF-pretreatment enhances the survival of neural stem cells following transplantation in a rat model of Parkinson's disease', *Neuroscience Research*, 71(1), pp. 92–98. doi: 10.1016/j.neures.2011.05.019.

Wang, H.-Y. *et al.* (2000) 'β-Amyloid1–42 Binds to α7 Nicotinic Acetylcholine Receptor with High Affinity IMPLICATIONS FOR ALZHEIMER'S DISEASE PATHOLOGY', *Journal of Biological Chemistry*, 275(8), pp. 5626–5632. doi: 10.1074/jbc.275.8.5626.

Wang, J.-Z. *et al.* (1995) 'Dephosphorylation of Alzheimer Paired Helical Filamnets by Protein Phosphatase-2A and 2B', *The Journal of biological chemistry*, 270(3), pp. 4854–4860.

Wang, Z. *et al.* (2009) 'Pre- and Postsynaptic Interaction of the Amyloid Precursor Protein Promotes Peripheral and Central Synaptogenesis', *J Neurosci*, 29(35), pp. 10788–10801. doi: 10.1523/JNEUROSCI.2132-09.2009.Pre-.

Wegiel, J., Henryk, W. and Soltysiak, Z. (1998) 'Region- and cell-type-specific pattern of tau phosphorylation in dog brain.', *Brain Research*, 802(1–2), pp. 259–266. doi: 10.1016/S0006-8993(98)00542-3.

Weidemann, A. *et al.* (1989) 'Identification, biogenesis, and localization of precursors of Alzheimer's disease A4 amyloid protein', *Cell*, 57(1), pp. 115–126. doi: 10.1016/0092-8674(89)90177-3.

Weingarten, M. D. *et al.* (1975) 'A protein factor essential for microtubule assembly.', *Proceedings of the National Academy of Sciences of the United States of America*, 72(5), pp. 1858–62. doi: 10.1073/pnas.72.5.1858.

Weissman, I. L., Anderson, D. J. and Gage, F. (2001) 'Stem and Progenitor Cells: Origins, Phenotypes, Lineage Commitments, and Transdifferentiations', *Annual Review of Cell and Developmental Biology*, 2001(17), pp. 387–403. doi: 10.1146/annurev.cellbio.17.1.387.

Wen, P. H. *et al.* (2004) 'The presenilin-1 familial Alzheimer disease mutant P117L impairs neurogenesis in the hippocampus of adult mice', *Experimental Neurology*, 188(2), pp. 224–237. doi: 10.1016/j.expneurol.2004.04.002.

Westerman, M. A. *et al.* (2002) 'The relationship between Abeta and memory in the Tg2576 mouse model of Alzheimer's disease.', *The Journal of Neuroscience*, 22(5), pp. 1858–67. doi: 22/5/1858 [pii].

White, D. M. *et al.* (2000) 'CREB contributes to the increased neurite outgrowth of sensory neurons induced by vasoactive intestinal polypeptide and activity-dependent neurotrophic factor', *Brain Research*, 868(1), pp. 31–38. doi: 10.1016/S0006-8993(00)02259-9.

William Rebeck, G. *et al.* (1993) 'Apolipoprotein E in sporadic Alzheimer's disease: Allelic variation and receptor interactions', *Neuron*, 11(4), pp. 575–80. doi: 10.1016/0896-6273(93)90070-8.

Wilson, R. S. *et al.* (2013) 'Life-span cognitive activity, neuropathologic burden, and cognitive aging', *Neurology*, 81(4), pp. 311–321. doi: 10.1212/WNL.0b013e31829c5e8a.

Wines-Samuelson, M. *et al.* (2010) 'Characterization of age-dependent and progressive cortical neuronal degeneration in Presenilin conditional mutant mice', *PLoS ONE*, 5(4), p. e10195. doi: 10.1371/journal.pone.0010195.

Wisniewski, K. E., Wisniewski, H. M. and Wen, G. Y. (1985) 'Occurrence of neuropathological changes and dementia of Alzheimer's disease in Down's syndrome', *Annals of Neurology*, 17(3), pp. 278–82. doi: 10.1002/ana.410170310.

Wolfe, M. S. *et al.* (1999) 'Two transmembrane aspartates in presenilin-1 required for presenilin endoproteolysis and γ-secretase activity', *Nature*, 398(6727), pp. 513–517. doi: 10.1038/19077.

Wong, P. C. *et al.* (1997) 'Presenilin 1 is required for Notch1 and DII1 expression in the paraxial mesoderm.', *Nature*, 387(6630), pp. 288–92. doi: 10.1038/387288a0.

Wörsdörfer, P. *et al.* (2019) 'Generation of complex human organoid models including vascular networks by incorporation of mesodermal progenitor cells', *Scientific Reports*, 9(1), pp. 1–13. doi: 10.1038/s41598-019-52204-7.

Wu, C. C. *et al.* (2016) 'Gain of BDNF Function in Engrafted Neural Stem Cells Promotes the Therapeutic Potential for Alzheimer's Disease', *Scientific Reports*. Nature Publishing Group, 6(June), pp. 1–16. doi: 10.1038/srep27358.

Wu, S. M. *et al.* (2010) 'Role of Sonic hedgehog signaling and the expression of its components in human embryonic stem cells.', *Stem cell research*, 4(1), pp. 38–49. doi: 10.1016/j.scr.2009.09.002.

Yagi, T. *et al.* (2011) 'Modeling familial Alzheimer's disease with induced pluripotent stem cells', *Human Molecular Genetics*, 20(23), pp. 4530–4539. doi: 10.1093/hmg/ddr394.

Yamanaka, S. (2010) 'Patient-Specific pluripotent stem cells become even more accessible', *Cell Stem*

Cell, pp. 1–2. doi: 10.1016/j.stem.2010.06.009.

Yan, S. D. *et al.* (1994) 'Glycated tau protein in Alzheimer disease: a mechanism for induction of oxidant stress.', *Proceedings of the National Academy of Sciences of the United States of America*, 91(16), pp. 7787–91. doi: 10.1073/pnas.91.16.7787.

Yan, S. Du *et al.* (1996) 'RAGE and amyloid-β peptide neurotoxicity in Alzheimer's disease', *Nature*, 382(6593), pp. 685–691. doi: 10.1038/382685a0.

Yan, W. *et al.* (2018) 'A Three-Dimensional Culture System with Matrigel Promotes Purified Spiral Ganglion Neuron Survival and Function In Vitro', *Molecular Neurobiology*. Molecular Neurobiology, 55(3), pp. 2070–2084. doi: 10.1007/s12035-017-0471-0.

Yang, J. *et al.* (2016) 'Early pathogenic event of Alzheimer's disease documented in iPSCs from patients with PSEN1 mutations', *Oncotarget*, 8(5), pp. 7900–7913. doi: 10.18632/oncotarget.13776.

Yankner, B. A. *et al.* (1989) 'Neurotoxicity of a fragment of the amyloid precursor associated with Alzheimer's disease.', *Science (New York, N.Y.)*, 245(4916), pp. 417–20. doi: 10.1126/science.2474201.

Yankner, B. A., Duffy, L. K. and Kirschner, D. A. (1990) 'Neurotrophic and neurotoxic effects of amyloid β protein: Reversal by tachykinin neuropeptides', *Science*. doi: 10.1126/science.2218531.

Ye, P. *et al.* (2004) 'Astrocyte-specific overexpression of insulin-like growth factor-I promotes brain overgrowth and glial fibrillary acidic protein expression', *Journal of Neuroscience Research*, 78(4), pp. 472–484. doi: 10.1002/jnr.20288.

Ye, P., Carson, J. and D'Ercole, A. J. (1995) 'In vivo actions of insulin-like growth factor-I (IGF-I) on brain myelination: studies of IGF-I and IGF binding protein-1 (IGFBP-1) transgenic mice.', *The Journal of neuroscience : the official journal of the Society for Neuroscience*, 15(11), pp. 7344–56.

Yu, G. *et al.* (2000) 'Nicastrin modulates presenilin-mediated notch/glp-1 signal transduction and

βAPP processing', *Nature*, 407(6800), pp. 48–54. doi: 10.1038/35024009.

Yu, H. *et al.* (2001) 'APP processing and synaptic plasticity in presenilin-1 conditional knockout mice.', *Neuron*, 31(5), pp. 713–26. doi: 10.1016/S0896-6273(01)00417-2.

Zaka, M. *et al.* (2005) 'Insulin-like growth factor-1 provides protection against psychosine-induced apoptosis in cultured mouse oligodendrocyte progenitor cells using primarily the PI3K/Akt pathway.', *Molecular and cellular neurosciences*, 30(3), pp. 398–407. doi: 10.1016/j.mcn.2005.08.004.

Zhang, C. *et al.* (2009) 'Presenilins are essential for regulating neurotransmitter release', *Nature*, 460(7255), pp. 632–636. doi: 10.1038/nature08177.

Zhang, D. *et al.* (2014) 'A 3D Alzheimer's disease culture model and the induction of P21-activated kinase mediated sensing in iPSC derived neurons', *Biomaterials*. Elsevier Ltd, 35(5), pp. 1420–1428. doi: 10.1016/j.biomaterials.2013.11.028.

Zhang, S. C. *et al.* (2001) 'In vitro differentiation of transplantable neural precursors from human embryonic stem cells', *Nature Biotechnology*, 19(12), pp. 1129–1133. doi: 10.1038/nbt1201-1129.